High Throughput Screens Against Heat Shock Protein 70 (Hsp70)

by

Chia Yin Chang

A dissertation submitted in partial fulfillment
of the requirements for the degree of
Doctor of Philosophy
(Chemical Biology)
In The University of Michigan
2011

Doctoral Committee:

Assistant Professor Jason E. Gestwicki, Chair
Professor Anna K. Mapp
Associate Professor Bruce A. Palfey
Associate Professor Zhaohui Xu

To my parents and friends

Acknowledgements

First and foremost, I would like to thank my advisor, Prof. Jason E. Gestwicki. I feel that I am extremely lucky to have such a great mentor; his intelligence, patience, kindness, and optimistic attitude guided me through all the challenges I faced in graduate school and helped me mature to an independent scientist. I am grateful that Jason always believed in the best in me, even when I was struggling with all the obstacles in research or writing in a foreign language (for me). I am also thankful that Jason allowed us to make and fix our own mistakes in research, and always looked at the bright side of everything. I wish that one day I can become a mentor as good as him. I also want to acknowledge and thank all the members of Gestwicki lab, both present and past; it is a pleasant experience to work along such a group of fun, intelligent, kind, and hard-working scientists. I especially like to thank Sussi, who kindly helped me adapt to this country when I first came and assisted me in the initial stage of my projects. I also like to thank Chris for patiently teaching me organic synthesis; although my endeavors in chemistry were not that successful. I also thank Srikanth, Katie, Ashley, and Andrea for always providing great insights for my research, presentations, and writings. I also want to thank Yoshi for nature product characterization and helps in high throughput screening; also, I would like to thank Peter for lots of help in computer modeling and providing useful insights for my projects. I thank Gladis and Anne for helps when I occasionally needed to do yeast experiments; also, I thank Leah for lots of

help in doing lab chores. I also like to thank Tomoko for letting me use her purified proteins; I wish I can be as energetic when I am over 70. To the rest of the lab, please know that you have helped me greatly in your own ways and I'll be forever thankful for that. I am also grateful for my thesis committee for providing useful insights into my project and helping me in applying for job and fellowships. Thank you for your time and commitment.

To my friends, both the old ones in Taiwan, and the new ones I've made in the last five years, thanks for all of your helps and supports. I especially like to thank Xiao Liu for her kindness, understanding, and patience; I learned the virtue of perseverance from her. Also, I would like to thank Wenjing for her friendship and for bringing a lot of energy to my life. I also like to thank Xin, Yipei, Jing Chen, Xiaomu, Chenxi, Ningkun, Uniko, Liuling, Jiang Jiang, and Yaru for being so nice to me and so much fun to hang out with. I also like to thank Wan Lim and Devayani for being great cohorts and helped me in many ways when I first came to United States. I also want to thank Willy Hong, a great friend who helped me a lot in research and school application when I was in Taiwan; I wish you are still alive to see my growth as a scientist.

To my parents, your love, patience, and wisdom guide me through every stage of my life. You are the wind beneath my wings. If I can achieve anything, that's because of you. Thank you for everything.

Table of Contents

List of Figures

List of Tables

List of Abbreviations

15-DSG	15-deoxyspergualin
Aβ	Amyloid beta
AD	Alzheimer's disease
ADP	Adenosine diphosphate
Apaf-1	apoptotic peptidase activating factor 1
APIase	cis/trans aminopeptidyl isomerase
ATP	Adenosine triphosphate
ATPase	Adenosine Triphosphatase
BAG	Bcl2-associated athanogene
Bax	Bcl-2-associated X protein
CFTR	cystic fibrosis transmembrane receptor
CHIP	C-terminal of Hsc70 interacting protein
DJA2	DnaJ (Hsp40) homolog, subfamily A, member 2
DMSO	Dimethyl sulfoxide
ELISA	enzyme-linked immunosorbent assay
ER	Endoplasmic reticulum
ERAD	ER-associated degradation
FP	fluorescence polarization
FRET	Förster resonance energy transfer
HD	Huntington's disease

HOP	Hsp70/Hsp90 Organizing Protein
HRP	horseradish peroxidase
HSBP1	Hsp70 binding protein 1
Hsc70	Heat shock cognate 70 kDa
HSF1	Heat shock factor 1
Hsp40	Heat shock protein 40 KDa
Hsp70	Heat shock protein 70 KDa
Hsp90	Heat shock protein 90 kDa
HTS	High throughput screening
IL-10	interleukin 10
ITC	Isothermal titration calorimetry
J protein	J domain-containing protein
MB	Methylene blue
MDH	Malate dehydrogenase
MG	Malachite green
mtHsp70	mitochondrial HSP70
NBD	Nucleotide binding domain
NEF	Nucleotide exchange factor
NFT	neurofibrillary tangles
NMR	Nuclear magnetic resonance
NR peptide	NRLLLTG peptide
PES	phenylethynesulfonamide
PolyQ	polyglutamine
PPAR	peroxisome proliferation-activated receptor

QR	Quinaldine red
SAR	Structure activity relationship
SBD	Substrate binding domain
SBMA	spinal and bulbar muscular dystrophy
SCA	spinocerebellar ataxia
Ssa1	stress seventy subfamily A
TNFa	tumor necrosis factor a
TPR	Tetratricopeptide repeat
WT	wild-type

ABSTRACT

High Throughput Screens Against Heat Shock Protein 70 (Hsp70)

by

Chia Yin Chang

Chair: Jason E. Gestwicki

The molecular chaperone Hsp70 plays important roles in protein quality control. Moreover, Hsp70 has been linked to diseases of protein misfolding, such as neurodegenerative disorders, suggesting that it could be a promising new drug target. However, the molecular mechanisms that link Hsp70 to these diseases remain unclear.

We hypothesized that one way to better understand the roles of Hsp70 would be to develop chemical probes that disrupt its specific functions. In this thesis, we developed the first high throughput screens for the ATPase activity of Hsp70. Using this platform, we explored the idea of "gray-box" screening, in which multiple components of the Hsp70 chaperone system are reconstituted *in vitro* to better approximate the biochemical properties of the physiological complexes. We wanted to understand

whether this approach would provide a compromise between “black box” cell-based screens and assays that rely on individual purified proteins. Accordingly, we screened over 50,000 compounds and natural product extracts and reported a number of new Hsp70 inhibitors, including myricetin. Interestingly, we found that many of these inhibitors blocked the protein-protein interactions between the Hsp70, DnaK, and its important co-chaperone, DnaJ. Thus, we expect these compounds to be powerful probes for exploring the biological roles of the DnaK-DnaJ complex. Finally, we explored whether other Hsp70 chaperone functions, such as substrate binding or refolding, might also be useful targets for high throughput screening. Towards that goal, we generated point mutants in DnaK and human Hsc70 and studied how their different *in vitro* biochemical activities correlated with cellular functions. We found that luciferase refolding activity, not ATPase rate, was more predictive of certain cellular chaperone activities, such as heat shock rescue and effects on tau stability. These results suggest the need for multiple primary and secondary assays in searching for Hsp70 inhibitors. Together, these studies have provided important insights into the Hsp70 chaperone system and they have discovered molecules that could be used to further validate Hsp70 as a drug target.

Chapter 1

Introduction: Heat Shock Protein 70 as an Emerging Drug Target

1.1 Abstract

Heat shock protein 70 (Hsp70) is a molecular chaperone that is expressed in response to stress. In this role, Hsp70 binds to its protein substrates and stabilize them against denaturation or aggregation until conditions improve. In addition to its functions during a stress response, Hsp70 has multiple responsibilities during normal growth; it assists in the folding of newly synthesized proteins, the subcellular transport of proteins and vesicles, the formation and dissociation of complexes, and the degradation of unwanted proteins. Thus, this chaperone broadly shapes protein homeostasis by controlling protein quality control and turnover during both normal and stress conditions. Consistent with these diverse activities, genetic and biochemical studies have implicated it in a range of diseases, including cancer, neurodegeneration, allograft rejection and

infection. This review provides a brief overview of Hsp70 structure and function and then explores some of the emerging opportunities and challenges for drug discovery.

1.2 The Structure and Enzymatic Activities of Hsp70s

1.2.1 Hsp70 Family Members are Highly Conserved

Members of the Hsp70 family are ubiquitously expressed and highly conserved; for example, the major Hsp70 from *Escherichia coli,* termed DnaK, is approximately 50% identical to human Hsp70s [1]. Eukaryotes often express multiple Hsp70 family members with major isoforms found in all the cellular compartments: Hsp72 (HSPA1A) and heat shock cognate 70 (Hsc70/HSPA8) in the cytosol and nucleus, BiP (Grp78/HSPA5) in the endoplasmic reticulum, and mtHsp70 (Grp75/mortalin/HSPA9) in mitochondria. Some of the functions of the cytosolic isoforms, Hsc70 and Hsp72, are thought to be redundant, but the transcription of Hsp72 is highly responsive to stress while Hsc70 is constitutively expressed. In the ER and mitochondria, the Hsp70 family members are thought to fulfill specific functions and have unique substrates, with BiP playing key roles in the folding and quality control of ER proteins and mtHsp70 being involved in the import and export of proteins from the mitochondria. For the purposes

of this review, we will often use Hsp70 as a generic term to encompass the shared properties of the family members.

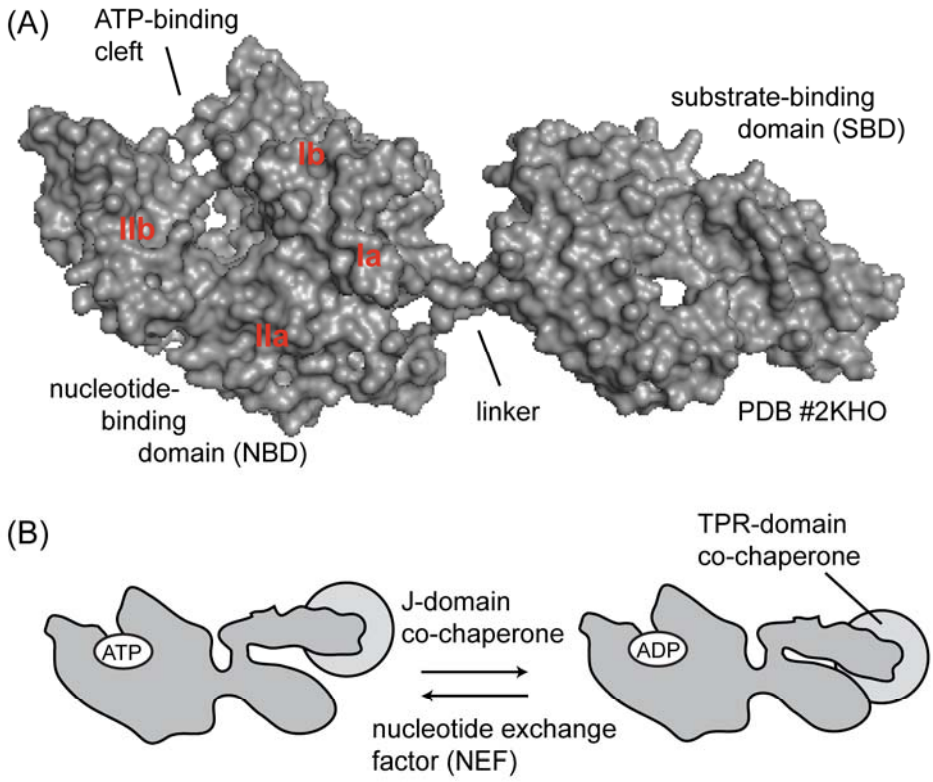

Figure 1.1 Structure and ATPase cycle of Hsp70. (A) Heat shock protein 70 is composed of a 45 kDa nucleotide-binding domain (NBD), connected to a 30kDa substrate-binding domain (SBD) by a short, hydrophobic linker. The SBD contains a beta-sandwich and a helical lid domain. The representative structure shown is of prokaryotic DnaK in complex with ADP and a peptide substrate (PDB # 2KHO). (B) Schematic of ATP hydrolysis and the role of co-chaperones.

1.2.2 The Domain Architecture and Substrate Binding Activity of Hsp70

All members of the Hsp70 family have an N-terminal nucleotide binding domain (NBD) (~40 kDa) and a C-terminal substrate-binding domain (SBD) (~25 kDa) connected by a short linker (**Figure 1.1A**) [2]. The NBD consists of two subdomains, I and II, which are

further divided into regions a and b. The Ia and IIa subdomains interact with ATP through a nucleotide-binding cassette related to those of hexokinase, actin and glycerol kinase [3, 4]. The SBD consists of a 10-kDa α-helix subdomain and a 15-kDa β-sandwich. Crystal structures suggest that substrate peptides are bound in an extended conformation between loops of the β-sandwich and that the α-helix subdomain acts as a "lid" [5]. The substrates of Hsp70 are thought to include both linear polypeptides, such as those found in newly synthesized proteins or folding intermediates [6], and exposed regions of fully or partially folded proteins. For example, Hsp70 is known to interact with clathrin, components of the transcriptional activation complex, nuclear hormone receptors and many others [7-9]. This diversity of substrates is allowed by the low sequence selectivity of the SBD, which binds to most peptides composed of most non-polar amino acids [10].

1.2.3 The ATPase Activity of Hsp70

Many of the functions of Hsp70 appear to revolve around crosstalk between ATPase activity in the NBD and substrate binding in the SBD. Hsp70 binds tightly to ATP, with some reports of *E. coli* DnaK binding with a K_d of 1 nM [11]. Through an inter-domain, allosteric mechanism, ATP binding increases the on- and off-rate of peptide binding in

the adjacent SBD. In turn, nucleotide hydrolysis to ADP closes the "lid" and enhances the affinity for substrate (**Figure 1.1B**) [12]. Likewise, interactions between the SBD and its substrates increase the rate of ATP hydrolysis in the NBD, suggesting that communication between the two domains is two-way [12]. The mechanisms of inter-domain communication have been studied extensively and appear to involve the conserved, hydrophobic linker [13, 14]. Thus, from a drug discovery viewpoint, this allostery in Hsp70 provides multiple opportunities for chemical intervention, including inhibition of ATP turnover, substrate binding or even blocking inter-domain allostery.

1.2.4 The Co-chaperones of Hsp70s

As isolated proteins, the ATP hydrolysis rates of Hsc70 and DnaK are extremely slow, 0.003 and 0.0003 s^{-1}, respectively [11, 15]. *In vivo*, this property provides the opportunity for regulation by co-chaperones, which associate with Hsp70s and control their nucleotide turnover. For example, the J proteins (or Hsp40s) are a large group of co-chaperones that stimulate ATP hydrolysis (**Figure 1.1B**) [16]. In the human genome, at least 40 different J protein genes have been identified [17] and each contains the conserved, ~70 amino acid J domain required for binding and stimulation of Hsp70s [18]. NMR, mutagenesis and crystallography studies indicate that at least one binding

site of the J domain is on the NBD [19, 20]. Protein-protein interactions between the J domain and Hsp70 trigger an allosteric “hotwire” through the NBD that enhances ATP turnover by approximately 7-fold. Thus, in the presence of a J-protein, the release of ADP becomes the rate-limiting step [21]. To complete the ATPase cycle, a distinct class of co-chaperones, the nucleotide exchange factors (NEFs) catalyze ADP release. The major NEF families include, the GrpE-like family [22], BAG family proteins [23], HspBP1 [24] and the atypical Hsp70 homologs (*e.g.* Hsp110) [25]. All of these NEFs appear to bind the NBD and favor ADP release, but each class uses a different structural mechanism to achieve this effect [26]. Together, the J-domain proteins and NEFs regulate ATP cycling, and therefore they also control substrate binding. In addition, some of the co-chaperones independently bind substrates and, through this activity, have the potential to influence substrate selection by the Hsp70 complex [27, 28]. Thus, although these co-chaperones do not have enzymatic activity, they are important regulatory factors and they are required for many chaperone functions of Hsp70.

A final group of co-chaperones, the tetratricopeptide repeat (TPR)-containing proteins, bind to the EEVD sequence at the extreme C-terminus of Hsp70. Interestingly, the evolutionarily unrelated molecular chaperone, Hsp90, also contains the EEVD motif,

allowing it to also interact with TPR domains. The TPR is characterized by a 34-amino acid motif that forms an antiparallel α-helical hairpin [29]. Most proteins that have TPR domains also have additional domains with other activities and, thus, these co-chaperones are thought to recruit unique capabilities to the Hsp70 complex. For example, HOP has three domains (TPR1, TPR2A, and TPR2B) with three TPR motifs each [30]. HOP preferably binds to the ADP-bound form of Hsp70 via TPR1 and TPR2B, while TPR2A specifically binds to Hsp90 [31-33]. In this way, Hop bridges Hsp70 and Hsp90, assists substrate transfer between these chaperones and is believed to promote substrate folding [34]. Another TPR-domain protein, CHIP, also contains a U-box domain and it supervises the triage of Hsp70- or Hsp90-bound proteins [35, 36]. Thus, although both HOP and CHIP bind via TPR domains, the outcomes of these interactions are diametrically opposed: HOP favors folding, while CHIP favors degradation. Based on these observations and many others, it is thought that competition between co-chaperones might drive combinatorial assembly of chaperone complexes with specific functions [8, 37, 38]. Together, these features suggest that protein-protein contacts in the Hsp70 complex may be potential drug targets.

1.3 The Roles of Hsp70 in Human Diseases

1.3.1 Cancer and Apoptosis

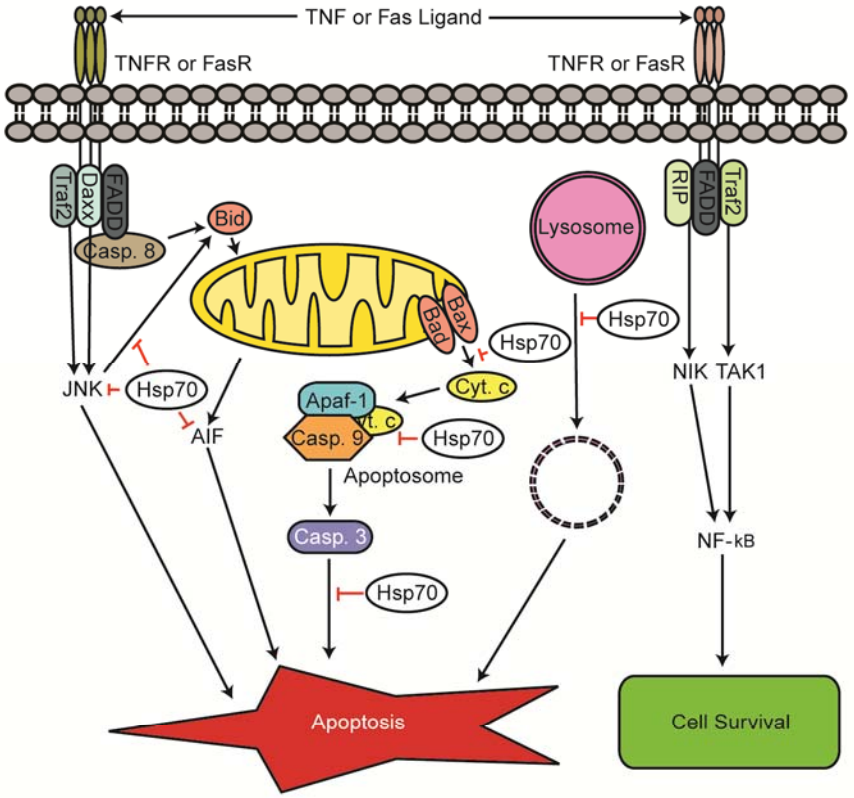

Figure 1.2 Roles of Hsp70 in anti-apoptotic signaling. Hsp70 is thought to promote survival and block apoptosis through interactions with multiple steps in the pathway. For some substrates, Hsp70's role appears to be stabilization of the substrate, while it appears to mediate the degradation of other substrates. The regulatory mechanisms that govern these activities are not known. See the main text and Table 1 for references.

Hsp70 expression has been routinely associated with poor prognosis in multiple forms of cancer [39]. For example, high Hsp70 levels are associated with adverse outcomes in breast, endometrial, oral, colorectal, prostate cancers as well as certain leukemias [40-43]. Moreover, transgenic over-expression of Hsp70 is sufficient to induce T cell lymphoma in some models [42]. This observation is important because induction of

Hsp70 can be misregulated in cancer, potentially mediated by altered activity of the heat shock transcription factor 1 (HSF1) [39, 44, 45]. In cancer cells, over-expression of Hsp70 is thought to provide a survival advantage because it is able to interact with multiple components of both the caspase-dependent and –independent apoptotic pathways (**Figure 1.2** and **Table 1.1**) [39, 46, 47]. For example, this chaperone was

Table 1.1 Roles of Hsp70 in Apoptotic Signaling

Process	Role of Hsp70	Ref.
Caspase-Dependent Pathway		
Bid	Hsp72 inhibits TNF activation of the Bid pathway	[49]
Caspase-9	Hsp70 inhibits recruitment of procaspase-9 to the apoptosome	[53]
	Hsp70 binds to Apaf-1, preventing formation of the active apoptosome	[188]
BCL2	Hsp70 inhibits the proteasomal degradation of Bcl2 proteins	[48]
	Hsp70 inhibits cytochrome c release from mitochondria by inhibiting Bad and Bax	[189]
Caspase-3	Hsp70 inhibits caspase-3 induced apoptosis	[189]
Caspase-Independent Pathway		
JNK	Hsp72 inhibits JNK induced apoptosis, but its ATPase activity is dispensable	[56, 190-194]
AIF	Hsp70 prevents the release of AIF from mitochondria	[195-197]
Lysosome	Hsp70 stabilizes lysosomal membrane integrity	[54, 198, 199]
p53	Hsp70 blocks p53-induced senescence through PI3K	[41, 55, 200-202]

reported to regulate the important apoptotic mediator, Bcl-2 [48]. Similarly, expression of Hsp70 blocks TNF-induced apoptosis, activation of caspase-3, translocation of Bax and cleavage of PPAR [49-52]. Some of these interactions are thought to be direct. For example, immunoprecipitation has shown an interaction between Hsp72 and Bax [50]. In this context, Hsp72 prevents Bax translocation by blocking its oligomerization, a step necessary for disruption of the mitochondrial membrane [51, 52]. By influencing

multiple steps in the same cascade, Hsp70 is likely to exert even more potent anti-apoptotic activity than if it was acting on an individual protein. Similarly, Hsp70 has also been found to block caspase-independent signaling through activity on cathepsins and Apaf-1 [53]. For example, Hsp70 knockdown increases cathepsin B release and protects lysosomes from photo- and H_2O_2-mediated permeabilization [54]. In addition to these effects on the caspase-dependent and –independent apoptotic pathways, Hsp72 also plays roles in senescence through effects on the p53-p21 pathway [55]. Together, these results suggest that Hsp70 interacts with multiple partners in the apoptosis and senescence pathways, a model that is consistent with Hsp70's known substrate promiscuity. Importantly, the ATPase activity of Hsp70 doesn't appear to be required for all of these activities, as the action of Hsp70 on JNK and AIF occurs independent of nucleotide hydrolysis [56-58]. This is an important observation, because many of the early Hsp70 inhibitors target its ATPase activity. While shRNA-mediated knockdown of Hsp70 induces apoptosis and slows cell proliferation in multiple cancer cell models [41, 59, 60], it is unclear whether inhibitors of specific Hsp70 functions, such as nucleotide turnover, will mimic this favorable cellular effect. Regardless, these studies suggest that cancer cells become "addicted" to Hsp70 through this chaperone's activity on multiple, parallel signaling pathways [61].

Hsp70 over-expression has also been documented to provide resistance to chemotherapeutic agents, such as imatinib, etopiside, cisplatin and MG-132 [62, 63]. Although the detailed mechanisms of resistance remain to be elucidated, recent evidence suggests that reduced activation of ERK, NF-κB, and JNK pathways may be responsible [63]. The protective effects of Hsp70 are particularly striking in response to treatment with Hsp90 inhibitors, such as geldanamycin and its derivatives [61, 64]. Like Hsp70, Hsp90 is an ATP-utilizing molecular chaperone with roles in protein turnover [65]. However, Hsp90 is often considered the more "specialized" chaperone, with a relatively restricted set of cellular substrates. Among Hsp90's are key anti-apoptotic proteins, including Akt, Cdk4, Raf1 and Her2 [65, 66]. Inhibiting the binding of Hsp90 to ATP leads to proteasomal degradation of these substrates and corresponding anti-proliferative activity [45, 67, 68]. In the context of our discussion, treatment with Hsp90 inhibitors has also been found to induce expression of Hsp70, likely through activation of HSF1 [64]. As discussed above, this compensatory mechanism can cause resistance to apoptosis and stabilization of some shared protein substrates, such as Akt [61, 64]. Together, these observations suggest that dual therapy against both Hsp90 and Hsp70

might be beneficial. This hypothesis is strongly supported by observations that RNAi knockdown of Hsp70s enhances the efficacy of Hsp90 inhibitors [69, 70].

Table 1.2 The Roles of Hsp70 in Neurodegenerative Diseases

Disease	Role of Hsp70	Ref.
HD	Hsp70 co-localizes with polyQ aggregates	[203]
	Hsp70 and Hsp40 prevent aggregation of purified HD exon 1	[79]
	Over-expression of Hsp70 and Hsp40 reduces polyQ aggregation and cytotoxicity	[82, 203]
	Hsp70 inhibits polyQ-induced caspase 3 and 9 activation and M3/6 JNK phosphatase aggregation	
	Over-expression of Hsp70 does not significantly ameliorate the disease symptoms of R6/2 HD model mice	[88, 204]
	HSF-1 activating compounds reduce polyQ aggregation and rescue neurodegeneration in cultured cells and HD model mice	[87]
		[94, 96, 97]
SCA1	Hsp70 over-expression suppresses neurodegeneration and improves motor function in *SCA1* mice	[85]
SCA3	Hsp70 co-localizes with nuclear inclusions of ataxin-3	[83, 205]
	Over-expression of Hsp70 suppresses polyQ-mediated neuropathy in a *Drosophila* model of *SCA3*	[83]
SCA7	Hdj2 and Hsp70 prevent mutant ataxin-7 aggregation in cultured cells but not in a mouse model	[86]
SBMA	Hsp70 co-localizes with nuclear inclusions of polyQ expanded androgen receptor (AR)	[84, 206]
	Hsp70 and Hsp40 increases the SDS-solubility and proteasomal degradation of mutated AR in cultured cells	
	Over-expression Hsp70 ameliorates disease phenotypes in a SBMA model	[207]
	Oral administration of GGA, an HSF1 inducer, ameliorates the SBMA phenotype in mouse models	[84] [95]
AD-Aβ	Hsp70 and Hsp40 block *in vitro* Aβ self assembly	[100]
	Hsp70 reduces steady state Aβ levels and Aβ-induced cytoxicity in cultured cells	[101]
AD-Tau	Hsp70 interacts with sites in tau important for aggregation	[103]
	Hsp70-Bag2 captures and delivers insoluble and phosphorylated tau to the proteasome for ubiquitin-independent degradation	[110]
	Hsp70-Bag1 associates with tau and inhibits proteasomal degradation	[109]
PD	Lewy bodies contain Hsp40 and Hsp70	[208]
	Over-expression of Hsp70 reduces α-synuclein aggregation and cytotoxicity	[209]
	Hsp70 over-expression prevents dopaminergic neuronal loss in PD models	[208, 210]
CF	Immature CFTR and ΔF508 CFTR form complexes with Hdj-2 and Hsc70	[211]
	Inactivation of Hsc70 and CHIP in cultured cell increase surface expression of ΔF508 CFTR	[212]

1.3.2 Protein Misfolding and Neurodegenerative Diseases

One of the other important roles of Hsp70 is to assist protein folding and turnover. In normal cells, quality control systems prevent the accumulation of toxic misfolded protein species. However, in response to mutagenesis, aging or oxidative stress, misfolding can often occur [71-73]. As post-mitotic cells, neurons appear to be particularly sensitive to these effects and many neurodegenerative disorders, such as Alzheimer's, Parkinson's and Huntington's diseases, involve aberrant accumulation of misfolded or misprocessed proteins. Genetic studies have routinely linked Hsp70 and its co-chaperones to this process and, thus, it has emerged as a potential drug target (**Table 1.2**). For example, one recent study has shown that Hsp70 directly stabilizes lysozomes and plays a key role in Niemann-Pick disease [74]. We will discuss two models here and further information can be found in recent reviews [75, 76].

1.3.2.1 Polyglutamine Diseases

Polyglutamine (polyQ) diseases are a family of at least nine inherited neurodegenerative disorders, including Huntington's disease (HD), spinocerebellar ataxia (SCA), and spinal and bulbar muscular atrophy (SBMA), caused by the expansion of trinucleotide CAG repeats in the disease genes [77]. This expansion leads to the formation of an abnormally long glutamine tract in the synthesized protein [78]. PolyQ expansion

renders disease proteins prone to aggregation, and the extent of aggregation is correlated with the length of the polyQ [78]. *In vitro*, Hsp70 (along with its J-domain co-chaperone Hdj1) can partially suppress the aggregation of the polyQ-expanded exon 1 of huntingtin (htt) in an ATP-dependent remodeling process [79]. Importantly, these chaperones are only active when added during the lag phase of the aggregation reaction, which suggests that Hsc70 and Hdj1 preferably act on early, prefibrillar states

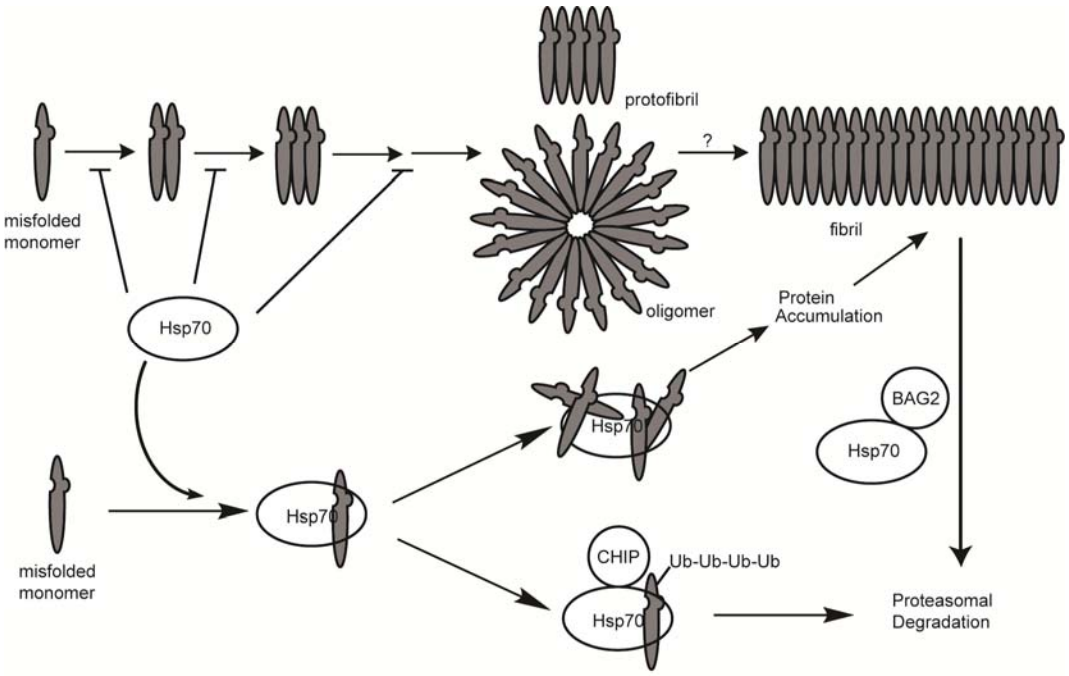

Figure 1.3 Potential roles for Hsp70 in protein misfolding and aggregation. Hsp70 has been linked to multiple steps of the protein misfolding and aggregation pathway, including in preventing misfolding, blocking early stages of aggregation and in mediating the degradation of misfolded intermediates through coupling to the ubiquitin-proteasome system. The Hsp70 co-chaperones BAG2 and CHIP have both been linked to clearance of misfolded substrates. In some systems (including yeast prions), Hsp70 activity is required for fibril formation. For simplicity, this schematic encompasses broad aspects of the misfolding pathway of amyloid beta, polyglutamines and tau, although important differences likely exist. See the main text and Table 2 for references.

(**Figure 1.3**) [79]. Similarly, in a yeast model, over-expression of the yeast Hsp70, Ssa1, decreases aggregation of htt and increased its SDS solubility [80]. However, these relationships appear to be complex because, in O23, COS-7, PC12, SH-SY5Y, and HEK293 cells, Hsp70 over-expression showed little effect on htt aggregation [81, 82]. Similar themes are observed in animal models. For example, in fly models of SCA1 and mouse models of SCA1 and SBMA, over-expression of Hsp70 suppresses the neurodegenerative phenotypes [83-85], while no significant effect is observed in mouse models of HD or SCA7 [86, 87]. It is worth noting that it is not clear whether polyQ aggregation is a good surrogate for toxicity. Moreover, it is not clear if Hsp70's effects on cell viability are always mediated by direct effects on polyQ assembly or through more general buffering of pro-survival signaling [88].

Despite these uncertainties, it is interesting to note that several co-chaperones, including J-domain proteins, CHIP and BAG, have dramatic effects on polyQ aggregate formation, either on their own or in concert with Hsp70. For example, over-expression of yeast Ydj1 (a J-domain co-chaperone) increase the solubility of htt [79], whereas a related J-domain co-chaperone, Sis1, splits large inclusions into smaller loci [80]. The TPR-domain co-chaperone, CHIP, ubiquitinates htt and facilitates its degradation in a U-

box dependent manner (**Figure 1.3**) [89]. The over-expression of CHIP also significantly rescues neurodegenerative symptoms in animal models of SCA1, SCA3, SBMA, and HD, while CHIP -/- mice have exaggerated disease progression in models of HD and SCA3 [90-93]. The role of Hsp70 in CHIP-mediated protection remains to be established, but current models suggest that Hsp70 is required for the CHIP–mediated effects.[89, 90] Together, those observations suggest that protection against polyQ toxicity might require interplay between multiple components of the complex between chaperone and co-chaperones. Indeed, it has been shown that chemical stimulators of the heat shock response, such as geldanamycin, 17-(allylamino)-17-demethoxy geldanamycin, geranylgeranylacetone, and celastrol, upregulate multiple chaperone components and rescue neurodegenerative symptoms in cell culture, fly, and mouse models of SCA1, HD, and SBMA [94-97].

1.3.2.2 Alzheimer's Disease

Alzheimer's disease (AD) is the most common neurodegenerative disease and its patients are characterized by progressive memory loss and the accumulation of senile plaques (SP) composed of β-amyloid (Aβ) and neurofibrillary tangles (NFTs) assembled from tau [98]. Current models suggest that self-association of Aβ or tau into β-sheet rich

oligomers leads to neuronal cell death (**Figure 1.3**) [98, 99]. Hsp70 has been shown to play important roles in the cytotoxicity of both Aβ and tau. For example, Hsp72 blocks the early stages of Aβ aggregation *in vitro* at substoichiometric levels [100] (**Figure 1.3**), and Hsp70 has been shown to alter processing of the amyloid precursor protein [101]. Also, this chaperone protects against Aβ-induced cytotoxicity via inhibiting caspase-9 and accelerating the elimination of Aβ [102]. In addition to these effects on Aβ, Hsc70 also binds tau at two sites within its tubulin-binding repeats, which is the same region required for tau self-association [103]. This finding suggests that Hsc70 might compete with aggregation and toxicity [103] and, consistent with this model, over-expression of Hsp70 reduces aggregated tau in mouse models [104]. Moreover, increasing Hsp70 levels promotes tau binding to microtubules and reduces the levels of hyperphosphorylated tau [105]. Similar to the polyQ examples listed above, co-chaperones of Hsp70 also play roles in tau processing. For example, CHIP ubiquitinates phosphorylated tau in an Hsc70-dependent manner [106, 107] and its over-expression accelerates tau degradation, reduces formation of insoluble tau and rescues tau-induced cell death (**Figure 1.3**) [107, 108]. The co-chaperones, BAG-1 and BAG-2, also impact tau aggregation, but in opposing ways [109, 110]. An Hsc70-BAG-1 complex binds to tau and inhibits its turnover [109]. In contrast, BAG-2 and Hsc70 form a

microtubule-tethered complex that can capture and deliver insoluble and phosphorylated tau to the proteasome for degradation (**Figure 1.3**), likely through a ubiquitin-independent mechanism [110]. Together, these results illuminate the complex relationships between Hsp70, its co-chaperones and their impact on AD and other tauopathies.

1.3.3 Infectious Disease and Immunity

The prokaryotic Hsp70, DnaK, is required for survival of bacteria under stressful conditions, such as thermal stress and challenge with heavy metals or antibiotics [111-113]. Consistent with this activity, *S. aureus dnaK* mutants have reduced viability and are susceptible to stress [114]. Most strikingly, these mutations increase sensitivity to oxacillin and methicillin in normally resistant *S. aureus* strains. Likewise, *dnaK* or *dnaJ* mutations in *E. coli* make the cells susceptible to fluoroquinolones [115, 116]. These chaperones are also necessary for *S. enterica* to invade epithelial cells and for *L. monocytogenes* to survive in macrophages [117, 118]. Thus, Hsp70 and its co-chaperones appear to be potential drug targets that would sensitize prokaryotes to stress, such as that provided by antibiotics or host responses (**Table 1.3**).

Table 1.3 The Roles of Hsp70 in Infection and Immunity

Disease/Process	Role of Hsp70	Ref.
Bacterial Infection		
Invasion	Mutations in DnaK make *S. aureus* less infective and inhibit biofilm formation in *S. mutans*	[112, 114, 213]
	S. enterica DnaK required for invasion of epithelial cells	[117]
	Hsc70 enhances internalization of *Brucella* by trophoblasts	[214]
	H. pylori Hsp70 allows for its attachment to the gastric epithelia	[215]
Survival	DnaK mutants are susceptible to stress	[111-114]
	S. enteric and *L. monocytogenes* DnaK required for survival in macrophages	[117, 118]
	Over-expression of Hsp70 in *M. tuberculosis* reduces survival during the chronic phase of infection	[216]
Replication	DnaK necessary for replication of *Brucella suis* in macrophages	[217]
Immune System Evasion	Hsp70 protects macrophages from cell death when infected with *Salmonella choleraesuis*	[119]
Immune Function		
Antigen Presentation	Hsp70s involved in MHC class II antigen presentation and endocytic maturation	[218, 219]
Viral Infection		
Cell Entry and Exit	Hsc70 involved in rotavirus entry into cells	[220, 221]
	Hsp70 involved in the disassembly of Polyomavirus and Papillomaviruses in mouse cells	[222]
Replication	Hsp70 associates with RSV polymerase complex in lipid rafts	[223]
	Interaction between Hsc70 and T-antigen required for the replication of Simian Virus 40	[224-228]
	Hsp72 involved in Epstein-Barr virus replication	[229]
	Hsp70 can replace viral protein R in the pre-integration complex of HIV	[230]
Immune Response	Hsp70 prevents cell cycle arrest and apoptosis in HIV infected cells	[231]
Viral Assembly	Hsp70 is associated with capsid formation in Polyomavirus and Papillomaviruses	[232]

In addition to its roles in bacterial physiology, Hsp70 is also important in host immunological responses and cell-cell interactions. For example, in mammalian cells infected with a virulent form of *S. choleraesuis*, the levels of Hsp70 correlate with an increase in TNF-α induced cell death [119]. Hsc70 and other heat shock proteins also play important roles in IKK signaling, endocytic trafficking and possibly in antigen presentation, suggesting roles in activation and regulation of immune cells [120-122].

1.4 Chemical Targeting of Hsp70s

Given these complex roles of Hsp70 in disease, it is not immediately apparent whether a good therapeutic strategy would be to stimulate, inhibit or otherwise re-direct the activity of this chaperone with chemical agents. For example, would stimulation of Hsp70's ATPase activity provide protection from neurodegeneration? Would inhibition sensitize cancer cells to apoptosis? Moreover, should the ATPase activity of Hsp70 be the ideal target or is another function (*e.g.* protein folding, protein trafficking *etc.*) more appropriate? Given the promiscuity of Hsp70's interactions with proteins, is it possible to influence the processing of individual substrates or will inhibitors have global effects? Although the answers to many of these important questions remain unknown, work over the last decade has provided first-generation, Hsp70-targeted compounds [123, 124]. Interestingly, these compounds belong to a broad range of structural classes and some have distinct, non-overlapping binding sites on the Hsp70 surface. These observations suggest that there are multiple ways to impact Hsp70's functions, such as through modulating its ATPase activity, its contacts with co-chaperones or binding to misfolded substrates. Importantly, these early probes have also begun to reveal unexpected aspects of Hsp70's biology. Thus, even if these compounds do not directly

lead to approved drugs, they have started to define Hsp70's roles in disease and its potential as a drug target. In the following sections, we review the known chemical classes and briefly highlight the medicinal chemistry efforts and biological findings enabled by these probes.

1.4.1 Spergualin-like Compounds.

In 1981, Umezawa and colleagues reported the identification of a compound with antibiotic and anti-tumor activity from a *Bacillus sp* [125]. They further characterized the active compound as the polyamine, (-)-spergualin **1** (**Figure 1.4**) [126]. Kondo and colleagues carried out the total synthesis of this compound in 14% overall yield [127]. However, **1** was found to have poor stability *in vitro* and *in vivo*, which led to the synthesis of analogues, including **2** (15-deoxyspergualin; 15-DSG) [128, 129]. In an aqueous environment at pH 7, removal of the labile 15-hydroxyl group was found to improve stability to 2 days [130]. The route to **2** and its derivatives involves formaldehyde-mediated cyclization of spermidine, followed by coupling of the free amine to an amino acid and installation of the ω-guanidino fatty acid [131]. Thus, this approach allows ready variation of the amino acid identity. However, in antitumor assays against L1210 leukemia cells, only the glycine (**3**) and L-serine (**4**) derivatives

retained activity, whereas even conservative replacements with alanine or leucine abolished function [131]. Likewise, variations in the polyamine regions, such as the number of methyl groups or secondary amines, decreased efficacy [129]. Taken together, these results suggest that the activity profile of spergualin analogues is surprisingly narrow.

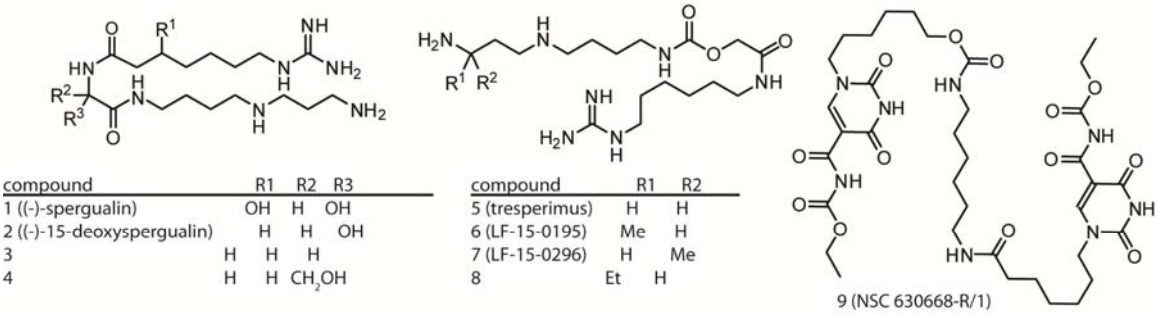

Figure 1.4 Structures of spergualin and related polyamines. Selected structures from larger series are shown for clarity. See the text for references

Despite the improved stability of **2**, this compound still retained relatively poor bioavailability [132]. In an attempt to circumvent some of these shortcomings, a series of derivatives was developed in which the amides are inverted and this change was found to greatly improve the molecule's stability and activity [130]. Following from these efforts, the hydroxyglycine moiety was substituted with a carbomoyl group, producing the promising derivatives **5** (tresperimus) and **6** (LF 15-0195) (**Figure 1.4**).

However, in this series, only minor methyl substitutions were tolerated in a few positions without a dramatic loss of activity [133]. For example, an *R* methyl group appended near the terminus, as in compound **6**, was tolerated, while the opposite stereochemistry, as in compound **7**, had no apparent Hsp70 binding and 3-fold reduced immunosuppressive activity [134]. Likewise, conservative replacement of this methyl with an ethyl, as in compound **8**, greatly reduced activity. Other portions of the molecule were equally sensitive to manipulation; for example, replacement of the guanidine with a pyridine reduced activity by approximately 4-fold [134]. Taken together, the structure-activity studies have revealed a surprisingly limited range of acceptable modifications.

Using immobilized compound, **2** and its derivatives were found to bind to several proteins, including Hsc70 and Hsp90 [135, 136]. Based on mass spectrometry and competition studies, it was further proposed that **2** binds to the EEVD domain of these chaperones with an affinity ~ 5 μM [137, 138]. This interaction appears to impact some of Hsp70's functions, because **2** was able to increase Hsc70's ATPase rate by approximately 20 to 40% [139]. Although this change in ATP turnover rate seems minor, the biological activities of these compounds suggest that either (a) modest changes in

enzymatic activity might disproportionately impact chaperone function or (b) ATP turnover is not the most relevant *in vitro* assay to describe the activity of these compounds on chaperone functions. Another possibility is that **2** has multiple cellular targets; for example 1-acid glycoprotein has been suggested as a potential partner [140].

Although compound **1** was first identified as an anti-infective and anti-tumor agent, **2** was subsequently identified as a potent immunosuppressant. The molecular mechanisms of this activity are not entirely clear, but **2** has been proposed to block NF-B trafficking and antigen presentation, two known cellular roles of Hsc70.[122, 141] Regardless, **2** decreases the incidence of acute rejection in combination with cyclosporin and tacrolimus [142] and it prolongs renal allograft survival [143]. These immunological activities appear to arise from effects on dendritic cells [144] and leukocyte [145] and monocyte [141] activation; for example, Birck and colleagues looked at T-cell activation in patients with Wegener's granulomatosis and found that patients treated with **2** had lower levels of proliferation markers, such as INF-γ and IL-10 [143]. Similarly, treatment with **2** leads to decreased mucosal injury and reduced TNF-α in a mouse model of colitis [146].

Based on these activities, **2** has been explored in multiple clinical trials, with allograft rejection and malignant cancers being the most widely studied indications. For additional details an excellent review is available [140]. Briefly, **2** is poorly bioavailable (5%), so it is typically delivered by *i.v.* infusion [132]. It displays a bi-exponential decay, with an alpha half-life ($t_{1/2}$) of 5 to 12 minutes and terminal half-life of approximately 2 hours [147]. Metabolism is believed to occur, in part, through amine oxidases, with seven, inactive metabolites known [140]. In rodents, infusion of 25 mg/kg/day for 9 days leads to a 4-6_{log} reduction in tumor burden in a L1210 leukemia model [148]. However, a Phase I clinical trial of **2** as a monotherapy against advanced malignancies showed no efficacy at 75 mg/kg/day [140]. Similarly, a Phase II trial against metastatic breast cancer in 14 patients at 1800 or 2150 mg/m^2/day by *i.v.* infusion for 5 days also showed no efficacy. However, in both trials, **2** was well tolerated and only low toxicity was observed (mild neuromuscular side effects as the only grade III toxicities) [149]. The activity of **2** in studies on immunological indications has been more promising. Since 1994, **2** has been used in Japan for acute kidney allograft rejection [140]. The advantage of this compound is that, unlike FK506 or cyclosporin, it can be used up to 48 hrs after initiation of rejection and, therefore, can reverse ongoing organ rejection in animal models and

humans. For example, 81% (25 of 31) of patients undergoing acute renal allograft rejection in one study showed reversal of rejection, even as a monotherapy in some cases [150]. Importantly, **2** is not a P_{450} substrate and it can be used with cyclosporin or steroids [147]. In fact, studies of kidney and liver allograft rejections in Western Europe revealed 65% reversion in combination with bolus steroids [151]. In addition to these examples, many other pilot clinical studies in Japan and the U.S. have been reported, and these generally document good tolerability, low toxicity and efficacy in transplant models [140]. While **2** has been used successfully in the clinic, the mechanism by which it exerts this effect is not fully understood. For example, how specific is this compound for Hsp70? If it is specific, how does binding to the EEVD control chaperone functions? Does the seemingly minor change in ATPase rate (20 to 40%) lead directly to the robust cellular effects? Is binding to both Hsp70 and Hsp90 important for activity? Clearly, additional structural and mechanistic experiments are needed.

Given the promising biological activity of these polyamines, Brodsky and colleagues searched the Developmental Therapeutics database at the National Cancer Institute for related compounds. This effort yielded, **9** (NSC 630668-R/1), which inhibits Hsc70's ATPase activity and partially blocks chaperone-mediated protein translocation (**Figure**

1.4) [152]. However, unlike compound **2**, which is a mild ATPase stimulator, **9** specifically inhibits Hsc70's ATPase activity in the presence of a J-domain co-chaperone [152]. This result is interesting because, although **9** was originally identified as a spergualin-like analogue, it might operate by a different mechanism.

1.4.2 Dihydropyrimidines

ollowing the successful identification of **9**, Brodsky and colleagues searched for other scaffolds able to alter Hsp70's ATPase activity. Guided by structural similarity to **2** and **9**, they focused on a series of functionalized dihydropyrimidines (**Figure 1.5**) [153]. The route to these compounds leveraged consecutive, Biginelli and Ugi multi-component reactions to yield diversity. In an ATPase assay, several compounds from this series were shown to inhibit ATP hydrolysis (e.g. compound **10**), while others enhanced this activity (e.g. compound **11**) [153]. Moreover, the activity of these compounds was dependent on the presence of a J-domain co-chaperone, similar to what had been seen with **9** [152]. For example, compound **10** had no effect on ATP hydrolysis by Hsc70 at up to 600 µM, but it gave a 4-fold reduction at 300 µM when added to the combination of Hsc70 and the J-domain of T-antigen [153]. Approximately 30 compounds were tested in these experiments and, accordingly, quantitative SAR was not readily apparent. To further

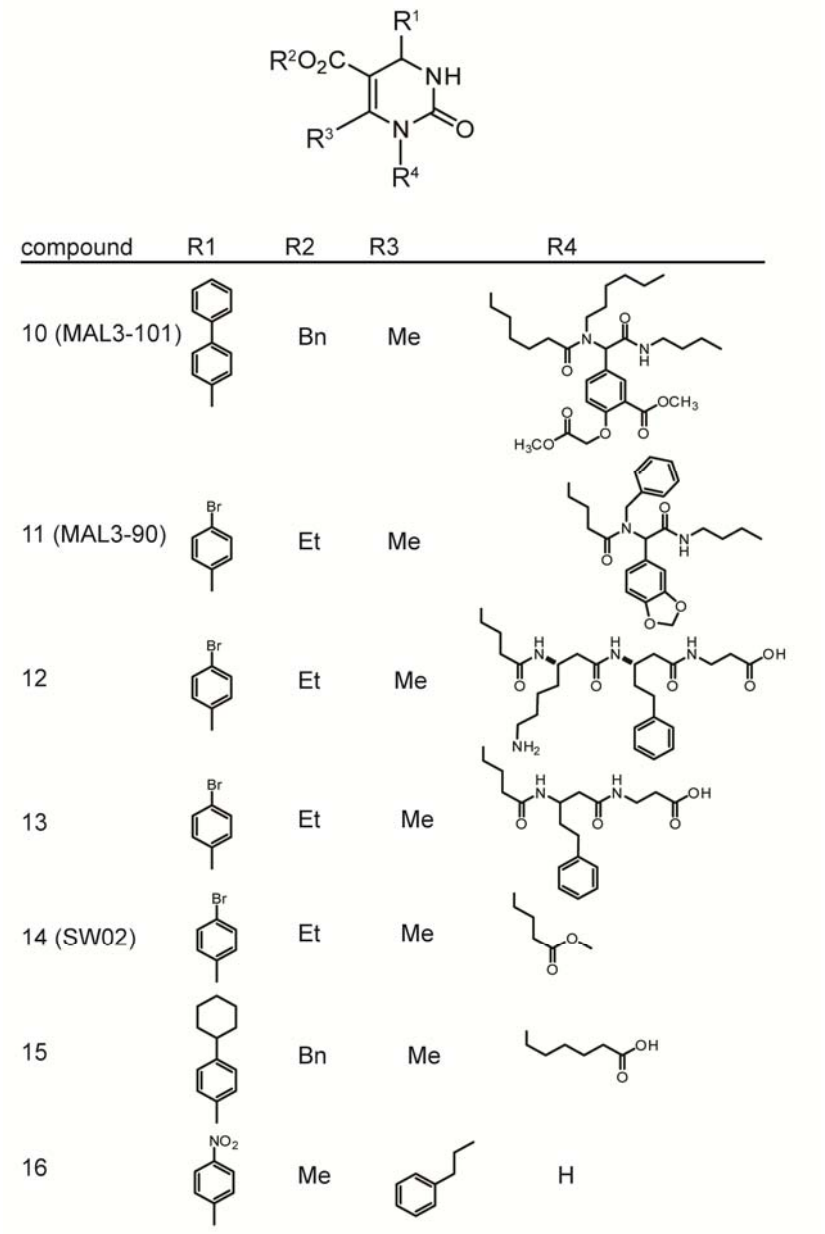

Figure 1.5 Structures of dihydropyrimidines with activity against Hsp70 family members. Select compounds from larger series are shown for clarity. See the text for references.

explore this series, seventeen additional dihydropyrimidines were synthesized in which the Ugi-derived peptoid portion was replaced with a protease-resistant, beta-peptide [154]. The activity of these derivatives was tested against the ATPase activity of two

Hsp70s (either Hsc70 or DnaK) in complex with a J-domain co-chaperone. The results of that study suggest that hydrophobic substitutions near the dihydropyrimidine core (R4; **Figure 1.5**) may be important for activity. For example, compounds **12** and **13**, which have phenyl substitutions in this region, changed ATP turnover by between 20 and 45% [154]. Interestingly, **12** was an inhibitor of ATPase activity, while **13** was a stimulator, consistent with the general observations that compounds of this class can have either type of activity when J-domains are present. Also, **13** only stimulated bovine Hsc70 and not *E. coli* DnaK, suggesting that these highly homologous proteins might be independently targeted. Despite these efforts, the potency of these compounds is very weak (EC_{50} values ~ 75 to 300 μM), making it challenging to interpret the SAR and to confirm selectivity for Hsp70 in cells. Part of the challenge, until recently, was that compounds had to be tested in small numbers because a high throughput assay for Hsp70's ATPase activity had not been available. To improve this capacity, Chang *et al.* converted a malachite green assay into a high-throughput platform. Importantly, this assay employs purified DnaK and its co-chaperones, DnaJ, and GrpE, to boost the signal and provide physiological turnover rates [155]. This advance allowed screening of a collection of more than 180 dihydropyrimidines and, from these efforts, several promising derivatives, such as **15**, which blocks more than 80% of DnaK's activity at 150

μM, were identified. To complement this approach, a medium throughput luciferase-refolding assay was developed. In this assay, denatured firefly luciferase is diluted in the presence of the three-component chaperone complex and refolding is monitored by recovered luminescence. The ~180 member dihydropyrimidine collection was screened in 96-well format and the best of these compounds, such as **16**, had EC_{50} values around 4 μM [156]. Interestingly, there was not obvious structural similarity between the active compounds from the ATPase assay and the luciferase-folding assay.

Even though the dihydropyrimidines identified to date have weak activity and their selectivity remains to be established, the first-generation compounds have been employed in a variety of biological systems. Importantly, these studies have provided unexpected insights into Hsp70's functions in disease models. In one example, the stimulatory dihydropyrimidine, **14**, was found to enhance the Hsp70-mediated inhibition of amyloid-β aggregation [100]. Conversely, a weak inhibitor of ATPase activity led to suppression, suggesting that the ATP hydrolysis rate of the chaperone might impact its anti-aggregation activity *in vitro*. To test this model in cells, Jinwal *et al.* used both inhibitors and activators of Hsp70's ATPase activity in a model of tau aggregation [157]. Surprisingly, they found that stimulators, including **14**, led to

dramatic accumulation of tau, while inhibitors had the opposite effect. The inhibitors reduced tau levels via rapid ubiquitination with EC_{50} values of ~5 to 10 μM. Importantly, over-expression of Hsp70 promoted the activity of the inhibitors and lowered their EC_{50} values, consistent with this chaperone as an important cellular target. Finally, intracranial injection was found to reduce tau in transgenic mice, which suggests that inhibiting the ATPase activity of Hsp70 might be a viable strategy for reducing the accumulation of misfolded tau.

In addition to these studies on protein misfolding and aggregation, dihydropyrimidines have also been employed to explore the potential of Hsp70 as a target in cancer. For example, compound **10** was found to have anti-proliferative activity against SKBr3 cells [158]. This activity appears to be mediated by the ability of the dihydropyrimidines to interrupt stimulation of Hsp70 by J-protein co-chaperones, because the GI_{50} values for a series of peptoid-modified dihydropyrimidines tend to correlate with their activity in a J-stimulated ATPase assay [159]. Moreover, the best compounds (of the nearly 50 derivatives tested) had promising GI_{50} values of approximately 6 to 10 μM against SKBR3 cells, suggesting the possibility that inhibition of Hsp70 alone is sufficient to induce apoptosis. To explore the potential mechanisms for anti-cancer activity, the effects of

activators and inhibitors on stability of the pro-survival target, Akt, were explored [160]. In that study, it was found that activators promote Akt stabilization, while inhibitors promote Akt degradation and subsequent cell death in a panel of cancer cells [160]. This mechanism is similar to that proposed for Hsp90 inhibitors; namely, that selective destabilization of chaperone substrates leads to apoptosis [66]. Because Hsp90 and Hsp70 often cooperate, it is not yet entirely clear what role Hsp90 might play in the response to the Hsp70 inhibitors. Further work is needed to understand the molecular mechanisms; however, these collective findings, across multiple models of protein misfolding and apoptosis, have begun to reveal potential avenues towards therapeutic intervention.

1.4.3 Fatty Acids

Sulfogalactosyl ceramide and sulfogalactoglycerolipid are two sulfoglycolipids that have been found to bind Hsp70. Mamelak and Lingwood identified their putative binding site on the NBD through deletional analysis and site-directed mutagenesis; specifically, mutation of two residues in the NBD (Arg 342 and Phe 198) led to reduced binding of 3'sulfogalactolipid [161]. It was further shown that the aglycone portion determines whether the molecules bind to bacterial or eukaryotic Hsp70s. Eukaryotic Hsp70 bound

$SG^{24}Cer$, $SG^{18}Cer$, and $SG^{20:OH}Cer$ while DnaK preferentially bound to $SG^{18:1}Cer$ and $SG^{20:OH}Cer$ [162]. Other substitutions on the aglycone or manipulations of the sulfation (or phosphorylation) pattern on the sugar ablated binding, demonstrating the narrow tolerance in these regions [163]. A full SAR analysis of this class of molecules awaits expanded library synthesis and additional structural studies. However, early studies revealed that substituting the acyl chain with an adamantyl group improved affinity for Hsp70 (**Figure 1.6**). Specifically, **17** (adaSGC) was found to have an IC_{50} value of ~50 μM [161]. Interestingly, **17** is a noncompetitive inhibitor of ATPase activity, but the molecular mechanism of inhibition is not entirely clear [164]. In cells, **17** increases the protein levels of ΔF508CFTR [164], a mutant of the cystic fibrosis transmembrane receptor (CFTR) that is prone to misfolding and degradation through ER-associated degradation (ERAD). Thus, this finding suggests that inhibition of Hsp70's ATPase activity might suppress the ERAD pathway that normally acts to reduce the levels of mutated CFTR. Moreover, the activity of **17** was found to be dependent on the actions of both Hsp70 and a J-domain containing co-chaperone, consistent with this complex as a cellular target. These results might have important implications for the use of Hsp70 as a

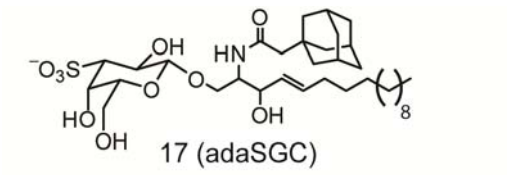

Figure 1.6 Chemical structures of a representative sulfoglycolipid (adaSGC).

drug target in cystic fibrosis and other misfolding diseases. Despite these insights, the binding site for these glycolipids is only loosely defined and, further, their selectivity has yet to be firmly established.

Another example of a fatty acid-like derivative that inhibits Hsp70 function is the acyl benzamide family. This class of compounds arose from work by the Schiene-Fisher group in which they targeted the cis/trans aminopeptidyl isomerase (APIase) activity of DnaK, in an effort to identify potential antibiotics. DnaK has been shown to catalyze isomerase activity yielded acyl benzamides with IC_{50} values as low as 2.7 µM [165]. Further, they found that the length of the fatty acid chain is an important determinant of the molecule's activity (**Figure 1.7**). For example, short acyl chains, such as those in **18**, gave

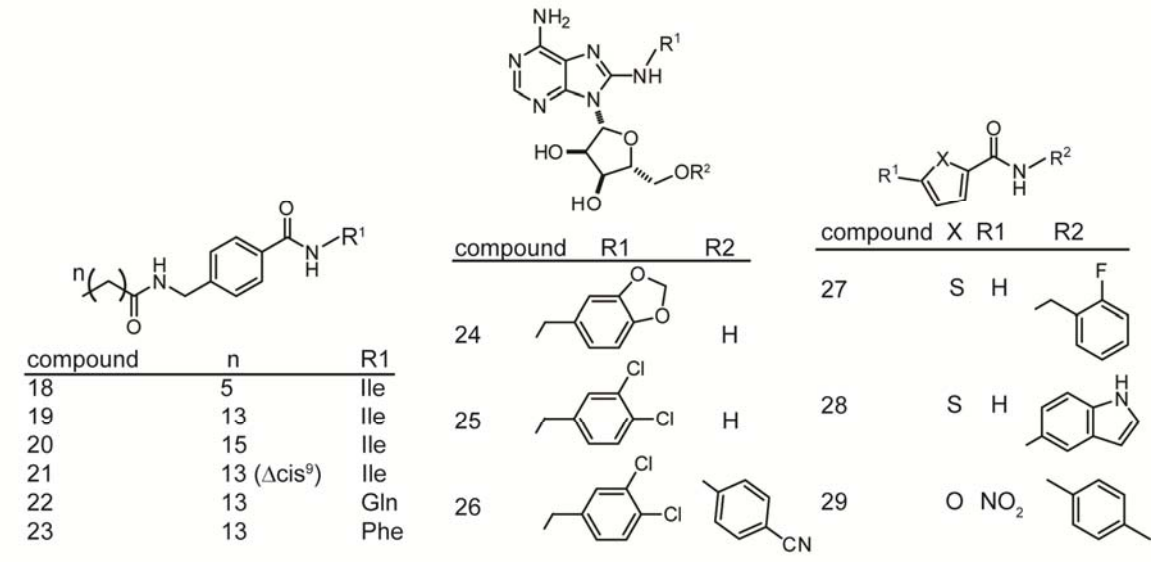

Figure 1.7 Chemical structures of Hsp70 inhibitors. Select compounds from larger series are shown for clarity. See the text for references.

compounds with poor activity in both APIase and bacterial growth assays. Increasing the length of the chain tended to enhance potency: compound **19** had an IC_{50} in the APIase assay of 5 μM and an MIC against *E. coli* of 380 μg/mL, while **20** had an IC_{50} of 1.2 μM and MIC of 180 μg/mL. However, increasing the fatty acid chain-length also enhanced undesirable erythrocyte hemolytic activity. Hemolytic activity could be partially avoided by installation of unsaturations in the fatty acid; for example, compound **21**, with a cis alkene at C9, had an EC_{50} >1500 μg/mL in the hemolytic assay, while it retained activity against APIase (36 μM) and bacterial growth (280 μg/mL). Substitutions in the amino acid portion (R1; **Figure 1.7**) altered the MIC values, with less predictable effects in the other *in vitro* assays [165]. For example, dramatic substitutions of the isoleucine for a glutamine (**22**) or phenylalanine (**23**) caused modest changes in APIase inhibition but they increased the MIC by approximately 3- to 7-fold. Together, these findings suggest that the *in vitro* activity assays proscribed to Hsp70 might not best reflect the key mechanistic roles played by this chaperone in bacteria. This is a re-occurring theme in the Hsp70 field because the roles of measurable Hsp70 functions (*e.g.* ATPase, APIase, refolding, *etc.*) in controlling its biology *in vivo* remain uncertain. Despite this discrepancy, the MIC of the best acyl benzylamide is approximately 7-fold lower than that of ampicillin, which suggests that these compounds or their derivatives may be

useful. However, it is important to note that their selectivity for Hsp70 has not been formally established and any off-target effects of these compounds remain unexplored.

1.4.4 Peptides

As mentioned above, DnaK is considered a potential target for anti-bacterials, but this model has only recently been tested with pharmacological agents. For example, a series of 18-20 amino acid, proline-rich peptides, including drosocin, pyrrhocoricin, and apidaecin (**Table 1.4**), were described that bind DnaK (and another prokaryotic chaperone, GroEL) and kill susceptible bacteria without impacting mammalian cells [166]. Pyrrhocoricin inhibits the ATPase activity of *E. coli* DnaK and it binds in the SBD with a K_d of 50 μM.[167] This interaction is thought to keep the "lid" domain in the closed position, preventing substrate release, a model supported by computational simulations and mutagenesis studies, which identified the SBD residues Glu589, Gln595, and Met598 as the key targets in DnaK [168]. Interestingly, pyrrhocoricin does not bind to *S. aureus* DnaK [167], suggesting a potential difference between gram-positive and –negative strains. In an effort to

Table 1.4 The Sequences of Anti-bacterial Peptides Targeting DnaK

Peptide	sequence
drosocin	GKPRPYSPRPTSHPRPIRV
apidaecin	GNNRPVYIPQPRPPHPRI
pyrrhocoricin	VDKGSYLPRPTPPRPIYNRN

optimize the pharmacokinetics and antibacterial activity of these peptides, several analogues representing combinations of the peptide sequences were generated. Of these derivatives, GRPDKPRPYLPRPRPPRPVRL is the most active and it also has improved serum stability [169]. Importantly, this compound has activity against both *E. coli* and a resistant strain of *Enterobactericeae sp.*, with an MIC approximately 4 times better than ciprofloxacin. Moreover, it was not toxic to eukaryotic cells at concentrations up to 1.5 mg/mL [169]. Cudic *et al.* recently generated dimers of pyrrhocoricin in an effort to further improve stability and potency. Some of these compounds have increased serum stability compared to pyrrhocoricin and activity against isolates normally resistant to β-lactams, tetracycline, or aminoglycosides [170]. While these compounds have not advanced to the clinic, they have shown that targeting DnaK may be a viable anti-bacterial strategy.

1.4.5 ATP Mimics

Given that Hsp70's ATPase activity appears to be one central determinant of chaperone function, compounds that are competitive for binding to ATP might be expected to have potent activity. This hypothesis arises, in part, from analogy with Hsp90, in which ATP competitive compounds, such as geldanamycin derivatives, induce degradation of

Hsp90 substrates. Recently, Williamson *et al.* published the first compounds that can be used to test this important hypothesis in Hsp70. Using a fluorescence polarization assay, they screened adenosine derivatives and identified 8-amino adenosines with affinity for the ATP-binding site, with the most active (**24**) having an IC_{50} of 4.9 μM (**Figure 1.7**) [171]. The intended binding orientation was confirmed by a co-crystal structure. Further, when the 8-amino group was substituted with 3,4-dichlorobenzyl (**25**), it retained activity (IC_{50} ~ 9.1 μM) and had an improved toxicity profile. Subsequent modifications optimized the π-stacking with residues in Hsc70 and the 5-substituent (R2; **Figure 1.7**) was further substituted with a 4-cyanophenyl group to yield a tight binding compound **26** (IC_{50} value of 0.5 μM). Importantly, **26** also had activity against HCT 116 colon carcinoma cells (GI_{50} of 5 μM) and it reduced the levels of Her2, a substrate that is sensitive to Hsp70 knockdown.[171] Most recently, compounds from this class were also found to have synergy with an Hsp90 inhibitor in HCT116 cells [172], which might be expected based on shared functions of these chaperones. Together, these studies represent an important step towards submicromolar affinities and structure-guided design of Hsp70 inhibitors.

1.4.6 Thiophene-2-carboxamides.

Celliti *et al.* recently used NMR spectroscopy to identify compounds that bind to DnaK [173]. They specifically explored the protons in the aliphatic region of the 1D ^{1}H NMR spectra of *E. coli* DnaK SBD (residues 393-507) in an effort to find scaffolds that interact with that domain. These efforts yielded a pocket near Leu484 and Pro419, which forms a groove important for allosteric communication between the SBD and the NBD. The compounds that bound this site were principally thiophene-2-carboxamides, such as **27**, and their binding was confirmed by isothermal titration calorimetry (ITC), with K_d values around 70 μM. Based on these results, fifteen derivatives with either a thiophene or furan core and a variety of hydrophobic groups appended to the 2-position were synthesized (**Figure 1.7**). Adding bulk to the R2 substituent seemed to improve affinity and these efforts yielded the indole-substituted **28**, which bound with a K_d of 12.7 μM. Finally, members of this series of compounds were found to inhibit growth of *E. coli* and *Yersinia pseudotuberculosis*, with MIC values of approximately 10 to 400 μM depending on the strain and growth temperature. The best compound was the 2-substituted furan **29**, which had an MIC of less than 12 μM against *Y. pseudotuberculosis* at 40 °C. Interestingly, the most potent inhibitor of microbial growth was not the compound with the highest affinity to DnaK as determined by ITC, again suggesting a complex relationship between Hsp70 binding and *in vivo* potency.

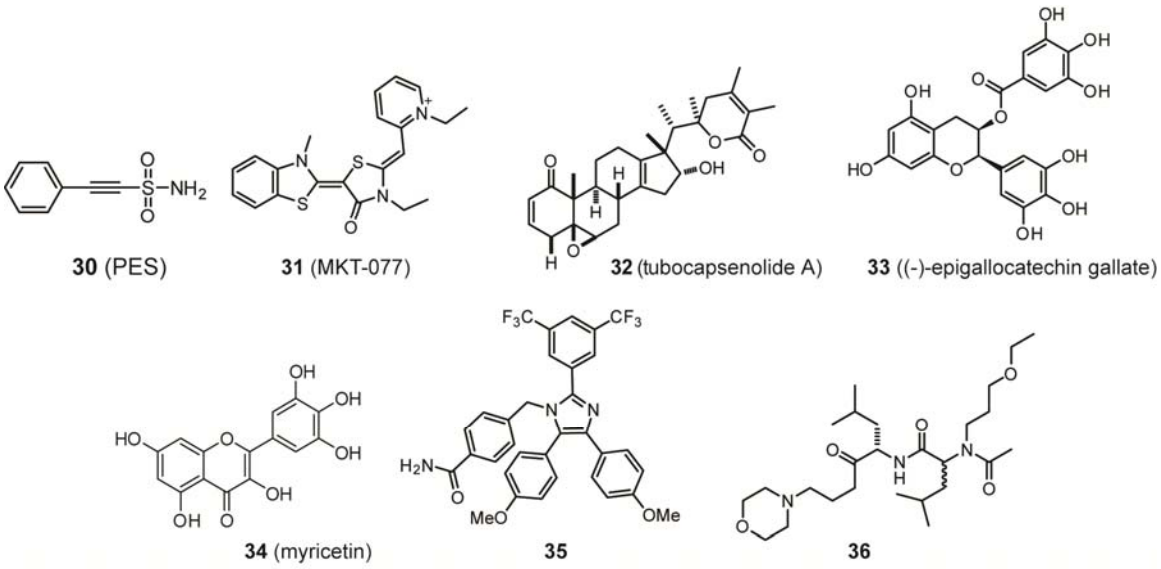

Figure 1.8 Chemical structures of miscellaneous Hsp70 inhibitors.

1.4.7 Phenylethynesulfonamide

Recently, Leu and colleagues reported the identification of 2-phenylethynesulfonamide (**30**) as a compound that binds Hsp72 (**Figure 1.8**) [174]. Compound **30** (also known as Pfithrin-μ) has been shown to be selectively toxic to cancer cell lines and it was proposed effect p53, but its mechanism of action had not been clear. Biotin-conjugated PES revealed Hsp72 (but not Hsc70, BiP or Hsp90) as a target and deletional analysis further restricted the binding site to the C-terminus [174]. Using immunoprecipitations, the authors characterized the effects of **30** on assembly of the Hsp70 chaperone complex in different cell lines. They hypothesized that **30** would alter co-chaperone associations with Hsp72 and, thereby, alter chaperone functions. These studies revealed

that **30** prevents the interaction between Hsp72 and some BAG proteins, depending on the cell type. Moreover, **30** blocks association of Hsp72 with p53, consistent with the ability of **30** to kill cancer cells and block caspase activation. Finally, **30** appears to interrupt the interaction of Hsp72 and LAMP2, an important protein in chaperone-mediated autophagy. Consistent with this idea, long-lived proteins are degraded at a reduced rate in response to **30** and this compound causes build up of procathespin L, indicating that autophagy and lysosomal enzyme processing are impaired [174]. Together, these studies suggest that **30** changes the interactions of Hsp70 with some of its co-chaperone partners and, through this activity, impacts substrate fate. Moreover, **30** has a relatively simple structure and it seems likely that additional synthetic studies might improve its activity and, potentially, its selectivity. Those efforts will likely benefit from improved structural analysis and further biophysical studies on the mechanism for changes in Hsp70 complex assembly.

1.4.8 MKT-077

The rhodacyanine **31** (MKT-077; **Figure 1.8**), has been reported to bind to mtHsp70 in pull-down studies.[175, 176] More specifically, deletion analysis revealed that **31** binds near the ATP-binding site of the mtHsp70 NBD. However, the cellular selectivity of

mtHsp70 over other Hsp70 isoforms is likely driven, in part, from its cationic character. Cationic compounds are known to accumulate across the mitochondrial proton gradient in rapidly dividing cancer cells. In early experiments, **31** was found to inhibit proliferation of multiple human cancer cell lines, including colon, bladder and breast carcinoma cells, with IC_{50} values ranging from 1 to 5 μM with no toxicity against normal kidney cells [177]. Based on these findings, pre-clinical evaluation in rats revealed low toxicity below 3 mg/kg/day and primarily renal impairment above that dose. In mouse xenograft studies, continuous infusion was required for anti-tumor activity [178]. Based on the preclinical findings, a Phase I clinical trial against solid tumors was performed using daily infusions carried out five times over three weeks at 30-50 mg/m^2/day [179]. In a subset of these patients, renal toxicity was again seen as the major toxicity. Importantly, pharmacokinetic measurements failed to detect **31** above one micromolar in the serum, suggesting that therapeutic dose was not achieved. Consistent with this, little improvement in disease was seen (1 out of 10 patients achieved stable disease) [179]. However, these studies suggest that targeting mitochondrial Hsp70 might be a viable strategy if the toxicity and pharmacokinetics of this scaffold could be improved. In addition, more detail about the selectivity and mtHsp70-binding activity of this compound might guide these efforts.

1.4.9 Other Examples

Included in a comprehensive list of compounds with activity on Hsp70 are several molecules that are either recently discovered or older ones that await further study. For example, the steroid-like molecule **32** (tubocapsenolide A) was found to oxidize thiols on both Hsp70 and Hsp90, causing their inactivation [180]. Also, there are several reports suggesting that **33** ((-)-epigallocatechin gallate) can inhibit Hsp70s, including BiP, allowing initiation of apoptotic pathways.[181-183] Likewise, the flavonoid **34** (myricetin) inhibits the ATPase activity of Hsp70s, reduces tau levels and has anti-cancer activity in multiple models [157, 160]. It should be clearly noted that polyphenols, such as **33** and **34**, are notoriously promiscuous. However, uncovering their binding site(s) and mechanism(s) on Hsp70 might reveal new "druggable" sites and opportunities for structure-guided design. Recently, an imidazole **35** was reported by Williams *et al.* to induce apoptosis through interactions with Hsp70 and Hsc70[184] and Haney *et al.* reported that Ugi-derived peptoids, such as **36**, modulate Hsp70's ATPase activity by up to 40% through binding to the SBD [185]. Finally, peptides derived from BAG1 were shown to inhibit the BAG1-Hsc70 interaction and inhibit proliferation of breast cancer cells [186]. These last results further emphasize the important contribution of co-

chaperones in guiding the activity of the Hsp70 complex. While much work remains to optimize these compounds and establish their selectivity for Hsp70, they provide an illustration of the wide diversity of structures found to interact with this chaperone.

1.5 Analysis and Prospectus

Hsp70 is a critical molecular chaperone in cell survival signaling and protein homeostasis. As such, it has gathered significant attention as a potential, emerging drug target [39, 61, 123, 124]. Genetic studies (e.g. knockdown and over-expression) have clearly demonstrated that Hsp70 and its co-chaperones are involved in cancer, neurodegeneration and other diseases. The next steps are to determine if the various functions of Hsp70 can be pharmacologically manipulated and, further, whether the outcomes of this intervention will be well tolerated. On first glance, targeting of a core mediator of protein homeostasis might be considered challenging, given its widespread cellular roles and ample opportunities for toxicity. In part, enthusiasm for Hsp70 as a drug target is based on the success of programs targeting other core molecular chaperones, such as Hsp90 [61]. As mentioned above, Hsp90 inhibitors specifically destabilize pro-survival signaling proteins in cancer cells and the results of early anti-cancer trials appear promising. However, the field of Hsp70 inhibitors is less mature and

many, important questions remain before Hsp70 can be considered an equally good drug target.

In this review, we have discussed some of the early efforts to identify inhibitors of Hsp70 and highlighted some of the biological findings enabled by these reagents. However, many questions remain before Hsp70 can be considered a fully validated drug target. For example, there are multiple assays used to measure Hsp70 activity *in vitro* (*e.g.* ATPase activity, APIase activity, substrate folding, anti-apoptotic signaling, *etc*) and the relationships between any of these measurable functions and the chaperone roles of Hsp70 *in vivo* remain unclear. Additionally, there is a general lack of selectivity information for the first-generation, Hsp70-targeted compounds. Thus, it seems likely that at least some of these compounds are enacting their cellular activities through multiple pathways, which precludes definitive statements on Hsp70 as a drug target.

1.5.1 Consensus Assays are needed for Characterizing Chemical Modulators of Hsp70s

Clearly, one of the major problems in the field is that consensus assays for studying Hsp70 are lacking. By analogy, Hsp90 inhibitors are often tested against a battery of standard assays, including those that measure chaperone binding *in vitro* and the ability

to reduce the levels of Hsp90 substrates, such as Akt, Cdk4, Raf and Her2, in cells [68]. Future efforts on Hsp70 will benefit from similar, routine utilization of (a) *in vitro* binding assays, (b) examination of cellular effects on putative Hsp70 substrates, such as tau, Akt and Her2, and (c) studying the effects of Hsp70 over-expression on compound efficacy. This last point is particularly important because, in our opinion, the interpretations of pull-down studies (which are often used to document Hsp70 binding in cells) are complicated by both the hydrophobic promiscuity of this chaperone and its abundance. Thus, over-expression studies may provide a more readily interpretable alternative. Another interesting approach is transcriptional profiling, which was previously used to identify novel Hsp90 inhibitor [187]. Finally, a greater emphasis on structural studies seems warranted, to permit insights into the binding sites of putative Hsp70 inhibitors. In the Hsp90 field, extensive crystallography studies have yielded important molecular details into the binding sites. As the field of Hsp70 inhibitors matures, increasing utilization of structural analysis and broader assay profiling will ultimately accelerate discovery.

1.5.2 Multiple Potential Drug-binding Sites on Hsp70s that Accommodate Various Chemical Scaffolds

It is interesting to note that a wide variety of chemical scaffolds (e.g. polyamines, fatty acids, sulfoglycolipids, peptides, adenosines, *etc.*) have been identified with affinity for Hsp70. Although some of these scaffolds are likely promiscuous, this observation still suggests that Hsp70 harbors an unusual number of potential drug-binding sites that can accommodate a variety of chemical scaffolds. These sites might include deep pockets, such as those found in the ATP-binding cleft and substrate-binding region, and more shallow surfaces, such as those involved in allostery and protein-protein interactions with co-chaperones. Although not all of the compounds discussed herein have been explored in sufficient molecular detail, the early findings suggest that there are multiple ways to impact Hsp70's functions. For example, compounds **9**, **10**, **14**, **30** and the BAG1-related peptides seem to interrupt Hsp70's contacts with co-chaperones, while **26** directly competes for nucleotide binding.

1.5.3 Targeting the Multiprotein Complexes formed by Hsp70s and Co-chaperones

One interesting aspect of Hsp70 biology that remains to be more fully leveraged is the ability of this chaperone to form multi-protein complexes. As discussed above, Hsp70 interacts with multiple classes of co-chaperones and these partners are known to shape

its activities. Thus, specifically targeting the interactions between Hsp70 and its regulatory partners would be expected to control specific chaperone activities [38]. This approach might be expected to have more limited toxicity because of reduced global impairment of protein homeostasis. Moving forward, we propose that an emphasis on the structural biology of co-chaperones, combined with a deeper insight into how these factors shape the proteome, will be required to rationally leverage Hsp70 as an effective drug target.

In summary, genetic and biochemical studies support Hsp70 as an interesting, potential drug target in a remarkably wide range of diseases. Early studies on Hsp70 inhibitors support this general conclusion. However, the field of Hsp70 inhibitors is clearly in its infancy and extensive work remains before it is clear how this chaperone can be best exploited.

Notes

This review was written by Lyra Chang, Christopher G. Evans, and Jason E. Gestwicki, and was published as “Heat shock protein 70 (hsp70) as an emerging drug target” **2010** *Journal of Medicinal Chemistry* 53: 4585-602

1.6 References

1. Daugaard, M., M. Rohde, and M. Jaattela, *The heat shock protein 70 family: Highly homologous proteins with overlapping and distinct functions.* FEBS Lett, 2007. **581**(19): p. 3702-10.
2. Bertelsen, E.B., et al., *Solution conformation of wild-type E. coli Hsp70 (DnaK) chaperone complexed with ADP and substrate.* Proc Natl Acad Sci U S A, 2009. **106**(21): p. 8471-6.
3. Flaherty, K.M., C. DeLuca-Flaherty, and D.B. McKay, *Three-dimensional structure of the ATPase fragment of a 70K heat-shock cognate protein.* Nature, 1990. **346**(6285): p. 623-8.
4. Bork, P., C. Sander, and A. Valencia, *An ATPase domain common to prokaryotic cell cycle proteins, sugar kinases, actin, and hsp70 heat shock proteins.* Proc Natl Acad Sci U S A, 1992. **89**(16): p. 7290-4.
5. Zhu, X., et al., *Structural analysis of substrate binding by the molecular chaperone DnaK.* Science, 1996. **272**(5268): p. 1606-14.
6. Frydman, J., *Folding of newly translated proteins in vivo: the role of molecular chaperones.* Annu Rev Biochem, 2001. **70**: p. 603-47.
7. Erbse, A., M.P. Mayer, and B. Bukau, *Mechanism of substrate recognition by Hsp70 chaperones.* Biochem Soc Trans, 2004. **32**(Pt 4): p. 617-21.
8. Young, J.C., J.M. Barral, and F. Ulrich Hartl, *More than folding: localized functions of cytosolic chaperones.* Trends Biochem Sci, 2003. **28**(10): p. 541-7.
9. Xing, Y., et al., *Structure of clathrin coat with bound Hsc70 and auxilin: mechanism of Hsc70-facilitated disassembly.* EMBO J, 2010. **29**(3): p. 655-65.
10. Flynn, G.C., et al., *Peptide-binding specificity of the molecular chaperone BiP.* Nature, 1991. **353**(6346): p. 726-30.
11. Russell, R., R. Jordan, and R. McMacken, *Kinetic characterization of the ATPase cycle of the DnaK molecular chaperone.* Biochemistry, 1998. **37**(2): p. 596-607.
12. Mayer, M.P., et al., *Multistep mechanism of substrate binding determines chaperone activity of Hsp70.* Nat Struct Biol, 2000. **7**(7): p. 586-93.
13. Vogel, M., M.P. Mayer, and B. Bukau, *Allosteric regulation of Hsp70 chaperones involves a conserved interdomain linker.* J Biol Chem, 2006. **281**(50): p. 38705-11.
14. Han, W. and P. Christen, *Mutations in the interdomain linker region of DnaK abolish the chaperone action of the DnaK/DnaJ/GrpE system.* FEBS Lett, 2001. **497**(1): p. 55-8.
15. Ha, J.H. and D.B. McKay, *ATPase kinetics of recombinant bovine 70 kDa heat shock cognate protein and its amino-terminal ATPase domain.* Biochemistry, 1994. **33**(48): p. 14625-35.
16. Laufen, T., et al., *Mechanism of regulation of hsp70 chaperones by DnaJ cochaperones.* Proc Natl Acad Sci U S A, 1999. **96**(10): p. 5452-7.
17. Qiu, X.B., et al., *The diversity of the DnaJ/Hsp40 family, the crucial partners for Hsp70 chaperones.* Cell Mol Life Sci, 2006. **63**(22): p. 2560-70.

18. Wall, D., M. Zylicz, and C. Georgopoulos, *The NH2-terminal 108 amino acids of the Escherichia coli DnaJ protein stimulate the ATPase activity of DnaK and are sufficient for lambda replication.* J Biol Chem, 1994. **269**(7): p. 5446-51.
19. Greene, M.K., K. Maskos, and S.J. Landry, *Role of the J-domain in the cooperation of Hsp40 with Hsp70.* Proc Natl Acad Sci U S A, 1998. **95**(11): p. 6108-13.
20. Jiang, J., et al., *Structural basis of J cochaperone binding and regulation of Hsp70.* Mol Cell, 2007. **28**(3): p. 422-33.
21. Pierpaoli, E.V., et al., *The power stroke of the DnaK/DnaJ/GrpE molecular chaperone system.* J Mol Biol, 1997. **269**(5): p. 757-68.
22. Harrison, C., *GrpE, a nucleotide exchange factor for DnaK.* Cell Stress Chaperones, 2003. **8**(3): p. 218-24.
23. Kabbage, M. and M.B. Dickman, *The BAG proteins: a ubiquitous family of chaperone regulators.* Cell Mol Life Sci, 2008. **65**(9): p. 1390-402.
24. Kabani, M., et al., *HspBP1, a homologue of the yeast Fes1 and Sls1 proteins, is an Hsc70 nucleotide exchange factor.* FEBS Lett, 2002. **531**(2): p. 339-42.
25. Shaner, L. and K.A. Morano, *All in the family: atypical Hsp70 chaperones are conserved modulators of Hsp70 activity.* Cell Stress Chaperones, 2007. **12**(1): p. 1-8.
26. Bukau, B., J. Weissman, and A. Horwich, *Molecular chaperones and protein quality control.* Cell, 2006. **125**(3): p. 443-51.
27. Vos, M.J., et al., *Structural and functional diversities between members of the human HSPB, HSPH, HSPA, and DNAJ chaperone families.* Biochemistry, 2008. **47**(27): p. 7001-11.
28. Kota, P., et al., *Identification of a consensus motif in substrates bound by a Type I Hsp40.* Proc Natl Acad Sci U S A, 2009. **106**(27): p. 11073-8.
29. Blatch, G.L. and M. Lassle, *The tetratricopeptide repeat: a structural motif mediating protein-protein interactions.* Bioessays, 1999. **21**(11): p. 932-9.
30. Scheufler, C., et al., *Structure of TPR domain-peptide complexes: critical elements in the assembly of the Hsp70-Hsp90 multichaperone machine.* Cell, 2000. **101**(2): p. 199-210.
31. Carrigan, P.E., et al., *Multiple domains of the co-chaperone Hop are important for Hsp70 binding.* J Biol Chem, 2004. **279**(16): p. 16185-93.
32. Flom, G., et al., *Definition of the minimal fragments of Sti1 required for dimerization, interaction with Hsp70 and Hsp90 and in vivo functions.* Biochem J, 2007. **404**(1): p. 159-67.
33. Hernandez, M.P., W.P. Sullivan, and D.O. Toft, *The assembly and intermolecular properties of the hsp70-Hop-hsp90 molecular chaperone complex.* J Biol Chem, 2002. **277**(41): p. 38294-304.
34. Onuoha, S.C., et al., *Structural studies on the co-chaperone Hop and its complexes with Hsp90.* J Mol Biol, 2008. **379**(4): p. 732-44.
35. Connell, P., et al., *The co-chaperone CHIP regulates protein triage decisions mediated by heat-shock proteins.* Nat Cell Biol, 2001. **3**(1): p. 93-6.
36. Ballinger, C.A., et al., *Identification of CHIP, a novel tetratricopeptide repeat-containing protein that interacts with heat shock proteins and negatively regulates chaperone functions.* Mol Cell Biol, 1999. **19**(6): p. 4535-45.

37. Hohfeld, J., D.M. Cyr, and C. Patterson, *From the cradle to the grave: molecular chaperones that may choose between folding and degradation.* EMBO Rep, 2001. **2**(10): p. 885-90.
38. Meimaridou, E., S.B. Gooljar, and J.P. Chapple, *From hatching to dispatching: the multiple cellular roles of the Hsp70 molecular chaperone machinery.* J Mol Endocrinol, 2009. **42**(1): p. 1-9.
39. Mosser, D.D. and R.I. Morimoto, *Molecular chaperones and the stress of oncogenesis.* Oncogene, 2004. **23**(16): p. 2907-18.
40. Ciocca, D.R. and S.K. Calderwood, *Heat shock proteins in cancer: diagnostic, prognostic, predictive, and treatment implications.* Cell Stress Chaperones, 2005. **10**(2): p. 86-103.
41. Rohde, M., et al., *Members of the heat-shock protein 70 family promote cancer cell growth by distinct mechanisms.* Genes Dev, 2005. **19**(5): p. 570-82.
42. Seo, J.S., et al., *T cell lymphoma in transgenic mice expressing the human Hsp70 gene.* Biochem Biophys Res Commun, 1996. **218**(2): p. 582-7.
43. Sliutz, G., et al., *Drug resistance against gemcitabine and topotecan mediated by constitutive hsp70 overexpression in vitro: implication of quercetin as sensitiser in chemotherapy.* Br J Cancer, 1996. **74**(2): p. 172-7.
44. Whitesell, L. and S. Lindquist, *Inhibiting the transcription factor HSF1 as an anticancer strategy.* Expert Opin Ther Targets, 2009. **13**(4): p. 469-78.
45. Powers, M.V. and P. Workman, *Inhibitors of the heat shock response: biology and pharmacology.* FEBS Lett, 2007. **581**(19): p. 3758-69.
46. Buzzard, K.A., et al., *Heat shock protein 72 modulates pathways of stress-induced apoptosis.* J Biol Chem, 1998. **273**(27): p. 17147-53.
47. Garrido, C., et al., *Heat shock proteins: endogenous modulators of apoptotic cell death.* Biochem Biophys Res Commun, 2001. **286**(3): p. 433-42.
48. Yang, J., et al., *HSP70 protects BCL2L12 and BCL2L12A from N-terminal ubiquitination-mediated proteasomal degradation.* FEBS Lett, 2009. **583**(9): p. 1409-14.
49. Gabai, V.L., et al., *Hsp72 and stress kinase c-jun N-terminal kinase regulate the bid-dependent pathway in tumor necrosis factor-induced apoptosis.* Mol Cell Biol, 2002. **22**(10): p. 3415-24.
50. Gotoh, T., et al., *hsp70-DnaJ chaperone pair prevents nitric oxide- and CHOP-induced apoptosis by inhibiting translocation of Bax to mitochondria.* Cell Death Differ, 2004. **11**(4): p. 390-402.
51. Stankiewicz, A.R., et al., *Hsp70 inhibits heat-induced apoptosis upstream of mitochondria by preventing Bax translocation.* J Biol Chem, 2005. **280**(46): p. 38729-39.
52. Li, B. and Q.P. Dou, *Bax degradation by the ubiquitin/proteasome-dependent pathway: involvement in tumor survival and progression.* Proc Natl Acad Sci U S A, 2000. **97**(8): p. 3850-5.
53. Beere, H.M., et al., *Heat-shock protein 70 inhibits apoptosis by preventing recruitment of procaspase-9 to the Apaf-1 apoptosome.* Nat Cell Biol, 2000. **2**(8): p. 469-75.

54. Nylandsted, J., et al., *Heat shock protein 70 promotes cell survival by inhibiting lysosomal membrane permeabilization.* J Exp Med, 2004. **200**(4): p. 425-35.
55. Yaglom, J.A., V.L. Gabai, and M.Y. Sherman, *High levels of heat shock protein Hsp72 in cancer cells suppress default senescence pathways.* Cancer Res, 2007. **67**(5): p. 2373-81.
56. Volloch, V., et al., *ATPase activity of the heat shock protein hsp72 is dispensable for its effects on dephosphorylation of stress kinase JNK and on heat-induced apoptosis.* FEBS Lett, 1999. **461**(1-2): p. 73-6.
57. Meriin, A.B., et al., *Protein-damaging stresses activate c-Jun N-terminal kinase via inhibition of its dephosphorylation: a novel pathway controlled by HSP72.* Mol Cell Biol, 1999. **19**(4): p. 2547-55.
58. Yaglom, J.A., et al., *The function of HSP72 in suppression of c-Jun N-terminal kinase activation can be dissociated from its role in prevention of protein damage.* J Biol Chem, 1999. **274**(29): p. 20223-8.
59. Nylandsted, J., K. Brand, and M. Jaattela, *Heat shock protein 70 is required for the survival of cancer cells.* Ann N Y Acad Sci, 2000. **926**: p. 122-5.
60. Nylandsted, J., et al., *Selective depletion of heat shock protein 70 (Hsp70) activates a tumor-specific death program that is independent of caspases and bypasses Bcl-2.* Proc Natl Acad Sci U S A, 2000. **97**(14): p. 7871-6.
61. Powers, M.V., P.A. Clarke, and P. Workman, *Death by chaperone: HSP90, HSP70 or both?* Cell Cycle, 2009. **8**(4): p. 518-26.
62. Pocaly, M., et al., *Overexpression of the heat-shock protein 70 is associated to imatinib resistance in chronic myeloid leukemia.* Leukemia, 2007. **21**(1): p. 93-101.
63. Gabai, V.L., K.R. Budagova, and M.Y. Sherman, *Increased expression of the major heat shock protein Hsp72 in human prostate carcinoma cells is dispensable for their viability but confers resistance to a variety of anticancer agents.* Oncogene, 2005. **24**(20): p. 3328-38.
64. Bagatell, R., et al., *Induction of a heat shock factor 1-dependent stress response alters the cytotoxic activity of hsp90-binding agents.* Clin Cancer Res, 2000. **6**(8): p. 3312-8.
65. Wegele, H., L. Muller, and J. Buchner, *Hsp70 and Hsp90--a relay team for protein folding.* Rev Physiol Biochem Pharmacol, 2004. **151**: p. 1-44.
66. Richter, K. and J. Buchner, *Hsp90: chaperoning signal transduction.* J Cell Physiol, 2001. **188**(3): p. 281-90.
67. Chaudhury, S., T.R. Welch, and B.S. Blagg, *Hsp90 as a target for drug development.* ChemMedChem, 2006. **1**(12): p. 1331-40.
68. Taldone, T. and G. Chiosis, *Purine-scaffold Hsp90 inhibitors.* Curr Top Med Chem, 2009. **9**(15): p. 1436-46.
69. Powers, M.V., P.A. Clarke, and P. Workman, *Dual targeting of HSC70 and HSP72 inhibits HSP90 function and induces tumor-specific apoptosis.* Cancer Cell, 2008. **14**(3): p. 250-62.
70. Zaarur, N., et al., *Targeting heat shock response to sensitize cancer cells to proteasome and Hsp90 inhibitors.* Cancer Res, 2006. **66**(3): p. 1783-91.

71. Soskic, V., K. Groebe, and A. Schrattenholz, *Nonenzymatic posttranslational protein modifications in ageing.* Exp Gerontol, 2008. **43**(4): p. 247-57.
72. Zeng, B.Y., et al., *Proteasomal activity in brain differs between species and brain regions and changes with age.* Mech Ageing Dev, 2005. **126**(6-7): p. 760-6.
73. Shpund, S. and D. Gershon, *Alterations in the chaperone activity of HSP70 in aging organisms.* Arch Gerontol Geriatr, 1997. **24**(2): p. 125-31.
74. Kirkegaard, T., et al., *Hsp70 stabilizes lysosomes and reverts Niemann-Pick disease-associated lysosomal pathology.* Nature, 2010. **463**(7280): p. 549-53.
75. Witt, S.N., *Hsp70 molecular chaperones and Parkinson's disease.* Biopolymers, 2010. **93**(3): p. 218-28.
76. Liberek, K., A. Lewandowska, and S. Zietkiewicz, *Chaperones in control of protein disaggregation.* EMBO J, 2008. **27**(2): p. 328-35.
77. Bauer, P.O. and N. Nukina, *The pathogenic mechanisms of polyglutamine diseases and current therapeutic strategies.* J Neurochem, 2009. **110**(6): p. 1737-65.
78. Williams, A.J. and H.L. Paulson, *Polyglutamine neurodegeneration: protein misfolding revisited.* Trends Neurosci, 2008. **31**(10): p. 521-8.
79. Muchowski, P.J., et al., *Hsp70 and hsp40 chaperones can inhibit self-assembly of polyglutamine proteins into amyloid-like fibrils.* Proc Natl Acad Sci U S A, 2000. **97**(14): p. 7841-6.
80. Krobitsch, S. and S. Lindquist, *Aggregation of huntingtin in yeast varies with the length of the polyglutamine expansion and the expression of chaperone proteins.* Proc Natl Acad Sci U S A, 2000. **97**(4): p. 1589-94.
81. Wyttenbach, A., et al., *Effects of heat shock, heat shock protein 40 (HDJ-2), and proteasome inhibition on protein aggregation in cellular models of Huntington's disease.* Proc Natl Acad Sci U S A, 2000. **97**(6): p. 2898-903.
82. Rujano, M.A., H.H. Kampinga, and F.A. Salomons, *Modulation of polyglutamine inclusion formation by the Hsp70 chaperone machine.* Exp Cell Res, 2007. **313**(16): p. 3568-78.
83. Warrick, J.M., et al., *Suppression of polyglutamine-mediated neurodegeneration in Drosophila by the molecular chaperone HSP70.* Nat Genet, 1999. **23**(4): p. 425-8.
84. Adachi, H., et al., *Heat shock protein 70 chaperone overexpression ameliorates phenotypes of the spinal and bulbar muscular atrophy transgenic mouse model by reducing nuclear-localized mutant androgen receptor protein.* J Neurosci, 2003. **23**(6): p. 2203-11.
85. Cummings, C.J., et al., *Over-expression of inducible HSP70 chaperone suppresses neuropathology and improves motor function in SCA1 mice.* Hum Mol Genet, 2001. **10**(14): p. 1511-8.
86. Helmlinger, D., et al., *Hsp70 and Hsp40 chaperones do not modulate retinal phenotype in SCA7 mice.* J Biol Chem, 2004. **279**(53): p. 55969-77.
87. Hansson, O., et al., *Overexpression of heat shock protein 70 in R6/2 Huntington's disease mice has only modest effects on disease progression.* Brain Res, 2003. **970**(1-2): p. 47-57.

88. Zhou, H., S.H. Li, and X.J. Li, *Chaperone suppression of cellular toxicity of huntingtin is independent of polyglutamine aggregation.* J Biol Chem, 2001. **276**(51): p. 48417-24.
89. Jana, N.R., et al., *Co-chaperone CHIP associates with expanded polyglutamine protein and promotes their degradation by proteasomes.* J Biol Chem, 2005. **280**(12): p. 11635-40.
90. Miller, V.M., et al., *CHIP suppresses polyglutamine aggregation and toxicity in vitro and in vivo.* J Neurosci, 2005. **25**(40): p. 9152-61.
91. Williams, A.J., et al., *In vivo suppression of polyglutamine neurotoxicity by C-terminus of Hsp70-interacting protein (CHIP) supports an aggregation model of pathogenesis.* Neurobiol Dis, 2009. **33**(3): p. 342-53.
92. Al-Ramahi, I., et al., *CHIP protects from the neurotoxicity of expanded and wild-type ataxin-1 and promotes their ubiquitination and degradation.* J Biol Chem, 2006. **281**(36): p. 26714-24.
93. Adachi, H., et al., *CHIP overexpression reduces mutant androgen receptor protein and ameliorates phenotypes of the spinal and bulbar muscular atrophy transgenic mouse model.* J Neurosci, 2007. **27**(19): p. 5115-26.
94. Sittler, A., et al., *Geldanamycin activates a heat shock response and inhibits huntingtin aggregation in a cell culture model of Huntington's disease.* Hum Mol Genet, 2001. **10**(12): p. 1307-15.
95. Katsuno, M., et al., *Pharmacological induction of heat-shock proteins alleviates polyglutamine-mediated motor neuron disease.* Proc Natl Acad Sci U S A, 2005. **102**(46): p. 16801-6.
96. Zhang, Y.Q. and K.D. Sarge, *Celastrol inhibits polyglutamine aggregation and toxicity though induction of the heat shock response.* J Mol Med, 2007. **85**(12): p. 1421-8.
97. Fujikake, N., et al., *Heat shock transcription factor 1-activating compounds suppress polyglutamine-induced neurodegeneration through induction of multiple molecular chaperones.* J Biol Chem, 2008. **283**(38): p. 26188-97.
98. Findeis, M.A., *The role of amyloid beta peptide 42 in Alzheimer's disease.* Pharmacol Ther, 2007. **116**(2): p. 266-86.
99. Ballatore, C., V.M. Lee, and J.Q. Trojanowski, *Tau-mediated neurodegeneration in Alzheimer's disease and related disorders.* Nat Rev Neurosci, 2007. **8**(9): p. 663-72.
100. Evans, C.G., S. Wisen, and J.E. Gestwicki, *Heat shock proteins 70 and 90 inhibit early stages of amyloid beta-(1-42) aggregation in vitro.* J Biol Chem, 2006. **281**(44): p. 33182-91.
101. Kumar, P., et al., *CHIP and HSPs interact with beta-APP in a proteasome-dependent manner and influence Abeta metabolism.* Hum Mol Genet, 2007. **16**(7): p. 848-64.
102. Veereshwarayya, V., et al., *Differential effects of mitochondrial heat shock protein 60 and related molecular chaperones to prevent intracellular beta-amyloid-induced inhibition of complex IV and limit apoptosis.* J Biol Chem, 2006. **281**(40): p. 29468-78.
103. Sarkar, M., J. Kuret, and G. Lee, *Two motifs within the tau microtubule-binding domain mediate its association with the hsc70 molecular chaperone.* J Neurosci Res, 2008. **86**(12): p. 2763-73.

104. Petrucelli, L., et al., *CHIP and Hsp70 regulate tau ubiquitination, degradation and aggregation.* Hum Mol Genet, 2004. **13**(7): p. 703-14.
105. Dou, F., et al., *Chaperones increase association of tau protein with microtubules.* Proc Natl Acad Sci U S A, 2003. **100**(2): p. 721-6.
106. Shimura, H., et al., *CHIP-Hsc70 complex ubiquitinates phosphorylated tau and enhances cell survival.* J Biol Chem, 2004. **279**(6): p. 4869-76.
107. Hatakeyama, S., et al., *U-box protein carboxyl terminus of Hsc70-interacting protein (CHIP) mediates poly-ubiquitylation preferentially on four-repeat Tau and is involved in neurodegeneration of tauopathy.* J Neurochem, 2004. **91**(2): p. 299-307.
108. Dickey, C.A., et al., *The high-affinity HSP90-CHIP complex recognizes and selectively degrades phosphorylated tau client proteins.* J Clin Invest, 2007. **117**(3): p. 648-58.
109. Elliott, E., P. Tsvetkov, and I. Ginzburg, *BAG-1 associates with Hsc70.Tau complex and regulates the proteasomal degradation of Tau protein.* J Biol Chem, 2007. **282**(51): p. 37276-84.
110. Carrettiero, D.C., et al., *The cochaperone BAG2 sweeps paired helical filament-insoluble tau from the microtubule.* J Neurosci, 2009. **29**(7): p. 2151-61.
111. Henderson, B., E. Allan, and A.R. Coates, *Stress wars: the direct role of host and bacterial molecular chaperones in bacterial infection.* Infect Immun, 2006. **74**(7): p. 3693-706.
112. Lemos, J.A., Y. Luzardo, and R.A. Burne, *Physiologic effects of forced down-regulation of dnaK and groEL expression in Streptococcus mutans.* J Bacteriol, 2007. **189**(5): p. 1582-8.
113. Wolska, K.I., et al., *Antibiotic susceptibility of Escherichia coli dnaK and dnaJ mutants.* Microb Drug Resist, 2000. **6**(2): p. 119-26.
114. Singh, V.K., et al., *Role for dnaK locus in tolerance of multiple stresses in Staphylococcus aureus.* Microbiology, 2007. **153**(Pt 9): p. 3162-73.
115. Yamaguchi, Y., et al., *Effects of disruption of heat shock genes on susceptibility of Escherichia coli to fluoroquinolones.* BMC Microbiol, 2003. **3**: p. 16.
116. Sell, S.M., et al., *Isolation and characterization of dnaJ null mutants of Escherichia coli.* J Bacteriol, 1990. **172**(9): p. 4827-35.
117. Takaya, A., et al., *The DnaK/DnaJ chaperone machinery of Salmonella enterica serovar Typhimurium is essential for invasion of epithelial cells and survival within macrophages, leading to systemic infection.* Infect Immun, 2004. **72**(3): p. 1364-73.
118. Hanawa, T., et al., *The Listeria monocytogenes DnaK chaperone is required for stress tolerance and efficient phagocytosis with macrophages.* Cell Stress Chaperones, 1999. **4**(2): p. 118-28.
119. Nishimura, H., et al., *Hsp70 protects macrophages infected with Salmonella choleraesuis against TNF-alpha-induced cell death.* Cell Stress Chaperones, 1997. **2**(1): p. 50-9.
120. Salminen, A., et al., *Innate immunity meets with cellular stress at the IKK complex: regulation of the IKK complex by HSP70 and HSP90.* Immunol Lett, 2008. **117**(1): p. 9-15.
121. Todryk, S.M., M.J. Gough, and A.G. Pockley, *Facets of heat shock protein 70 show immunotherapeutic potential.* Immunology, 2003. **110**(1): p. 1-9.

122. Li, Z., A. Menoret, and P. Srivastava, *Roles of heat-shock proteins in antigen presentation and cross-presentation.* Curr Opin Immunol, 2002. **14**(1): p. 45-51.
123. Brodsky, J.L. and G. Chiosis, *Hsp70 molecular chaperones: emerging roles in human disease and identification of small molecule modulators.* Curr Top Med Chem, 2006. **6**(11): p. 1215-25.
124. Patury, S., Y. Miyata, and J.E. Gestwicki, *Pharmacological targeting of the Hsp70 chaperone.* Curr Top Med Chem, 2009. **9**(15): p. 1337-51.
125. Takeuchi, T., et al., *A new antitumor antibiotic, spergualin: isolation and antitumor activity.* J Antibiot (Tokyo), 1981. **34**(12): p. 1619-21.
126. Umezawa, H., et al., *Structure of an antitumor antibiotic, spergualin.* J Antibiot (Tokyo), 1981. **34**(12): p. 1622-4.
127. Kondo, S., et al., *The total synthesis of spergualin, an antitumor antibiotic.* J Antibiot (Tokyo), 1981. **34**(12): p. 1625-7.
128. Umeda, Y., et al., *Synthesis and antitumor activity of spergualin analogues. I. Chemical modification of 7-guanidino-3-hydroxyacyl moiety.* J Antibiot (Tokyo), 1985. **38**(7): p. 886-98.
129. Umeda, Y., et al., *Synthesis and antitumor activity of spergualin analogues. III. Novel method for synthesis of optically active 15-deoxyspergualin and 15-deoxy-11-O-methylspergualin.* J Antibiot (Tokyo), 1987. **40**(9): p. 1316-24.
130. Lebreton, L., et al., *Structure-immunosuppressive activity relationships of new analogues of 15-deoxyspergualin. 1. Structural modifications of the hydroxyglycine moiety.* J Med Chem, 1999. **42**(2): p. 277-90.
131. Nishizawa, R., et al., *Synthesis and biological activity of spergualin analogues. I.* J Antibiot (Tokyo), 1988. **41**(11): p. 1629-43.
132. Thomas, F.T., et al., *15-Deoxyspergualin: a novel immunosuppressive drug with clinical potential.* Ann N Y Acad Sci, 1993. **685**: p. 175-92.
133. Lebreton, L., et al., *Structure-immunosuppressive activity relationships of new analogues of 15-deoxyspergualin. 2. Structural modifications of the spermidine moiety.* J Med Chem, 1999. **42**(23): p. 4749-63.
134. Komesli, S., C. Dumas, and P. Dutartre, *Analysis of in vivo immunosuppressive and in vitro interaction with constitutive heat shock protein 70 activity of LF08-0299 (Tresperimus) and analogues.* Int J Immunopharmacol, 1999. **21**(5): p. 349-58.
135. Nadler, S.G., et al., *Interaction of the immunosuppressant deoxyspergualin with a member of the Hsp70 family of heat shock proteins.* Science, 1992. **258**(5081): p. 484-6.
136. Mazzucco, C.E. and S.G. Nadler, *A member of the Hsp70 family of heat-shock proteins is a putative target for the immunosuppressant 15-deoxyspergualin.* Ann N Y Acad Sci, 1993. **685**: p. 202-4.
137. Nadler, S.G., et al., *Identification of a binding site on Hsc70 for the immunosuppressant 15-deoxyspergualin.* Biochem Biophys Res Commun, 1998. **253**(1): p. 176-80.
138. Nadeau, K., et al., *Quantitation of the interaction of the immunosuppressant deoxyspergualin and analogs with Hsc70 and Hsp90.* Biochemistry, 1994. **33**(9): p. 2561-7.

139. Brodsky, J.L., *Selectivity of the molecular chaperone-specific immunosuppressive agent 15-deoxyspergualin: modulation of Hsc70 ATPase activity without compromising DnaJ chaperone interactions.* Biochem Pharmacol, 1999. **57**(8): p. 877-80.
140. Kaufman, D.B., et al., *15-Deoxyspergualin: Immunotheray in solid organ and cellular transplantation.* Transplant. Rev., 1996. **10**(3): p. 160-174.
141. Hoeger, P.H., et al., *Immunosuppressant deoxyspergualin inhibits antigen processing in monocytes.* J Immunol, 1994. **153**(9): p. 3908-16.
142. Amada, N., et al., *Deoxyspergualin prophylaxis with tacrolimus further improves long-term graft survival in living-related renal-transplant recipients transfused with donor-specific blood.* Transplant Proc, 2005. **37**(2): p. 927-9.
143. Birck, R., et al., *15-Deoxyspergualin in patients with refractory ANCA-associated systemic vasculitis: a six-month open-label trial to evaluate safety and efficacy.* J Am Soc Nephrol, 2003. **14**(2): p. 440-7.
144. Sugawara, A., et al., *Polyamine compound deoxyspergualin inhibits heat shock protein-induced activation of immature dendritic cells.* Cell Stress Chaperones, 2009. **14**(2): p. 133-9.
145. Kalsch, A.I., et al., *In vivo effects of cyclic administration of 15-deoxyspergualin on leucocyte function in patients with Wegener's granulomatosis.* Clin Exp Immunol, 2006. **146**(3): p. 455-62.
146. Lee, J., et al., *15-deoxyspergualin prevents mucosal injury by inhibiting production of TNF-alpha and down-regulating expression of MD-1 in a murine model of TNBS-induced colitis.* Int Immunopharmacol, 2007. **7**(8): p. 1003-12.
147. Ohlman, S., et al., *Pharmacokinetics of 15-deoxyspergualin studied in renal transplant patients receiving the drug during graft rejection.* Transpl Int, 1994. **7**(1): p. 5-10.
148. Plowman, J., et al., *Preclinical antitumor activity and pharmacological properties of deoxyspergualin.* Cancer Res, 1987. **47**(3): p. 685-9.
149. Dhingra, K., et al., *Phase II study of deoxyspergualin in metastatic breast cancer.* Invest New Drugs, 1994. **12**(3): p. 235-41.
150. Okubo, M., et al., *15-Deoxyspergualin "rescue therapy" for methylprednisolone-resistant rejection of renal transplants as compared with anti-T cell monoclonal antibody (OKT3).* Transplantation, 1993. **55**(3): p. 505-8.
151. Ohlman, S., et al., *Treatment of renal transplant rejection with 15-deoxyspergualin--a dose-finding study in man.* Transplant Proc, 1992. **24**(1): p. 318-20.
152. Fewell, S.W., B.W. Day, and J.L. Brodsky, *Identification of an inhibitor of hsc70-mediated protein translocation and ATP hydrolysis.* J Biol Chem, 2001. **276**(2): p. 910-4.
153. Fewell, S.W., et al., *Small molecule modulators of endogenous and co-chaperone-stimulated Hsp70 ATPase activity.* J Biol Chem, 2004. **279**(49): p. 51131-40.
154. Wisen, S., et al., *Chemical modulators of heat shock protein 70 (Hsp70) by sequential, microwave-accelerated reactions on solid phase.* Bioorg Med Chem Lett, 2008. **18**(1): p. 60-5.

155. Chang, L., et al., *High-throughput screen for small molecules that modulate the ATPase activity of the molecular chaperone DnaK.* Anal Biochem, 2008. **372**(2): p. 167-76.
156. Wisen, S. and J.E. Gestwicki, *Identification of small molecules that modify the protein folding activity of heat shock protein 70.* Anal Biochem, 2008. **374**(2): p. 371-7.
157. Jinwal, U.K., et al., *Chemical manipulation of hsp70 ATPase activity regulates tau stability.* J Neurosci, 2009. **29**(39): p. 12079-88.
158. Rodina, A., et al., *Selective compounds define Hsp90 as a major inhibitor of apoptosis in small-cell lung cancer.* Nat Chem Biol, 2007. **3**(8): p. 498-507.
159. Wright, C.M., et al., *Pyrimidinone-peptoid hybrid molecules with distinct effects on molecular chaperone function and cell proliferation.* Bioorg Med Chem, 2008. **16**(6): p. 3291-301.
160. Koren, J., et al., *Facilitating Akt clearance via manipulation of Hsp70 activity and levels.* J Biol Chem, 2009.
161. Mamelak, D. and C. Lingwood, *The ATPase domain of hsp70 possesses a unique binding specificity for 3'-sulfogalactolipids.* J Biol Chem, 2001. **276**(1): p. 449-56.
162. Mamelak, D., et al., *Hsp70s contain a specific sulfogalactolipid binding site. Differential aglycone influence on sulfogalactosyl ceramide binding by recombinant prokaryotic and eukaryotic hsp70 family members.* Biochemistry, 2001. **40**(12): p. 3572-82.
163. Mamelak, D., et al., *The aglycone of sulfogalactolipids can alter the sulfate ester substitution position required for hsc70 recognition.* Carbohydr Res, 2001. **335**(2): p. 91-100.
164. Park, H.J., et al., *A soluble sulfogalactosyl ceramide mimic promotes Delta F508 CFTR escape from endoplasmic reticulum associated degradation.* Chem Biol, 2009. **16**(4): p. 461-70.
165. Liebscher, M., et al., *Fatty acyl benzamido antibacterials based on inhibition of DnaK-catalyzed protein folding.* J Biol Chem, 2007. **282**(7): p. 4437-46.
166. Otvos, L., Jr., et al., *Interaction between heat shock proteins and antimicrobial peptides.* Biochemistry, 2000. **39**(46): p. 14150-9.
167. Kragol, G., et al., *The antibacterial peptide pyrrhocoricin inhibits the ATPase actions of DnaK and prevents chaperone-assisted protein folding.* Biochemistry, 2001. **40**(10): p. 3016-26.
168. Kragol, G., et al., *Identification of crucial residues for the antibacterial activity of the proline-rich peptide, pyrrhocoricin.* Eur J Biochem, 2002. **269**(17): p. 4226-37.
169. Otvos, L., Jr., et al., *Designer antibacterial peptides kill fluoroquinolone-resistant clinical isolates.* J Med Chem, 2005. **48**(16): p. 5349-59.
170. Cudic, M., et al., *Development of novel antibacterial peptides that kill resistant isolates.* Peptides, 2002. **23**(12): p. 2071-83.
171. Williamson, D.S., et al., *Novel adenosine-derived inhibitors of 70 kDa heat shock protein, discovered through structure-based design.* J Med Chem, 2009. **52**(6): p. 1510-3.

172. Massey, A.J., et al., *A novel, small molecule inhibitor of Hsc70/Hsp70 potentiates Hsp90 inhibitor induced apoptosis in HCT116 colon carcinoma cells.* Cancer Chemother Pharmacol, 2009.
173. Cellitti, J., et al., *Small molecule DnaK modulators targeting the beta-domain.* Chem Biol Drug Des, 2009. **74**(4): p. 349-57.
174. Leu, J.I., et al., *A small molecule inhibitor of inducible heat shock protein 70.* Mol Cell, 2009. **36**(1): p. 15-27.
175. Wadhwa, R., et al., *Selective toxicity of MKT-077 to cancer cells is mediated by its binding to the hsp70 family protein mot-2 and reactivation of p53 function.* Cancer Res, 2000. **60**(24): p. 6818-21.
176. Deocaris, C.C., et al., *Mortalin sensitizes human cancer cells to MKT-077-induced senescence.* Cancer Lett, 2007. **252**(2): p. 259-69.
177. Koya, K., et al., *MKT-077, a novel rhodacyanine dye in clinical trials, exhibits anticarcinoma activity in preclinical studies based on selective mitochondrial accumulation.* Cancer Res, 1996. **56**(3): p. 538-43.
178. Chiba, Y., et al., *MKT-077, localized lipophilic cation: antitumor activity against human tumor xenografts serially transplanted into nude mice.* Anticancer Res, 1998. **18**(2A): p. 1047-52.
179. Propper, D.J., et al., *Phase I trial of the selective mitochondrial toxin MKT077 in chemo-resistant solid tumours.* Ann Oncol, 1999. **10**(8): p. 923-7.
180. Chen, W.Y., et al., *Tubocapsenolide A, a novel withanolide, inhibits proliferation and induces apoptosis in MDA-MB-231 cells by thiol oxidation of heat shock proteins.* J Biol Chem, 2008. **283**(25): p. 17184-93.
181. Ermakova, S.P., et al., *(-)-Epigallocatechin gallate overcomes resistance to etoposide-induced cell death by targeting the molecular chaperone glucose-regulated protein 78.* Cancer Res, 2006. **66**(18): p. 9260-9.
182. Tang, X.Y. and Y.Q. Zhu, *Epigallocatechin-3-gallate suppressed the over-expression of HSP 70 and MDR1 induced by heat shock in SGC 7901.* J Chemother, 2008. **20**(3): p. 355-60.
183. Li, M., et al., *Synergistic promotion of breast cancer cells death by targeting molecular chaperone GRP78 and heat shock protein 70.* J Cell Mol Med, 2008.
184. Williams, D.R., et al., *An apoptosis-inducing small molecule that binds to heat shock protein 70.* Angew Chem Int Ed Engl, 2008. **47**(39): p. 7466-9.
185. Haney, C.M., et al., *Identification of Hsp70 modulators through modeling of the substrate binding domain.* Bioorg Med Chem Lett, 2009. **19**(14): p. 3828-31.
186. Sharp, A., et al., *Short peptides derived from the BAG-1 C-terminus inhibit the interaction between BAG-1 and HSC70 and decrease breast cancer cell growth.* FEBS Lett, 2009. **583**(21): p. 3405-11.
187. Lamb, J., et al., *The Connectivity Map: using gene-expression signatures to connect small molecules, genes, and disease.* Science, 2006. **313**(5795): p. 1929-35.
188. Saleh, A., et al., *Negative regulation of the Apaf-1 apoptosome by Hsp70.* Nat Cell Biol, 2000. **2**(8): p. 476-83.
189. Schmitt, E., et al., *Intracellular and extracellular functions of heat shock proteins: repercussions in cancer therapy.* J Leukoc Biol, 2007. **81**(1): p. 15-27.

190. Volloch, V., et al., *HSP72 can protect cells from heat-induced apoptosis by accelerating the inactivation of stress kinase JNK.* Cell Stress Chaperones, 2000. **5**(2): p. 139-47.
191. Meriin, A.B., et al., *Proteasome inhibitors activate stress kinases and induce Hsp72. Diverse effects on apoptosis.* J Biol Chem, 1998. **273**(11): p. 6373-9.
192. Gabai, V.L., et al., *Role of Hsp70 in regulation of stress-kinase JNK: implications in apoptosis and aging.* FEBS Lett, 1998. **438**(1-2): p. 1-4.
193. Gabai, V.L., et al., *Suppression of stress kinase JNK is involved in HSP72-mediated protection of myogenic cells from transient energy deprivation. HSP72 alleviates the stress-induced inhibition of JNK dephosphorylation.* J Biol Chem, 2000. **275**(48): p. 38088-94.
194. Gabai, V.L., et al., *Hsp72-mediated suppression of c-Jun N-terminal kinase is implicated in development of tolerance to caspase-independent cell death.* Mol Cell Biol, 2000. **20**(18): p. 6826-36.
195. Ruchalski, K., et al., *Distinct hsp70 domains mediate apoptosis-inducing factor release and nuclear accumulation.* J Biol Chem, 2006. **281**(12): p. 7873-80.
196. Ruchalski, K., et al., *HSP72 inhibits apoptosis-inducing factor release in ATP-depleted renal epithelial cells.* Am J Physiol Cell Physiol, 2003. **285**(6): p. C1483-93.
197. Ravagnan, L., et al., *Heat-shock protein 70 antagonizes apoptosis-inducing factor.* Nat Cell Biol, 2001. **3**(9): p. 839-43.
198. Dudeja, V., et al., *Heat shock protein 70 inhibits apoptosis in cancer cells through simultaneous and independent mechanisms.* Gastroenterology, 2009. **136**(5): p. 1772-82.
199. Gyrd-Hansen, M., J. Nylandsted, and M. Jaattela, *Heat shock protein 70 promotes cancer cell viability by safeguarding lysosomal integrity.* Cell Cycle, 2004. **3**(12): p. 1484-5.
200. Gabai, V.L., et al., *Heat shock protein Hsp72 controls oncogene-induced senescence pathways in cancer cells.* Mol Cell Biol, 2009. **29**(2): p. 559-69.
201. Sherman, M.Y., et al., *Molecular chaperones regulate p53 and suppress senescence programs.* FEBS Lett, 2007. **581**(19): p. 3711-5.
202. Park, M.A., Yacoub, A., Rahmani, M., Zhang, G., Hart, L., Hagan, M., Calderwood, S. K., Sherman, M. Y., Koumenis, C., Spiegel, S., Chen, C., Graf, M., Curiel, D. T., Fisher, P. B., Grant, S., Dent, P., *OSU-03012 stimulates PRK-like endoplasmic reticulum-dependent increases in 70-kDa heat shock protein expression, attenuating its lethal actions in transformed cells.* Mol Pharmacol, 2008. **73**(4): p. 1168-1184.
203. Jana, N.R., et al., *Polyglutamine length-dependent interaction of Hsp40 and Hsp70 family chaperones with truncated N-terminal huntingtin: their role in suppression of aggregation and cellular toxicity.* Hum Mol Genet, 2000. **9**(13): p. 2009-18.
204. Merienne, K., et al., *Polyglutamine expansion induces a protein-damaging stress connecting heat shock protein 70 to the JNK pathway.* J Biol Chem, 2003. **278**(19): p. 16957-67.
205. Chai, Y., et al., *Analysis of the role of heat shock protein (Hsp) molecular chaperones in polyglutamine disease.* J Neurosci, 1999. **19**(23): p. 10338-47.

206. Kobayashi, Y., et al., *Chaperones Hsp70 and Hsp40 suppress aggregate formation and apoptosis in cultured neuronal cells expressing truncated androgen receptor protein with expanded polyglutamine tract.* J Biol Chem, 2000. **275**(12): p. 8772-8.
207. Bailey, C.K., et al., *Molecular chaperones enhance the degradation of expanded polyglutamine repeat androgen receptor in a cellular model of spinal and bulbar muscular atrophy.* Hum Mol Genet, 2002. **11**(5): p. 515-23.
208. Auluck, P.K., et al., *Chaperone suppression of alpha-synuclein toxicity in a Drosophila model for Parkinson's disease.* Science, 2002. **295**(5556): p. 865-8.
209. Klucken, J., et al., *A single amino acid substitution differentiates Hsp70-dependent effects on alpha-synuclein degradation and toxicity.* Biochem Biophys Res Commun, 2004. **325**(1): p. 367-73.
210. Dong, Z., et al., *Hsp70 gene transfer by adeno-associated virus inhibits MPTP-induced nigrostriatal degeneration in the mouse model of Parkinson disease.* Mol Ther, 2005. **11**(1): p. 80-8.
211. Meacham, G.C., et al., *The Hdj-2/Hsc70 chaperone pair facilitates early steps in CFTR biogenesis.* Embo J, 1999. **18**(6): p. 1492-505.
212. Younger, J.M., et al., *A foldable CFTR{Delta}F508 biogenic intermediate accumulates upon inhibition of the Hsc70-CHIP E3 ubiquitin ligase.* J Cell Biol, 2004. **167**(6): p. 1075-85.
213. Wild, J., et al., *Partial loss of function mutations in DnaK, the Escherichia coli homologue of the 70-kDa heat shock proteins, affect highly conserved amino acids implicated in ATP binding and hydrolysis.* Proc Natl Acad Sci U S A, 1992. **89**(15): p. 7139-43.
214. Watanabe, K., et al., *Heat shock cognate protein 70 contributes to Brucella invasion into trophoblast giant cells that cause infectious abortion.* BMC Microbiol, 2008. **8**: p. 212.
215. Hoffman, P.S. and R.A. Garduno, *Surface-associated heat shock proteins of Legionella pneumophila and Helicobacter pylori: roles in pathogenesis and immunity.* Infect Dis Obstet Gynecol, 1999. **7**(1-2): p. 58-63.
216. Stewart, G.R., et al., *Overexpression of heat-shock proteins reduces survival of Mycobacterium tuberculosis in the chronic phase of infection.* Nat Med, 2001. **7**(6): p. 732-7.
217. Kohler, S., et al., *Induction of dnaK through its native heat shock promoter is necessary for intramacrophagic replication of Brucella suis.* Infect Immun, 2002. **70**(3): p. 1631-4.
218. Tobian, A.A., D.H. Canaday, and C.V. Harding, *Bacterial heat shock proteins enhance class II MHC antigen processing and presentation of chaperoned peptides to CD4+ T cells.* J Immunol, 2004. **173**(8): p. 5130-7.
219. Lagaudriere-Gesbert, C., et al., *Uncoating ATPase Hsc70 is recruited by invariant chain and controls the size of endocytic compartments.* Proc Natl Acad Sci U S A, 2002. **99**(3): p. 1515-20.
220. Guerrero, C.A., et al., *Heat shock cognate protein 70 is involved in rotavirus cell entry.* J Virol, 2002. **76**(8): p. 4096-102.

221. Zarate, S., et al., *Interaction of rotaviruses with Hsc70 during cell entry is mediated by VP5.* J Virol, 2003. **77**(13): p. 7254-60.
222. Chromy, L.R., et al., *Chaperone-mediated in vitro disassembly of polyoma- and papillomaviruses.* J Virol, 2006. **80**(10): p. 5086-91.
223. Brown, G., et al., *Evidence for an association between heat shock protein 70 and the respiratory syncytial virus polymerase complex within lipid-raft membranes during virus infection.* Virology, 2005. **338**(1): p. 69-80.
224. May, E., et al., *Immunological evidence for the association between simian virus 40 115-kDa super T antigen and hsp70 proteins in rat, monkey, and human cells.* Virology, 1991. **180**(1): p. 285-93.
225. Campbell, K.S., et al., *DnaJ/hsp40 chaperone domain of SV40 large T antigen promotes efficient viral DNA replication.* Genes Dev, 1997. **11**(9): p. 1098-110.
226. Sullivan, C.S., et al., *Species-specific elements in the large T-antigen J domain are required for cellular transformation and DNA replication by simian virus 40.* Mol Cell Biol, 2000. **20**(15): p. 5749-57.
227. Sainis, L., et al., *HSC70 interactions with SV40 viral proteins differ between permissive and nonpermissive mammalian cells.* Cell Stress Chaperones, 2000. **5**(2): p. 132-8.
228. Salma, A., A. Tsiapos, and I. Lazaridis, *The viral SV40 T antigen cooperates with dj2 to enhance hsc70 chaperone function.* Febs J, 2007. **274**(19): p. 5021-7.
229. Peng, C.-W., Zhoa, B., Chen, H.-C., Chou, M.-L., Lai, C.-Y., Lin, S.-Z., Hsu, H.-Y., Kieff, E., *Hsp72 up-regulates Epstein-Barr virus EBNALP coactivation with EBNA2.* Blood, 2007. **109**: p. 5447-5454.
230. Agostini, I., et al., *Heat-shock protein 70 can replace viral protein R of HIV-1 during nuclear import of the viral preintegration complex.* Exp Cell Res, 2000. **259**(2): p. 398-403.
231. Iordanskiy, S., et al., *Heat-shock protein 70 exerts opposing effects on Vpr-dependent and Vpr-independent HIV-1 replication in macrophages.* Blood, 2004. **104**(6): p. 1867-72.
232. Chromy, L.R., J.M. Pipas, and R.L. Garcea, *Chaperone-mediated in vitro assembly of Polyomavirus capsids.* Proc Natl Acad Sci U S A, 2003. **100**(18): p. 10477-82.

Chapter 2

Development of High Throughput Screens to Find Compounds that Modulate the ATPase Activity of DnaK

2.1 Abstract

As discussed in Chapter 1, DnaK is a molecular chaperone of *Escherichia coli* that belongs to a family of conserved 70 kDa heat shock proteins. The Hsp70 chaperones are well known for their crucial roles in regulating protein homeostasis. Given the complexity of their molecular functions, a chemical method for controlling these chaperones might provide a useful experimental tool. However, there are only a handful of Hsp70-binding molecules known. To expand our ability to find new inhibitors, we developed a robust, colorimetric, high throughput screening (HTS) method in 96-well plates that reported on the ATPase activity of DnaK. Using this approach, we screened a 204-member, focused library of compounds that shared a dihydropyrimidine core that had been shown to be common to known Hsp70-binding leads. This process resulted in the identification of 7 new inhibitors. To further improve the throughput of the method, we adapted an energy transfer strategy to miniaturize the assay for use in 384-well format. Briefly, in this method, the intrinsic fluorescence of white, 384-well plates was quenched by energy transfer with the quinaldine red-based chromophore. Using this more sensitive approach,

we tested 55,400 compounds against the DnaK-DnaJ complex. The assay performance was good (Z' ~0.6, CV ~8%) and at least one promising new inhibitor was identified. In secondary assays, this compound specifically blocked stimulation of DnaK by its co-chaperone, DnaJ. In sum, we have developed reliable HTS methods that will likely accelerate the discovery of small molecules that modulate DnaK/Hsp70 function. Moreover, because this family of chaperones has been linked to numerous diseases, this platform might be used to generate new therapeutic leads.

2.1.1 Hsp70s are Important for Cellular Proteostasis and They Are Related to Many Diseases

DnaK is an extensively studied member of the family of 70 kDa heat shock proteins. These proteins are evolutionarily conserved at the amino acid level; for example, *E. coli* DnaK and human Hsp70 are 46% identical and 65% similar [1]. Moreover, they are functionally conserved; like other Hsp70s, DnaK acts as a molecular chaperone that assists in protein folding, aids in trafficking of newly synthesized polypeptides, and helps dissolve protein aggregates [2-6]. In humans, Hsp70s have also been implicated in numerous diseases, including cancer, neurodegenerative disorders and viral infections [7-12]. However, the complexity of their functions has made studying the specific roles of Hsp70 challenging. Even for the relatively well-studied DnaK, there are numerous questions regarding how this chaperone carries out its myriad cellular tasks and, thus, its roles in disease and suitability as a drug target are uncertain.

2.1.2 *E. coli* Hsp70, DnaK, has ATPase Activity that is Tightly Controlled by its Co-chaperones, DnaJ and GrpE

DnaK (like all Hsp70 family members) consists of three domains: a 25 kDa substrate binding domain (SBD), a 45 kDa N-terminal nucleotide binding domain (NBD) that harbors ATPase activity and a 10 kDa helical "lid" region [2, 13]. Allosteric communication between these modules provides regulatory control. The ATP-bound form of DnaK has a "loose" configuration and weak affinity for peptide substrates [13, 14]. Hydrolysis of the nucleotide causes conformational changes in the adjacent SBD that enhance the affinity for the peptide substrate [2, 15]. Thus, ATP hydrolysis is one driving force behind chaperone structure and function. Importantly, DnaK's intrinsic rate of nucleotide hydrolysis is slow (~ 0.14 µmole ATP/µmole DnaK/min *vide infra*) when compared to other, typical ATPases, such as porcine Na,K-ATPase (~ 75 µmole ATP/µmole enzyme/min) [16]. This modest intrinsic rate permits tight regulation of the cycle by co-chaperones. For example, the binding of the co-chaperone, DnaJ, stimulates ATP hydrolysis (and, thus, enhances affinity for substrate), while the nucleotide exchange factor, GrpE, promotes ADP release to complete the catalytic cycle [17]. In addition to its role in ATP hydrolysis, DnaJ recruits DnaK into its various cellular functions and, consequently, there are typically more DnaJ-like proteins in a cell than core DnaK/Hsp70 chaperones [4, 18-22]. For example, there are six DnaJ homologs in *E. coli*, 22 in *Saccharomyces cerevisiae*, and 41 putative family members in humans. In this way, co-chaperones steer DnaK/Hsp70 into various combinatorial partnership and likely coordinate different responses to cellular stress, signaling or protein aggregation.

2.1.3 Chemical Modulators of Hsp70s Might Be Used as Research Tools and Potential Leads for Therapeutics: Lessons from the Related Chaperone, Hsp90

In contrast to the questions surrounding Hsp70 function, the roles of the related heat shock protein, Hsp90, are becoming increasingly well characterized. This is especially true in relation to Hsp90's prominent roles in cancer. In part, knowledge about Hsp90 has been accelerated by the availability of potent and selective chemical inhibitors, such as geldanamycin and radicicol [23]. In addition, these reagents have facilitated the development of anti-cancer drugs that are currently undergoing clinical trials [24-27]. This success suggests that a parallel "chemical genetic" approach might be used to dissect the complex Hsp70 network and, moreover, that this process might also lead to the discovery of new Hsp70-based therapeutics. Of particular interest are compounds that can selectively recognize specific DnaK-DnaJ combinations because these complexes are likely to be involved in only subsets of the total chaperone functions.

2.1.4 Despite the Importance of Hsp70, Only a Few Chemical Modulators Have Been Reported

As discussed in Chapter 1, only a handful of small molecules that bind DnaK or Hsp70 have been reported. Among the first partners identified was the polyamine, 15-deoxyspergualin (DSG), which binds Hsp70 in pull-down assays and, later, was found to enhance its steady-state ATPase activity by 20-40% [23, 28-31]. Based on structural similarity to DSG, a small-scale (~40 compounds) search for new Hsp70 modulators led

to the discovery of NSC 630668-R/1 (R/1), which inhibits ATPase activity and also blocks Hsp70-mediated trafficking of polypeptides [32]. More recently, another collection of ~30 dihydropyrimidines related to R/1 was studied using single-turnover ATP hydrolysis reactions [33]. In that work, unique classes of chaperone modulators were uncovered: some directly inhibited ATPase activity while others, such as MAL3-101, selectively blocked the ATPase-enhancing ability of specific J domain proteins [33]. Interestingly, despite their diverse activities, many known Hsp70-binding compounds share a central dihydropyrimidine core and only vary in their pendant functionality. However, this is not the only chemical scaffold that has affinity for Hsp70-class proteins. For example, a family of acylated benzamido derivatives was reported to bind DnaK's SBD, inhibit its chaperone function, and thereby display antibacterial activity [34]. Thus, multiple chemical classes have been reported to modify Hsp70's functions. Despite the potential uses of these reagents, structure activity relationships (SAR) that govern potent effects on ATPase activity are not yet clear. One factor contributing to this lack of information is that only a small number of compounds have been screened in low-throughput formats. We hypothesized that a high throughput screen (HTS) would be a useful platform for identifying new, potent chemical modulators and discerning SAR between similar compounds.

2.1.5 Our Strategies of Developing High Throughput Screens against Hsp70s

Surprisingly, Hsp70 has not been subjected to extensive HTS. In contrast, a number of different assays have been developed to uncover new inhibitors of Hsp90 [35-39]. One

of these platforms employed the inorganic phosphate chelator, malachite green (MG), to monitor the ATPase activity of Hsp90 [38]. The MG assay is colorimetric and has the advantages of being robust, cost effective, and suitable for automated screening [40-42]. These advantages led us to explore whether this method could be employed to screen for compounds that alter the ATPase activity of DnaK. Because of DnaK's relatively slow ATP turnover rate, this assay required modification to improve the signal and reduce the noise from spontaneous nucleotide hydrolysis. Importantly, we found that, using optimized conditions, the signal was linear for up to 4 hours; therefore, an end-point measurement was sufficient to represent the steady-state rate. Using this assay, we discovered 7 new inhibitors of DnaK from a focused collection of 204 dihydropyrimidines. Next, we sought to identify more chemical scaffolds by screening larger compound collections in high throughput ATPase assays. Unfortunately, our attempts to further miniaturize the absorbance platforms to low volume 384-well microtiter plates were frustrated by significantly decreased sensitivity. Guided by the work of Zuck and coworkers [43], we explored whether sensitivity could be enhanced using energy transfer methodology. Briefly, we found that the fluorescence method improved sensitivity for phosphate and permitted screening of over 55,000 compounds with good assay performance (Z' ~ 0.6, CV ~ 8%). These experiments yielded at least one new inhibitor of DnaK, which appears to block stimulation by DnaJ. In sum, we developed a useful platform for discovering small molecule modulators against DnaK. These selected compounds, in turn, might be applied as chemical genetic tools to understand DnaK's biology and they might be used in the future development of

medicines that target Hsp70-related diseases.

2.2 Results

2.2.1 Influence of DnaK Concentration and ATP on the Malachite Green Signal

In an effort to adapt an existing MG-based method [38] for use in monitoring DnaK's ATPase activity, we first measured OD_{620} while varying the concentration of DnaK and ATP. We found that, between 0.3 µM and 0.9 µM, the signal increased with DnaK levels (**Figure 2.1A**). At constant DnaK (0.6 µM), ATP concentration was varied from 0.13 to 8.0 mM, and we found that, above 4 mM, the OD_{620} was independent of nucleotide (**Figure 2.1B**). Based on these studies, we chose 0.6 µM DnaK and 1 mM ATP for screening conditions because these parameters provided good signal:noise values while minimizing reagent costs.

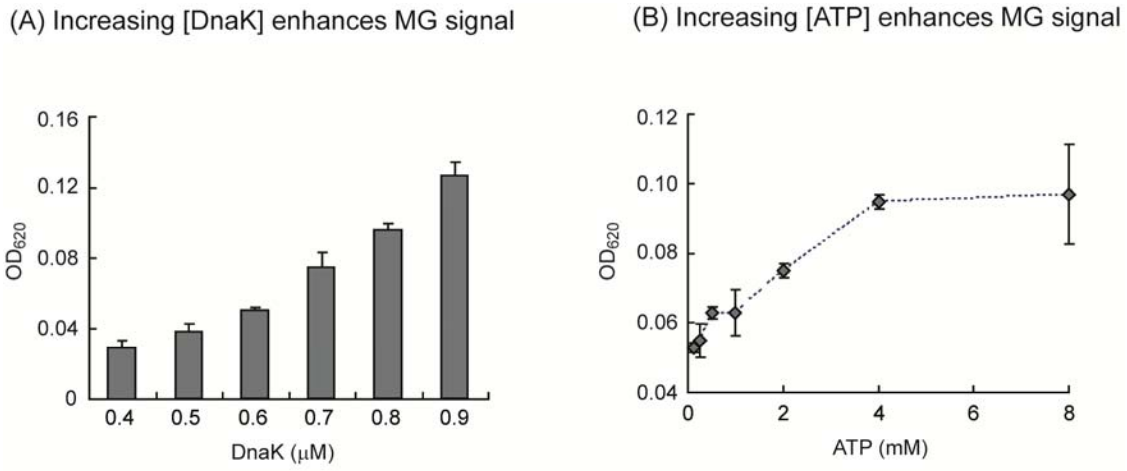

Figure 2.1 Dependence of MG signal on the concentration of DnaK and ATP. (A) The concentration dependence of DnaK was observed at 1 mM ATP. (B) DnaK was fixed at 0.6 µM while changing the concentration of ATP. The OD_{620} value of the ATP control (OD_{620} = ~ 0.25) was subtracted in all figures shown. These results are the average of triplicate and the error is standard deviation.

2.2.2 Influence of DnaJ and GrpE Concentration on MG Signal

During its normal physiological function, DnaK is assisted by the action of DnaJ and GrpE [2, 17]. Moreover, certain small molecules that are known to modulate Hsp70's ATPase activity are only active in the presence of co-chaperones [33]. Therefore, we sought to develop a screen protocol that includes these components. Our approach was to vary the levels of recombinant DnaJ or GrpE and monitor their effects on ATP hydrolysis by DnaK. In these studies, we were interested in both the rate enhancement and the co-chaperone concentration that yielded half-maximal stimulation ($K_{0.5}$). Rate enhancement is calculated by comparing the turnover rate of the co-chaperone-stimulated system against the rate due to DnaK alone and the $K_{0.5}$ can be used to approximate the affinity for DnaK. Using the MG assay, we found that the $K_{0.5}$ of DnaJ was around 0.8 μM, and that it provided up to ~11-fold stimulation of ATPase activity (**Figure 2.2A**). On the other hand, GrpE had better apparent affinity for DnaK

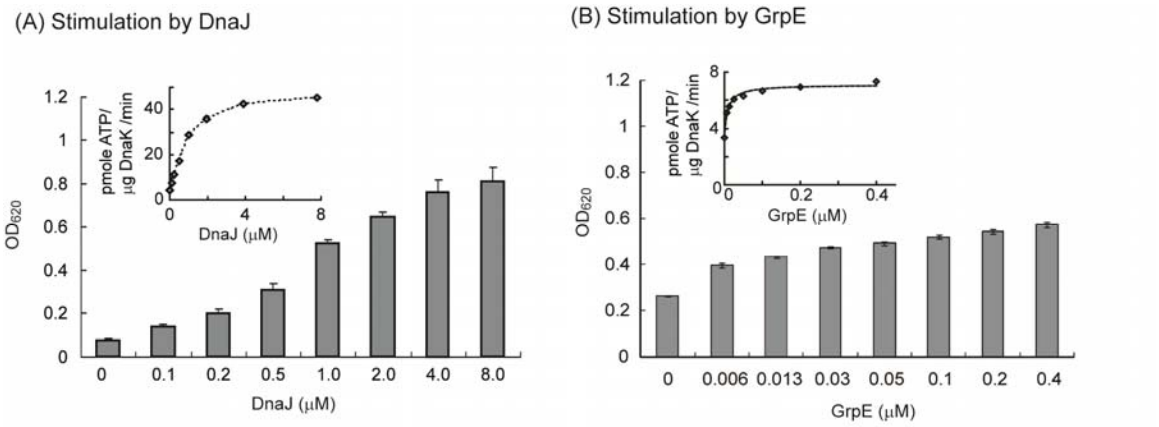

Figure 2.2 The stimulatory effect of co-chaperones, DnaJ and GrpE. The ATPase activity of DnaK at different concentrations of (A) DnaJ and (B) GrpE was measured at 1 mM ATP and 0.6 μM DnaK. The OD_{620} signal was determined after 3 hours incubation at 37°C. In the insets, the OD_{620} values were converted into ATP hydrolysis rates based on a standard curve. The GrpE protein used in this figure was purified as indicated in the experimental procedure section of Chapter 4. These results are the average of triplicate and the error is standard deviation.

($K_{0.5}$= 0.01 μM) but only stimulated ATPase activity approximately 2-fold (**Figure 2.2B**). These results are generally consistent with the findings of McCarty *et al*., who used single turnover ATP assays to define that when DnaK was fixed at 0.7 μM, 1.4 μM DnaJ and 0.7 μM GrpE stimulate DnaK ATPase by 13 fold and 1.3 fold, respectively [44]. Next, we were interested in finding a ternary combination that would provide the most robust signal and the broadest dynamic range because this information could be used to select optimal screening conditions. To explore this idea, we fixed the concentration of DnaK (0.6 μM) and either DnaJ (1.0 μM) or GrpE (0.9 μM) and changed the concentration of GrpE or DnaJ, respectively. We discovered that, at a saturating level of GrpE, the $K_{0.5}$ of DnaJ increased to around 3.1 μM and ATPase activity was stimulated an additional 15.5-fold compared to the DnaK:GrpE complex in the absence of DnaJ. This ternary combination lead to a 130-fold stimulation over DnaK alone (**Figure 2.3A**). Alternatively,

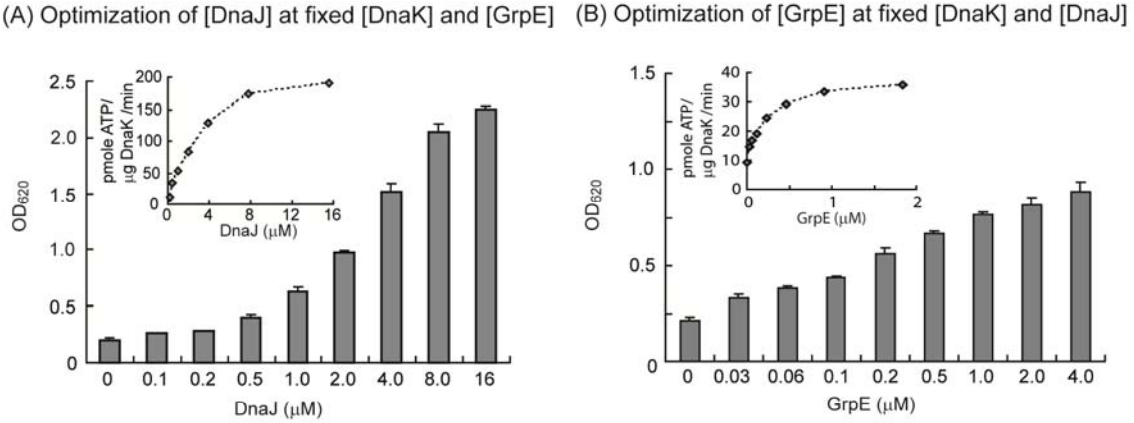

Figure 2.3 Optimization of the concentrations of DnaJ and GrpE for screening. (A) DnaJ stimulates ATP hydrolysis at fixed DnaK (0.6 μM) and GrpE (0.9 μM). (B) GrpE promotes the ATPase activity of 0.6 μM DnaK and 1.0 μM DnaJ. In the insets, the OD_{620} values were converted into ATP hydrolysis rates based on a standard curve. The OD620 value was determined after 1.5 hours incubation at 37°C. These results are the average of triplicate and the error is standard deviation.

when DnaJ and DnaK were held constant, the $K_{0.5}$ of GrpE did not change. Under these conditions, we observed a 3.5-fold stimulation over DnaJ alone and only a 30-fold total

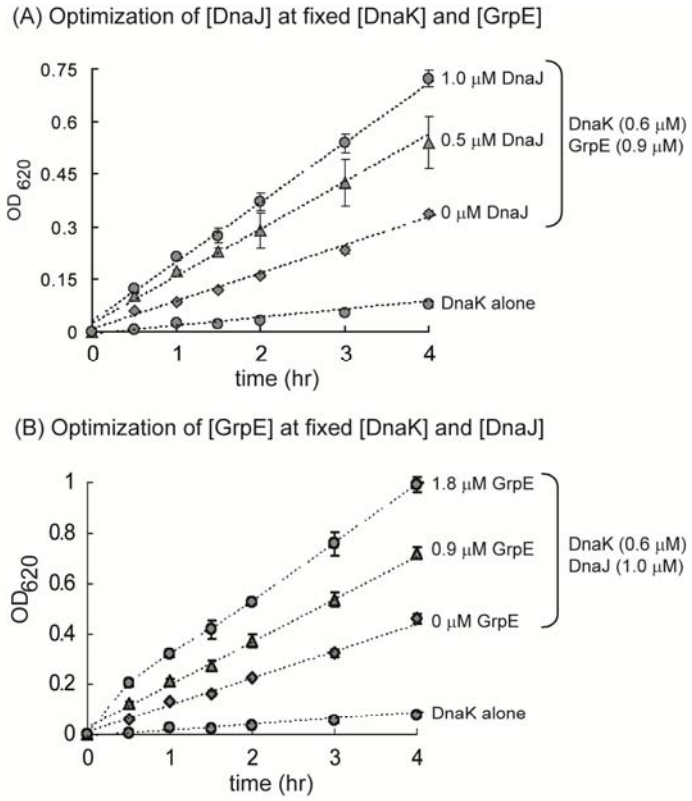

Figure 2.4 ATPase activity over time at different combination of co-chaperones. (A) Variable concentrations of DnaJ were mixed with 0.6 μM DnaK and 0.9 μM of GrpE. (B) The DnaK (0.6 μM) and DnaJ (1.0 μM) concentrations were fixed, whereas different amount of GrpE was added. At given times, the reaction was stopped and the OD620 value measured. These results are the average of triplicate and the error is standard deviation.

increase in ATP hydrolysis (**Figure 2.3B**). Next, the rate of DnaK's ATPase activity over time was measured at different combinations of DnaK, DnaJ, and GrpE. A linear increase was observed in all conditions up to 4 hours (**Figure 2.4**). Finally, we sought to ensure that this platform faithfully reproduces known kinetic parameters of the enzyme. The V_{max} and k_{cat} of each reaction condition were calculated and, as shown in **Table 2.1**, we found that these parameters were in good agreement with previous data [44, 45]. Thus, we hypothesized that, despite the slow turnover rate of DnaK alone, these

co-chaperone-stimulated conditions appeared to provide sufficient signal for screening.

Table 2.1 Calculated and reported V_{max} and K_{cat} values for DnaK system

DnaK (μM)	DnaJ (μM)	GrpE (μM)	V_{max} (pmole ATP/ug DnaK/min	$K_{cat}(min^{-1})$	ref.
0.58	0	0	1.9± 0.12	0.12± 0.01	This work
0.58	0	0.91	6.5± 0.14	0.45± 0.01	This work
0.58	0.48	0.91	11 ± 0.56	0.75± 0.04	This work
0.58	0.97	0.91	14 ± 0.59	0.94± 0.04	This work
0.58	0.97	0	8.6± 0.24	0.59± 0.02	This work
0.58	0.97	1.8	17 ± 0.72	1.1 ± 0.05	This work
0.69	0	0	0.65		[49]
0.93	0	0	2.29	0.16	[50]
0.69	0	0.69	0.87		[49]
0.69	1.40	0	8.25		[49]

2.2.3 Screen a Focused Chemical Library against the DnaK-DnaJ-GrpE Enzyme Mix

Using the optimized reaction conditions, we screened a small chemical library for compounds that modulate DnaK activity. This collection is composed of 204 dihydropyrimidines that are structurally similar to the lead candidate, MAL3-101 [33]. These compounds were assembled from three sources: “cherry-picked” molecules from commercially available collections, those synthesized by the University of Pittsburgh’s Center for Chemical Methodologies and Library Development (UPCMLD), and those generated internally by our group. Together, these compounds form a focused library from which we sought to identify potent modulators of DnaK.

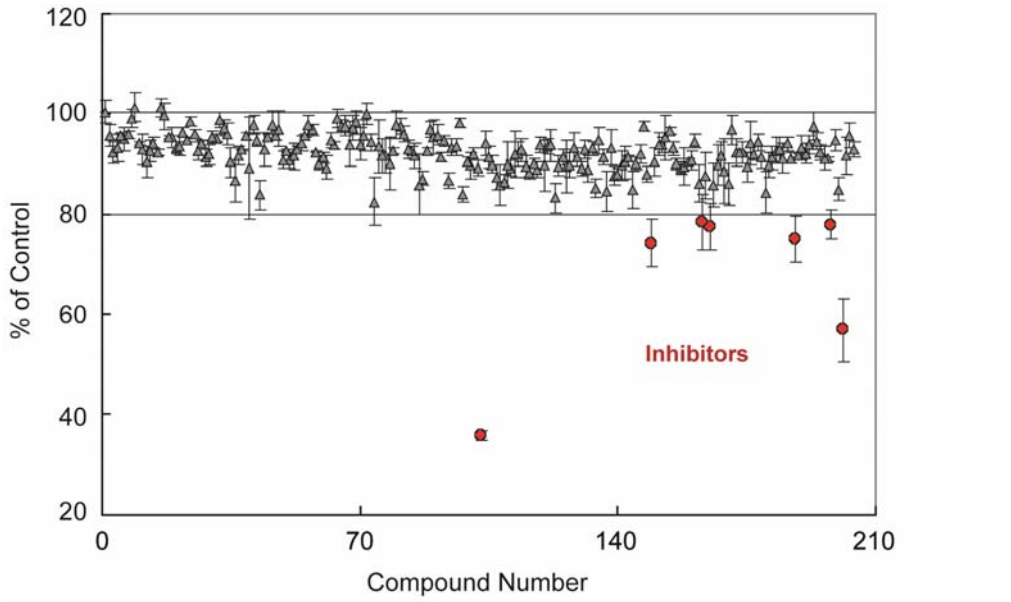

Figure 2.5 Screening of a 204-compound focused library. Each spot represents the average of triplicate wells for a single compound and the error is standard deviation. Triplicates were performed to demonstrate that screening results are reproducible. All compounds were screened at 200 μM with 0.6 μM DnaK, 1.0 μM DnaJ, 0.9 μM GrpE, 0.01% Triton X-100, and 1 mM ATP. Compounds resulting in <80% original DnaK ATPase activity were defined as inhibitors. As a control, 200 μM each compound was incubated with 1 mM ATP and 0.01% Triton X-100 and the resultant OD_{620} value was subtracted from the measured signal at the presence of DnaK, DnaJ, and GrpE for the specific compound before calculating the percentage of control activity.

Using the MG assay, we screened each compound individually at 200 μM in 96 well plates. During our first screening attempt, we found that most (~90%) of the compounds displayed weak ATPase-stimulating ability (**Appendix 2.5.1A**). We suspected that this might result from nonspecific binding of the largely hydrophobic compounds to the SBD. It has been reported that detergents can remove promiscuous hits and improve the reliability of HTS methods [46]. Therefore, we repeated the screen in the presence of 0.01% Triton X-100 (**Figure 2.5**). Consistent with our hypothesis, the mild stimulation effects disappeared. Moreover, the activity of the inhibitors remained largely unchanged or became more pronounced. We defined compounds that decreased activity >20% as inhibitors and, by this definition, 7 candidates were identified (3.5% of the library; **Table**

2.2). These results demonstrated that the MG assay can be used to readily screen a chemical collection.

Table 2.2 Distribution of the screening results

Class	% Control	Hits	% Total Compounds
Inhibitor	< 50	1	0.5
	50 ~ 80	6	3
Inactive	80 ~ 90	46	23
	90 ~ 100	149	73

2.2.4 Confirming "Hits" from the Screen

Based on their availability and synthetic tractability, we selected 4 of the 7 inhibitors, 0116-2F, 0116-4G, 0116-7G and 0116-9E, for further study (**Figure 2.6**). First, we determined their IC_{50} values by varying compound concentration between ~50 and 400 µM and studying the effects on DnaK's ATPase activity. Importantly, we found that the inhibitory effect was reproducible and the IC_{50} values were between 120 and 200 µM (**Figure 2.6**). At saturating concentrations, 0116-4G, 0116-7G, and 0116-9E provide ~50% inhibition of DnaK ATPase activity whereas the potency of 0116-2F is modest (80% original activity). The effects of the validated inhibitors were independent of detergent (**Appendix 2.5.1B**).

2.2.5 Characterization of the Binding of Candidate Compounds to DnaK

The substrate-binding domain (SBD) of DnaK has affinity for exposed hydrophobic regions on unfolded polypeptides. Because the selected inhibitors all have hydrophobic

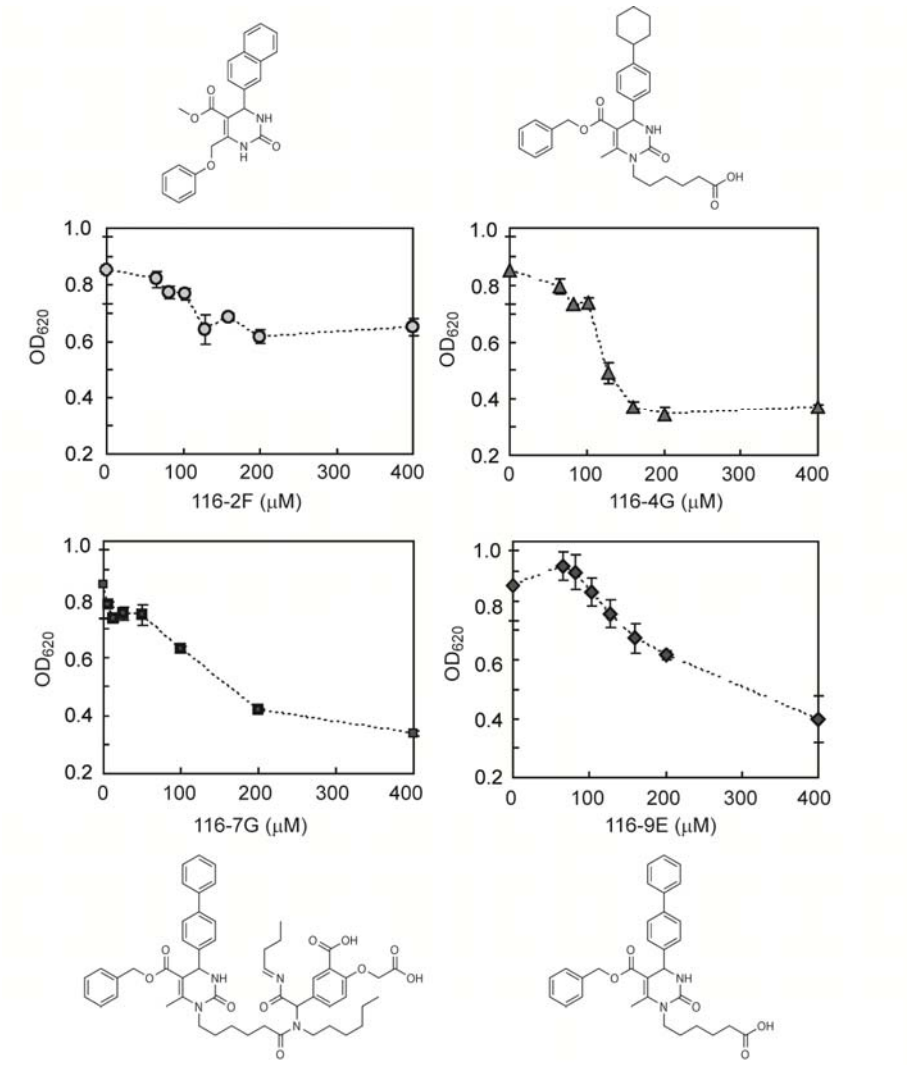

Figure 2.6 Dose dependence curves and IC_{50} values for selected inhibitors.
The curve was fitted in GraphPad Prism using the equation: y=Min + (Max-Min)/ (1+10^((LogIC50-x)*HillSlope)); (x = log[compound]).

regions, we assumed that they might bind to SBD. To test this hypothesis, we used a known Dnak substrate (NRLLLTG) to compete for the SBD binding site [47]. First, we confirmed that the peptide stimulates ATPase function as previously reported [48]. In these studies, we found that the peptide provides ~5-fold stimulation at concentrations above 100 μM (**Figure 2.7**). Next, we explored the activity of the candidate compounds, 0116-2F, 0116-4G, 0116-7G and 0116-9E, in the presence of saturating levels of peptide.

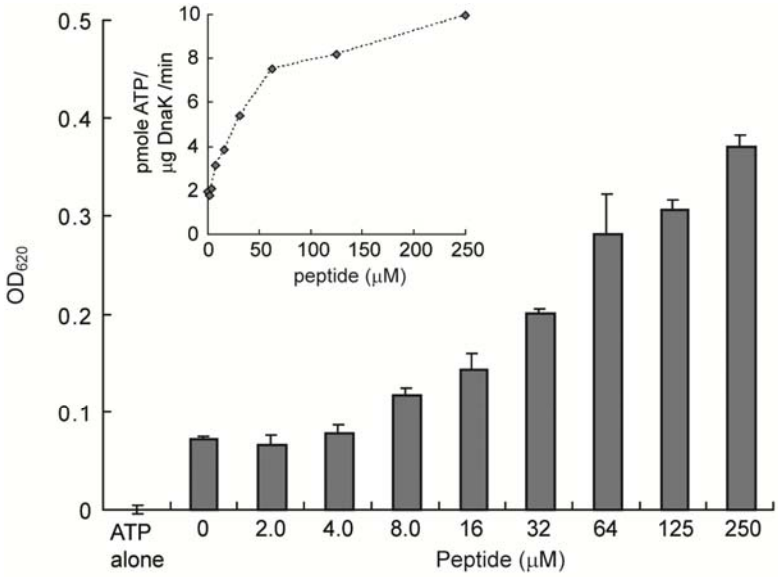

Figure 2.7 Peptide substrate stimulates ATPase activity. The experiment was carried out at 0.6 μM DnaK, 1 mM ATP, and the OD_{620} signal was measured after 3 hours incubation at 37 °C. In the inset figures, the OD_{620} values were converted into ATP hydrolysis rates based on a phosphate standard curve. These results are the average of triplicate and the error is standard deviation.

In these experiments, geranylgeraniol, with a structure similar to reported SBD-binding anti-bacterials [34], was also included as a control; we expected that peptide substrates would compete with this compound for binding to the SBD. Consistent with this idea, the ATPase enhancing activity of geranylgeraniol was eliminated (**Figure 2.8A**). Intriguingly, for 3 out of 4 selected compounds, inhibition remained largely unchanged in the presence of peptide (**Figure 2.8B and Appendix 2.5.2**). These experiments suggest that the dihydropyrimidines act via a site independent of the substrate-binding groove of the SBD to modulate ATPase activity. These compounds and their derivatives have been further studied in secondary assays by other members of the Gestwicki group (Wisen et al. 2008 Anal. Biochem.; Wisen et al. 2008 Bioorg. Med. Chem. Lett.; Wisen et al. 2010 ACS Chem. Biol.) and they have been used to explore the roles of Hsp70 in tau biology

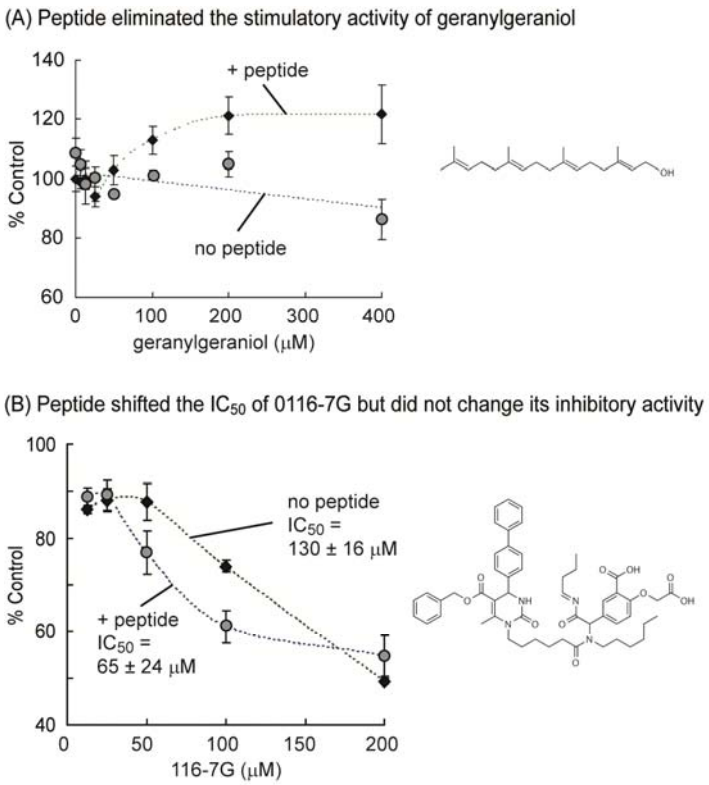

Figure 2.8 Dose dependence of (A) geranylgeraniol, and (B) inhibitor, 0116-7G in the presence and absence of 50 μM SBD-binding peptide. These results are the average of triplicate and the error is standard deviation.

(Jinwal et al. 2009 J. Neurosci). Moreover, this assay has become a "workhorse" method in our group to identify an characterize new inhibitors of Hsp70.

2.2.6 Using Energy Transfer to Convert the Colorimetric Phosphate Assay into a Fluorescence Format Method in 384-well, White Low-Volume Plates

Our next goal was to screen larger compound collections to identify new scaffolds that inhibit DnaK or other Hsp70 family members. However, in preliminary studies, we found that the colorimetric, absorbance-based MG assay described above had poor performance in 384-well plates (data not shown). This finding wasn't too surprising, as it is well known that absorbance-based assays have reduced sensitivity in higher density

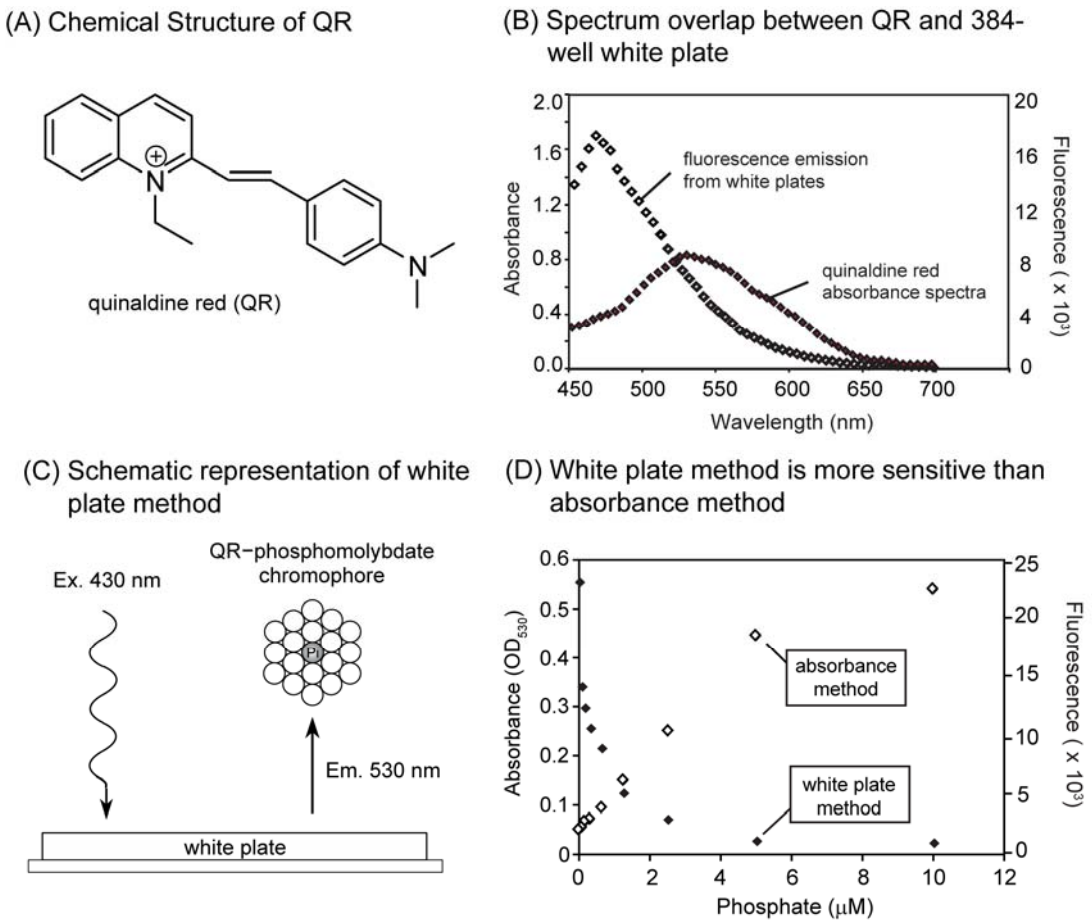

Figure 2.9 Model for converting an absorbance assay into a fluorescence quenching method. (A) Chemical structure of quinaldine red (QR). (B) Overlap between QR-phosphomolybdate chromophore and intrinsic fluorescence of white opaque 384-well plates. When irradiated at 430 nm, white plates emit broadly between 450 and 550 nm. (C) Schematic representation of white plate method. Fluorescence emission from white plates is quenched by QR in the presence of molybdate and inorganic phosphate (spheres). (D) Comparison of sensitivity for phosphate between absorbance and fluorescence methods. Results are the average of at least triplicates and error bars are standard error of the mean (some bars are smaller than the symbols).

formats. The primary technical challenge in performing absorbance assays in high-density formats, such as 384- and 1536-well plates, is that the sensitivity is typically decreased ~2.5 fold by the restrictive well geometry [49, 50]. In addition, absorbance assays demand flat, clear-bottomed microtiter plates that consume more reagents than other well geometries (*e.g.* round, concave). However, absorbance assays are often

inexpensive and robust, so there is interest in finding ways to adopt them to higher density. One promising approach was reported by Zuck *et al.*, who successfully converted a QR-based phosphate assay for use in 384-well format (**Figure 2.9A**) [43]. They observed that when white, opaque microtiter plates are irradiated at 430 nm, they emit fluorescence in a broad range between approximately 450 and 600 nm (**Figure 2.9B**). Because the QR-complex absorbs light at 530 nm, the emission from wells containing phosphate is quenched; thus, this simple modification converts the absorbance assay into a fluorescence-quenching format (**Figure 2.9C**). Zuck and colleagues found that this strategy improves sensitivity because both the fluorescence emission and excitation are absorbed by the chromophore [43]. Further, the Walt group has explored the mechanistic underpinnings of a similar process, and they found that both radiative and non-radiative energy transfer events contribute to improved sensing [51].

Based on these findings, we became interested in using this approach to screen for new inhibitors of DnaK. Before adapting this platform for use against DnaK, we were first interested in discerning the lowest concentration of phosphate that could be robustly detected. Accordingly, we prepared phosphate standard solutions and directly compared the sensitivity of the absorbance- and fluorescence-based methods. For these experiments, we found that the linear detection range of the absorbance method was approximately 0.5 to 5 μM (**Figure 2.9D**), in agreement with previous reports [52]. We found that the white plates gave a linear range of approximately 0.06 to 0.6 μM, an

approximately 10-fold improvement in sensitivity.

2.2.7 Fluorescence Method Has Superior Performance in Pilot Screens.

To our knowledge, a high throughput screening application of this fluorescence method has not yet been reported. Therefore, we first performed a pilot screen in 384-well plates to gauge its performance. Briefly, we found that the combination of 0.4 μM DnaK and 0.7 μM DnaJ gave a signal that was linear for at least 2-3 hours when incubated with 1 mM ATP (**Appendix 2.5.3**). From these experiments, we developed a protocol that was adopted from the previous 96-well version (**Figure 2.10A**) [53]. For calculation of Z' scores, we defined the negative control as the signal from enzyme plus DMSO and the positive control as buffer plus DMSO (see below). Using these conditions, we screened the MS2000 collection of bioactive compounds. We had previously screened this collection in the 96-well version of the assay and, thus, we knew it contained five DnaK inhibitors; thus, it could be used to probe the performance of the 384-well version [54]. Also, we directly compared the absorbance and energy transfer methods by splitting the reactions into either clear plates or low volume, white plates. Using this side-by-side approach, we confirmed our previous observations that the absorbance-based assay is a relatively poor HTS method, with a Z' score of approximately 0.2. Moreover, this method only identified one of five known inhibitors and it gave two false positives (**Figure 2.10B**). In contrast, the fluorescence method yielded a Z' score of 0.6 and it correctly identified all five known inhibitors. We also confirmed that the fluorescence method could accurately replicate the IC_{50} of one inhibitor (myricetin) (**Appendix 2.5.3**). Together,

(A) Detail protocol of 384-well fluorescence based method

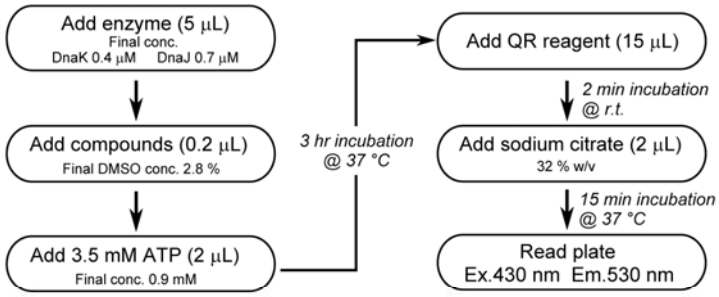

(B) Fluorescence-based method identify more known inhibitors than absorbance-based method in the pilot screen

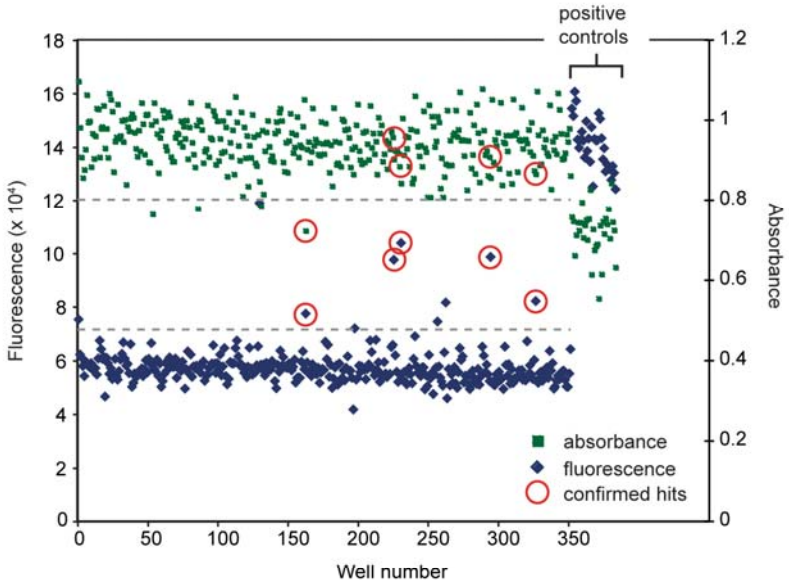

Figure 2.10 Comparison of screening performances between absorbance and fluorescence methods. (A) Detailed protocol for fluorescence quenching method in 384-well plates. (B) Representative data from the side-by-side pilot screen for absorbance method and fluorescence method. Each dotted line represents three times standard deviation from the negative control. Data points for known inhibitors (as determined from previous 96-well assays) are circled. Fluorescence based method successfully identified all of the five known inhibitors whereas absorbance based method only detected one. The fluorescence method yielded ~4-fold higher signal-to-noise ratio than the absorbance method

these results suggest that the fluorescence method is suitable for screening in low volume 384-well plates.

2.2.8 384-well Based High Throughput Screen for Inhibitors of DnaK's ATPase Activity

Based on the promising results from the pilot experiments, we screened an additional 55,400 small molecules and natural product crude extracts against the ATPase activity of DnaK-DnaJ (**Figure 2.11A**). In these experiments, we found that the Z' factors ranged from 0.10 - 0.75 with an average of 0.58 (**Figure 2.11B**). Interestingly, we found that the occasional poor Z' values were partially attributable to plates with intrinsic fluorescence that were either significantly above or below average (See **Appendix 2.5.4**). Because these microtiter plates were not originally manufactured for use in fluorescence applications, we expect that the amount of fluorescent material may be unevenly distributed, resulting in occasional plates with higher or lower signal. These unsatisfactory plates (Z' value < 0.4) were excluded from further analyses (3 % of total plates), increasing the average Z' score to 0.60. More recently, we have started "pre-screening" fresh, empty plates to remove these outliers.

Samples were screened at a single concentration (between 10 to 40 μM) against DnaK-DnaJ, with the addition of 0.01% Triton X-100 to minimize false discovery of aggregators. From these screens, samples that exhibited effects of 35% or higher by plate were considered inhibitors. Samples with signals at least 3-times the standard deviation from the negative controls and samples on their given plate were also included. Of 55,400 samples tested, 598 fell into this category (hit rate: 1.1 %). In our previous studies, activators of Hsp70s have also proven to be powerful chemical tools [54, 55]. With the aim of potentially expanding the number of activators, the HTS results were

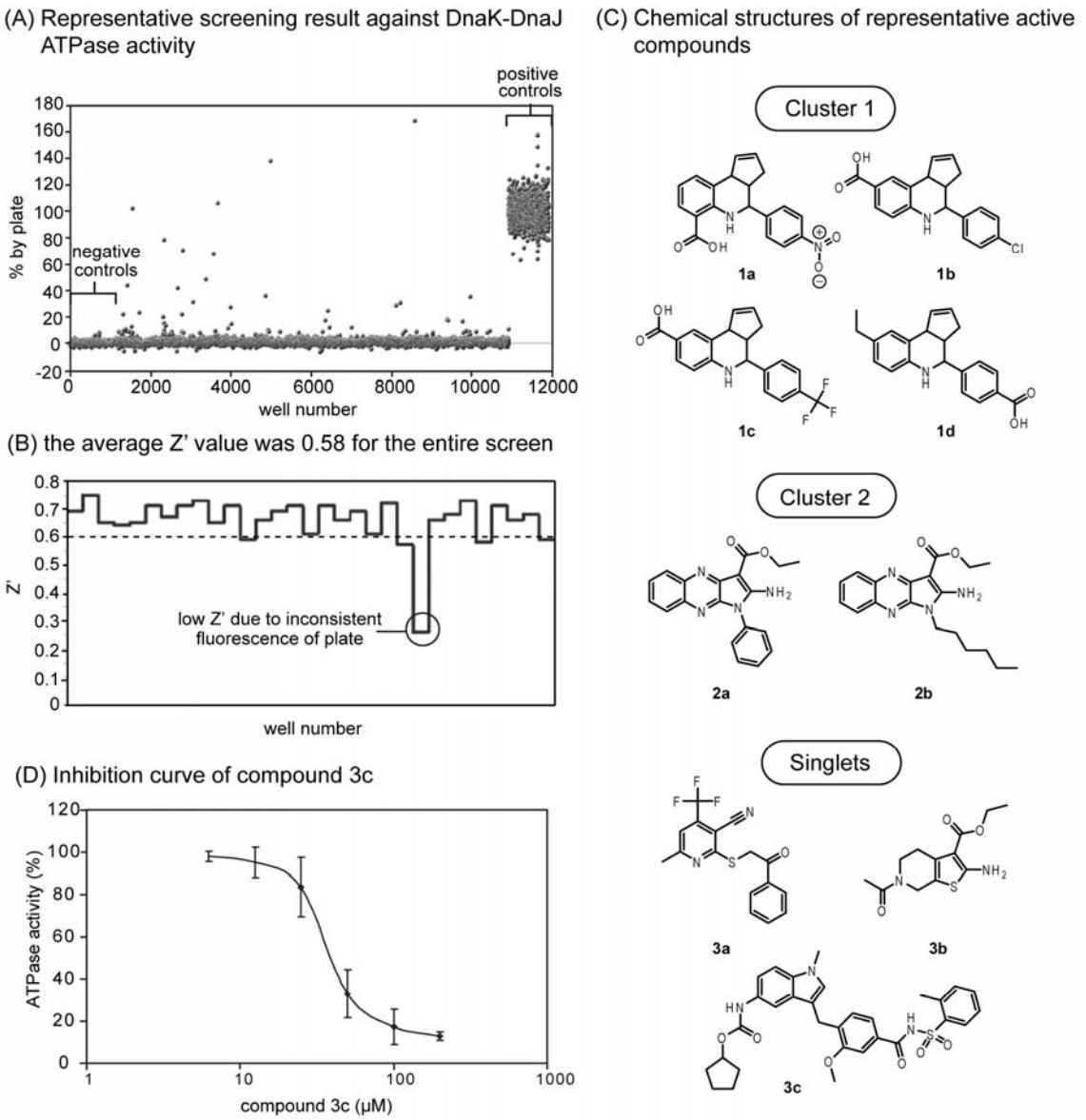

Figure 2.11 Screening of 55,400 samples. (A) Representative data from the screening campaign. Positive controls (buffer plus DMSO) and negative controls (enzyme plus DMSO) are shown. Some examples of false positives are clearly shown above the 100% line. (B) Representative Z' values by plate from the screen. The average Z' for the entire screening was 0.58. We observed occasional low Z', which is likely due to plates' irregular fluorescence properties (circled). (C) Chemical structures of representative active compounds. A total of 36 inhibitors were identified in this screen; 26 cluster I compounds, 6 cluster II and 4 singlets. The structures of the re-tested compounds are shown. (D) Inhibition curve for compound 3c. IC_{50} value was calculated to be 37 ± 1 μM. The assay was performed in triplicates and error bars represent standard error of mean.

reviewed for samples with signals of -2.5 standard deviations or lower. Using this modest criterion, 122 unique samples were identified as activators (hit rate: 0.22 %).

To confirm their activities, the samples were subjected to confirmatory retesting in duplicate. Prior to this experiment, 10 compounds containing a heavy metal and 11 compounds with a molecular weight above 650 Da were excluded, because they were expected to have unfavorable properties. In addition, the natural product extracts were excluded and their analysis will be reported elsewhere. Thus, a total of 508 unique compounds (400 inhibitors and 108 activators) were assayed and 73 inhibitors confirmed. None of the activators confirmed upon retesting, although it should be noted that they only exhibited weak activity in the primary screen and the assay conditions were optimized to identify inhibitors. The Z' factors for the confirmation assay ranged from 0.65 and 0.70.

The confirming structures were subsequently clustered to determine if series were present. Clustering at 65% + similarity with the fingerprints (Unity) and clustering algorithms (Optisim) by Benchware DataMiner produced 55 clusters. It has been shown that a compound with 85% or greater structural similarity to an active compound will have a ~30% probability of also being active [56]. Therefore, we analyzed our internal database of ~150,000 compounds and retrieved structures that have 85% or greater similarity to any of the confirmed inhibitors. Based on this analysis, we selected 76 compounds that belong to three largest clusters for testing in dose dependence assays. These assays were performed using a 2-fold dilution series of eight compound concentrations (1 to 125 μM). Of the 127 compounds tested, 70 showed dose dependent

inhibition curves. In order to minimize false positives, these 70 compounds were then evaluated for autofluorescence. Briefly, compounds were excluded if their intrinsic fluorescence (Ex: 430 nm, Em: 530 nm) at 5 μM was at least 10% of the positive control or if their dose dependence plateau was above the positive control (see examples in **Figure 2.11A**). These filters excluded 34 samples, leaving 36 unique compounds as potential DnaK-DnaJ inhibitors. These compounds were clustered to reveal six unique chemical scaffolds. Finally, each of these compounds was manually reviewed for the possession of reactive groups such as Michael acceptors, epoxides, and free thiols. However, none of them had such functional groups.

To further evaluate the identified actives, we repurchased four examples that belong to the largest cluster (cluster I, containing 26 of the 36 remaining compounds); **1a** (4-(4-nitrophenyl) -3a,4,5,9b-tetrahydro-3H-cyclopenta[c]quinoline-6-carboxylic acid) (ChemBridge, cat. 5585430), **1b** (4-(4-chlorophenyl)-3a,4,5,9b-tetrahydro-3H-cyclopenta[c]quinoline-8-carboxylicacid) (ChemDiv, cat. 2374-0013), **1c** (4-(3-(trifluoromethyl)phenyl)-3a,4,5,9b-tetrahydro-3H-cyclo-penta[c]quinoline-8-carboxylic acid) (ChemDiv, cat. 5408-1849), **1d** (4-(4-ethylphenyl)-3a,4,5,9b- tetrahydro-3H-cyclopenta[c]quinoline-8-carboxylic acid) (ChemDiv, cat. 6415-0967) (**Figure 2.11C**). Unexpectedly, none of these compounds were inhibitors upon re-testing. These samples were subsequently subjected to a side-by-side assay against the original stock solutions. Interestingly, the two series had significantly

different inhibitory profiles; the “old” samples were highly active whereas the repurchased compounds were inactive. Despite these differences, analysis by mass spectrometry and ^{1}H NMR suggested that both sets of compounds were relatively pure and that they had the correct molecular formulae. One potential clue to this discrepancy came from observations made during the assay setup, in which we noticed differences in the color of these samples. Specifically, over the span of 5 days at room temperature in DMSO, the re-purchased compounds would eventually become slightly colored. Moreover, these aged samples now had anti-DnaK ATPase activity upon re-testing. Based on the reported synthesis of this scaffold [57] and the presence of a free acid in the active structures, we suspected that the color difference (and perhaps the activity differences) might arise due to metal chelation. Indeed, treatment with EDTA inhibited the color change and extraction of the "active" form with an EDTA solution led to a loss of its activity (data not shown). Thus, we concluded that the active sample appears to involve a metal and no further investigation was pursued.

Compounds belonging to the other clusters were studied in a similar manner. Briefly, we repurchased two compounds from cluster II [**2a** (ethyl 2-amino-1-phenyl-1H-pyrrolo[2,3-b] quinoxaline-3-carboxylate) (ChemDiv, cat. 5122-1769), **2b** (ethyl 2-amino-1-hexyl-1H-pyrrolo [2,3-b]quinoxaline-3-carboxylate) (ChemDiv, cat. 6256-4951)] and the three singlets that were available for resupply [**3a** (6-methyl-2-((2-oxo-2-phenylethyl)thio)-4-(trifluoromethyl) nicotinonitrile) (ChemDiv, cat. 3076-0200), **3b** (ethyl 6-acetyl-2-amino-4,5,6,7-tetrahydrothieno

[2,3-c]pyridine-3-carboxylate) (ChemDiv, cat. K813-0112), **3c** (cyclopentyl (3-(2-methoxy-4- ((o-tolylsulfonyl)carbamoyl)benzyl)-1-methyl-1H-indol-5-yl) carbamate) (Cayman Chemical Inc., cat. 10008282)]. We confirmed the structure of these compounds by mass spectrometry and then determined their IC_{50} values. Compounds **2a**, **2b**, **3a** and **3b** had poor activity (> 500 μM) and were not further pursued. However, compound **3c** inhibited ATPase activity with an IC_{50} value of 37 ± 1 μM (**Figure 2.11D**). Previously identified, allosteric Hsp70 inhibitors also have relatively modest, micromolar IC_{50} values [58]. Thus, the activity of **3c** is comparable to some of the known compounds.

2.2.9 Compound 3c Binds DnaK, Favors High Affinity Binding to Luciferase and Blocks DnaK's Stimulation by DnaJ

To characterize compound **3c** in secondary assays, we first investigated its ability to directly bind DnaK. Using tryptophan fluorescence, we found that the compound bound the chaperone with an estimated K_D of 13 ± 1.7 μM, in relatively good agreement with the IC_{50} value from the ATPase assay (**Figure 2.12A**). Next, we wanted to explore how compound **3c** might influence the structure of DnaK and, specifically, its interactions with substrates. As mentioned above, the ATP-bound form of DnaK has relatively poor affinity for substrate, while the ADP-bound form has enhanced affinity (**Figure 2.12B**) [59]. To test whether compound **3c** might change DnaK's apparent affinity for substrate, we measured binding of the chaperone to the model substrate, firefly luciferase (**Figure 2.12B**). By this method, the affinity of DnaK for luciferase was 260 ± 50 nM (**Figure 2.12C**) and addition of compound **3c** significantly improved the apparent affinity (**Figure 2.12D**).

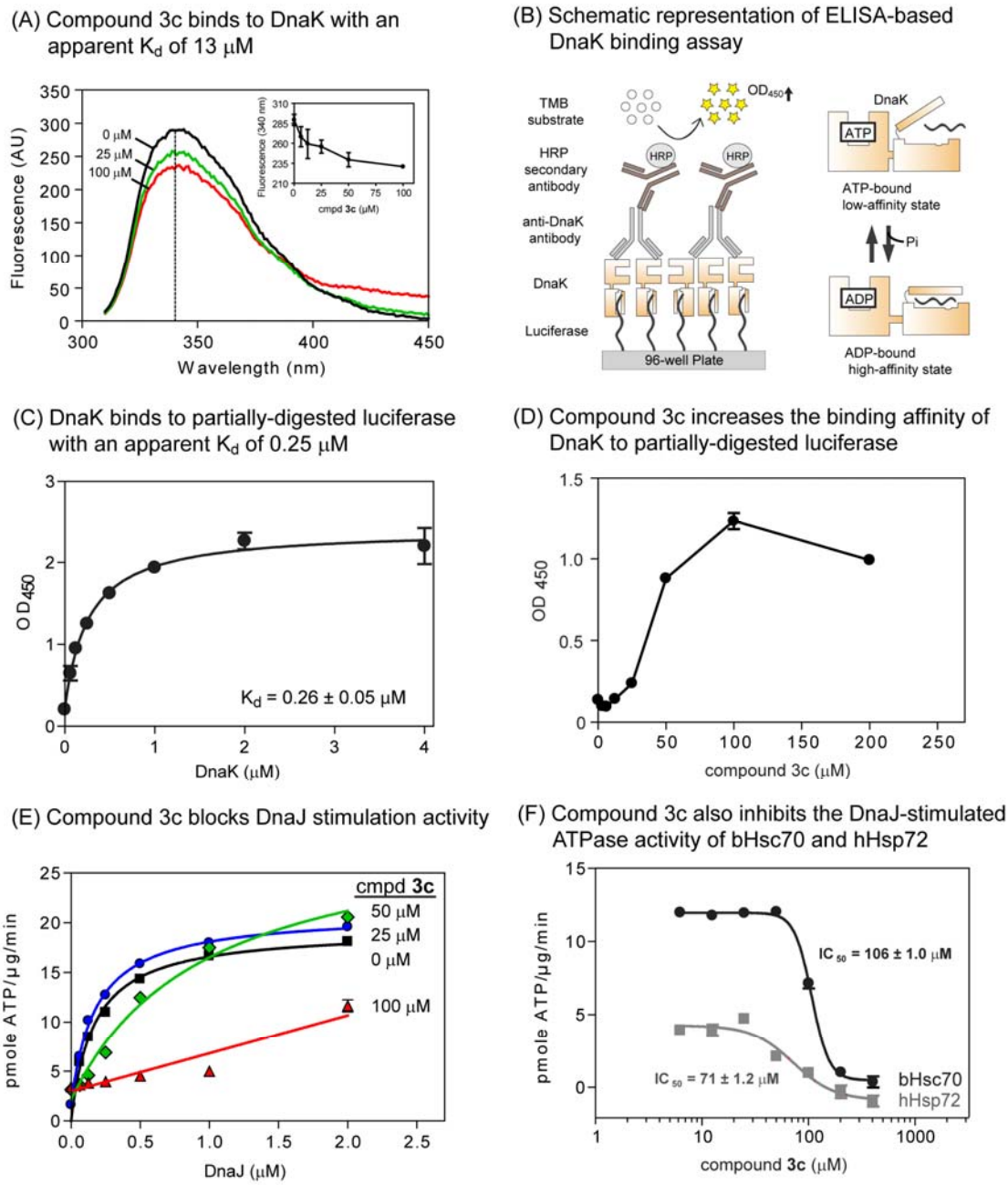

Figure 2.12 Compound 3c binds DnaK and blocks DnaJ-stimulated ATPase activity. (A) Tryptophan fluorescence was used to measure binding of compound to DnaK. Inset: The dose-dependence experiments were carried out at 340 nm (dotted line). (B) On the left is a schematic of the ELISA for DnaK binding to a model substrate, firefly luciferase. On the right is a schematic of the ADP-bound form of DnaK, which binds tighter than the ATP-bound form to substrates. (C) Measurement of DnaK binding to luciferase, using the ELISA approach. (D) Compound 3c favored the high affinity form of DnaK. The chaperone (0.05 μM DnaK + 1 mM ATP) was treated with 3c at the indicated concentrations for 20 minutes prior to the ELISA. (E) Compound 3c specifically blocked DnaJ-mediated stimulation of ATP turnover by DnaK. The DnaK concentration was 0.6 μM and ATPase activity was measured using the absorbance version of the assay. The results are the average of triplicates and the error bars represent standard error of mean. (F) Compound 3c also inhibited the DnaJ-stimulated ATPase activity of bovine Hsc70 and human Hsp72, as measured using the absorbance version of the assay. The protein concentrations were: Hsc70 or Hsp72 (0.6 μM) and DnaJ (1.0 μM). All data points are the average of triplicates and the error bars represent standard error of mean.

Because much of the signal from the ATPase assay is due to the stimulatory activity of the co-chaperone DnaJ, we hypothesized that compound **3c** might alter the interaction between DnaK and DnaJ. To explore that model, we determined the $K_{0.5}$ of DnaJ to estimate the strength of the protein-protein interaction. In the absence of inhibitor, we found that the $K_{0.5}$ of DnaJ was 0.17 ± 0.01 μM (**Figure 2.12E**). Addition of low levels (25 μM) of compound **3c** did not significantly alter this value ($K_{0.5}$ = 0.18 ± 0.01 μM). However, higher concentrations (50 or 100 μM) increased the $K_{0.5}$ to 0.96 ± 0.16 μM and greater than 2 μM, respectively (**Figure 2.12E**). These results suggested that binding of compound **3c** to DnaK might interrupt its interactions with DnaJ.

Finally, members of the Hsp70 family are highly conserved, with DnaK sharing nearly 50% sequence identity with human Hsp72 (HSPA1A) and bovine Hsc70 (HSPA8). To test whether compound **3c** might inhibit the ATPase activity of these related family members, we carried out dose dependence experiments in the presence of DnaJ. We found that this compound had an IC_{50} of 71 ± 1.2 μM for human Hsp72, and an IC_{50} of 106 ± 1.0 μM against bovine Hsc70 (**Figure 2.12F**), showing that compound **3c** also inhibits the mammalian isoforms.

2.3 Discussion

2.3.1 Development of Two Reliable and Economic High Throughput Screening Methods for the DnaK Chaperone Complex

Hsp70 chaperones are central mediators of protein homeostasis and they are involved in

a variety of signaling pathways [2, 3, 7-9]. Therefore, small molecules that specifically modulate their activities are intriguing as research tools and, potentially, as therapeutic leads [23, 60]. In this chapter, we described both a colorimetric 96-well-based and a fluorescent 384-well based high throughput method against DnaK chaperone complexes. Both methods are reliable (Z = 0.7 and ~0.6, respectively) [61] and low cost [43]. By carefully varying the levels of chaperone and stimulatory co-chaperones, we were able to arrive at a ratio that provided good dynamic range and signal-to-noise. Moreover, because this system contains both chaperone and co-chaperone, it provides the opportunity for uncovering compounds that modify either protein. Of course, this feature requires subsequent follow-up studies to isolate the binding site and mode of action. Lastly, in MG-based method we observed a linear increase in OD_{620} signal for greater than four hours, which is a feature that permits usage of simple endpoint measurements.

2.3.2 The Applications of Chemical Probes Found in the 96-well Based Screen against Hsp70s

Using the 96-well based colorimetric method, we screened 204 compounds that share a dihydropyrimidine core similar to the previously reported lead, MAL3-101 [33]. In this relatively small collection, we successfully identified 7 inhibitors (>20% inhibition). All selected inhibitors (4 compounds) were reproducible and their IC_{50} values ranged from approximately 120 to 200 μM. While these potencies were modest, the library size was not large and we would predict that activity might be improved following additional lead

optimization and structural studies. Our further study led to the discovery of two dihydropyrimide-based compounds, 115-7c and SW02, that stimulated the ATPase of both human and bacterial Hsp70 [54, 62]. Interestingly, 115-7c could act as a chemical J protein and recover the heat and calcofluor white-sensitive phenotypes of Δ*ydj1* yeast cells (Ydj1 is a major J protein of yeast) [62]. Using NMR, we mapped the binding site of 115-7c to the cleft between IA and IIA subdomains in DnaK NBD, close to the reported DnaJ binding site [62], consistent with the current findings that the compounds do not bind the SBD (**Figure 2.8**). Using this established 96-well based screening assay, we also identified two benzothiazines, methylene blue (MB) and azure C, that inhibited the ATPase activity human Hsp70s (EC_{50} = 83 and 11 μM, respectively) [54]. Studies performed in collaboration with the Dr. Dickey's group correlated the Hsp70 ATPase inhibition or activation effects of 115-7c, SW02, MB, and Azure C to their effects on the stability of two Hsp70 substrates, tau and Akt, in mammalian cell-based assays [54, 55]. Counterintuitively, the ATPase activators 115-7c and SW02 improved the stability of substrates whereas the inhibitors MB and Azure C destabilized them [54, 55]. Since MB destabilized Akt, it selectively killed specific breast cancer cells that depended on Akt for survival [55]. Furthermore, Dr. Dickey's group found that MB rescued memory loss in a transgenic mouse model of tauopathy [63]. Because MB is already a FDA approved drug and has minimal side effect, it can potentially be very useful in treating Alzheimer's disease patients. Recently, Studies performed in collaboration with the Dr. Lieberman's group expanded the use of MB as a chemical probe to study Hsp70-dependent effects in three well-established biological systems with increased complexity [64]. Firstly, they

found that MB inhibited the activation of the glucocorticoid receptor for ligand binding by a purified Hsp70/Hsp90/HOP/Hsp40/p23 system through a specific inhibition of Hsp70 [64]. Secondly; MB blocked the ubiquitination of neuronal nitricoxide synthase (nNOS) by reticulocyte lysate, and this effect can be overcome by adding excess recombinant Hsp70 [64]. Finally, they found that MB promoted the accumulation of the overexpressed polyQ-containing androgen receptor (AR112Q) in HeLa cells [64]. These results revealed the complexity of substrate fate determination by Hsp70, because MB had completely opposite effect on tau – increasing its ubiquitination and degradation [54, 65]. Despite the high IC_{50} and promiscuity of our first generation probes, they are useful tools for studying the biological functions of Hsp70 and have exciting potentials as drugs against neurodegenerative diseases and cancers. We are currently screening bigger compound libraries against different combinations of human Hsp70s and their various co-chaperones to expand our collections of chemical probes. We believe that those new probes can help us better understand the functions of this complicate and interesting chaperone system.

2.3.3 Characterization of the Inhibition Mechanisms of Compound 3c (Zafirlukast)

Screening of 55,400 molecules identified compound **3c**, with an IC_{50} value of 37 ± 1 μM (see **Figure 2.11C**) and an affinity of 13 ± 1.7 μM (see **Figure 2.12A**). Compound **3c** is a known leukotriene receptor antagonist and an FDA-approved asthma drug, marketed by Astra-Zeneca as zafirlukast (Accolate®), thus it is likely not a selective DnaK inhibitor. However, this scaffold might still be a revealing chemical probe. Specifically, it might help

illuminate the currently cryptic mechanisms of allostery in the chaperone complex. For example, we found that compound **3c** selectively suppressed stimulation by DnaJ, while having little effect on the intrinsic ATPase activity (see **Figure 2.12**). Further, this compound did not block binding of DnaK to luciferase and, rather, it significantly enhanced this interaction (see **Figure 2.12D**). The high affinity form of DnaK is a poor partner for DnaJ [66], which might partially explain the observed behaviors. Future structural studies are expected to provide more insight into the mechanism of this compound and, more broadly, the pathways of allosteric regulation in the DnaK-DnaJ complex.

2.3.4 Conclusion

In conclusion, we have developed HTS methods for the DnaK•DnaJ•GrpE system. The main technical challenges were the low ATPase rate of DnaK, the poor performance of absorbance assays in 384-well plates and the complexity of using the three chaperone system. In this study, we have explored solutions to these problems and the resulting platform has the potential for uncovering new chemical probes of DnaK. In turn, these chemical modulators might be used to study chaperone biology and may provide leads for developing Hsp70-targeting therapeutics and antibiotics.

2.4 Materials and Methods

2.4.1 Protein Expression and Purification

DnaK, DnaJ and GrpE proteins were expressed in *E. coli* BL21 (DE3) using T7-based

vectors. DnaK and GrpE were expressed at 37 °C, while DnaJ was expressed at 25 °C in order to increase the fraction of soluble protein. All purification steps were carried out at 4 °C. Protein concentration was estimated by Bradford assay, using BSA as the standard. Following purification, proteins were frozen on liquid nitrogen and stored at –80 °C until use.

Purification of DnaK was accomplished by a modification of established procedures [67, 68]. Briefly, cell pellets were suspended in buffer A (25 mM Tris, 10 mM KCl, 5 mM $MgCl_2$, pH 7.5) containing 0.01 mM PMSF and 1 mM DTT, and disrupted using a microfluidizer (Microfluidics). Cleared extracts were applied to a Q-Sepharose fast-flow column (GE Healthcare), and the protein was eluted with a 10-500 mM gradient of KCl in buffer A. Fractions containing DnaK were pooled and applied to ATP-agarose (Sigma). After extensive washing with Buffer A and Buffer A containing 1 M KCl, the protein was eluted with Buffer A containing 3 mM ATP. The pure protein was concentrated and exchanged to buffer A for storage.

DnaJ was purified using a streamlined version of established methodology [69, 70]. Briefly, cell pellets were resuspended in buffer B (25 mM Tris, 2 M urea, 0.1% Brij-58, 2 mM DTT, pH 7.5) containing 0.01 mM PMSF and disrupted using a microfluidizer. Cleared extracts were applied to a Source SP (GE Healthcare) column, and the protein was eluted with a gradient of 0-350 mM KCl in buffer B. Fractions containing DnaJ were pooled and applied to a hydroxyapatite (BioGel HTP, Bio-Rad Laboratories) column that had been

equilibrated with buffer C (buffer B containing 50 mM KCl and no detergent). After extensive washing with buffer C and buffer C containing 1.0 M KCl, the protein was eluted with a 0-350 mM gradient of potassium phosphate, pH 7.4. Fractions containing DnaJ were pooled, diluted two-fold with 25 mM Tris, 50 mM KCl, 2 M urea, pH 9.0, and applied to a Q-Sepharose fast-flow column. Pure DnaJ was collected in the flow-through, concentrated, and exchanged into buffer A containing 150 mM KCl for storage.

GrpE was purified as follows: Cell pellets were resuspended in buffer D (25 mM Tris, pH 7.5) containing 0.01 mM PMSF and disrupted using a microfluidizer. Cleared extracts were applied to a Q-Sepharose fast-flow column, and protein was eluted with a 0-500 mM gradient of KCl in buffer D. Fractions containing GrpE were pooled, supplemented with 1 M ammonium sulfate, and applied to a phenyl-Sepharose high-performance 16/10 column (GE Healthcare). Protein was eluted with a 1.0-0 M gradient of ammonium sulfate in buffer D. Fractions containing GrpE were pooled, concentrated, and applied to a Superdex 200 26/60 column (GE Healthcare). Protein was eluted at 0.5 ml/min in buffer D. Fractions containing GrpE were pooled, concentrated, and the protein was exchanged into buffer A for storage. The protein was greater than 90% pure as judged by SDS-PAGE and Coomassie staining.

2.4.2 Colorimetric Determination of ATPase Activity in 96-well Format

The assay procedure was adopted from previous reports [38] with modifications where indicated. Stock solutions of malachite green (0.081% w/v), polyvinyl alcohol (2.3% w/v),

and ammonium heptamolybdate tetrahydrate (5.7% w/v in 6 M HCl) were prepared, stored at 4 °C, and mixed with water in the ratio of 2:1:1:2 to prepare the malachite green reagent. This reagent was stable at 4 °C for at least one week. All components were from Sigma and used without further purification.

For compound library screening, a master mix of DnaK : DnaJ : GrpE (1.0 : 1.7 : 1.6 µM) was prepared in assay buffer (0.017% Triton X-100, 100 mM Tris-HCl, 20 mM KCl, and 6 mM $MgCl_2$, pH 7.4). An aliquot (14 µL) of this mixture was added into each well of a 96 well plate. To this solution, 1 µL of either compound (5 mM) or DMSO was added and the plate was incubated for 30 min at 37 °C before adding 10 µl of 2.5 mM ATP to start the reaction. Thus, the final reaction volume was 25 µL and the conditions were: 0.6 µM DnaK, 1.0 µM DnaJ, 0.9 µM GrpE, 4% DMSO, 0.01% Triton X-100 and 1 mM ATP. These concentrations were chosen because they provide intermediate signal and thereby encourage the possibility of discovering both inhibitors and (potentially) activators. After 1-3 hours incubation at 37 °C, 80 µL of malachite green reagent was added into each well. Immediately following this step, 10 µL 34% sodium citrate was used to halt the nonenzymatic hydrolysis of ATP. The samples were mixed thoroughly and incubated at 37 °C for 15 min before measuring OD_{620} on a SpectraMax M5 (Molecular Devices, Sunnyvale, CA). To control these results for intrinsic hydrolysis, the signal from ATP in identically treated-buffer lacking chaperones was subtracted. To permit comparisons between screens performed at different times, a phosphate standard curve (using sodium phosphate) was generated each day (**Figure 2.13**).

2.4.3 Chemical Synthesis of Dihydropyrimidine Library

The dihydropyrimidine compounds used in this study were synthesized by a microwave-accelerated Biginelli cyclocondensation reaction, utilizing methods modified from the independent work of Kappe and Wipf [28, 71]. The collection of 204 compounds we used in this work includes those generated in-house, members received from the University of Pittsburgh's Center for Chemical Methodologies and Library Development (UPCMLD) and those purchased from ChemBridge. A more detailed description of the synthesis and characterization of this collection will be reported elsewhere. Geranylgeraniol was obtained from Sigma and the peptide substrate (NRLLLTG**)** was provided by SynPep [47]. None of the compounds had appreciable absorbance at 620 nm and, thus, did not interfere with the MG signal (data not shown).

2.4.4 Source of the Compound Libraries Stored in 384-well format

The MicroSource MS2000 library contains ~2,000 bioactive compounds with a minimum of 95% purity. Briefly, the collection includes 958 known therapeutic drugs, 629 natural products and derivatives, 343 compounds with reported biological activities and 70 compounds approved for agricultural use. The University of Michigan Center for Chemical Genomics (CCG) small molecule library consists of 16,000 Maybridge HitFinder, 13,000 ChemBridge, 20,000 ChemDiv, 3,000 NCI, 450 NIH Clinical Collection (NCC) compounds and ~20,000 natural product extracts. The activity of promising compounds was confirmed using repurchased samples from original vendors. Compound 3c was

purchased from Cayman Chemical Inc. (Ann Arbor, MI). Compounds were used without further purification.

2.4.5 Screening Against DnaK-DnaJ Complex by Absorbance Method in 384-well Format

The assay procedure was adopted from previous reports with modifications where indicated [53]. All components other than compounds were added by a Multidrop dispensor (Thermo Fisher Scientific, Inc., Waltham, MA). Stock solutions of 0.05% w/v quinaldine red (QR), 2% w/v polyvinyl alcohol, 6% w/v ammonium heptamolybdate tetrahydrate in 6 M HCl and water were mixed in a 2:1:1:2 ratio to prepare the QR reagent. This reagent was prepared fresh prior to each experiment. For compound screening, a stock solution of DnaK and DnaJ was prepared in assay buffer (100 mM Tris-HCl, 20 mM KCl, and 6 mM $MgCl_2$, 0.01% Triton X-100, pH 7.4) so that the final concentration of DnaK was 0.4 µM and DnaJ was 0.7 µM (unless noted). This solution (10 µL) was then added to each well of a 384-well clear plate (Thermo Fisher Scientific, Inc., Waltham, MA). To this solution, 0.4 µL of either compound (1.5 mM) or DMSO was added to each well by Biomek HDR (Beckman, Fullerton, CA). Finally, 4 µL of a 7 mM ATP solution was added to begin the reaction. The plates were then incubated for 3 hrs at 37 °C. After incubation, each well received 40 µL of the QR reagent, allowing 2 min of reaction time, and then quenched by addition of 32% w/v solution of sodium citrate (4 µL). The plates were then incubated for an additional 15 min at 37 °C before measuring absorbance at 530 nm on a PHERAstar plate reader (BMG Labtech, Cary, NC).

2.4.6 Screening Against DnaK-DnaJ Complex by Fluorescence Method in 384-well Format

The QR reagent was prepared exactly as indicated above. All components other than compounds were added by a Multidrop dispensor (Thermo Fisher Scientific, Inc., Waltham, MA). The DnaK-DnaJ stock solution was prepared so that the final concentration of DnaK was 0.4 µM and DnaJ was 0.7 µM (unless noted). This solution (5 µL) was then added to each well of a 384-well opaque, white, low-volume, non-sterile, polystyrene 384-well plates (Greiner Bio-One North America Inc., Monroe, NC). To this solution, 0.2 µL of either compound (1.5 mM) or DMSO was added to each well by Biomek HDR (Beckman, Fullerton, CA). Finally, 2 µL of a 3.5 mM ATP solution was added to begin the reaction. The plates were then incubated for 3 hrs at 37 °C. After incubation, each well received 15 µL of the QR reagent, allowing 2 min of reaction time, and then quenched by addition of 32% w/v solution of sodium citrate (2 µL). These plates were incubated for 15 min at 37 °C and the fluorescence intensity measured (excitation 430 nm, emission 530 nm) on a PHERAstar plate reader. Standard curves were obtained using stock solutions of dibasic potassium phosphate.

2.4.7 Tryptophan Fluorescence Assay

The method for measuring binding to DnaK was carried out as previously described [72]. Briefly, DnaK (5 µM) in 1 mM ATP was incubated with the indicated concentration of compound 3c in a total volume of 25 µL for 20 min at 37°C. The emission spectrum

between 300 - 450 nm was recorded (excitation at 290 nm) using a SpectraMax M5 microplate reader (Molecular Devices, Sunnyvale, CA).

2.4.8 Enzyme-linked Immunosorbant Assay

The procedure for DnaK binding to luciferase was adapted from a previous report [73]. Briefly, firefly luciferase (0.2 mg/mL) was first incubated with 0.1 µM trypsin at 37 °C for 1 hr in HEPES buffer (40 mM HEPES, 8 mM $MgCl_2$, 20 mM NaCl, 20 mM KCl, 0.3 mM EDTA, pH 7.2), the reaction was quenched with 1 mM PMSF and diluted to 5 µg/mL with PBS buffer (pH 7.4). An aliquot (50 µL) was then added to 96-well plates (ThermoFisher brand, clear, non-sterile, flat bottom). After 1 hr of incubation at 37 °C, the wells were washed three times with 100 µL PBS-T (0.05% Tween-20). A solution of DnaK (at the indicated concentrations), compound 3c, and 1 mM ATP was pre-incubated in HEPES with 0.01% Tween for 30 min. From this solution, 50 µL was added to wells and allowed to bind for 30 min at room temperature. After washing three times with PBS-T, 5% non-fat milk (w/v) in 100 µL TBS-T was used to block the non-specific binding sites. Primary antibody was then added (1:3000 dilution of rabbit anti-DnaK serum in TBS-T, 50 µL/well) and the plates were incubated for 1 hr at room temperature. Wells were then washed three times with TBS-T, followed by addition of HRP-conjugated secondary (1:3000 dilution of goat anti-rabbit serum in TBS-T, 50 µL/well). After an 1 hr incubation, the wells were washed three times and signal developed for 20 min using the TMB kit from Cell Signaling Technology (Danvers, MA). The absorbance was measured using a SpectraMax M5 microplate reader (Molecular Devices, Sunnyvale, CA) at 450 nm.

Notes

This work was partially published as “High-throughput screen for small molecules that modulate the ATPase activity of the molecular chaperone DnaK” **2008** Anal Biochem. 372 :167-76 and “High-throughput screen for Escherichia coli heat shock protein 70 (Hsp70/DnaK): ATPase assay in low volume by exploiting energy transfer” **2010** J Biomol Screen. 15: 1211-9.

Lyra Chang and Jason E. Gestwicki designed the experiments. Lyra Chang conducted the experiments. Yoshinari Miyata did the follow-up studies on the “hits” we found in the DnaK 384-well based high throughput screen. In 96-well based HTS assay, the DnaK, DnaJ, and GrpE proteins were purified by Eric B. Bertelsen. Thomas J. Mcquade, Martha J. Larsen, and Paul Kirchhoff helped with high throughput screening and scaffold clustering. Anthony Bainor and Christopher P. Walczak carried out the absorbance-based 384-well HTS assay against DnaK-DnaJ complex. Yaru Zhang helped to optimize the ELISA-based DnaK binding assay.

2.5 Appendix

2.5.1 The effect of Triton X-100 on high throughput screening and compound activity

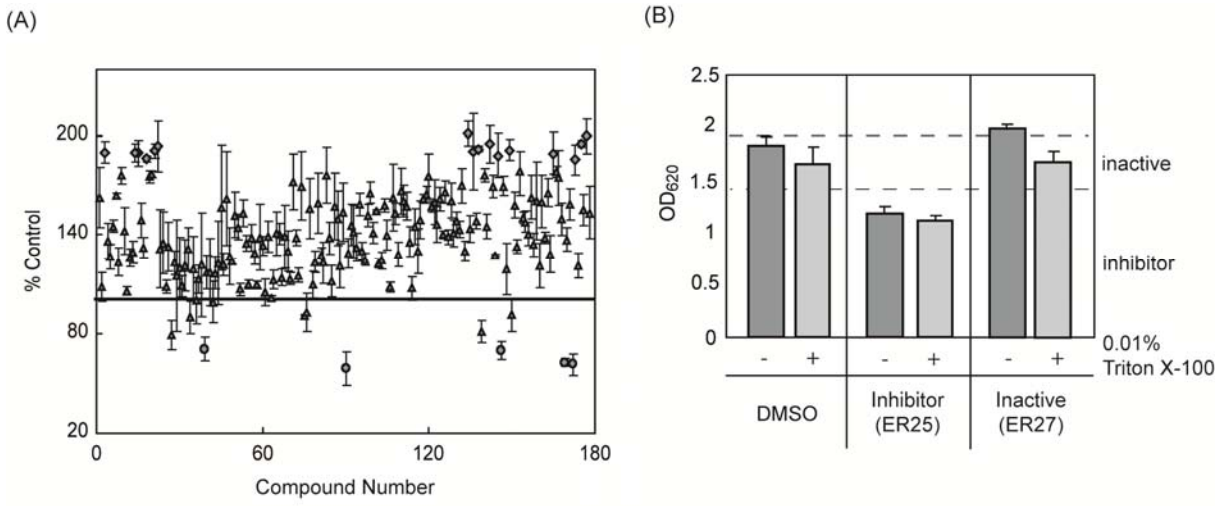

Appendix 2.5.1 Addition of Triton X-100 removed non-specific stimulation but did not impact inhibitory activity. (A) Screening in the absence of Triton X-100 provides high background. Note that the order of the compounds is different in this plot than those shown in Figure 2.5 (B) Adding Triton X-100 reduced non-specific stimulation of DnaK ATPase activity by ER27 but not affected the inhibition effect of ER25. Two representative compounds are shown and similar effects were seen in other comparisons. For both (A) and (B), the compound concentrations are 200 μM, and the reactions were carried out with 0.6 μM DnaK, 1.0 μM DnaJ, 0.9 μM GrpE, and 1 mM ATP. In both figures, the results are the average of triplicates and the errors represent the standard deviations.

2.5.2 Dose dependent curves of the selected hits at the presence of peptide

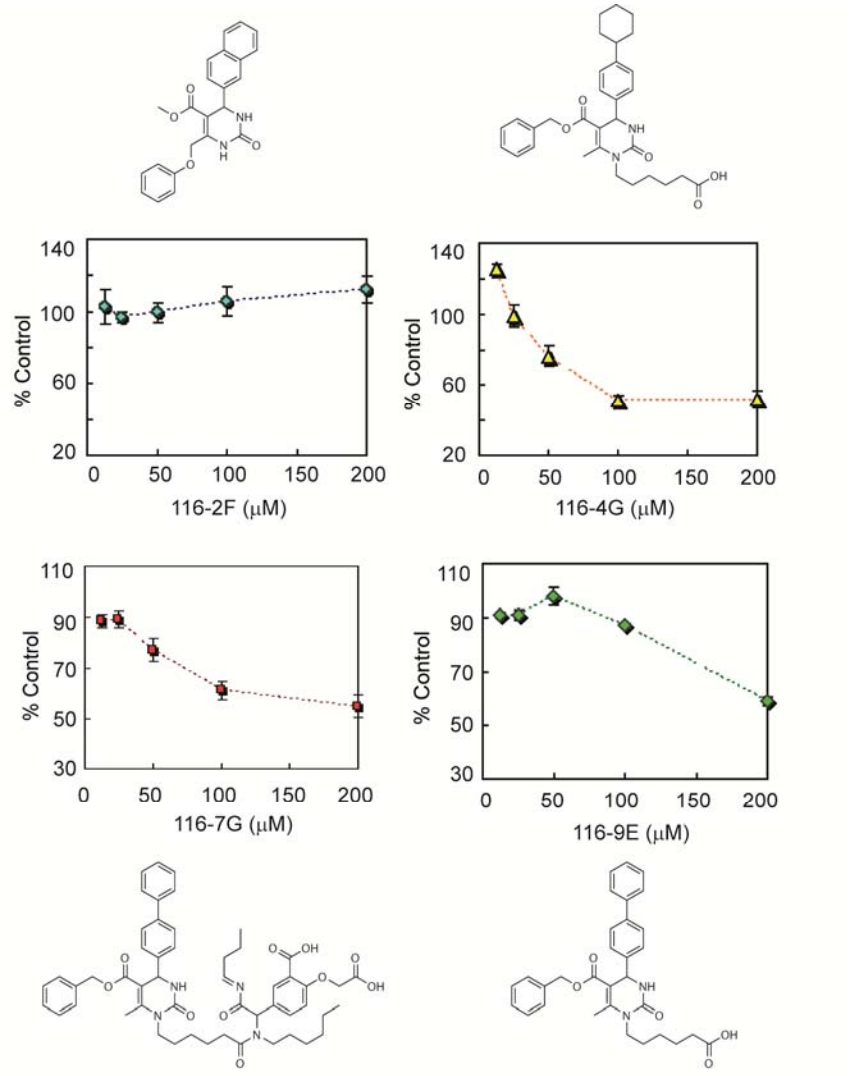

Appendix 2.5.2 Dose dependent curves of 0116-2F, 0116-4G, 0116-7G and 0116-9E at the presence of 50 μM SBD-binding peptide.

2.5.3 Optimization of the 384-well white plate assay

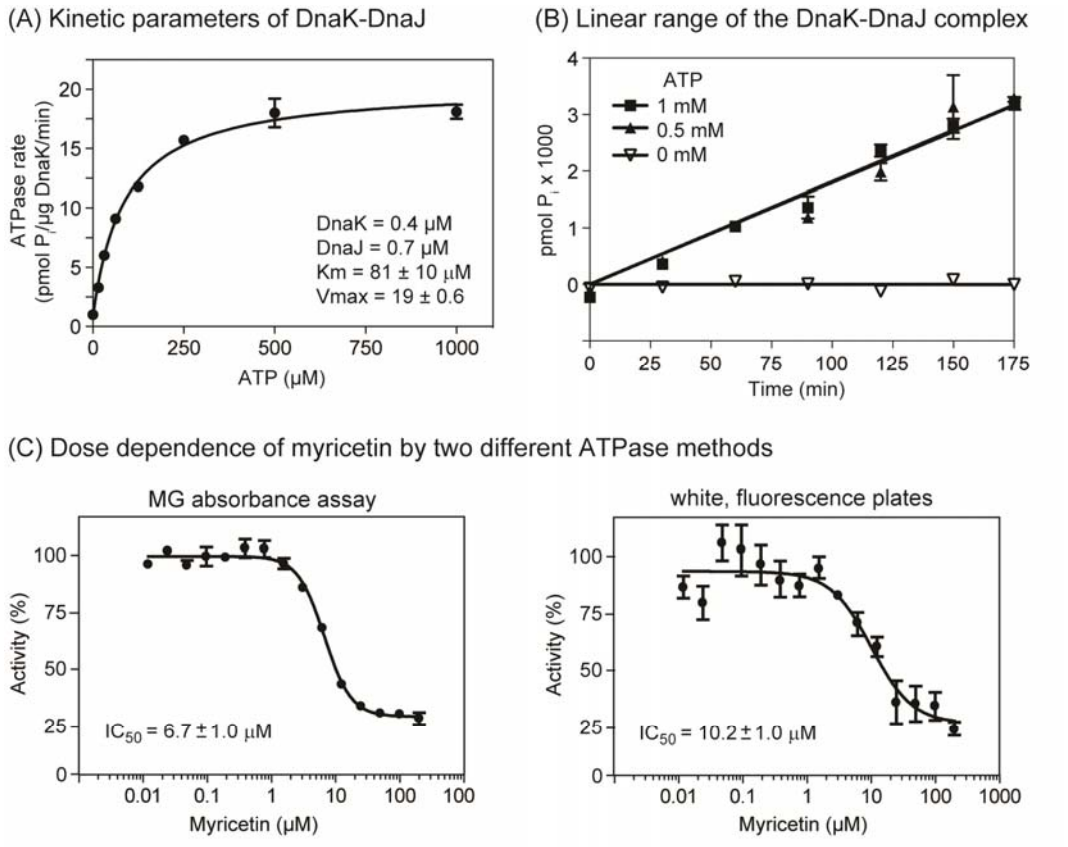

Appendix 2.5.3 Characterization of the white plate, fluorescent assay. (A) Determination of the kinetic parameters of DnaK-DnaJ in the fluorescence method, under the screening conditions. (B) Determination of the linear range. The concentration of DnaK was 0.4 µM and DnaJ was 0.7 µM. (C) Direct comparison of the IC_{50} values of a known inhibitor in the normal, malachite green-based absorbance assay and the white, fluorescent plate assay. The concentration of DnaK was 0.4 µM, DnaJ was 0.7 µM and ATP was 1 mM. Results are the average of triplicates and the error bars represent standard error of the mean.

2.5.4 Occasional outliers in white, opaque 384-well plates

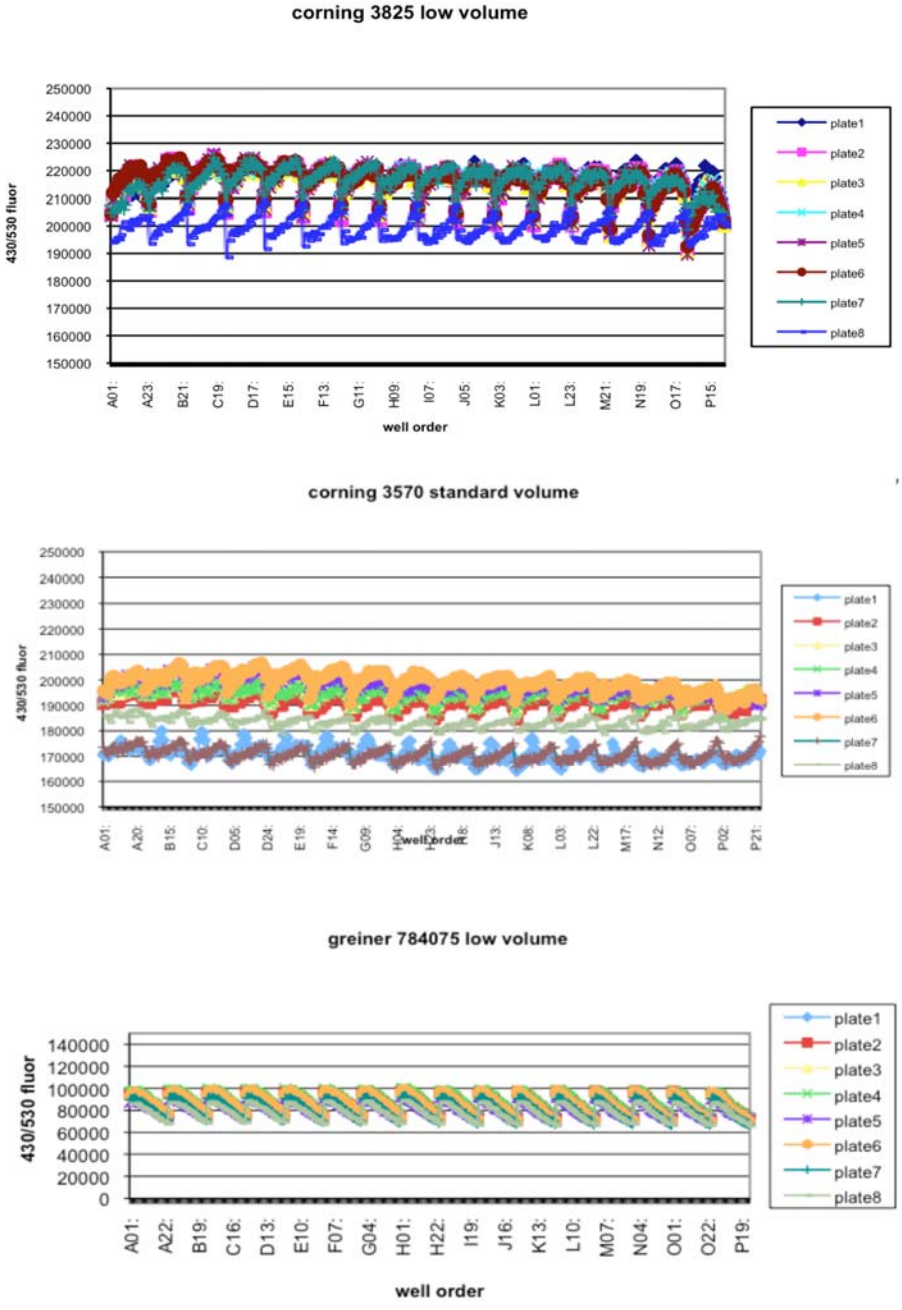

Appendix 2.5.4 Occasional outliers in white, opaque mirotiter plates. Stacks of untreated microtiter plates were monitored for fluorescence (ex. 430 nm. em. 530 nm). Note that occasional plates show significantly different fluorescence patterns and that all the plates show a “sharktooth” pattern. Representative data sets are shown for three manufacturers. Based on these results, we chose Greiner 784075 low volume plates for our experiments.

2.6 References

1. Rensing, S.A. and U.G. Maier, *Phylogenetic analysis of the stress-70 protein family.* J Mol Evol, 1994. **39**(1): p. 80-6.
2. Mayer, M.P. and B. Bukau, *Hsp70 chaperones: cellular functions and molecular mechanism.* Cell Mol Life Sci, 2005. **62**(6): p. 670-84.
3. Morishima, N., *Control of cell fate by Hsp70: more than an evanescent meeting.* J Biochem (Tokyo), 2005. **137**(4): p. 449-53.
4. Bukau, B., J. Weissman, and A. Horwich, *Molecular chaperones and protein quality control.* Cell, 2006. **125**(3): p. 443-51.
5. Feder, M.E. and G.E. Hofmann, *Heat-shock proteins, molecular chaperones, and the stress response: evolutionary and ecological physiology.* Annu Rev Physiol, 1999. **61**: p. 243-82.
6. Young, J.C., J.M. Barral, and F. Ulrich Hartl, *More than folding: localized functions of cytosolic chaperones.* Trends Biochem Sci, 2003. **28**(10): p. 541-7.
7. Macario, A.J. and E. Conway de Macario, *Sick chaperones, cellular stress, and disease.* N Engl J Med, 2005. **353**(14): p. 1489-501.
8. Muchowski, P.J. and J.L. Wacker, *Modulation of neurodegeneration by molecular chaperones.* Nat Rev Neurosci, 2005. **6**(1): p. 11-22.
9. Pierpaoli, E.V., *The role of Hsp70 in age-related diseases and the prevention of cancer.* Ann N Y Acad Sci, 2005. **1057**: p. 206-19.
10. Westerheide, S.D. and R.I. Morimoto, *Heat shock response modulators as therapeutic tools for diseases of protein conformation.* J Biol Chem, 2005. **280**(39): p. 33097-100.
11. Mosser, D.D. and R.I. Morimoto, *Molecular chaperones and the stress of oncogenesis.* Oncogene, 2004. **23**(16): p. 2907-18.
12. Barral, J.M., et al., *Roles of molecular chaperones in protein misfolding diseases.* Semin Cell Dev Biol, 2004. **15**(1): p. 17-29.
13. Swain, J.F., E.G. Schulz, and L.M. Gierasch, *Direct comparison of a stable isolated Hsp70 substrate-binding domain in the empty and substrate-bound states.* J Biol Chem, 2006. **281**(3): p. 1605-11.
14. Swain, J.F., et al., *Hsp70 chaperone ligands control domain association via an allosteric mechanism mediated by the interdomain linker.* Mol Cell, 2007. **26**(1): p. 27-39.
15. Slepenkov, S.V. and S.N. Witt, *The unfolding story of the Escherichia coli Hsp70 DnaK: is DnaK a holdase or an unfoldase?* Mol Microbiol, 2002. **45**(5): p. 1197-206.
16. Cohen, E., et al., *Purification of Na+,K+-ATPase expressed in Pichia pastoris reveals an essential role of phospholipid-protein interactions.* J Biol Chem, 2005. **280**(17): p. 16610-8.
17. Siegenthaler, R.K. and P. Christen, *Tuning of DnaK chaperone action by nonnative protein sensor DnaJ and thermosensor GrpE.* J Biol Chem, 2006. **281**(45): p. 34448-56.
18. Harrison, C., *GrpE, a nucleotide exchange factor for DnaK.* Cell Stress Chaperones, 2003. **8**(3): p. 218-24.

19. Qiu, X.B., et al., *The diversity of the DnaJ/Hsp40 family, the crucial partners for Hsp70 chaperones.* Cell Mol Life Sci, 2006. **63**(22): p. 2560-70.
20. Walsh, P., et al., *The J-protein family: modulating protein assembly, disassembly and translocation.* EMBO Rep, 2004. **5**(6): p. 567-71.
21. Hennessy, F., et al., *Analysis of the levels of conservation of the J domain among the various types of DnaJ-like proteins.* Cell Stress Chaperones, 2000. **5**(4): p. 347-58.
22. Sahi, C. and E.A. Craig, *Network of general and specialty J protein chaperones of the yeast cytosol.* Proc Natl Acad Sci U S A, 2007. **104**(17): p. 7163-8.
23. Smith, D.F., L. Whitesell, and E. Katsanis, *Molecular chaperones: biology and prospects for pharmacological intervention.* Pharmacol Rev, 1998. **50**(4): p. 493-514.
24. Chaudhury, S., T.R. Welch, and B.S. Blagg, *Hsp90 as a target for drug development.* ChemMedChem, 2006. **1**(12): p. 1331-40.
25. Janin, Y.L., *Heat shock protein 90 inhibitors. A text book example of medicinal chemistry?* J Med Chem, 2005. **48**(24): p. 7503-12.
26. Ansar, S., et al., *A non-toxic Hsp90 inhibitor protects neurons from Abeta-induced toxicity.* Bioorg Med Chem Lett, 2007. **17**(7): p. 1984-90.
27. Xu, W. and L. Neckers, *Targeting the molecular chaperone heat shock protein 90 provides a multifaceted effect on diverse cell signaling pathways of cancer cells.* Clin Cancer Res, 2007. **13**(6): p. 1625-9.
28. Arthur G. Schultz, C.-K.S., *Chemistry of Naturally Occurring Polyamines. 1. Total Synthesis of Celacinnine, Celabenzine, and Maytenine.* J. Org. Chem., 1980. **45**: p. 2041-2042.
29. Komesli, S., C. Dumas, and P. Dutartre, *Analysis of in vivo immunosuppressive and in vitro interaction with constitutive heat shock protein 70 activity of LF08-0299 (Tresperimus) and analogues.* Int J Immunopharmacol, 1999. **21**(5): p. 349-58.
30. Nadler, S.G., et al., *Identification of a binding site on Hsc70 for the immunosuppressant 15-deoxyspergualin.* Biochem Biophys Res Commun, 1998. **253**(1): p. 176-80.
31. Nadler, S.G., et al., *Elucidating the mechanism of action of the immunosuppressant 15-deoxyspergualin.* Ther Drug Monit, 1995. **17**(6): p. 700-3.
32. Fewell, S.W., B.W. Day, and J.L. Brodsky, *Identification of an inhibitor of hsc70-mediated protein translocation and ATP hydrolysis.* J Biol Chem, 2001. **276**(2): p. 910-4.
33. Fewell, S.W., et al., *Small molecule modulators of endogenous and co-chaperone-stimulated Hsp70 ATPase activity.* J Biol Chem, 2004. **279**(49): p. 51131-40.
34. Liebscher, M., et al., *Fatty acyl benzamido antibacterials based on inhibition of DnaK-catalyzed protein folding.* J Biol Chem, 2007. **282**(7): p. 4437-46.
35. Avila, C., et al., *High-throughput screening for Hsp90 ATPase inhibitors.* Bioorg Med Chem Lett, 2006. **16**(11): p. 3005-8.
36. Avila, C., B.A. Kornilayev, and B.S. Blagg, *Development and optimization of a useful assay for determining Hsp90's inherent ATPase activity.* Bioorg Med Chem, 2006. **14**(4): p. 1134-42.
37. Howes, R., et al., *A fluorescence polarization assay for inhibitors of Hsp90.* Anal

Biochem, 2006. **350**(2): p. 202-13.
38. Rowlands, M.G., et al., *High-throughput screening assay for inhibitors of heat-shock protein 90 ATPase activity.* Anal Biochem, 2004. **327**(2): p. 176-83.
39. Galam, L., et al., *High-throughput assay for the identification of Hsp90 inhibitors based on Hsp90-dependent refolding of firefly luciferase.* Bioorg Med Chem, 2007. **15**(5): p. 1939-46.
40. Geladopoulos, T.P., T.G. Sotiroudis, and A.E. Evangelopoulos, *A malachite green colorimetric assay for protein phosphatase activity.* Anal Biochem, 1991. **192**(1): p. 112-6.
41. Fisher, D.K. and T.J. Higgins, *A sensitive, high-volume, colorimetric assay for protein phosphatases.* Pharm Res, 1994. **11**(5): p. 759-63.
42. Cogan, E.B., G.B. Birrell, and O.H. Griffith, *A robotics-based automated assay for inorganic and organic phosphates.* Anal Biochem, 1999. **271**(1): p. 29-35.
43. Zuck, P., et al., *Miniaturization of absorbance assays using the fluorescent properties of white microplates.* Anal Biochem, 2005. **342**(2): p. 254-9.
44. McCarty, J.S., et al., *The role of ATP in the functional cycle of the DnaK chaperone system.* J Mol Biol, 1995. **249**(1): p. 126-37.
45. Barthel, T.K., J. Zhang, and G.C. Walker, *ATPase-defective derivatives of Escherichia coli DnaK that behave differently with respect to ATP-induced conformational change and peptide release.* J Bacteriol, 2001. **183**(19): p. 5482-90.
46. Ryan, A.J., et al., *Effect of detergent on "promiscuous" inhibitors.* J Med Chem, 2003. **46**(16): p. 3448-51.
47. Stevens, S.Y., et al., *The solution structure of the bacterial HSP70 chaperone protein domain DnaK(393-507) in complex with the peptide NRLLLTG.* Protein Sci, 2003. **12**(11): p. 2588-96.
48. Chesnokova, L.S., S.V. Slepenkov, and S.N. Witt, *The insect antimicrobial peptide, L-pyrrhocoricin, binds to and stimulates the ATPase activity of both wild-type and lidless DnaK.* FEBS Lett, 2004. **565**(1-3): p. 65-9.
49. Kreusch, S., et al., *UV measurements in microplates suitable for high-throughput protein determination.* Anal Biochem, 2003. **313**(2): p. 208-15.
50. Lavery, P., M.J. Brown, and A.J. Pope, *Simple absorbance-based assays for ultra-high throughput screening.* J Biomol Screen, 2001. **6**(1): p. 3-9.
51. Yuan, P. and D.R. Walt, *Calculation for Fluorescence Modulation by Absorbing Species and Its Application to Measurements Using Optical Fibers.* Analytical Chemistry, 1987. **59**(19): p. 2391-2394.
52. Carter, S.G. and D.W. Karl, *Inorganic phosphate assay with malachite green: an improvement and evaluation.* J Biochem Biophys Methods, 1982. **7**(1): p. 7-13.
53. Chang, L., et al., *High-throughput screen for small molecules that modulate the ATPase activity of the molecular chaperone DnaK.* Anal Biochem, 2008. **372**: p. 167-176.
54. Jinwal, U.K., et al., *Chemical manipulation of hsp70 ATPase activity regulates tau stability.* J Neurosci, 2009. **29**(39): p. 12079-88.
55. Koren, J., 3rd, et al., *Facilitating Akt clearance via manipulation of Hsp70 activity and levels.* J Biol Chem, 2010. **285**(4): p. 2498-505.

56. Martin, Y.C., J.L. Kofron, and L.M. Traphagen, *Do structurally similar molecules have similar biological activity?* J Med Chem, 2002. **45**(19): p. 4350-8.
57. Kiselyov, A., L. Smith, and R. Armstrong, *Solid support synthesis of polysubstituted tetrahydroquinolines via three-component condensation catalyzed by Yb(OTf)(3).* Tetrahedron, 1998. **54**: p. 5089-5096.
58. Patury, S., Y. Miyata, and J.E. Gestwicki, *Pharmacological targeting of the Hsp70 chaperone.* Curr Top Med Chem, 2009. **9**(15): p. 1337-51.
59. Mayer, M.P., et al., *Multistep mechanism of substrate binding determines chaperone activity of Hsp70.* Nat Struct Biol, 2000. **7**(7): p. 586-93.
60. Brodsky, J.L. and G. Chiosis, *Hsp70 molecular chaperones: emerging roles in human disease and identification of small molecule modulators.* Curr Top Med Chem, 2006. **6**(11): p. 1215-25.
61. Zhang JH, C.T., Oldenburg KR., *A Simple Statistical Parameter for Use in Evaluation and Validation of High Throughput Screening Assays.* Journal of Biomolecular Screening, 1999. **4**(2): p. 67-73.
62. Wisen, S., et al., *Binding of a small molecule at a protein-protein interface regulates the chaperone activity of hsp70-hsp40.* ACS Chem Biol, 2010. **5**(6): p. 611-22.
63. O'Leary, J.C., 3rd, et al., *Phenothiazine-mediated rescue of cognition in tau transgenic mice requires neuroprotection and reduced soluble tau burden.* Mol Neurodegener, 2010. **5**: p. 45.
64. Wang, A.M., et al., *Inhibition of hsp70 by methylene blue affects signaling protein function and ubiquitination and modulates polyglutamine protein degradation.* J Biol Chem, 2010. **285**(21): p. 15714-23.
65. Jinwal, U.K., et al., *Hsc70 rapidly engages tau after microtubule destabilization.* J Biol Chem, 2010. **285**(22): p. 16798-805.
66. Szabo, A., et al., *The ATP hydrolysis-dependent reaction cycle of the Escherichia coli Hsp70 system DnaK, DnaJ, and GrpE.* Proc Natl Acad Sci U S A, 1994. **91**(22): p. 10345-9.
67. Zylicz, M., et al., *The dnaK protein of Escherichia coli possesses an ATPase and autophosphorylating activity and is essential in an in vitro DNA replication system.* Proc Natl Acad Sci U S A, 1983. **80**(21): p. 6431-5.
68. Mensa-Wilmot, K., K. Carroll, and R. McMacken, *Transcriptional activation of bacteriophage lambda DNA replication in vitro: regulatory role of histone-like protein HU of Escherichia coli.* Embo J, 1989. **8**(8): p. 2393-402.
69. Zylicz, M., et al., *Purification and properties of the dnaJ replication protein of Escherichia coli.* J Biol Chem, 1985. **260**(12): p. 7591-8.
70. Linke, K., et al., *The roles of the two zinc binding sites in DnaJ.* J Biol Chem, 2003. **278**(45): p. 44457-66.
71. Kappe, C.O., *High-speed combinatorial synthesis utilizing microwave irradiation.* Curr Opin Chem Biol, 2002. **6**(3): p. 314-20.
72. Ha, J.H. and D.B. McKay, *Kinetics of nucleotide-induced changes in the tryptophan fluorescence of the molecular chaperone Hsc70 and its subfragments suggest the ATP-induced conformational change follows initial ATP binding.* Biochemistry, 1995. **34**(36): p. 11635-44.

73. Wawrzynow, A. and M. Zylicz, *Divergent effects of ATP on the binding of the DnaK and DnaJ chaperones to each other, or to their various native and denatured protein substrates.* J Biol Chem, 1995. **270**(33): p. 19300-6.

Chapter 3

Chemical Screens against a Reconstituted Multi-Protein Complex: Myricetin Blocks DnaJ Regulation of DnaK through an Allosteric Mechanism

3.1 Abstract

As discussed in Chapters 1 and 2, DnaK is a molecular chaperone responsible for multiple aspects of proteostasis. The intrinsically slow ATPase activity of DnaK is stimulated by its co-chaperone, DnaJ, and these proteins often work in concert. To identify inhibitors, we screened plant-derived extracts against a re-constituted mixture of DnaK and DnaJ using the high throughput assay first developed and described in Chapter 2. This approach resulted in the identification of flavonoids, including myricetin, which inhibited activity by up to 75%. Interestingly, myricetin prevented DnaJ-mediated stimulation of ATPase activity, with minimal impact on either DnaK's intrinsic turnover rate or its stimulation by another co-chaperone, GrpE. Using NMR, we found that myricetin binds DnaK at an unanticipated site between the IB and IIB subdomains and

that it allosterically blocked binding of DnaJ. Together, these results highlight a “gray box” screening approach, which approximates a limited amount of the complexity expected in physiological multi-protein systems.

3.1.1 The Potential Advantages of Screening against Multiprotein Complexes – The “Gray Box” Strategy

Many emerging drug targets operate as part of multi-protein complexes *in vivo* [1]. Often, these ensembles have a single enzymatic output, such as ATP consumption, that is catalyzed by one core component. The non-enzyme partners typically regulated this activity, by impacting subcellular localization, substrate selection and/or turnover rates. Because the protein partners are often important for tuning biological function and integrating information from signaling pathways, there is interest in identifying molecules that specifically target the protein-protein interactions in complexes [2, 3]. Such inhibitors are often identified by either screening for protein-protein contacts in purified systems or by structure-guided design [4-8]. These strategies are increasingly useful, but all *in vitro* screens are prone to attrition when the active compounds are taken into cell-based or animal systems. An alternative approach is to use “black box” cell-based, phenotypic screens. Cell-based approaches are powerful because they

incorporate multiple parameters, such as an intact plasma membrane, a full complement of regulatory pathways and native multi-protein complexes, which better approximate physiological states. However, post-screen target identification can often be challenging. We have been pursuing an approach that might be considered a compromise between these platforms. In this strategy, multiple components of a known protein complex are purified and re-constituted *in vitro* [9, 10]. Only one component typically has measurable activity, yet the other, ancillary partners are likely to impact the turnover rate, approximating a more physiological enzymatic output. In addition, protein-protein interactions between the core enzyme and its partners might mask some potential drug-binding sites, while inducing conformers that reveal other, latent sites. We term this approach "gray box", because it is expected to find the middle ground between biochemical and cell-based assays, providing some limited amount of physiological complexity while reducing investment in downstream target identification.

3.1.2 The DnaK Chaperone Complex as a Test Case for the "Gray Box" Screening Strategy

As a model system, we have principally focused on the *Escherichia coli* DnaK protein. As discussed in Chapters 1 and 2, the nucleotide turnover by DnaK is tightly controlled by its

co-chaperones, including DnaJ and GrpE [11]. DnaJ belongs to the Hsp40 family of co-chaperones and it is thought to bind the IA and IIA subdomains of DnaK [12-14] (**Figure 3.1A**). In turn, this protein-protein interaction allosterically stimulates the ATPase activity of DnaK. In the presence of DnaJ, ADP release becomes rate-limiting and another co-chaperone, GrpE, assists nucleotide exchange via protein-protein interactions with the IB and IIB subdomains [11, 15]. Thus, the combination of DnaK, DnaJ and GrpE efficiently turns over ATP and allows control over chaperone activity [11, 16, 17]. While only the core chaperone, DnaK, has any enzymatic activity, knockouts of *dnaJ* or *grpE* share some phenotypes, such as temperature-sensitivity, in common with Δ*dnaK* cells [18, 19]. These results suggest that the entire network is required for efficient chaperone activity. Further, mutants that specifically disrupt interactions between DnaK and DnaJ give similar phenotypes [12], further suggesting that protein-protein contacts among the components are required.

As discussed in Chapter 2, we have developed screens to specifically target the DnaK-DnaJ system [9, 10]. The key design elements in this assay include the use of high ATP levels to reduce discovery of nucleotide-competitive inhibitors and the inclusion of DnaJ to stimulate ATP turnover and provide a more physiological output. We had

previously used this approach to identify dihydropyrimidines and other scaffolds impact the ATPase activity of DnaK-DnaJ. Moreover, we found that these compounds specifically impacted the stimulatory activity of DnaJ, without affecting the intrinsic enzymatic functions of DnaK (Wisen et al 2010 ACS Chem Biol.; Miyata et al. 2010 JBS). Here, we use this approach to screen a library of plant-derived, natural product extracts in an effort to identify additional scaffolds. Moreover, part of our goal was to determine if compounds identified in an unbiased search would have specific activity against the DnaK-DnaJ protein-protein interaction, to test the utility of the "gray-box" approach.

3.2 Results

3.2.1 Screening for Natural Products that Inhibit the DnaK-DnaJ Complex

To initiate a screen for potential inhibitors of the DnaK-DnaJ combination, we assembled a collection of organic extracts from 36 commercial spices and crude plant materials. For this specific study, we chose to use common plant materials, containing largely known compounds, to facilitate downstream identification of active components. Also, because the Hsp70-Hsp40 family is highly conserved and expressed in many plant pathogens, we were interested in whether natural product extracts might be particularly enriched for inhibitors of this system.

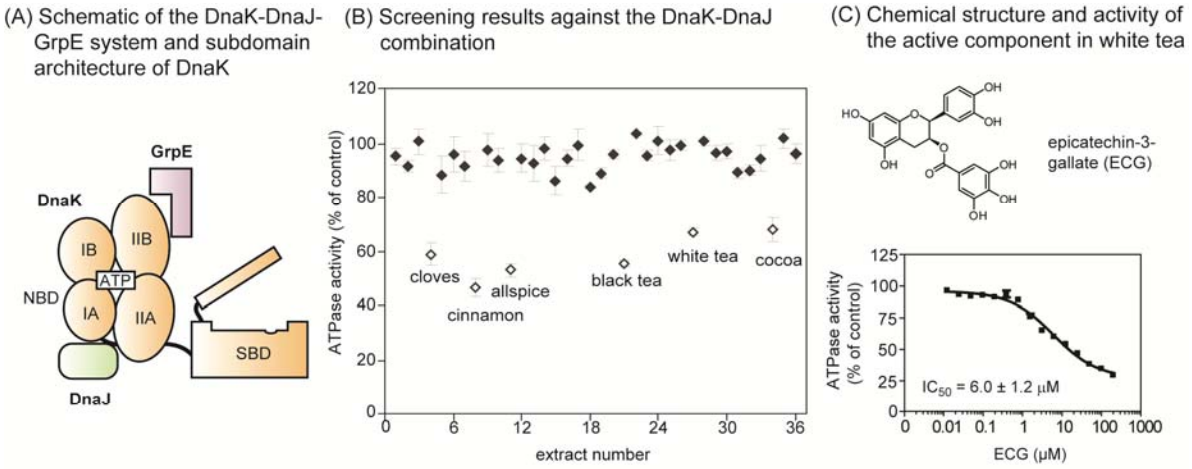

Figure 3.1 Screening plant extracts against the DnaK-DnaJ system reveals epicatechin-3-gallate as the major inhibitor in white tea. (A) Schematic of the DnaK chaperone, with the nuceotide-binding domain (NBD), substrate-binding domain (SBD) and the NBD subdomains (IA, IIA, IB, IIB) highlighted. The co-chaperones DnaJ and GrpE are shown near their approximate binding sites on DnaK's NBD. (B) Results of the screen of natural product extracts (40 µg / mL) against the ATPase activity of the DnaK (0.6 µM) and DnaJ (1 µM). Each extract was screened in duplicate and the range is shown relative to a solvent control. The active compounds (> 25% inhibition) are shown in open symbols (Table S1). (C) Chemical structure of ECG and its dose dependent inhibition of DnaK-DnaJ. The active component of white tea was identified by bio-assay guided fractionation and the structure confirmed by comparing the NMR spectra to an authentic sample (Figure S1). The dose dependence experiment was performed against DnaK-DnaJ in triplicate and the error bars represent standard error of the mean.

This collection was arrayed in 96-well plates and screened at 40 µg/mL using a previously established, high throughput ATPase assay [9]. The key design criteria included the use of high ATP concentrations (1 mM, >> K_m) to minimize discovery of nucleotide-competitive inhibitors. Secondly, we employed an optimized ratio of DnaK (0.6 µM) to DnaJ (1 µM) that gives robust ATP turnover and good Z' scores (~ 0.6), to favor identification of inhibitors [9, 10]. Using this approach, we screened each crude extract in triplicate and found that only 6 of 36 extracts (allspice, black tea, cocoa, cinnamon, cloves, and white tea) inhibited ATPase activity by more than 30% (**Figure**

3.1B). Using activity-guided fractionation on reverse phase HPLC columns, we identified the major active component from the white tea extract as epicatechin-3-gallate (ECG) (**Figures 3.1C and Appendix 3.5.1**). ECG is known to be prevalent in this plant [20]. In dose dependence experiments, the IC_{50} of authentic ECG was 6.0 $\pm$ 0.9 μM against the DnaK-DnaJ system (**Figure 3.1D**).

3.2.2 Identification of the Structure-Activity Relationships (SAR) of Flavonoid-Based Inhibitors.

ECG is a member of a large family of plant-derived flavonoids that possess a variety of anti-oxidation and other activities [20, 21]. Although these well-known scaffolds often have modest selectivity, they can be powerful probes for identifying new drug-binding sites [22, 23]. Therefore, we chose to further explore the structure-activity relationships (SAR) of flavonoids in the specific context of the DnaK-DnaJ system. Towards that goal, we collected 80 related flavonoids (structures available in **Appendix 3.5.2**) and determined their activity against DnaK-DnaJ (**Figure 3.2A**). This approach provided a number of key SAR observations, which are summarized in **Figure 3.2B**. For example, we found that the free phenolic groups on ring A were required for activity; quercetin provided up to 67% inhibition (IC_{50} = 27.6 μM), whereas its tetramethoxy derivative,

(A) Selected results of screening ~80 flavonoids against DnaK-DnaJ

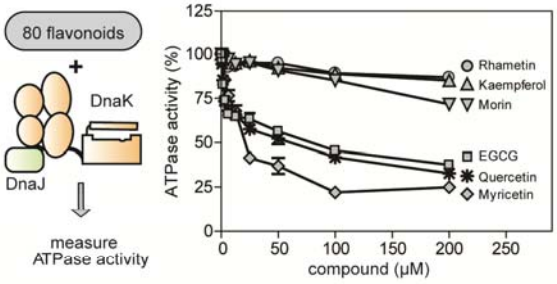

(B) Summary of structure-activity relationships

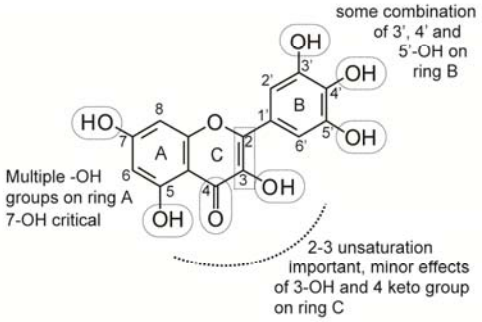

(C) Summary of the activities of select flavonoids

Compund Name	2, 3 DB [a]	C=O at 4 [b]	3 [c]	5	7	2'	3'	4'	5'	IC_{50} (μM)	% Inhibition at 200 μM
Quercetin	+	+	OH	OH	OH	H	OH	OH	H	24.9 ± 4.3	67 ± 2
QTE [d]	+	+	OH	OCH_3	OCH_3	H	OCH_3	OCH_3	H	> 200	ND
Rhamnetin	+	+	OH	OH	OCH_3	H	OH	OH	H	> 200	13 ± 1
Myricetin	+	+	OH	OH	OH	H	OH	OH	OH	14.5 ± 1.5	75 ± 4
Kaempferol	+	+	OH	OH	OH	H	H	OH	H	> 200	15 ± 1
Morin	+	+	OH	OH	OH	OH	H	OH	H	> 200	28 ± 2
Hieracin	+	+	H	OH	OH	H	OH	OH	OH	28.2 ± 15.1	48 ± 3
Luteolin	+	+	H	OH	OH	H	OH	OH	H	9.4 ± 1.5	54 ± 2
Taxifolin	-	+	OH	OH	OH	H	H	OH	OH	> 200	12 ± 2
(+) Catechin	-	-	OH	OH	OH	H	H	OH	OH	> 200	ND
(-)-Epigallocatechin	-	-	OH	OH	OH	H	OH	OH	OH	> 200	0 ± 3
ECG	-	-	Gal [e]	OH	OH	H	OH	OH	H	6.0 ± 0.9	70 ± 1
EGCG	-	-	Gal	OH	OH	H	OH	OH	OH	12.0 ± 5.8	62 ± 1

[a] 2-3 double bond
[b] 4-keto group
[c] position on flavonoid rings
[d] QTE (quercetin tetramethyl (5, 7, 3', 4') ether)
[e] gallate group.

Figure 3.2 The structure activity relationship of flavonoid-based inhibitors of DnaK-DnaJ. (A) Approximately 80 flavonoids were chosen based on their structural similarity to EGC (Figure S2) and screened against the DnaK-DnaJ ATPase activity. The activities of select examples are shown in relation to a DMSO solvent control. The ATPase assays were performed in triplicate and the error bars represent standard error of the mean. (DnaK, 0.6 μM; DnaJ, 1 μM) (B) A summary of the structure-activity relationships, highlighting the key structural featuresof the flavonoid scaffold important for activity against DnaK-DnaJ. (C) Summary of the functional group decoration and activity of select flavonoids. These examples were selected to highlight key SAR observations.

quercetin tetramethyl (5,7,3',4') ether (QTE), had no significant activity (IC_{50} > 200 μM) (**Figure 3.2C**). Most strikingly, rhamnetin, which differs from quercetin only by a 7-methoxy substitution on ring A, was also inactive, suggesting a particularly important role for the C7 phenolic group (**Figure 3.2C**). On ring B, hydroxyl groups at the 3', 4' and 5' positions appeared to improve activity. For example, myricetin, with hydroxyls at all

three positions, provided the highest percent inhibition (75 % at 200 μM; IC_{50} = 14.5 μM), while the 4' mono-hydroxylated kaempferol lacked activity (IC_{50} > 200 μM) (**Figure 3.2C**). On ring C, we found that, although the alkene was clearly required, the hydroxyl group on position 3 made only minor contributions to activity, as revealed by comparing myricetin and quercetin to their counterparts lacking this modification, hieracin (IC_{50} = 28.2 μM) and luteolin (IC_{50} = 9.4 μM) (**Figure 3.2C**). It is worth noting that epicatechin-3-gallate (ECG) and epigallocatechin 3-gallate (EGCG), which contain an extra gallate group appended to ring C did not fit the general SAR patterns, which might suggest that they have a different binding mode (**Figure 3.2C**). Because myricetin provided the best overall inhibition, we chose to further characterize its binding and mechanism.

3.2.3 Myricetin Binds to the IB and IIB Subdomains of DnaK

To gain insight into how flavonoids inhibit ATPase activity, we first performed nuclear magnetic resonance (NMR) experiments to examine whether the compound might bind DnaK. In these studies, ^{1}H-^{15}N labeled DnaK NBD (250 μM, in the presence of 1 mM ADP) was titrated with myricetin and a two dimensional ^{1}H-^{15}N HSQC-TROSY experiment was performed. These experiments revealed a set of chemical shift perturbations mainly in

the IB and IIB subdomains facing the nucleotide binding cleft, along with scattered residues of the IA and IIA (**Figure 3.3A and Appendix 3.5.3A**). Interestingly, these results suggested that myricetin did not bind to the same sites as ATP or DnaJ; instead, the binding site appeared to be in a distinct location "above" the nucleotide-binding cleft **(Figure 3.3A)**.

To further explore this model, we used intrinsic tryptophan fluorescence to study myricetin-induced, structural changes in DnaK. This chaperone has a single tryptophan (Trp102), which is present at the NBD-SBD interface, which has been extensively used as a probe for nucleotide-induced structural transitions [24]. Briefly, ATP is known to induce a blue shift (349 to 345 nm), with a corresponding 18% decrease in intensity [24, 25]. When we saturated DnaK with myricetin (100 μM), tryptophan fluorescence responded normally to ATP binding, suggesting that the compound did not strongly influence the nucleotide-induced structural changes (**Figure 3.3B**). Additionally, it was reported that when flavonoids bind near a tryptophan residue, they quench its fluorescence [26]. Based on our NMR results, myricetin appeared to interact near (~10 Å) Trp102; therefore, we expected to see a fluorescence quench as myricetin bound to DnaK. Indeed, myricetin quenched the Trp fluorescence of nucleotide-free (Apo) DnaK

(**Figure 3.3C**). Further, when we added saturating levels of ATP (2 mM), the apparent affinity (K_{app}) of myricetin decreased from ~600 µM to 38 µM, suggesting that myricetin

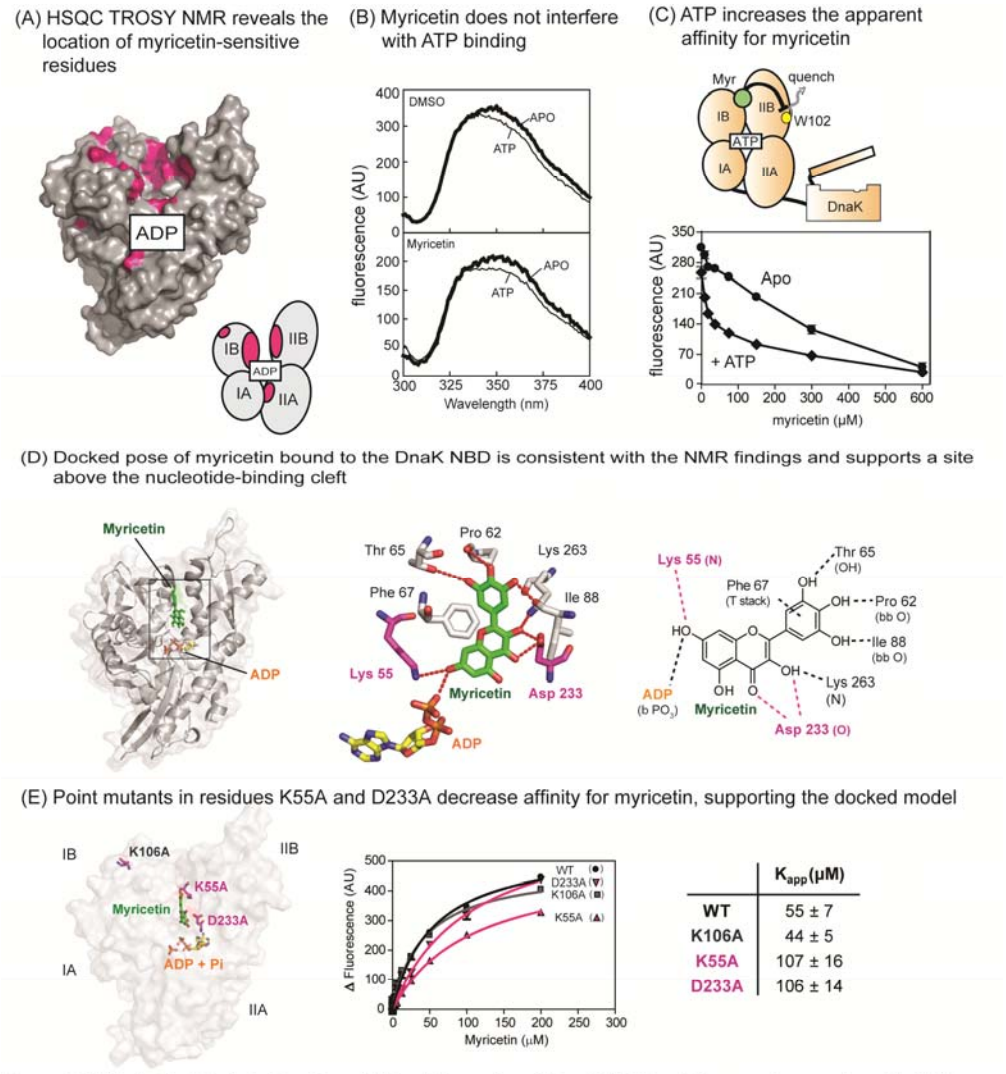

Figure 3.3 Myricetin binds to the IB and IIB subdomains of DnaK NBD and does not compete with ATP. (A) Mapping of the chemical shifts above 0.02 ppm (pink; Figure S3A) onto DnaK suggests that myricetin binds to the upper nucleotide cleft, between the IB and IIB subdomains. (PDB: 1DKG). The approximate position of the nucleotide is shown for orientation and the cartoon schematic is used to identify the subdomains. (B) Saturating myricetin (100 µM) did not block tryptophan fluorescence (excitation 295 nm) in response to ATP. DnaK = 5 µM, ATP = 100 µM. Results are representative of experiments performed in triplicate. (C) ATP (2 mM) enhanced the apparent affinity of myricetin for DnaK, as measured by tryptophan fluorescence (Ex 295 / Em. 342 nm). DnaK = 5 µM. Results are the average of triplicates and the error bars represent standard error of the mean. Error bars are often smaller than the symbols. (D) A representative conformation of myricetin in DnaK, determined by LD simulations of the myrecitin+ADP+Pi DnaK NBD (see the Methods section for details). Contacts observed are in good agreement with observed NMR shifts and SAR data. (E) Point mutations in K55A and D233A (highlighted in purple) significantly reduce binding of myricetin to DnaK, as measured by tryptophan fluorescence, compared to wild type and a control mutant (K106A). Results are the average of triplicate experiments and the error is standard

had even better binding affinity when ATP was present (**Figure 3.3C**). These results support a model in which myricetin binds to a site on DnaK that is distinct from the ATP-binding site and that ATP might even improve its affinity for DnaK.

The NMR chemical shift results were initially puzzling because the distance between the responsive residues on the IB and IIB subdomains in the available crystal structure (PDB code: 1DKG; [15]) seemed unlikely to be filled by myricetin. However, the 1DKG crystal structure likely represents an "open" form of DnaK's NBD because it is a co-complex with GrpE and the IB and IIB subdomains have been proposed to be closer to each other during the ATPase cycle [27, 28]. To explore possible conformational changes in DnaK and how they might impact myricetin binding, we turned to computer simulations. First, a more dynamic structure of DnaK's NBD was examined using unrestrained all-atom Langevin Dynamics (LD) simulations. In these simulations, the presence of ATP or ADP/P_i significantly altered the conformation of DnaK, bringing the IB and IIB subdomains into proximity. Docking calculations based on those "closed" forms of DnaK revealed that myricetin could occupy a position that satisfied the observed NMR shifts (data not shown). While it was satisfying that the observed contacts were consistent with the NMR studies, the conformations were obtained without myricetin present. Therefore,

to determine a conformation for the system that could incorporate any induced-fit phenomena we next conducted additional LD simulations of DnaK's NBD with myricetin, ADP, and P_i bound. The simulations started from the open form, and the protein was allowed to collapse to a closed structure that best incorporated myricetin. These simulations also supported the binding site between the IB and IIB subdomains that was suggested by docking (**Figure 3.3D**). There was a wide degree of sampling seen for myricetin, but the conformation shown in the figure represents over half of the observed conformations. Importantly, the observed binding mode was consistent with the SAR. For example, the critical 7-hydroxyl on ring A could form hydrogen bonds to the □-phosphate of ADP and Lys55. Further, the three hydroxyls of the B ring formed hydrogen bonds with the side-chain hydroxyl of Thr65 and the backbone carbonyl oxygens of Pro62 and Ile88. Finally, the unsaturation in ring C is most likely required for aligning ring B to form those hydrogen bonds and van der Waals contacts with Pro90, and a T-shaped aromatic stacking interaction with Phe67. Together, these contacts appeared to assist the closing of the upper nucleotide-binding cleft, with myrectin interacting with both the IB and IIB subdomains.

To test this model, we generated point mutants designed to disrupt the interaction. Specifically, we targeted Lys55 and Asp233, which are proposed to make contacts with the 7-position hydroxyl on ring A and oxygens on ring C. In addition, we selected another residue far from the proposed myricetin-binding site (Lys106) as a negative control (**Figure 3.3E**). Substituting alanine in these location generated the mutants K55A, D233A and K106A, which were well behaved by circular dichroism [29]. Using tryptophan fluorescence, we then measured their apparent affinity for myricetin. Consistent with the previous studies, the K55A and D233A mutants bound myricetin only weakly (K_{app} >100 μM), while the control mutant, K106A, was similar to the wild type (K_{app} 43 ± 5 and 55 ± 7 μM, respectively) (**Figure 3.3E**). These results further supported the proposed flavonoid interaction site.

Thus far, these studies have focused on potential binding of myricetin to DnaK. However, it also seemed possible that this compound might directly interact with DnaJ, so we performed isothermal titration calorimetry (ITC) studies to test this idea. Briefly, we titrated myricetin into a solution of DnaJ (10 μM) and found that it had no apparent affinity (**Appendix 3.5.3B**). However, these titrations were “noisy”, which precluded a definitive conclusion. Therefore, we performed similar titrations into the truncated J

domain (residues 2-108), which is better behaved in ITC experiments (unpublished observations and **Appendix 3.5.3B**). In these studies, myricetin clearly failed to bind the J domain (**Appendix 3.5.3B**). Although these findings do not preclude weak binding of myricetin to full length DnaJ, they support a model in which the major partner for myricetin is DnaK.

3.2.4 Myricetin Specifically Blocks DnaJ's Ability to Stimulate ATP Turnover

To better understand the implications of these interactions, we next measured whether myricetin could inhibit the ability of DnaJ to stimulate DnaK's ATPase activity. In the absence of compound, DnaJ stimulated ATPase activity by approximately 4-fold, with a half-maximal value (K_{DnaJ}) of 0.37 ± 0.03 μM (**Figure 3.4A**). Addition of myricetin at 200 μM completely suppressed the stimulatory activity of DnaJ (**Figure 3.4A**) and, even at 50 μM, this compound dramatically weakened DnaJ's activity (**Figure 3.4A**). Conversely, it had no effect on the intrinsic ATPase activity of DnaK (**Appendix 3.5.4D**) and it did not influence the stimulation of DnaK by the other co-chaperone, GrpE (**Figures 3.4B and Appendix 3.5.4C**). Finally, peptide substrates are known to stimulate ATP turnover [30], so we tested whether myricetin could block this activity. Using the high affinity model substrate, NRLLLTG, we found that myricetin had no effect on peptide-mediated

stimulation (**Figure 3.4C and Appendix 3.5.4B**). Together, these results strongly suggest that myricetin selectively blocks the co-chaperone activity of DnaJ, without impacting the function of other DnaK partners.

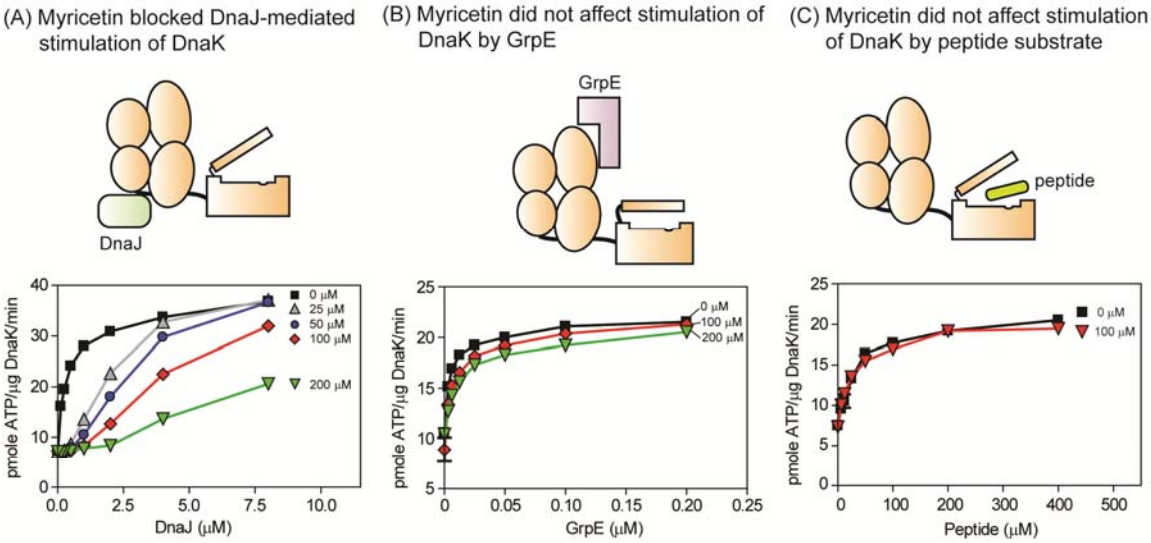

Figure 3.4 Myricetin specifically blocked DnaJ cochaperone activities. (A) In ATPase assays, myricetin blocked DnaJ-mediated stimulation. In all the ATPase experiments, the results are the average of triplicates and the error bars represent standard error of the mean. (B) Even at the highest concentrations, myricetin did not impact GrpE-mediated stimulation of ATP turnover. (C) Similarly, myricetin was unable to block stimulation by a model substrate peptide. Additional tests of this idea can be found in Figure S4.

As mentioned above, we found that myricetin did not bind to the truncated J domain by ITC (see **Appendix 3.5.4b**). Therefore, we wanted to specifically test whether this compound could block J domain activity. Consistent with previous reports [11], we found that the J domain stimulates DnaK's ATP turnover (**Appendix 3.5.4A**). Similar to what we observed with full length DnaJ, myricetin was able to block this stimulatory activity (**Appendix 3.5.4A**).

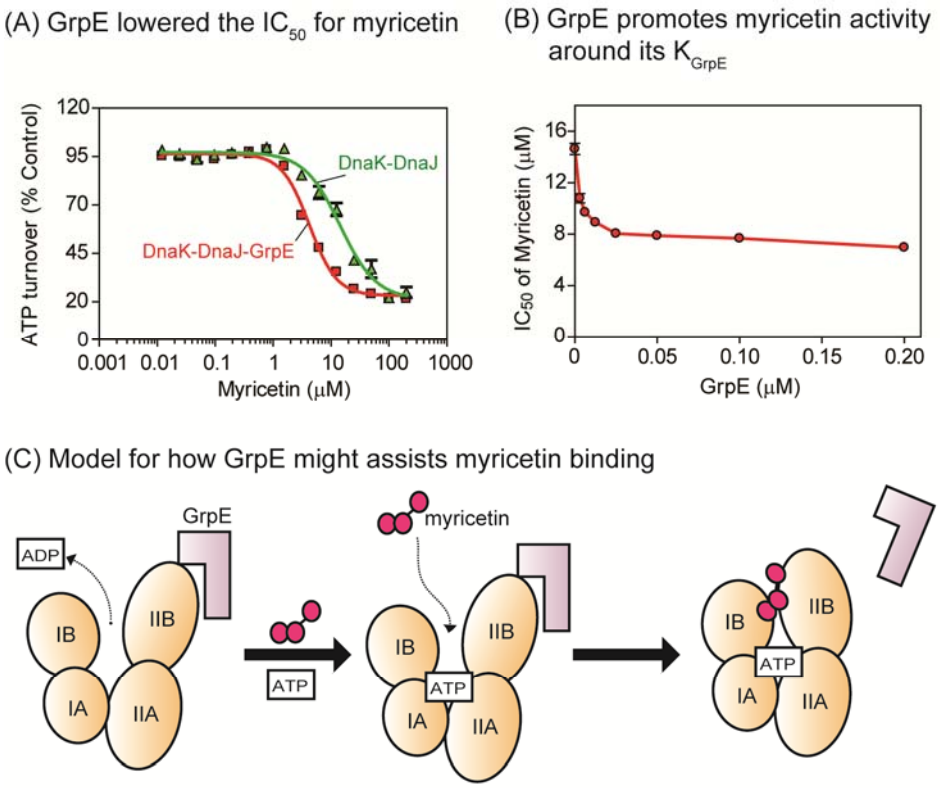

Figure 3.5 GrpE enhanced myricetin activity on DnaK-DnaJ. (A) GrpE (2 μM) decreased the IC_{50} of myricetin for the DnaK-DnaJ complex. (B) Dose dependence of GrpE action on the IC_{50} value of myricetin. DnaK = 0.6 μM and DnaJ = 1 μM. Results are the average of triplicates and the error bars represent standard error of the mean. (C) Model for how GrpE might impact myricetin binding. Only the NBD is shown for clarity.

Because the binding sites for GrpE and myricetin are both in the IB and IIB subdomains, we were interested in how this co-chaperone might influence compound binding. We had already found that myricetin did not suppress the stimulatory activity of GrpE, but we were also interested in whether the co-chaperone might impact myricetin-binding affinity. Towards that question, we tested the activity of myricetin in the presence of both DnaJ and GrpE. At saturating concentration of GrpE, we found that the apparent affinity of myricetin was significantly enhanced (**Figure 3.5A**). By altering the

concentration of GrpE and measuring the IC_{50} value of myricetin, we confirmed that the co-chaperone potentiated the activity of the compound (**Figure 3.5B**). This result suggests that GrpE, by opening the nucleotide-binding cleft of DnaK, may promote binding to myricetin; thereby increase affinity during ATP cycling (**Figure 3.5C**).

3.2.5 Myricetin reduces the ability of DnaJ to stimulate the substrate binding activity of DnaK

Because myricetin appeared to block the ability of DnaJ to accelerate ATP turnover in DnaK, we hypothesized that it might also interrupt substrate binding by reducing conversion to the high affinity, ADP-bound state. To test this hypothesis, we measured DnaK's binding to a model substrate, luciferase, using an ELISA-based approach. Briefly, we partially digested luciferase to increase the exposed hydrophobic regions and then absorbed this substrate into 96-well microtiter plates. Using an anti-DnaK antibody to measure bound chaperone, we first confirmed that DnaJ is able to stimulate DnaK's binding to immobilized luciferase (**Figure 3.6A**) [31]. Maximal stimulation was observed at 60 nM of DnaJ and, at higher levels, DnaK's binding gradually diminished, likely because of competition between DnaJ and DnaK for shared sites on luciferase. We found that 20 μM myricetin inhibited DnaJ-mediated stimulation of binding, with the amount

of DnaJ required to promote binding increased from 62 nM to 1 μM and the maximal amount of bound DnaK also decreased by approximately 40% (**Figure 3.6A**).

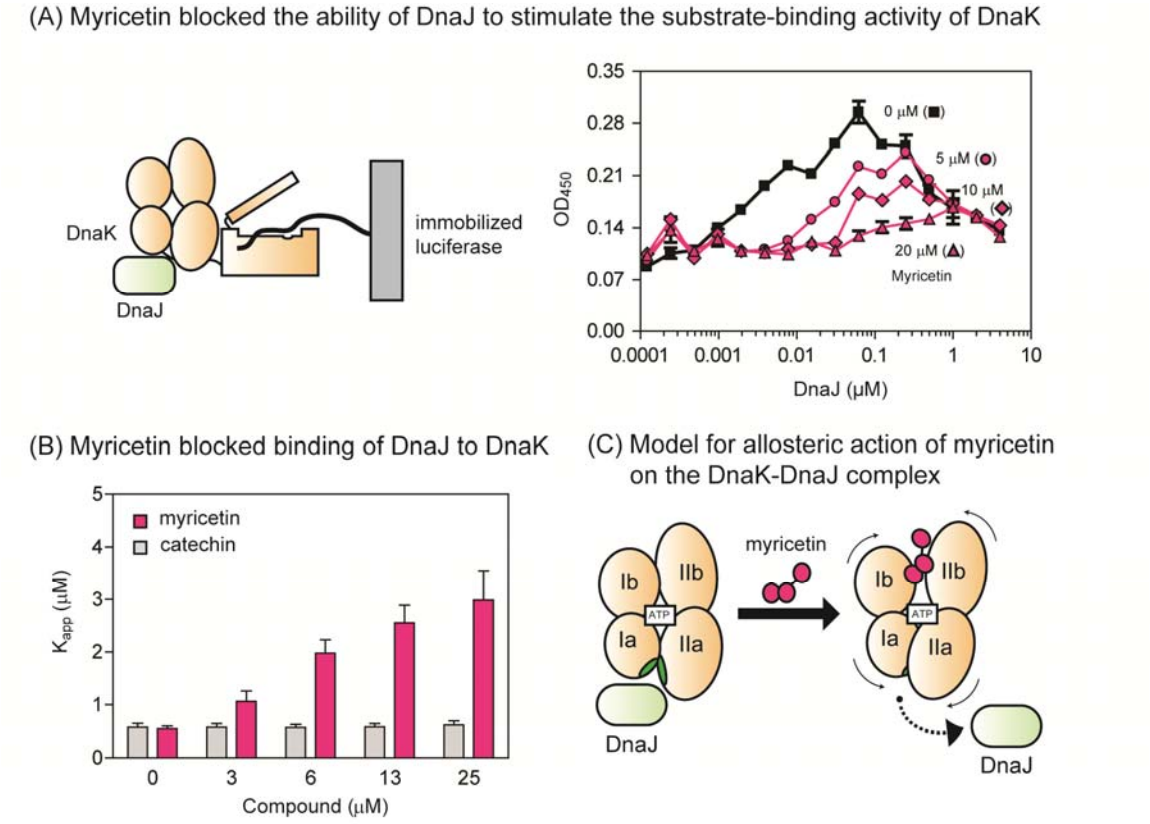

Figure 3.6 Myricetin blocked DnaJ-mediated enhancement of DnaK's binding to substrate and interfered with the DnaK-DnaJ interaction. (A) Myricetin inhibited the DnaJ-mediated stimulation of DnaK binding to partially-digested firefly luciferase. Each data point is the average of triplicates and the error bars represent the standard error of the mean. (B) Labeled DnaJ was titrated into fluorescent DnaK and the apparent binding affinity (K_{app}) measured by FRET. Myricetin, but not the control compound (catechin), partially blocked binding. The results are the average of triplicate and the error bars represent standard error of the mean. Further results are shown in Figure S5. (C) Model for the allosteric mechanism of myricetin. By impacting the clam-like motions of the subdomains, myricetin might impact DnaJ binding at a distal site. The hydrophobic cleft between subdomains IA and IIA is shown in green.

3.2.6 Myricetin inhibits binding of DnaJ to DnaK

Binding of myricetin to DnaK might block the ability of DnaJ to act on DnaK through at least two different mechanisms. In theory, myricetin might either (a) inhibit the physical interactions between DnaJ and DnaK or (b) block the allosteric activity of DnaJ on DnaK without directly impacting the strength of the protein-protein interaction. To begin to differentiate between these models, we directly measured the binding of DnaJ to DnaK by Förster resonance energy transfer (FRET) [32]. Briefly, DnaK was labeled with the fluorescent donor Alexa-488 (Em. 525 nm) and DnaJ with Black Hole Quencher-10 (BHQ-10), a FRET acceptor that absorb strongly around 507 nm. In the absence of myricetin, the apparent affinity (K_{app}) between DnaJ and DnaK was estimated to be approximately 560 nM, consistent with previous studies [13]. Addition of myricetin significantly reduced binding of DnaJ to DnaK (**Figure 3.6B and Appendix 3.5.5**), with the K_{app} weakened by 5.3-fold (at 25 μM myricetin). A control flavonoid, (±)-catechin, did not inhibit this interaction (**Figure 3.6B**) Together, these results suggest that myricetin inhibits DnaJ by preventing contacts between the chaperone and co-chaperone **(Figure 3.6C)**.

3.3 Discussion

3.3.1 Design of High Throughput Screens for the DnaK-DnaJ Combination: Methods for Targeting Multi-Protein Complexes.

A key effort in chemical biology is to identify inhibitors of protein-protein interactions [33-35]. Further, allosteric modulators of these interactions are becoming an increasingly important goal in screening campaigns. With these concepts in mind, we targeted the DnaK-DnaJ combination. The key design criteria were (a) screen in the presence of high ATP concentrations (>> K_m) and (b) screen against the re-constituted combination of DnaK and DnaJ. The first design aspect (*i.e.* high ATP) was chosen to favor identification of allosteric, rather than competitive, modulators. For the DnaK system, this criterion is important because of the high cellular levels of ATP and its unusually tight binding to nucleotide (mid-nanomolar) [36]. The second design aspect (*i.e.* inclusion of DnaJ) was selected because a majority of the measurable signal would be expected to emerge from stimulatory activities of the co-chaperone. Thus, compounds appearing as "actives" in the screen might be expected to preferentially influence the co-chaperone dependent activity (*e.g.* following the axiom, "you get what you screen for"). Together, we term this approach "gray box" screening because its goals are distinct from experiments that target purified proteins. Rather, it has more in

common with “black box”, cell-based screens, but with fewer possible options for target deconvolution.

“Gray box” screens might be particularly appropriate for systems, such as Hsp70s, that are regulated by multiple stimulatory and inhibitory protein partners. Hsp70, being the hub of many cellular activities [37], is regulated by many co-chaperones, including J domain-containing proteins, nucleotide exchange factors (*e.g.* GrpE, BAGs, Hsp110 and HspBP1), and tetratricopeptide repeat (TPR) motif containing proteins (*e.g.* CHIP and HOP) [37-39]. Interestingly, many of these interactions appear to converge on modulation of ATPase rate, and it might be a particularly attractive surrogate for emergent chaperone functions. In fact, we have used this method to identify chemical probes against the mammalian Hsp70 system that have revealed critical roles for ATP turnover in models of protein misfolding disease [40, 41]. We anticipate that a variety of other, important multi-protein systems, such as chromatin remodeling complexes, the mTor complex, or the exocyst, might be similarly targeted. Finally, it is also worth strongly emphasizing that the phenotypic complexity of other systems or technical issues may make a “gray box” approach cumbersome or undesirable.

3.3.2 Identification of an Unanticipated Allosteric Site on DnaK-DnaJ

In our natural product screens, we identified flavonoids as inhibitors of the DnaK-DnaJ complex. There are >9,000 naturally occurring flavonoids [42], and these compounds have been reported to have antioxidant, antitumor, antiviral, antifungal and antibacterial activities [20, 21, 43]. These compounds carry out their diverse biological activities by targeting various enzymes, including receptor tyrosine kinases, cyclin-dependent kinases, and P-glycoprotein [20, 26, 44, 45]. The diversity of these targets suggests that flavonoids have relatively promiscuous binding profiles. Yet, plant-derived flavonoids have been productive and interesting starting points for drug discovery [22, 23, 46]. Interestingly, one common feature of flavonoid targets is that they often bind ATP [44, 45]; however, NMR, fluorescence and modeling studies suggested that the binding site of myricetin on DnaK is distinct from the ATP-binding pocket (see **Figure 3.3**). This finding is consistent with recent studies on other flavonoids [47]. Despite this interesting mechanism, we found that the SAR for inhibition of DnaK-DnaJ is similar to that reported for flavonoids against other enzymes, such as receptor tyrosine kinase or protein kinase C [44, 45]. Thus, it is highly unlikely that myricetin or its close derivatives will bind selectively to DnaK-DnaJ *in vivo*. Rather, they might have been selected through evolution for their broad spectrum of targets [21], an

interesting alternative to the single-target, drug discovery model.

Although myrecitin is not a selective or particularly potent inhibitor of DnaK-DnaJ, these results suggest a new “druggable” site on the chaperone and they reveal a previously unanticipated allosteric network in DnaK. We found that myricetin, by binding to the upper nucleotide binding cleft between the IB and IIB subdomains, specifically interfered with binding to DnaJ and, subsequently, it interrupted co-chaperone stimulated activities. How can myricetin binding in the IB and IIB subdomain affect a remote site between the IA and IIA subdomains, where DnaJ binds to DnaK? Both NMR and modeling studies suggest that the IB and IIB subdomains move closer to each other in the “closed”, ATP-bound conformation [27, 28]. Simultaneously, the hydrophobic surface between the IA and IIA subdomains is expected to be more accessible in the ATP-bound form [27, 28]. Thus, it seems plausible that domains I and II undergo a clam-like movement during ATP hydrolysis, linking closure of the IB and IIB subdomains to the opening of IA and IIA. For that reason, if myricetin inserts between the IB and IIB subdomains, it might disrupt the DnaJ docking site at the distal IA and IIA region (see **Figure 3.6C**). This model clearly requires additional structural evaluation.

3.3.3 Targeting the Myricetin-binding Site by "Scaffold Hopping"

Although the promiscuous nature of myricetin renders it unsuitable as a drug lead, its binding site might be “druggable” by other compounds. Thus, with the collaboration with Peter Ung in Carlson Lab, we seek to “hop” to new chemical scaffolds that are more specific and have higher bioavailability. To achieve this goal, Peter used both the chemical/physical properties and the topological elements (fused rings, ring size, elements in certain position, etc.) of myricetin and other active flavonoids to search for potential scaffolds, and the “hits” were further refined and ranked by multiple protein structure docking against the structure of ATP or ADP-bound NBD (modeled from the crystal structure of GrpE-bound apo-NBD). From the compounds that were ranked in the top 12.5%, we selected 19 compounds and tested their abilities to inhibit DnaJ-stimulated ATPase activity of DnaK. Surprisingly, none of them was active (S. Patury and J.E. Gestwicki, unpublished data). This result revealed the challenge of targeting flexible structures; perhaps only promiscuous compounds like myricetin can form enough hydrogen bounds and have sufficient hydrophobic interactions that stabilize the binding. This hypothesis was supported by our mutagenesis study: none of our 16 point mutants of DnaK, selected based on NMR footprints, blocked myricetin inhibition (L.

Chang and J.E. Geswicki unpublished result). This suggests that myricetin can bind to this flexible site on NBD via various interactions and orientations.

3.3.4 Conclusions

Hsp70s are highly conserved molecular chaperones that play crucial roles in maintaining cellular proteostasis. They are also emerging drug targets for a range of diseases, including cancer, microbial infection and neurodegeneration. In this study, we identified myricetin as a new inhibitor of the *E. coli* Hsp70, DnaK. NMR and modeling studies suggested that this compound binds to a flexible site between the IB and IIB subdomains of DnaK and that it specifically blocks the activities of the co-chaperone DnaJ. This mechanism is unexpected because myricetin's binding site is at least 20 Å from where DnaJ interacts with DnaK, in a region not previously implicated in DnaJ-mediated allostery. Thus, although myricetin, because of its poor selectivity and stability, is unlikely to be a suitable scaffold for drug development *per se*, this work identified an unanticipated allosteric site that might be suitable for targeting. Finally, this study provides a "gray box" strategy for identifying modulators of protein-protein interactions in reconstituted multiprotein complexes *in vitro*.

3.4 Materials and Methods

3.4.1 Materials and general protocols

Apigenin, baicalein, catechin, epigallocatechin-3-gallate, epigallocatechin, luteolin, morin, myricetin, quercetin, and rhamnetin were purchased from Sigma (St. Louis, MO). Taxifolin and kaempferol were bought from Fluka (Switzerland). Hieracin and epicatechin gallate were acquired from MicroSource (Gaylordsville, CT). The ATPase assays were performed using a previously established protocol [9].

3.4.2 Plasmid construction and protein purification

DnaK, GrpE and DnaJ were purified, and the His-tags were cleaved as previously indicated [29]. Nucleotide-free (apo) DnaK was purified by a slight modification of the previous protocol. Briefly, after the first low-salt washing step of the ATP column, apo-DnaK was eluted using 50 mM Tris buffer (pH 7.5) containing 1 M NaCl. His-tagged J-domain (residue 2-108) was first purified as previously mentioned [29], but an additional purification step using a Superdex 200 gel filtration column (GE Healthcare) was included. Purified DnaJ, J domain, GrpE and DnaK were dialyzed into 25 mM Tris buffer (pH 7.5) containing 10 mM KCl (for DnaJ and J domain, 150 mM KCl) and 5 mM $MgCl_2$, and stored at -80 °C.

3.4.3 Construction of natural extract library and screening against DnaK/DnaJ complex

Approximately 300 mg of powdered natural product was extracted with ~500 µL of methanol. After vortexing and 15 minutes of sonication, the samples were centrifuged at 10,000 rpm for 5 minutes and the supernatant collected. After removing the organic solvent, the dried material was suspended in DMSO at 1 mg/mL. The resulting extract library was screened in the ATPase assay at 40 µg/ml final concentration, using a previously described protocol [9]. The concentrations of DnaJ and DnaK were 1.0 and 0.6 µM, respectively.

3.4.4 Identification of the active component from tea

White tea leaves were extracted with EtOAc, MeOH and acetone. The combined extracts were then concentrated *in vacuo* and the residue was partitioned between H_2O and CH_2Cl_2. The organic phase was partitioned between 90% MeOH and *n*-hexanes and the aqueous MeOH fraction was further partitioned between 60% MeOH and CH_2Cl_2. Using ATPase assays for bioactivity-guided fractionation, we identified the 60% MeOH fraction as the sample with inhibitory activity against *E. coli* DnaK. This sample was then subjected to ODS flash chromatography (Supelco, Bellefonte, PA) with aqueous MeOH, yielding six fractions. The most active fraction was purified by reversed-phase HPLC

(Beckman-coulter, Brea, CA) on Waters Spherisorb ODS-2 using a linear gradient elution of an aqueous MeOH system followed by reversed-phase HPLC with 20% aqueous MeOH. This procedure yielded epicatechin 3-gallate (ECG) as the major active component. The identification of this compound was confirmed by comparison of the ^{1}H NMR spectrum and ESI-MS spectrum with those of an authentic sample purchased from MicroSource (see **Appendix 3.5.1**).

3.4.5 Structure activity relationship studies

To identify available molecules structurally similar to ECG, we performed similarity searches for the core 2-phenyl benzopyran in the >100,000 compounds of the M-screen database (University of Michigan). From this analysis, 80 flavonoids were selected. Within the collection, 59 compounds were selected from the MS2000 library MicroSource), 10 from the Maybridge Hit finder library (Maybridge), 4 from the NIH Clinical Collection (BioFocus), 4 from the ChemDiv library, 1 from the Chembridge library, and 1 from the National Cancer Institute Collection. The compounds were "cherry-picked" and serially diluted (1:2) in ddH_2O from 125 µM to 0.9 µM into white, 384-well low-volume plates (4 µL/well). Compounds were tested in duplicate, using a previously described protocol [48]. Flavonoids that showed inhibition or had structure

similar to active compounds were purchased and retested in 96-well malachite green-based ATPase assay against DnaK/J complex (at 0.6 and 1 μM) as described [9].

3.4.6 NMR spectroscopy

The NMR experiments were carried out as previously described [40]. Briefly, ^{15}N-labeled $DnaK_{2-388}$ was purified and concentrated to approximately 0.5 mM, exchanged into NMR buffer (25 mM Tris, 10 mM $MgCl_2$, 5 mM KCl, 10% $^{2}H_2O$, 0.01% sodium azide, pH 7.1), and stored at –80 °C. Prior to NMR analysis, $DnaK_{2-388}$ samples were thawed and supplemented with 5 mM ADP. After collecting reference spectra, myricetin was titrated to a final concentration of 1 mM from a 100 mM stock in DMSO. Control experiments showed that DMSO alone had had no detectable effects on the spectrum of $DnaK_{2-388}$ at concentrations up to 1 %, and that it had minimal effects on the spectra of $DnaK_{2-605}$ at the same concentration. 2D HSQC-TROSY NMR spectra were collected at 30 ºC on a cryoprobe-equipped Varian Inova 800 MHz spectrometer, with data collection times of approximately 2 hours per spectrum. NMR data were processed using NMRPipe and analyzed with Sparky. Combined ^{1}H and ^{15}N chemical shift changes were measured using a weighted function and the assignments generated previously. Residues were selected as significant if the chemical shift was greater than 0.02 ppm (**Appendix 3.5.3**).

3.4.7 Protein dynamic simulations

Coordinates of *E. coli* DnaK NBD were obtained from the PDB (PDB: 1DKG; [15]) and the co-crystallized nucleotide-exchange factor GrpE was discarded. The missing side chains and short loops (≤ 5 amino acids) of NBD were introduced using Molecular Operating Environment (v2005.06) (Chemical Computing Group, Inc., Quebec, Canada) and PyMOL (DeLano Scientific, Palo Alto, CA). AMBER 10 [49] package was used to perform unrestrained all-atom Langevin Dynamics (LD) simulations. The protein was modeled using the FF99SB force field [50]. Model II of a modified Generalized Born approach [51] was used to implicitly model aqueous solvation. Collision frequency of 1 ps^{-1} was used. Three states of DnaK were simulated using LD: apo-NDB, ATP-bound NDB, and ADP+P_i-bound NDB. Since 1DKG was crystallized without bound cofactors, positions for these cofactors were obtained by superimposing the crystal structures of the closely related homolog bovine Hsc70. ATP, Mg^{2+}, and K^+ ions were obtained from PDB: 1KAZ [52] and ADP, PO_4^{3-}, Mg^{2+}, and K^+ ions were obtained from PDB: 1BUP [53].

Parameters for P_i and Mg^{2+} were generated using the ANTECHAMBER (Wang et al. 2006) module of AMBER, and AM1-BCC charges [54] were applied. Nucleotide parameters

developed by Meagher et al. [55] were used for ATP and ADP. The SHAKE algorithm [56] was used to restrain hydrogen atoms. Hydrogen atoms were first minimized, followed by residue side chains and finally an all-atom minimization. Five independent LD simulations for each of the three different NBD states were initiated with different random-number seeds. The non-bonded interactions cutoff was set to 999 Å. Default dielectric values were used: interior = 1 and exterior = 78.5. Heating and restrained equilibrations were followed. The system was heated gradually from 100 K to 300 K during the first two equilibrations, and the temperature remained at 300 K for the remaining equilibrations and production phase. Restraints were placed on all heavy atoms and gradually relaxed over the first four equilibrations using force constants from 2.0 to 0.1 kcal/mol·Å^2. Restraints were maintained on backbone atoms in the fifth equilibration using a force constant of 0.1 kcal/mol·Å^2. All restraints were removed in the sixth equilibration. The first three equilibrations were performed for 20 ps each, followed by 50 ps for the fourth and fifth equilibrations. The sixth, unrestrained equilibration was run for 740 ps and the production phase was run for 5 ns. A time step of 1 fs was used and snapshots were collected every 1 ps.

For the simulations of myricetin bound to DnaK, myricetin was docked into the initial NBD+ADP+P_i structure using AutoDock 4.01 [57]. This was the same structure built from the crystal structures and used to initiate the LD simulations. A grid box of (90, 100, 94) points and 0.375 Å spacing was centered at the interface between IB/IIB subdomains and over the residues with myricetin-induced NMR chemical-shifts. The docking calculation involved a Lamarckian genetic algorithm [58]; an initial population size of 200 and a maximum of 75 million energy evaluations were applied. The lowest-energy pose of myricetin, which was consistent with the NMR chemical-shifts, was added to the NBD. GAFF [59] with AM1-BCC charges was used to parameterize myricetin in ANTECHAMBER. Five independent LD simulations of the myricetin+ADP+P_i+NBD system were generated using protocol described above.

3.4.8 Tryptophan fluorescence

The tryptophan fluorescence experiments were carried out as previously reported with slight modification [25]. To study whether myricetin blocked ATP binding, 6 µM apo-DnaK was incubated with 125 µM myricetin with total volume of 40 µL in a 96-well black plate (Corning) for one hour at 37 °C. Next, 10µL of 500 µM ATP or buffer (200 mM Tris, 40 mM KCl, 12 mM $MgCl_2$, pH 7.4) was added to each well, and then the emission

spectrum between 300 - 400 nm was recorded (excitation at 295 nm) using a SpectraMax M5 (Molecular Devices). Alternatively, the tryptophan fluorescence quench caused by myricetin was measured as follow. Myricetin, at concentration indicated in the figure, was added to 5 µM of DnaK in the presence or absence of 2 mM ATP with a total volume of 30 µL in a black 96-well plate and the fluorescence at 342 nm (excitation at 295 nm) was measured by SpectraMax M5 and the controls with every component except DnaK was subtracted from the final values. Experiments described in **Figure 3.3E** were carried out as above, but with slightly different DnaK and ATP concentrations (3 µM and 1 mM, respectively) in lower total volume (20 µL) and the readings were performed in black, 384-well round bottom plates (Corning).

3.4.9 Enzyme-linked Immunosorbant Assay.

Binding of DnaK to denatured luciferase was measured as described in Chapter 1.

3.4.10 Characterization of DnaK-DnaJ Interaction by FRET

The assays were carried out as recently reported with slight modifications [32]. DnaK (10 mg/mL; 200 µL) was labeled with Alexa Fluor 488 5-TFP (Invitrogen, Carlsbad, CA) and DnaJ (10 mg/mL; 300 µL) was labeled using the N-hydroxysuccinimide ester of BHQ-10

Carboxylic Acid (Biosearch Technologies, Novato, CA). Both reactions were carried out at 10:1 molar ratio of dye:protein in bicarbonate buffer (100 mM $NaHCO_3$, 5 mM $MgCl_2$, 10 mM KCl, pH = 9.5). DnaK was labeled for 1.5 hours at room temperature while DnaJ was labeled for 1 hour at 30 °C. After the incubation, the unreacted dye was removed and the buffer was exchanged to 25 mM HEPES buffer (pH = 7.4) using Zeba^{TM} Desalt Spin Columns (2 mL, MWCO = 7000 Da) (Thermo Scientific, Rockford, IL). The average extent of labeling for DnaK and DnaJ was then determined to be approximately 2.5 and 0.5 fluorophore/dye per protein, respectively, using the ε_{495} = 71,000 $M^{-1}cm^{-1}$ (Alexa Fluor 488) and ε_{507} = 30,000 M^{-1} cm^{-1} (BHQ-10). Labeled DnaK was diluted to 100 nM using 100 mM Tris-HCl buffer (20 mM KCl, 6 mM $MgCl_2$, 0.01% Triton-X-100, pH = 7.45) containing compound (or solvent control) and 2 mM ATP. After pre-incubation at room temperature for 30 minutes, 10 µL of this diluted sample was added to 384-well, black round bottom plates (Corning). Next, 10 µL of a BHQ-10-labeled DnaJ solution was added to each well and the samples were incubated at 37 °C for 30 minutes. After the incubation, the fluorescence at 525 nm (Ex. 480, cut-off 515 nm) was measured using a SpectraMax M5 microplate reader. The result were analyzed by GraphPad Prism 4.0 using a hyperbolic fit with a non-zero intercept ($\Delta F = \Delta F_{max} \cdot [J]/(K_{app}+[J])+b$). ΔF = fluorescence change; ΔF_{max} = maximum fluorescence change; K_{app} = apparent K_d; [J] =

DnaJ concentration.

Notes

This work has been published as “Chemical screens against a reconstituted multiprotein complex: myricetin blocks DnaJ regulation of DnaK through an allosteric mechanism” **2011** Chem Biol. 18; 210-21.

Lyra Chang and Jason E. Gestwicki designed the experiments. Lyra Chang conducted the experiments. In this study, Yoshinari Miyata helped to identify the active compounds in white tea extract, Eric B. Bertelsen identified the binding site of myricetin by NMR, Peter Ung performed computer modeling for myricetin-DnaK interaction and ligand-based “scaffold-hopping”, and Thomas J. McQuade helped with high throughput screening.

3.5 Appendix

3.5.1 Identify the active compound in white tea as (-)-epicatechin-3-gallate

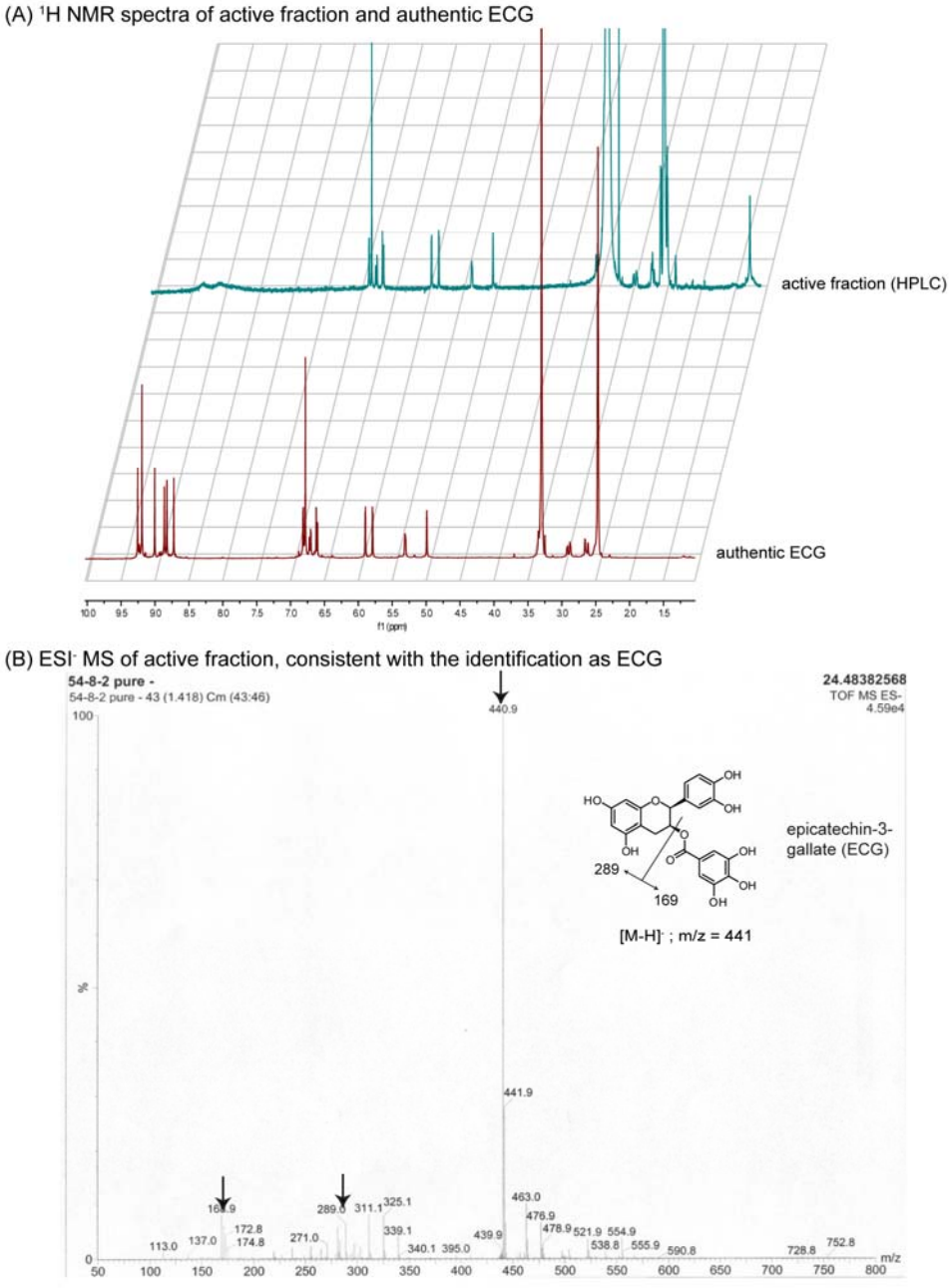

Appendix 3.5.1 Characterization of active component from white tea and identification as (-)-epicatechin-3-gallate. (A) ¹H-NMR spectra of active fraction and authentic ECG. (B) ESI- MS of the active fraction. For further details on the identification of ECG, see Mizooku *et al.* (2003) *Rapid Commun. Mass Spectrometry* 17:1915-1918.

3.5.2 The chemical structures of the inactive flavonoids

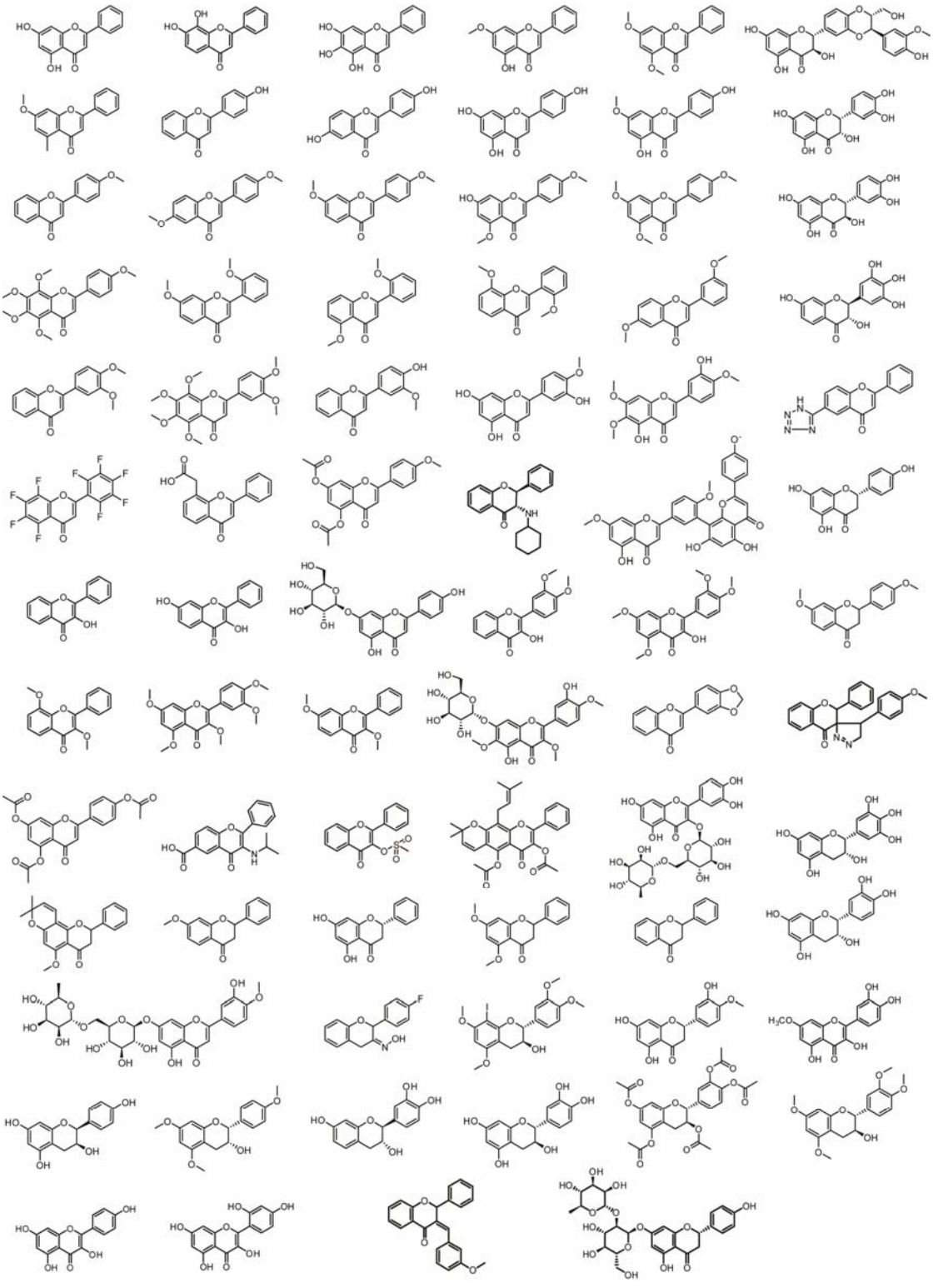

Appendix 3.5.2 Chemical structures of the inactive members of the flavonoid collection.

3.5.3 NMR result of myricetin binding to DnaK$_{NBD}$ and the ITC result of injecting myricetin to DnaJ and J domain

(A) Binding of myricetin to DnaK$_{NBD}$ by ^{1}H-^{15}N HSQC-TROSY NMR

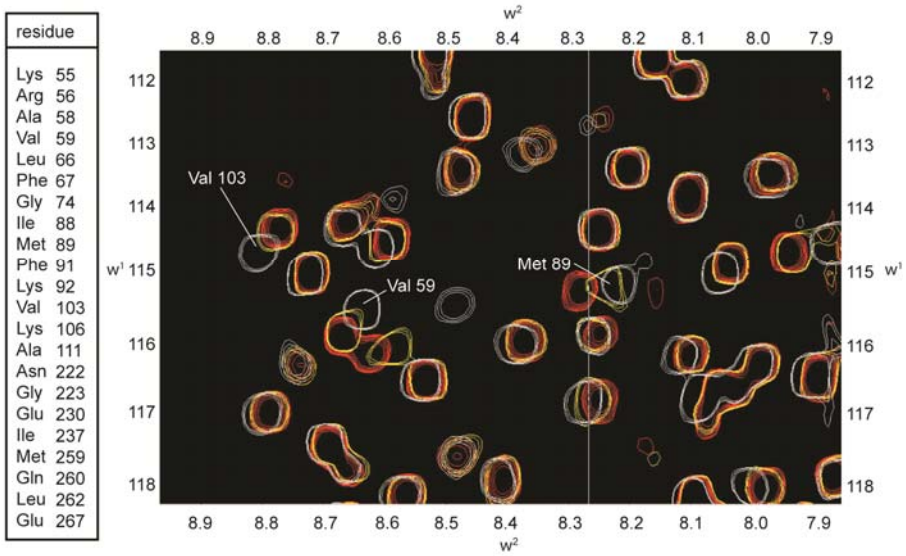

(B) Myricetin doesn't bind tightly to DnaJ or its J domain, by isothermal calorimetry

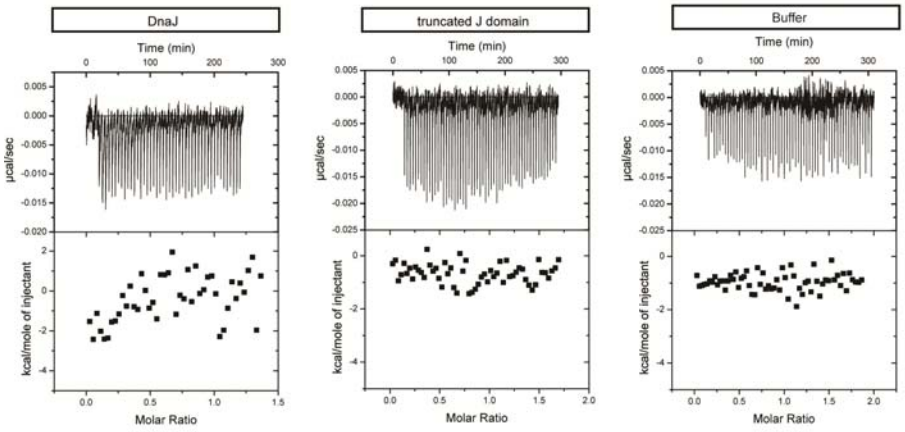

Appendix 3.5.3 ^{1}H-^{15}N HSQC-TROSY NMR results and ITC result of injecting myricetin into DnaJ, J domain, and buffer (A) (left) A list of the assigned residues that undergo at least a 0.02 ppm shift upon titration with myricetin. (right) A sample of the 2D HSQC-TROSY NMR spectra, highlighting residues Met 89 and Val 59. white = DMSO control; yellow = 0.5 mM myricetin; red = 1 mM myricetin. (B) Binding of myricetin to either full length DnaJ or a truncated J-domain was measured by ITC. Results are representative of experiments performed in duplicate or quadruplicate. Isothermal calorimetry titrations were performed using a VP-ITC microcalorimeter (MicroCal) at 25 °C. Titrations for J domain (10 µM) were performed in 25 mM HEPES buffer (5 mM MgCl2, 150 mM KCl, pH=7.4) whereas the experiments with DnaJ (10 µM) were carried out in 25 mM Tris buffer (5 mM MgCl2, 150 mM KCl pH=7.4). Both J domain and DnaJ were extensively dialyzed into the target buffer and then loaded into the calorimetric cell (cell volume = 1.43 mL). Protein samples were then titrated with 80 µM myricetin in 5 µL steps. The buffers used to prepare the myricetin samples were matched to the protein samples and control buffer injections were subtracted.

3.5.4 Myricetin specifically blocked DnaJ stimulation of DnaK ATPase activity

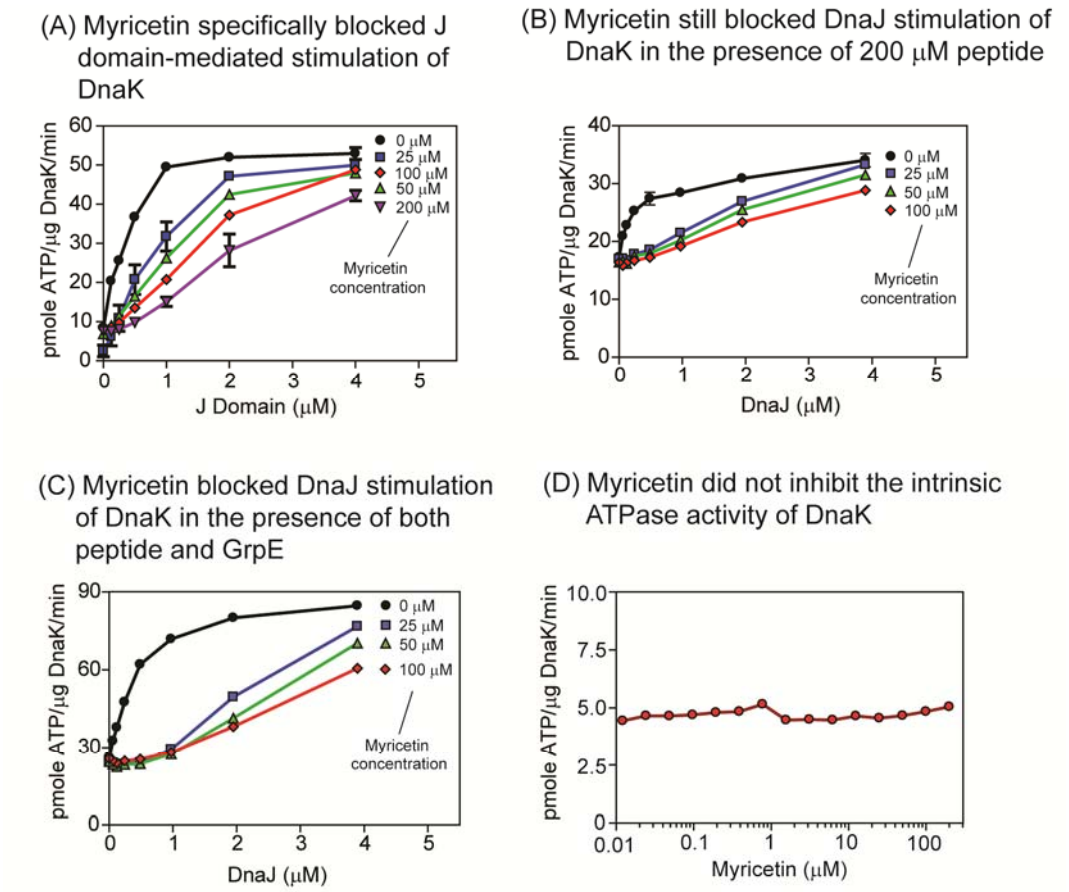

Appendix 3.5.4 Myricetin specifically blocked DnaJ stimulation of DnaK ATPase activity. (A) Myricetin specifically interfered with J domain (residues 2-108) mediated stimulation of DnaK's ATPase activity. Myricetin also blocked DnaJ stimulation in the presence of either (B) peptide (200 μM) or (C) peptide (200 μM) and GrpE (0.2 μM). (D) Myricetin did not impact the intrinsic ATPase activity of DnaK. Experimetns are the average of triplicates and the error bars represent standard error of the mean.

3.5.5 Myricetin blocked the interaction between DnaK and DnaJ (measured by FRET)

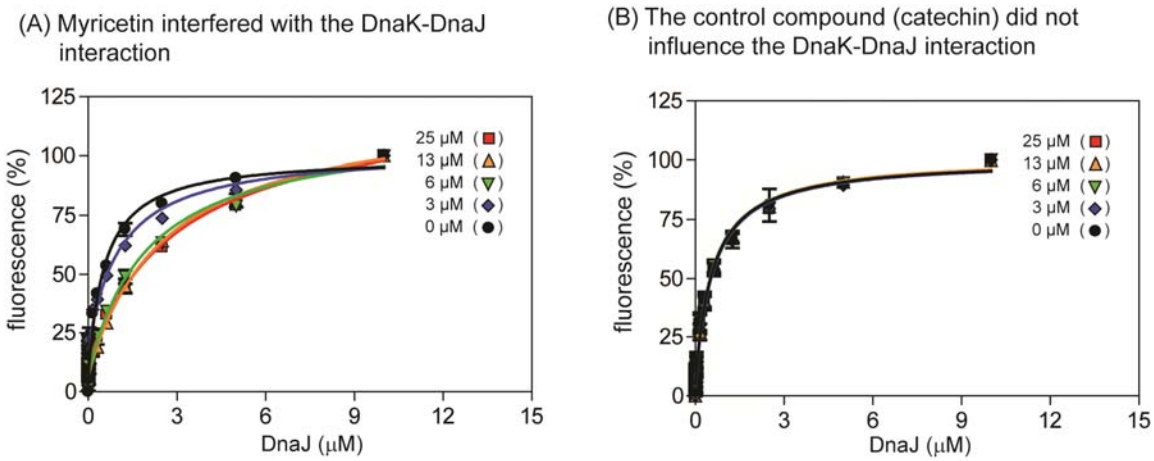

Appendix 3.5.5 Myricetin blocks the interaction between DnaK and DnaJ, as measured by FRET. DnaK was labeled with ALEXA-488 and DnaJ with the acceptor, BHQ-10. (A) Myricetin but not (B) catechin increased the K_{app} of DnaJ. Results are the average of triplicates and the error bars represent standard error of the mean.

3.6 References

1. Gavin, A.C., et al., *Functional organization of the yeast proteome by systematic analysis of protein complexes.* Nature, 2002. **415**(6868): p. 141-7.
2. MacBeath, G. and S.L. Schreiber, *Printing proteins as microarrays for high-throughput function determination.* Science, 2000. **289**(5485): p. 1760-3.
3. Arkin, M.R. and J.A. Wells, *Small-molecule inhibitors of protein-protein interactions: progressing towards the dream.* Nat Rev Drug Discov, 2004. **3**(4): p. 301-17.
4. Magliery, T.J., et al., *Detecting protein-protein interactions with a green fluorescent protein fragment reassembly trap: scope and mechanism.* J Am Chem Soc, 2005. **127**(1): p. 146-57.
5. Horswill, A.R., S.N. Savinov, and S.J. Benkovic, *A systematic method for identifying small-molecule modulators of protein-protein interactions.* Proc Natl Acad Sci U S A, 2004. **101**(44): p. 15591-6.
6. Vassilev, L.T., et al., *In vivo activation of the p53 pathway by small-molecule antagonists of MDM2.* Science, 2004. **303**(5659): p. 844-8.
7. Yin, H. and A.D. Hamilton, *Strategies for targeting protein-protein interactions with synthetic agents.* Angew Chem Int Ed Engl, 2005. **44**(27): p. 4130-63.
8. Kortemme, T. and D. Baker, *A simple physical model for binding energy hot spots in protein-protein complexes.* Proc Natl Acad Sci U S A, 2002. **99**(22): p. 14116-21.
9. Chang, L., et al., *High-throughput screen for small molecules that modulate the ATPase activity of the molecular chaperone DnaK.* Anal Biochem, 2008. **372**(2): p. 167-76.
10. Miyata, Y., et al., *High Throughput Screen for Escherichia coli Heat Shock Protein 70 (Hsp70/DnaK): ATPase Assay in Low Volume By Exploiting Energy Transfer.* J Biomol Screen, 2010: p. (accepted).
11. Liberek, K., et al., *Escherichia coli DnaJ and GrpE heat shock proteins jointly stimulate ATPase activity of DnaK.* Proc Natl Acad Sci U S A, 1991. **88**(7): p. 2874-8.
12. Gassler, C.S., et al., *Mutations in the DnaK chaperone affecting interaction with the DnaJ cochaperone.* Proc Natl Acad Sci U S A, 1998. **95**(26): p. 15229-34.
13. Suh, W.C., et al., *Interaction of the Hsp70 molecular chaperone, DnaK, with its cochaperone DnaJ.* Proc Natl Acad Sci U S A, 1998. **95**(26): p. 15223-8.
14. Jiang, J., et al., *Structural basis of J cochaperone binding and regulation of Hsp70.* Mol Cell, 2007. **28**(3): p. 422-33.
15. Harrison, C.J., et al., *Crystal structure of the nucleotide exchange factor GrpE bound*

to the ATPase domain of the molecular chaperone DnaK. Science, 1997. **276**(5311): p. 431-5.

16. Russell, R., R. Jordan, and R. McMacken, *Kinetic characterization of the ATPase cycle of the DnaK molecular chaperone.* Biochemistry, 1998. **37**(2): p. 596-607.
17. Schroder, H., et al., *DnaK, DnaJ and GrpE form a cellular chaperone machinery capable of repairing heat-induced protein damage.* Embo J, 1993. **12**(11): p. 4137-44.
18. Ang, D., et al., *Escherichia coli grpE gene codes for heat shock protein B25.3, essential for both lambda DNA replication at all temperatures and host growth at high temperature.* J Bacteriol, 1986. **167**(1): p. 25-9.
19. Sell, S.M., et al., *Isolation and characterization of dnaJ null mutants of Escherichia coli.* J Bacteriol, 1990. **172**(9): p. 4827-35.
20. Friedman, M., *Overview of antibacterial, antitoxin, antiviral, and antifungal activities of tea flavonoids and teas.* Mol Nutr Food Res, 2007. **51**(1): p. 116-34.
21. Khan, N. and H. Mukhtar, *Multitargeted therapy of cancer by green tea polyphenols.* Cancer Lett, 2008. **269**(2): p. 269-80.
22. Cuccioloni, M., et al., *Natural occurring polyphenols as template for drug design. Focus on serine proteases.* Chem Biol Drug Des, 2009. **74**(1): p. 1-15.
23. Shapiro, G.I., *Preclinical and clinical development of the cyclin-dependent kinase inhibitor flavopiridol.* Clin Cancer Res, 2004. **10**(12 Pt 2): p. 4270s-4275s.
24. Buchberger, A., et al., *Nucleotide-induced conformational changes in the ATPase and substrate binding domains of the DnaK chaperone provide evidence for interdomain communication.* J Biol Chem, 1995. **270**(28): p. 16903-10.
25. Theyssen, H., et al., *The second step of ATP binding to DnaK induces peptide release.* J Mol Biol, 1996. **263**(5): p. 657-70.
26. Conseil, G., et al., *Flavonoids: a class of modulators with bifunctional interactions at vicinal ATP- and steroid-binding sites on mouse P-glycoprotein.* Proc Natl Acad Sci U S A, 1998. **95**(17): p. 9831-6.
27. Bhattacharya, A., et al., *Allostery in Hsp70 chaperones is transduced by subdomain rotations.* J Mol Biol, 2009. **388**(3): p. 475-90.
28. Woo, H.J., et al., *ATP-induced conformational changes in Hsp70: molecular dynamics and experimental validation of an in silico predicted conformation.* Biochemistry, 2009. **48**(48): p. 11470-7.
29. Chang, L., et al., *Mutagenesis reveals the complex relationships between ATPase rate and the chaperone activities of Escherichia coli heat shock protein 70 (HSP70/DNAK).* J Biol Chem, 2010. **385**(28): p. 21282-91.

30. Buchberger, A., et al., *The chaperone function of DnaK requires the coupling of ATPase activity with substrate binding through residue E171.* Embo J, 1994. **13**(7): p. 1687-95.
31. Laufen, T., et al., *Mechanism of regulation of hsp70 chaperones by DnaJ cochaperones.* Proc Natl Acad Sci U S A, 1999. **96**(10): p. 5452-7.
32. Ruan, Q., J.P. Skinner, and S.Y. Tetin, *Using nonfluorescent Forster resonance energy transfer acceptors in protein binding studies.* Anal Biochem, 2009. **393**(2): p. 196-204.
33. Zhang, J., P.L. Yang, and N.S. Gray, *Targeting cancer with small molecule kinase inhibitors.* Nat Rev Cancer, 2009. **9**(1): p. 28-39.
34. Grant, S.K., *Therapeutic protein kinase inhibitors.* Cell Mol Life Sci, 2009. **66**(7): p. 1163-77.
35. May, L.T., et al., *Allosteric modulation of G protein-coupled receptors.* Annu Rev Pharmacol Toxicol, 2007. **47**: p. 1-51.
36. Massey, A.J., *ATPases as drug targets: insights from heat shock proteins 70 and 90.* J Med Chem, 2010. **53**(20): p. 7280-6.
37. Daugaard, M., M. Rohde, and M. Jaattela, *The heat shock protein 70 family: Highly homologous proteins with overlapping and distinct functions.* FEBS Lett, 2007. **581**(19): p. 3702-10.
38. Bukau, B., J. Weissman, and A. Horwich, *Molecular chaperones and protein quality control.* Cell, 2006. **125**(3): p. 443-51.
39. Meimaridou, E., S.B. Gooljar, and J.P. Chapple, *From hatching to dispatching: the multiple cellular roles of the Hsp70 molecular chaperone machinery.* J Mol Endocrinol, 2009. **42**(1): p. 1-9.
40. Wisen, S., et al., *Binding of a Small Molecule at a Protein-Protein Interface Regulates the Chaperone Activity of Hsp70-Hsp40.* ACS Chem Biol, 2010. **5**(6): p. 611-22.
41. Jinwal, U.K., et al., *Chemical manipulation of hsp70 ATPase activity regulates tau stability.* J Neurosci, 2009. **29**(39): p. 12079-88.
42. Martens, S. and A. Mithofer, *Flavones and flavone synthases.* Phytochemistry, 2005. **66**(20): p. 2399-407.
43. Yang, C.S., et al., *Cancer prevention by tea: animal studies, molecular mechanisms and human relevance.* Nat Rev Cancer, 2009.
44. Teillet, F., et al., *Flavonoids as RTK inhibitors and potential anticancer agents.* Med Res Rev, 2008. **28**(5): p. 715-45.
45. Gamet-Payrastre, L., et al., *Flavonoids and the inhibition of PKC and PI 3-kinase.* Gen

Pharmacol, 1999. **32**(3): p. 279-86.
46. Wiseman, R.L., et al., *Flavonol activation defines an unanticipated ligand-binding site in the kinase-RNase domain of IRE1.* Mol Cell. **38**(2): p. 291-304.
47. Wiseman, R.L., et al., *Flavonol activation defines an unanticipated ligand-binding site in the kinase-RNase domain of IRE1.* Mol Cell, 2010. **38**(2): p. 291-304.
48. Miyata, Y., et al., *High-Throughput Screen for Escherichia coli Heat Shock Protein 70 (Hsp70/DnaK): ATPase Assay in Low Volume by Exploiting Energy Transfer.* J Biomol Screen, 2010.
49. Case, D.A., et al., *AMBER 10, University of California, San Francisco.* 2008.
50. Hornak, V., et al., *Comparison of multiple Amber force fields and development of improved protein backbone parameters.* Proteins, 2006. **65**(3): p. 712-25.
51. Onufriev, A., D. Bashford, and D.A. Case, *Exploring protein native states and large-scale conformational changes with a modified generalized born model.* Proteins, 2004. **55**(2): p. 383-94.
52. O'Brien, M.C., K.M. Flaherty, and D.B. McKay, *Lysine 71 of the chaperone protein Hsc70 Is essential for ATP hydrolysis.* J Biol Chem, 1996. **271**(27): p. 15874-8.
53. Sousa, M.C. and D.B. McKay, *The hydroxyl of threonine 13 of the bovine 70-kDa heat shock cognate protein is essential for transducing the ATP-induced conformational change.* Biochemistry, 1998. **37**(44): p. 15392-9.
54. Jakalian, A., et al., *Fast, efficient generation of high-quality atomic charges. AM1-BCC model: I. Method.* J Comp Chem, 2000(21): p. 132-146.
55. Meagher, K.L., L.T. Redman, and H.A. Carlson, *Development of polyphosphate parameters for use with the AMBER force field.* J Comput Chem, 2003. **24**(9): p. 1016-25.
56. Ryckaert, J.P., G. Ciccotti, and H.J.C. Berendsen, *Numerical-integration of Cartesian equations of motion of a system with constraints-molecular-dynamics of N-Alkanes* J Comp Phys, 1977. **23**(327-41).
57. Morris, G.M., et al., *AutoDock4 and AutoDockTools4: Automated docking with selective receptor flexibility.* J Comput Chem, 2009. **30**(16): p. 2785-91.
58. Morris, G.M., et al., *Automated docking using a Lamarckian genetic algorithm and an empirical binding free energy function.1998.* J Comput Chem 1998. **19**: p. 1639-62.
59. Wang, J., et al., *Development and testing of a general amber force field.* J Comput Chem, 2004. **25**: p. 1157-74.

Chapter 4

In Search of the Best Screening Assays for Hsp70s: Mutagenesis Reveals that the Relationships between the ATPase Rates and Chaperone Activities of DnaK are Complex and Indirect

4.1 Abstract

The *E. coli* 70kDa heat shock protein, DnaK, is a molecular chaperone that engages in a variety of cellular activities, including the folding of proteins. During this process, DnaK binds its substrates in coordination with a catalytic ATPase cycle. Both the ATPase and protein-folding activities of DnaK are stimulated by its co-chaperones, DnaJ and GrpE. However, it is not yet clear how changes in the stimulated ATPase rate of DnaK impact the folding process. In this study, we performed mutagenesis throughout the nucleotide-binding domain of DnaK to generate a collection of mutants in which the stimulated ATPase rates varied from 0.7 to 13.6 pmol/mg/min^{-1}. We found that this range was largely established by differences in the ability of the mutants to be stimulated by one or both of the co-chaperones. Next, we explored how changes in

ATPase rate might impact refolding of denatured luciferase *in vitro* and found that the two activities were poorly correlated. Unexpectedly, we found several mutants that refold luciferase normally in the absence of significant ATP turnover, presumably by increasing the flexibility of DnaK. Finally, we tested whether DnaK mutants could complement growth of *ΔdnaK E. coli* cells under heat shock and found that the ability to refold luciferase was more predictive of *in vivo* activity than ATPase rate. This study provides insights into how flexibility and co-chaperone interactions affect DnaK-mediated ATP turnover and protein folding. These findings have important implications for next-generation high throughput screens against Hsp70/DnaK. Specifically, they suggest that ATPase assays need to be supported by multiple secondary assays to refine the impact of active compounds on other chaperone functions.

4.1.1 Nucleotide Induced Conformational Changes in DnaK

DnaK is a member of the highly conserved Hsp70 family and it is involved in a variety of cellular pathways, including protein folding, transport, and degradation [1, 2]. As a central player in protein quality control and homeostasis, Hsp70 has also been implicated in the pathogenesis of a variety of diseases [3-5]. These observations have led to an interest in understanding how the various activities of Hsp70 are correlated. One of

the main roles of DnaK is to enable the folding of nascent or otherwise unfolded proteins [6]. In this role, DnaK is thought to limit aggregation and facilitate folding by binding to the hydrophobic regions exposed in these substrates. Briefly, the binding of ATP to DnaK nucleotide binding domain (NBD) results in an “open” conformation of substrate binding domain (SBD) with low substrate affinity. Upon hydrolysis, the ADP-bound form assumes a “closed” conformation that binds substrate with higher affinity [7-13]. Thus, allosteric communication between NBD and SBD is thought to link nucleotide turnover to substrate binding and release.

4.1.2 Both the ATPase and Substrate-Binding Activities of DnaK are Regulated by its Co-chaperones, DnaJ and GrpE

DnaK alone has a low intrinsic ATPase rate, which facilitates regulation by the important co-chaperones, DnaJ and GrpE. DnaJ specifically stimulates ATP hydrolysis and thus favors high affinity substrate binding [14, 15]. In addition, DnaJ independently binds to substrates with its C-terminal domains and is thought to help these proteins bind to DnaK [16, 17]. GrpE, on the other hand, induces nucleotide exchange and leads to substrate release [18]. These co-chaperone activities appear to be required for the cellular functions of DnaK because deletion of either DnaJ or GrpE causes defects in

growth at elevated temperatures, similar to what is seen in *ΔdnaK* strains [5, 19, 20].

4.1.3 The ATPase Activity of DnaK is Necessary but not Sufficient for its *In Vitro* Refolding of Denatured Firefly Luciferase

Many of the key insights into the folding of substrates by DnaK have emerged from *in vitro* studies on the model substrate, firefly luciferase. For example, it was found that DnaK requires DnaJ and GrpE to refold denatured luciferase [6]. This platform has also been used to explore the roles of ATP hydrolysis in controlling substrate folding. For example, this process was found to require multiple cycles of ATP hydrolysis [5, 6]. Also, ATPγS blocks refolding, further suggesting an important role for nucleotide cycling [21-23]. However, truncated forms of DnaJ, which are able to stimulate ATP hydrolysis normally but cannot interact with substrates, are unable to stimulate luciferase refolding [15]. Together, these results suggest that ATP turnover is necessary but not sufficient to achieve luciferase folding.

4.1.4 Mutants that Abolish the ATPase Activity of DnaK Also Cannot Rescue the Heat Sensitive Phenotype of Δ*dnaK E. coli*

Finally, the chaperone function of DnaK can also be assayed *in vivo* by monitoring the

ability of DnaK mutants to complement growth of Δ*dnaK E. coli* cells under heat shock (also called heat shock rescue) [24]. At elevated temperatures, many proteins in *E. coli* become prone to unfolding and aggregation. One of the roles of DnaK is to bind these substrates, protecting them from aggregation [3, 25, 26]. Following a return to normal temperature, DnaK also participates in active refolding [27, 28]. Similar to what was observed in the *in vitro* luciferase refolding experiments, the ATPase activity of DnaK appears to be required during heat shock, because active site mutations that abolish nucleotide turnover are unable to rescue heat shock [21-23].

4.1.5 The Correlation between ATPase and Chaperone Activities of DnaK is Still Not Completely Clear

Taken together, these data suggest that ATPase rate may be an important modulator of chaperone activities. However, previous studies largely relied on either single mutations of residues involved in catalysis or non-hydrolyzable nucleotide mimics [21-23]. Thus, it remains unknown if changes in the rate of ATP hydrolysis lead to predictable changes in chaperone functions, such as luciferase folding and heat shock rescue. Insights into these relationships have been complicated by several factors. First, the DnaK chaperone system is impacted by a number of potential variables. For example, several studies have

highlighted substrate binding kinetics, interdomain communication, and the stimulation of DnaK's ATPase rate as important variables for refolding or cellular growth under heat shock [16, 29-37]. Secondly, the interdependence of these variables presents important challenges. For example, a mutation that disrupts interdomain communication might also interfere with substrate binding and DnaJ-mediated ATPase stimulation [31, 38].

4.1.6 Our Strategies to Study the Correlations between the ATPase and Chaperone Activities of DnaK

To better understand how ATPase rate might regulate chaperone activity, we have undertaken a strategy of performing mutagenesis on the NBD of DnaK to generate a battery of mutants that varied in their co-chaperone-stimulated ATPase rates by over 15-fold. We envisioned that this collection of mutants might reveal the trends between turnover rates and folding outcomes. Moreover, one of our main goals in this study was to support our ongoing efforts to discover chemical compounds that target Hsp70s [21, 39, 40]. As part of those studies, we wanted to evaluate if genetic modulation of DnaK's ATPase rate can predicatively modulate chaperone activities *in vitro* and *in vivo*. We anticipated that knowledge about these relationships would enable more predictive strategies for finding potent chemical probes for use in cellular and animal models.

4.2 Results

4.2.1 The Design of DnaK Mutants

In this study we aimed to assess if changes in the ATPase rate of DnaK lead to predictable changes in chaperone function. Toward this goal, we employed available mutational and structural data to select approximately 30 novel or established mutations in the NBD of DnaK [38, 41-44]. We avoided mutating the SBD to minimize direct disruption of substrate binding. Rather, these mutations were specifically designed to impact ATP turnover by four potential mechanisms (**Figure 4.1**). Known DnaK mutations, E171S and T199A, which alter residues in the ATP-binding pocket, made up Class I. Class II included L177A and I373A, which were predicted to disrupt DnaJ-mediated ATPase stimulation based on homology to mutations made in other Hsp70 family members [11, 31, 38]. Two mutants, V192A and Y193A, which are located near the proposed DnaJ-binding site, were also included in Class II. Class III included K55A and R56A, which are known to disrupt binding to GrpE [42, 45], and ten additional mutants in the IB and IIB subdomains that we hypothesized might impact nucleotide exchange. Finally, class IV mutations included residues around the proposed hinge region (residue 225 to 230) at the IIA / IIB subdomain interface. This region is proposed to undergo an ATP-induced structural

change [41, 43]. Together, this collection of DnaK mutants was intended to provide an analysis of contributions from multiple allosteric pathways.

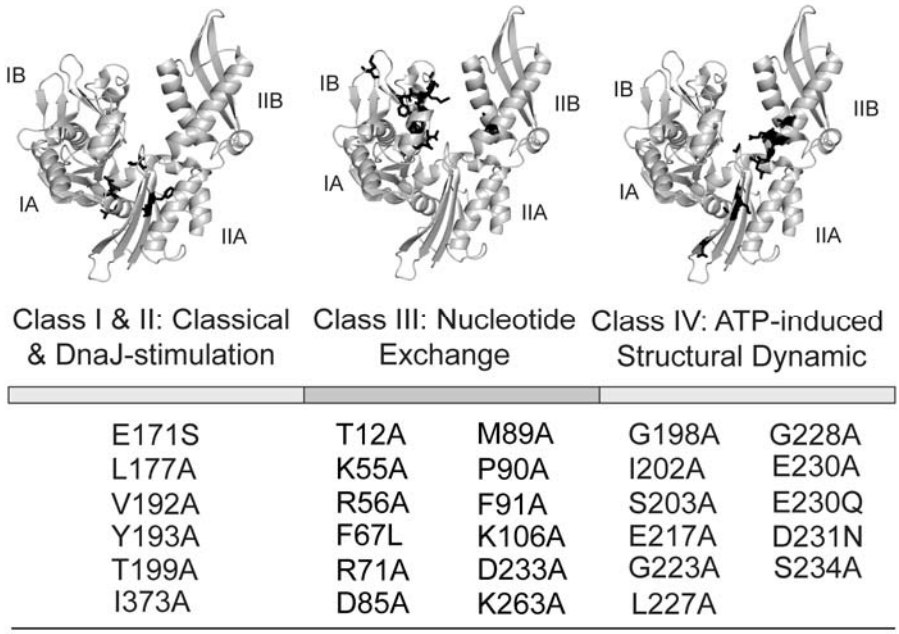

Figure 4.1 The location of DnaK mutants. The locations of mutations in DnaK are shown as black stick representations. Because the mutations are all present in the NBD, only this domain is shown for clarity. From left to right, as discussed in the main text, Class I mutations, E171S and T199A, are mutants known to disrupt ATPase and chaperone activities of DnaK. Class II mutations were designed to disrupt DnaJ-mediated stimulations. Next, Class III mutations were intended to disrupt GrpE-mediated stimulation. Finally, Class IV mutations were designed to disrupt ATP-induced structural dynamics.

To characterize these mutants, we first tested whether the mutants could bind to nucleotide by measuring their retention on an ATP affinity column. We found that all the mutants retained ATP-binding activity qualitatively similar to that of wild type (WT) DnaK.

We then confirmed that the mutants exhibited WT-like secondary structure, as measured by circular dichroism (**Appendix 4.5.1**). We also verified that each mutant bound to luciferase using a "holdase" assay. In this assay, the ability of DnaK to protect luciferase from heat denaturation was measured and we found that all of the mutants were able to bind this substrate (**Appendix 4.5.2**). Finally, we used an ELISA-based binding assay to confirm that all of the mutants bind to immobilized luciferase and malate dehydrogenase (MDH) (**Appendix 4.5.3-6**). During these characterization steps, we identified three mutations that resulted in unstable variants of DnaK (**Appendix 4.5.7**). These mutants were removed from further analysis. Thus, this design and selection process yielded a collection of 29 DnaK mutants for further investigation (**Figure 4.1**).

As mentioned above, the ATPase rate of DnaK is stimulated by three main factors: DnaJ, GrpE and substrate. Thus, we wanted to measure the ability of these factors to stimulate each of the DnaK mutants. Towards this goal, we calculated the K_m and V_{max} values for DnaJ, GrpE and a model DnaK substrate, NRLLLTG (**Table 4.1** and **Appendix 4.5.8**). From these experiments, we found that the mutants varied in their responses to these stimuli. Using K_m to estimate binding to DnaK, we found that most mutants varied in their affinity

Table 4.1 The ATPase activity of DnaK mutants

DnaK	Intrinsic ATPase rate	DnaJ Stimulation[b]		GrpE Stimulation[c]		Substrate Stimulation		
	$pmolP_i/\mu g/min$	$Vmax_{,J}$[d] $pmolP_i/\mu g/min$	$Km_{,J}$ μM	$Vmax_{,E}$ $pmolP_i/\mu g/min$	$Km_{,E}$ nM	$Vmax_{,sub}$ $pmolP_i/\mu g/min$	$Km_{,sub}$ μM	
WT	**1.7 ± 0.2**	**10.2 ± 0.5**	**0.58 ± 0.12**	**47.2 ± 4.0**	**108.3 ± 29.0**	**6.0 ± 0.9**	**90 ± 28**	
E171S	1.2 ± 0.1	NF[a]	NF	NF	NF	NF	NF	Class I
T199A	0.6 ± 0.2	NF	NF	NF	NF	NF	NF	
L177A	3.1 ± 0.3	8.8 ± 1.1	1.25 ± 0.50	19.5 ± 1.7	47.8 ± 16.2	5.4 ± 0.2	103.1 ± 6.5	
V192A	3.8 ± 1.0	6.7 ± 0.4	0.53 ± 0.13	84.2 ± 5.6	114.3 ± 23.5	5.0 ± 0.1	30.1 ± 1.4	Class II
Y193A	5.0 ± 0.3	13.4 ± 0.5	0.81 ± 0.12	57.0 ± 3.2	94.3 ± 17.4	7.0 ± 0.6	73.4 ± 12.2	
I373A	3.7 ± 1.2	NF	NF	26.4 ± 4.7	188.8 ± 82.9	NF	NF	
T12A	2.9 ± 0.4	40.5 ± 2.7	2.57 ± 0.39	11.7 ± 1.9	53.7 ± 34.6	7.1 ± 0.1	65.6 ± 2.8	
K55A	2.5 ± 0.4	30.4 ± 2.5	3.25 ± 0.54	NF	NF	NF	NF	
R56A	3.2 ± 0.3	19.5 ± 1.2	3.53 ± 0.42	64.2 ± 15.5	544.4 ± 210.2	13.3 ± 0.4	47.3 ± 3.9	
F67L	1.4 ± 0.3	NF	NF	NF	NF	NF	NF	
R71A	2.4 ± 0.3	NF	NF	NF	NF	NF	NF	
D85A	3.0 ± 0.3	14.1 ± 1.1	0.82 ± 0.22	17.4 ± 2.6	35.8 ± 21.5	NF	NF	Class III
M89A	3.5 ± 0.2	12.7 ± 0.9	0.56 ± 0.14	44.7 ± 17.4	364.6 ± 263.8	8.2 ± 0.2	39.6 ± 2.0	
P90A	1.8 ± 0.4	13.8 ± 4.4	4.3 ± 2.5	15.4 ± 1.9	5.2 ± 2.2	NF	NF	
F91A	1.6 ± 0.4	NF	NF	NF	NF	NF	NF	
K106A	5.0 ± 0.4	14.9 ± 0.6	0.96 ± 0.14	46.4 ± 4.6	64.5 ± 23.6	6.3 ± 0.1	8.4 ± 0.4	
D233A	5.7 ± 0.4	41.6 ± 1.4	1.15 ± 0.13	NF	NF	NF	NF	
K263A	3.4 ± 1.0	NF	NF	NF	NF	NF	NF	
G198A	2.2 ± 0.1	10.4 ± 0.6	0.50 ± 0.11	NF	NF	NF	NF	
I202A	1.5 ± 0.1	13.2 ± 0.8	0.67 ± 0.14	NF	NF	NF	NF	
S203A	3.9 ± 0.1	NF	NF	29.7 ± 0.7	6.9 ± 0.6	2.1 ± 0.2	17.5 ± 5.4	
E217A	1.2 ± 0.1	NF	NF	NF	NF	NF	NF	
G223A	0.5 ± 0.1	NF	NF	NF	NF	NF	NF	Class IV
L227A	1.0 ± 0.1	NF	NF	NF	NF	NF	NF	
G228A	2.5 ± 0.1	NF	NF	NF	NF	NF	NF	
E230Q	0.6 ± 0.4	19.1 ± 2.0	3.38 ± 0.70	NF	NF	NF	NF	
E230A	3.2 ± 0.4	14.3 ± 1.8	1.95 ± 0.65	12.5 ± 1.5	37.8 ± 18.3	NF	NF	
D231N	0.6 ± 0.1	NF	NF	NF	NF	NF	NF	
S234A	0.5 ± 0.1	9.9 ± 0.7	0.32 ± 0.09	NF	NF	NF	NF	

[a]The gray boxes (NF) indicate that either ATPase rate was not stimulated, as defined by a mutant in which the SEM of K_m or V_{max} encompassed zero, or when a non-linear fit could not be obtained. [b]DnaJ stimulation was tested in the presence of NR substrate (100 μM). [c]GrpE stimulation was tested in the presence of both DnaJ (1 μM) and NR substrate (100 μM). [d]The V_{max} value (calculated by the equation in the Materials and Methods) represents the increase in ATPase rate compared to solvent control. Raw data can be found in Supplemental Figure 2. Error is standard error of the mean.

for DnaJ by approximately 10-fold (0.50 to 5.4 μM). In addition, a few mutants, such as E217A and L227A had very weak stimulation, which precluded fitting of the curves (**Table 4.1** and **Appendix 4.5.8**). Similarly, the K_m of GrpE stimulation varied over a range of almost 100-fold, with multiple mutants unable to be stimulated. Finally, maximum stimulation (V_{max}) varied by approximately 6-fold for DnaJ, 7-fold for GrpE and 6-fold for

substrate. Thus, we found that this collection had the desired, wide range of K_m and V_{max} values for co-chaperone and substrate-mediated ATPase stimulation. Based on these findings, we reasoned that they could be used to probe the correlation between ATPase rate and luciferase folding.

4.2.2 The ATPase rate and refolding activity of DnaK mutants are weakly correlated.

One of the functions of DnaK is to refold damaged proteins, and this activity can be measured *in vitro* by luciferase refolding assays. In this experiment, chemically denatured firefly luciferase is diluted in the presence of DnaK, ATP, DnaJ and GrpE. This chaperone system gradually restores the misfolded luciferase and the refolding process can be monitored by an increase in luminescence. To directly explore the correlation between stimulated ATPase activity and chaperone-mediated refolding, we recorded both activities for each DnaK mutant at the same concentrations of DnaK, DnaJ, GrpE, luciferase and ATP (**Appendix 4.5.9**).

To explore potential correlations in these two activities of DnaK, we plotted the refolding activity against ATPase rate for each mutant (**Figure 4.2A**). This analysis revealed poor correlation (R^2 = 0.22), between the activities. A closer inspection of these results

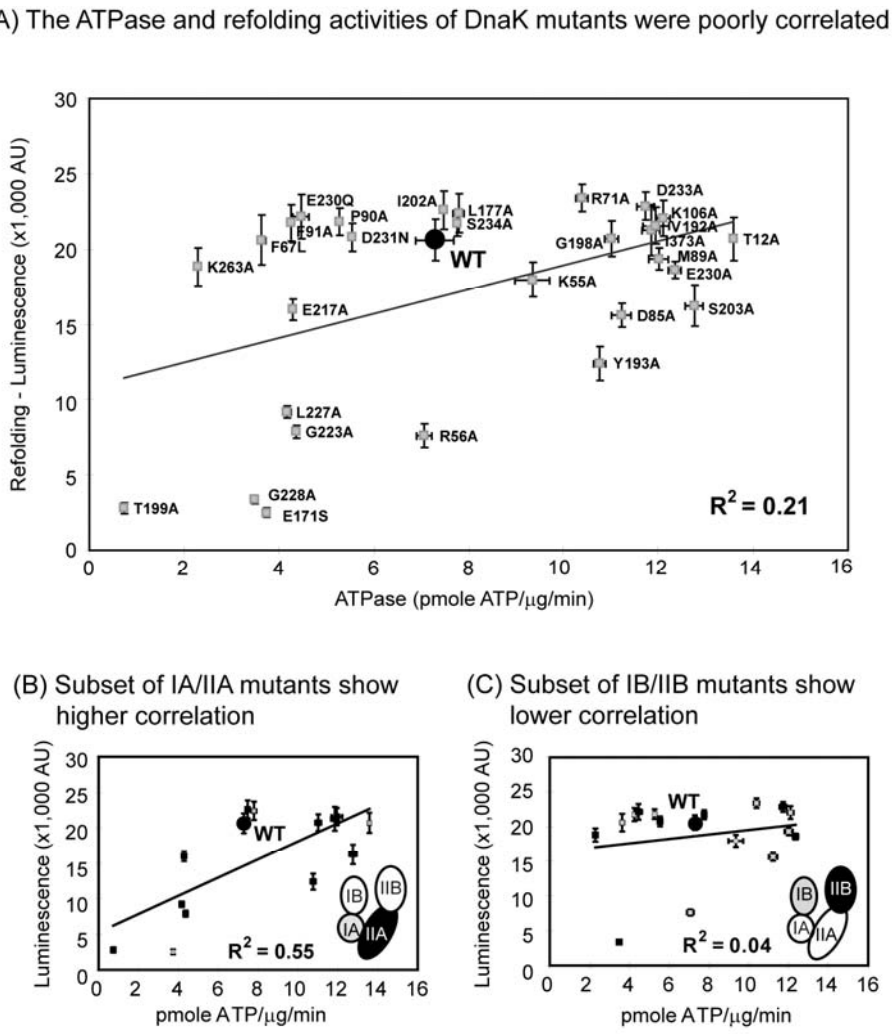

Figure 4.2 The ATPase and luciferase refolding activities of DnaK mutants were poorly correlated. (A) For wild-type (WT) DnaK and each mutant, the luciferase refolding activity and ATPase rate are shown. The final concentrations were: DnaK (1 μM), DnaJ (0.25 μM), GrpE (0.125 μM), denatured luciferase (8 nM) and ATP (1 mM). (B) & (C). Analysis of subsets of mutations based on their locations. Mutations in the IA/IIA subdomains (B) have a higher correlation (R^2 = 0.55) than those in the IB/IIB subdomains (C, R^2 = 0.04). In (B) and (C), IA/IB-subdomain mutants are shown as gray squares, IIA/IIB-subdomain mutants as black squares and WT as black circles. Although WT activity is shown in (B) and (C), it was not included for the calculation of R^2 value. Each data point is the average of triplicates and the error bars represent the standard error of the mean (SEM).

revealed some additional trends. For example, many mutants, such as T12A, had higher ATPase rate than WT but this enhanced turnover did not lead to correspondingly higher refolding activity. Further, some mutants, such as R56A, had the same ATPase rate as WT,

but decreased refolding activity. Curiously, there were also mutants such as F67L, P90A, F91A, E230Q, D231N and K263A, which had significantly lower ATP hydrolysis rates than WT DnaK, but they retained normal luciferase refolding activity. We named these DnaK mutants "decoupling mutants."

Because we found that many of the DnaK mutants had altered rates of intrinsic ATPase activity, we next analyzed the correlations between these values and luciferase refolding. Consistent with the previous findings, the intrinsic ATPase rates had almost no correlation with luciferase refolding activities (R^2 = 0.007; **Appendix 4.5.10**). Similarly, the ATPase rates of the mutants stimulated by DnaJ alone (*i.e.* no GrpE or substrate) also failed to correlate with refolding (R^2 = 0.071; **Appendix 4.5.10**). To confirm these findings, we also tested the correlations between the ATPase and refolding activity of DnaK mutants at higher substrate concentration (500 nM) using both luciferase and MDH as substrates (**Appendix 4.5.11-18**) and found even lower correlations (R^2=0.0049 and 0.0005 for luciferase and MDH, respectively; **Appendix 4.5.13-15**) under these conditions. Finally, we did not observe any correlations between the apparent K_d or maximal signal of DnaK mutants binding to denatured luciferase or MDH (measured by ELISA platform) and their refolding or ATPase activities (**Appendix 4.5.19-20**). In all of

these experiments, there was no dramatic difference between the responses of the DnaK mutants to the two substrates, although there were a few exceptions that will require additional follow-up studies (**Appendix 4.5.16-18**). Together, these studies suggest that the substrate binding and substrate refolding activities of DnaK mutants are poorly correlated with their ATPase rates.

We were particularly interested in exploring the activities of the decoupling mutants in greater detail. Interestingly, when the mutants were classified based on their locations, the decoupling mutants clustered on the IB and IIB subdomains. Most mutations in the IB and IIB subdomains had normal refolding activity regardless of ATPase rate (R^2 = 0.04; **Figure 4.2C**). Correspondingly, when only the IA/IIA subdomain mutants were examined, the overall ATPase rates became more positively associated with refolding activities (R^2 = 0.55) (**Figure 4.2B**).

4.2.3 The decoupling mutants of the IB subdomain make DnaK more flexible

Further analysis revealed that the decoupling mutants in the IB subdomain, F67L, P90A, and F91A, were co-localized in a hydrophobic patch adjacent to $loop_{74-96}$ (**Figure 4.3A**). $Loop_{74-96}$ has been shown to be crucial for cooperation with DnaJ and GrpE during both

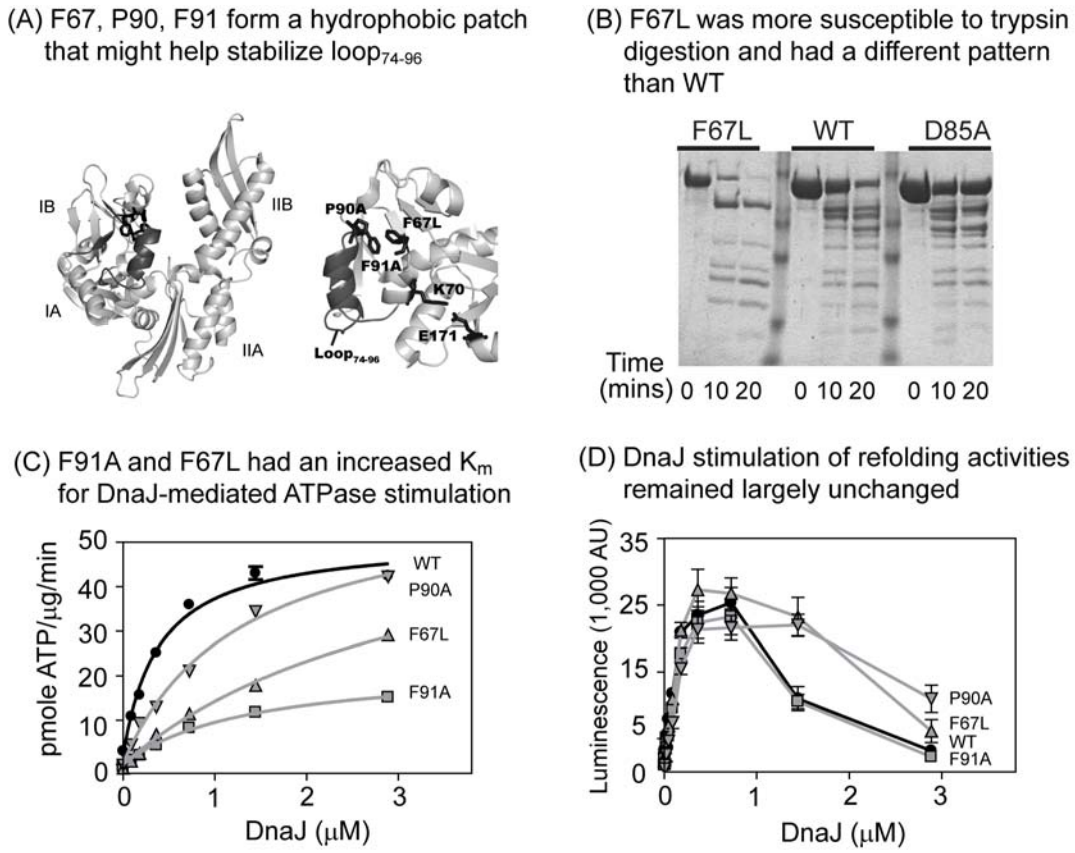

Figure 4.3 IB decoupling mutations increased DnaK flexibility and decreased DnaJ-mediated ATPase stimulation without impacting luciferase refolding activity. A. The NBD of DnaK is shown with a close-up on the region around residues F67, P90 and F91. These three residues appear to stabilize $loop_{74\text{-}96}$ (dark grey), which is connected to the critical catalytic residue, K70. B. Mutant F67L was more susceptible to trypsin digestion and demonstrated a different digestion pattern than WT-DnaK or a representative IB mutant, D85A. C. For decoupling mutants F91A and F67L, the Km for DnaJ-mediated ATPase stimulation was significantly increased. D. However, the decoupling mutants did not impact DnaJ-stimulated luciferase refolding. The final concentrations were: DnaK (1 μM), GrpE (0.125 μM), denatured luciferase (8 nM) and ATP (1 mM) in both C and D. Each data point is the average of triplicates and the error bars represent the standard error of the mean (SEM).

refolding and heat shock rescue [44]. Consistent with this important role, $loop_{74\text{-}96}$ is connected to a small helix containing K70, a residue that is essential for ATP hydrolysis [46]. Based on this analysis, we hypothesized that mutations to the hydrophobic triad of F67, P90, and F91 might destabilize $loop_{74\text{-}96}$. In turn, this increased flexibility might

disrupt positioning of K70, which would explain the low ATPase rates. In support of this hypothesis, we found that the three decoupling mutants were more sensitive to trypsin digestion and, further, that they exhibited a different digestion pattern than WT or other IB subdomain mutations (**Figure 4.3B** and **Appendix 4.5.21**). This result suggests that, through increased flexibility, the IB subdomain decoupling mutants may allow for productive interactions with misfolded luciferase without relying on structural transitions normally linked to ATP hydrolysis.

Because $loop_{74\text{-}96}$ was reported to be involved in interactions with DnaJ [44], we wanted to specifically test the ability of the decoupling mutants to be stimulated by this co-chaperone in the presence of denatured luciferase. In ATPase assays, we varied the concentration of DnaJ and found that F67L, P90A, and F91A had increased K_m values (2.4, 0.8, and 1.7 μM, respectively) compared to WT (0.3 μM) (**Figure 4.3C**). Despite these higher K_m values, the refolding activity of the three mutants in response to DnaJ remained similar to WT (**Figure 4.3D**). Thus, ATPase rate and refolding activity responded differently to DnaJ-mediated stimulation in these mutants, suggesting that these processes are separable.

4.2.4 IIB subdomain decoupling mutants are located near a previously predicted hinge region.

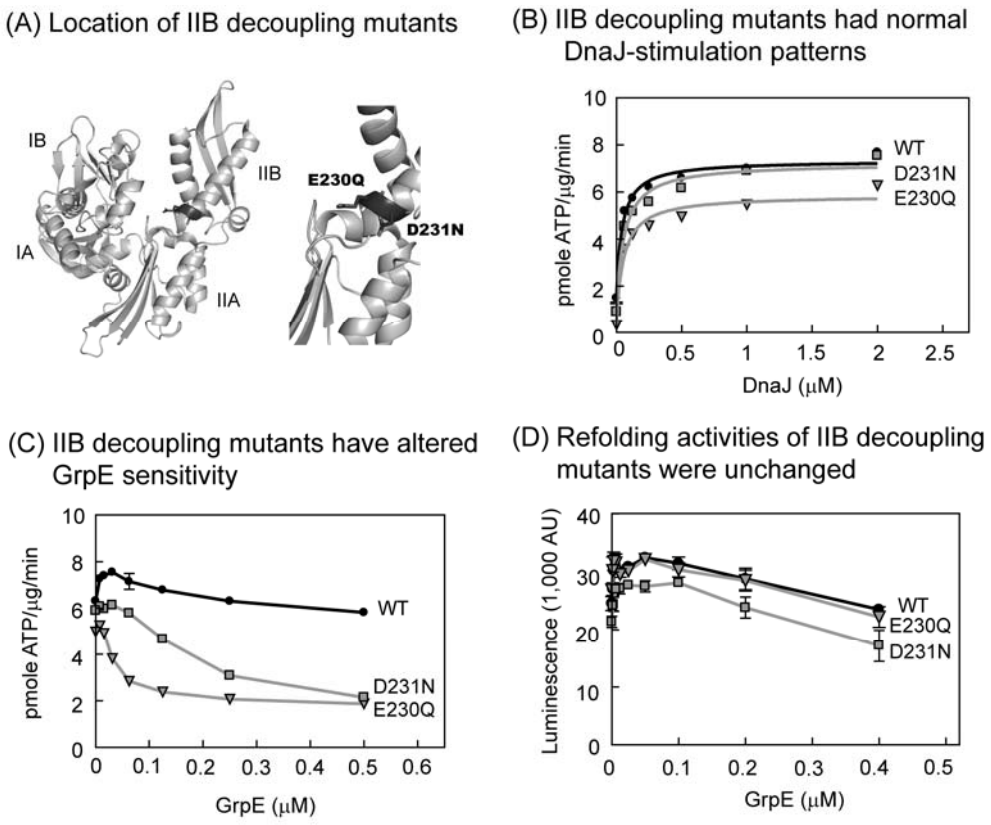

Figure 4.4 The ATPase activities of IIB decoupling mutants were inhibited by low concentration of GrpE but these mutants retained normal refolding activity. A. The NBD of DnaK is shown with the inset focused on the location of the IIB decoupling mutants, E320Q and D231N (stick representation). B. In ATPase assays, mutants E320Q and D231N had WT-like response to DnaJ-stimulation in the presence of 8 nM denatured luciferase. C. IIB decoupling mutants, E230Q and D231N, interacted with GrpE, but unlike WT, they were inhibited by a low concentration of GrpE. Notably, GrpE inhibited the ATPase activities of these mutants around the concentration used in the experiments shown in Figure 2 (0.1 μM). D. The refolding activities of E230Q and D231N responded to GrpE in a manner similar to WT DnaK. For both C and D, the final concentrations were: DnaK (1 μM), DnaJ (0.25 μM), denatured luciferase (8 nM) and ATP (1 mM). Each data point is the average of triplicates and the error bars represent the standard error of the mean (SEM).

Another class of decoupling mutations was interesting because the residues, E230 and D231, were located adjacent to each other in the IIB subdomain (**Figure 4.4A**). This

region is at the interface of the IIB and IIA subdomains, where a hinge region (residue 225 to 230 in DnaK) is thought to rotate the IIB subdomain away from the IB subdomain upon ATP hydrolysis [41]. This conformational change has been observed in GrpE-bound DnaK and it was previously proposed to be important for nucleotide release [42]. To explore the basis for the observed decoupling by mutations E230Q and D231N, we measured the stimulation of these mutants by DnaJ and GrpE. In ATPase assays, the decoupling mutants E230Q and D231N had normal responses to DnaJ (**Figure 4.4B**). However, unlike WT DnaK, the ATPase activities of these mutants were not stimulated by GrpE and, rather, were significantly inhibited by a low concentration of this co-chaperone (~0.1 μM) (**Figure 4.4C**). When these same mutations were tested in the refolding assay, they responded to GrpE in a manner similar to WT (**Figure 4.4D**). Thus, in these mutants, ATPase rate was decoupled from refolding largely by affecting the GrpE-mediated stimulation of these activities.

4.2.5 The refolding activity of DnaK mutants was more predictive of *in vivo* function.

Because this collection of DnaK mutants had revealed that ATPase rate and luciferase refolding activity were only weakly correlated, we wanted to explore which activity, if any, would be most predictive of a cellular function of DnaK. Towards this goal, we

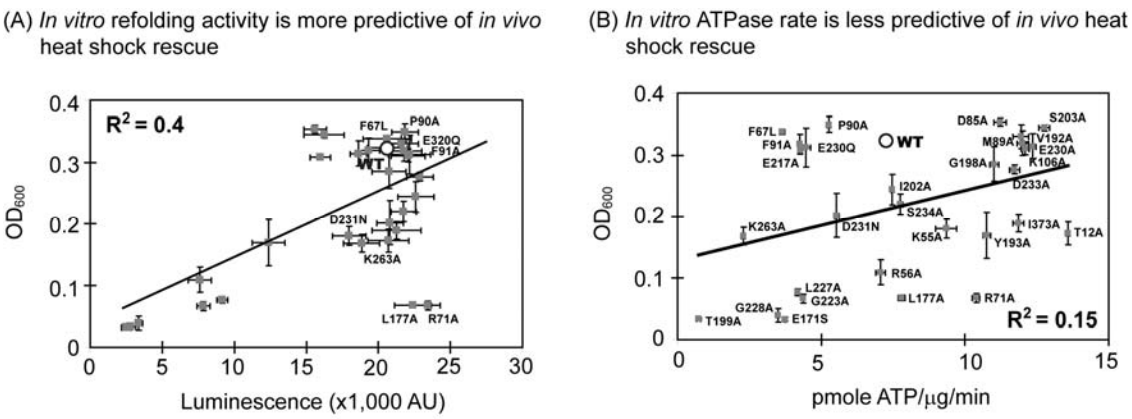

Figure 4.5 *In vitro* refolding activities of DnaK mutants were more predictive of their *in vivo* functions. (A) and (B) The luciferase refolding activities (R^2 = 0.4) of DnaK mutants were more predictive than ATPase rate (R^2 = 0.15) for their abilities to complement the growth of Δ*dnaK* (DE3) E. coli cells under heat shock. The growth of Δ*dnaK* (DE3) E. coli cells transformed with each dnaK mutant was measured using OD_{600} after a 6-hour incubation at 43°C. Each data point was measured in triplicate, and error bars represent the standard error of the mean (SEM).

explored the ability of the DnaK mutants to protect against heat shock in Δ*dnaK* (DE3) cells. *E. coli* strains lacking *dnaK* are temperature sensitive and unable to grow after exposure to elevated temperature. As expected, we found that WT DnaK, expressed from an inducible plasmid, could complement growth of Δ*dnaK E. coli* at 43 °C (**Appendix 4.5.22A**). Using the same procedure, we then tested each of the DnaK mutants. First, plasmids for each mutant were transformed into Δ*dnaK* (DE3) *E. coli* cells, and protein expression was confirmed (Supplemental Figure 7B). Following heat shock at 43 °C, the OD_{600} was measured and these results were plotted against the ATPase or refolding activity of each mutant (**Figure 4.5A** and **4.5B**). From this analysis, we found a strikingly poor correlation between ATPase rate and heat shock rescue (R^2 = 0.15). However, refolding activity was relatively better correlated (R^2 = 0.40). Interestingly, the

decoupling mutants of the IB and IIB subdomains, F67L, P90A, F91A, E230 and D231, were able to complement growth at 43 °C. This result demonstrated for the first time that mutants with a severe deficiency in their ATPase activity could rescue heat shock *in vivo*. Still, it is important to note that luciferase refolding was not fully predictive of heat shock rescue. Several mutants, such as L177A and R71A, were potent in the refolding assay yet they failed to rescue heat shock phenotypes. We interpret these results to mean that these relationships are complex and multiple factors are likely important for heat shock rescue.

4.3 Discussion

4.3.1 The relationship between ATPase and refolding activity of DnaK

As an isolated domain, the SBD of DnaK binds to substrate with the same affinity as ADP-bound DnaK and can slowly refold luciferase [47]. Thus, one major role of the NBD seems to be to power the transition of the SBD between open and closed states, which accelerates binding-and-release of substrates and increases refolding activity [11, 31, 48, 49]. Based on these findings, refolding and ATP turnover are thought to be closely linked functions of DnaK. Consistent with this idea, the co-chaperones DnaJ and GrpE stimulate both the ATPase rate and refolding activity of DnaK [45, 50, 51]. Previous data has

suggested that ATP hydrolysis is necessary but not sufficient for luciferase refolding (16, 22-24). To more deeply explore this finding, we examined if the ATPase rate of DnaK could predict its luciferase refolding activity using a series of mutants. We found that, in the 29 DnaK mutants tested, the two activities were poorly correlated. This result suggests that additional factors might contribute to refolding.

To explore what some of these contributing factors might be, we specifically investigated how the mutants were stimulated by co-chaperones and substrate (see **Table 4.1** and **Appendix 4.5.8**). This analysis showed that mutants unable to refold luciferase, such as E171S, T199A and G228A, were also defective in their ability to be stimulated by DnaJ, GrpE, and substrate in the ATPase assay. However, the converse was not necessarily true. For example, there were several mutants whose ATPase rate could not be stimulated, yet they still had the same refolding activity as WT DnaK. These results demonstrated that the relationship between ATPase and luciferase refolding activity is complex. More specifically, these results suggested that the ability of DnaK to be stimulated by DnaJ, GrpE or peptide substrate is not necessarily predictive of its activity in the refolding assay. This conclusion is illustrated by several mutants in which drastic changes in both the V_{max} and K_m of DnaJ-mediated ATPase stimulation were observed without a significant impact

on refolding activity (see **Table 4.1** and **Figure 4.3**). Most notably, the IB subdomain decoupling mutants, F67L, P90A and F91A, exhibited WT-like dependence on DnaJ for refolding, but had increased K_m for DnaJ-mediated stimulation of ATP hydrolysis. This observation suggests that DnaJ might promote ATPase and refolding activities by different mechanisms. In support of this model, DnaJ mutants that stimulate the ATPase rate of DnaK, but not its refolding activity, have been reported [14, 15, 52-54]. The structure of DnaJ might provide a clue into how these two activities can be separated. Residues 1 through 104 of DnaJ are essential for interactions with the NBD of DnaK. This region is composed of the J-domain and a glycine- and phenylalanine-rich region. The C-terminal half of DnaJ contains two zinc-binding sites and a domain important for binding to substrate [15-17, 54]. While the 1-104 fragment of DnaJ can fully stimulate ATP hydrolysis, it can not stimulate the refolding activity of DnaK [15]. More strikingly, Katrin *et al.* found that DnaJ lacking its second zinc-binding site had normal affinity for denatured luciferase and actively stimulated ATP hydrolysis by DnaK, but this mutant was unable to transfer substrate to DnaK or support luciferase refolding [14]. Those previous reports and our studies suggest that a secondary event, perhaps substrate presentation, may be important for refolding in the DnaK-DnaJ pair. We speculate that the decoupling mutations might interrupt ATPase activity without affecting

DnaJ-mediated substrate presentation. However, this model lacks structural support and the detailed mechanisms await further analysis. It is important to note that other factors may also help to account for the lack of correlation between ATPase rate and refolding activity. These factors might include substrate-binding kinetics, nucleotide dependent conformational changes, and co-chaperone complex formation [55-58].

4.3.2 The mechanisms of the IB and IIB decoupling mutants

We were particularly interested in understanding the mechanisms of the "decoupling" mutants, because this is, to our knowledge, the first report of DnaK mutants that have greatly decreased ATPase rates but normal refolding activities. Three of the decoupling mutants were mapped to a hydrophobic patch on the IB subdomain that appears to stabilize $loop_{74\text{-}96}$ and, therefore, regulate the position of K70, a key residue for ATP hydrolysis. These decoupling mutants had low ATPase rates, yet they retained both normal refolding activities and the ability to restore growth under heat shock in *E. coli*. We hypothesize that the unusual properties of these mutants might arise from their increased flexibility, as measured by trypsin susceptibility. Specifically, this flexibility might allow the mutants to sample the "open" and "closed" conformational states that facilitate refolding. To date, there is no structure of "open" ATP-bound full-length Hsp70,

but based on the structure of Hsp110, a member of the Hsp70 superfamily, the α-helical lid of the SBD interacts with IA and IB subdomains [59, 60]. Therefore, it is tempting to speculate that the same interactions stabilize the “open” structure in DnaK. Moreover, this interaction of the SBD with subdomains IA and IB might create a barrier for switching between “open” and “closed” conformations. In this model, F67L, P90A and F91A mutants, by destabilizing or otherwise repositioning loop $_{74\text{-}96}$, might reduce the barrier to conformational flexibility in the SBD, essentially mimicking the activity normally reserved for nucleotide hydrolysis. The net effect of this change might be to partially decouple ATP turnover from refolding activities. Further structural investigations of WT DnaK and these mutants may provide additional insight.

Interestingly, loop$_{74\text{-}96}$ is not present in Gram-positive bacteria. Moreover, the DnaK from *Tetragenococcus halophilus*, a Gram-positive bacterium, has excellent holdase activity, but its refolding and ATPase activities are not stimulated by *T. halophilus* DnaJ or GrpE [61]. Further, deletion of this loop from *E. coli* DnaK renders it unable to cooperate with co-chaperones in both ATP hydrolysis and luciferase refolding [44]. These results further suggest that loop$_{74\text{-}96}$ may play a role in the allosteric regulation of DnaK.

The mutations in the IIB subdomain, E230Q and D231N, also appear to decouple ATPase and refolding activities, but by a mechanism that is distinct from that used by the IB subdomain decoupling mutations. The IIB residues are co-localized at the interface between the IIA and IIB subdomains. This interface is proposed to contain a hinge region that controls the rotation of the IIB subdomain away from the IB subdomain upon ATP hydrolysis [41, 43]. Decoupling mutations, E230Q and D231N, which are located on an α-helix adjacent to this flexible hinge, exhibited normal refolding and DnaJ-stimulated ATPase activities. However, these mutants had an altered response to GrpE. Specifically, GrpE failed to stimulate the ATPase activity of these mutants and, moreover, it inhibited turnover at concentrations greater than around 0.1 μM. Since GrpE binding also induces rotation of the IIB subdomain away from the IB [42], it is possible that E230Q and D231N interfere with the proper movement or positioning of the α-helix in response to interaction with GrpE. However, this change does not appear to prevent the conformational changes required for refolding, because the GrpE-stimulated folding activity was unchanged.

Together, our findings with both the IB and IIB decoupling mutants suggest that alterations in co-chaperone-mediated stimulation of ATP turnover do not uniformly lead

to predictable changes in luciferase refolding. Based on published reports, it appears that ATP hydrolysis normally regulates structural transitions in DnaK that allow sampling of the "open" and "closed" conformers [62]. Thus, in some of the "decoupling" mutants, these conformers are likely sampled independent of nucleotide transitions. Although ATP hydrolysis is clearly required for WT DnaK to fold luciferase, as shown in previous studies with non-hydrolyzable nucleotide analogs [6], this enzymatic activity is not intrinsically or directly linked to substrate folding. Rather, the relationship between these activities may be driven by structural transitions in the two-domain chaperone and interactions with the co-chaperones DnaJ and GrpE.

4.3.3 Luciferase refolding is more predictive of cellular heat shock rescue than ATPase rate

Using this series of DnaK mutants, we found that luciferase refolding activity was more predictive (R^2 = 0.40) than ATPase rate (R^2 = 0.15) of heat shock rescue. Although ATPase rate clearly did not predict heat shock rescue in this system, we expect that it might be more predictive of other cellular functions of DnaK, such as lambda phage replication or other activities. On the other hand, we were interested in the correlation that was observed between luciferase folding and heat shock rescue because of its implications

for discovery of small molecules that can alter DnaK functions *in vivo*. However, it is important to note that the correlation between luciferase folding and heat shock rescue does not fully describe the factors that control DnaK's roles during heat shock. This fact is exemplified by the existence of outliers that were fully active in the luciferase-refolding assay but showed a decreased ability to rescue growth at 43 °C, such as R71A and L177A. Thus, there are likely additional factors that are important for heat shock rescue. For example, some of the outliers may be caused by the ability of DnaK mutants to work in cooperation with other protein quality control systems involved in heat shock rescue.

4.3.4 Implications of these findings for discovery of small molecules that target DnaK/Hsp70

Finally, the results reported herein have potential implications towards the discovery of small molecule inhibitors of Hsp70s. This chaperone has been identified through genetic studies as a potential therapeutic target for a variety of diseases including cancer, neurodegeneration, and bacterial infections [4, 63]. Therefore, recent efforts have focused on identifying drug-like compounds that target it [4, 64]. To date, early studies in this area have proven useful in identifying several compounds [39, 65-72]. However,

Hsp70s, such as DnaK, have many functions (e.g. ATP turnover, substrate binding, folding, modulation of the stress response, *etc.*) that could potentially be targeted. Therefore, it isn't readily obvious which *in vitro* activity of Hsp70 should be screened to find small molecules that modulate a desired *in vivo* function, such as heat shock rescue or anti-apoptotic activity in cancer cells.

In this work, we found that luciferase-folding activity is relatively predictive of the ability of DnaK to mediate a stress response, while ATPase activity was poorly correlated with this same function. This is an interesting finding because some attempts to identify Hsp70 inhibitors, including our own, have focused on the ATPase activity of this chaperone [21, 40, 67]. This approach has produced molecules with activity in cellular and animal models [39], However, the present findings suggest that other "measurable" activities, such as luciferase folding [21, 73] may help reduce attrition of lead compounds. More broadly, it is possible that specific *in vitro* assays need to be designed for each desired *in vivo* function. Future work in this area may improve our ability to rationally design better biochemical screens for an individual disease-modifying function of Hsp70 in both bacterial and eukaryotic systems.

4.4 Experimental Procedures

4.4.1 Materials

Reagents were obtained from the following sources; Platinum Pfx DNA Polymerase (Invitrogen, Calsbad, CA), pMCSG7 plasmid (Midwest Center for Structural Genomics, Bethesda, MD), ATP-agarose column (SIGMA, St. Louis, MO), NRLLLTG peptide (University of Michigan Peptide Core) [12], luciferase and Steady-Glo Reagent (Promega, Madison, WI), and *ΔdnaK E. coli* cells (a generous gift from Dr. Ursula Jacob). Further, all OD and luminescence measurements were performed using a SpectraMax M5 (Molecular Devices, Sunnyvale CA).

4.4.2 Plasmids and protein purification

The *E. coli dnaK* and *grpE* genes were amplified by PCR using Platinum Pfx DNA Polymerase and inserted into the pMCSG7 plasmid through ligation- independent cloning, as previously described [74]. The partial-overlapping site-directed mutagenesis primers for *dnaK* were designed based on the report of Zheng *et al.* [75] and mutagenesis of the *dnak* gene was carried out following the user manual of QuickChange site-directed mutagenesis kit (Stratagene, La Jolla, CA). Twenty-nine *dnaK* mutants were made; T12A, K55A, R56A, F67L, R71A, D85A, M89A, P90A, F91A, K106A,

E171S, L177A, V192A, Y193A, G198A, T199A, I202A, S203A, E217A, G223A, L227A, G228A, E230A, E230Q, D231N, D233A, S234A, K263A, I373A. The wild type (WT) His-tagged DnaK and its mutants were expressed in BL21(DE3) cells and first purified by batch purification with Ni-NTA His•Bind® Resin (Novagen, Darmstadt, Germany) following the user manual. The His-tag of eluted DnaK was then removed by His-tagged TEV protease (1 mM DTT, 4 °C, overnight incubation). After adjusting the $MgCl_2$ and KCl concentration to 10 mM, the sample was further purified by ATP-agarose column using previously established protocols [40]. Finally, the remaining cleaved His-tag was removed by Ni-NTA column. The purification of GrpE followed the same strategy except that the ATP-agarose column was excluded. DnaJ was purified as previously described [40] with the exclusion of hydroxyapatite and Q-Sepharose fast-flow column purification steps and the addition of a Superdex 200 gel filtration column (GE Healthcare, Piscataway, NJ) to remove contaminating ATPase activity. Finally, N-terminal His-tagged J-domain 2-108 was purified by Ni-NTA column as described above without cleaving the His-tag. All proteins were concentrated and exchanged into 25 mM Tris buffer (10 mM KCl (150 mM KCl for DnaJ), 5 mM $MgCl_2$, pH 7.5) and stored at -80 °C until use.

4.4.3 Circular Dichroism (CD)

WT DnaK and mutants were prepared in 10 mM sodium phosphate buffer (100 mM sodium fluoride, pH 7.4) and spectra collected at 0.1 mg/ml in a 0.1 cm cuvette at room temperature. CD spectra were recorded on a Jasco J-715 spectropolarimeter (Jasco, Easton, MD) at 1 nm intervals from 190-260 nm at a scanning speed of 50 nm/min and a 5.0 nm bandwith. Each spectrum reported is the average of 15 scans after the subtraction of the baseline spectrum (buffer without the addition of DnaK) and normalization (mdeg cm^2 $dmol^{-1}$).

4.4.4 ATPase Activity

This procedure was adapted from a previously described protocol [40]. Briefly, samples were prepared with the addition of DnaK, DnaJ, GrpE, NR substrate (NRLLLTG), and/or denatured luciferase to a total volume of 15 µl in each well. Next, 10 µl of 2.5 mM ATP was added to start the reaction. The final concentrations were: ATP (1 mM), DnaK (0.5 µM), and NR substrate (100 µM), unless otherwise noted. Intrinsic ATPase rate was measured with DnaK (0.6 µM) in the absence of co-chaperones or substrate. When ATPase rate was tested as a comparison to refolding activity (see Figures 2-4), guanidine hydrochloride (GuHCl) denatured luciferase at 8 nM and DnaK at 1 µM was used to match the conditions described in the luciferase refolding assay (below). The final

concentrations of DnaJ, GrpE, are reported for each experiment in the results section. For steady state conditions, samples were incubated at 37 °C for one to three hours, then 80 µl of malachite green reagent was added to each well, immediately followed by 10 µl of 32% (w/v) sodium citrate. Samples were mixed thoroughly and incubated at 37 °C for 15 minutes. Finally, OD_{620} was measured. All experiments were preformed in triplicate and the signal from non-specific ATP hydrolysis in controls lacking DnaK was subtracted. A phosphate standard curve (using potassium dibasic phosphate) was generated each day and used to convert the units to pmol P_i/µg DnaK/min.

Stimulation curves were evaluated by fitting the data using a hyperbolic fit with a non-zero intercept;

$$y = V_{max} * x / (K_m + x) + b$$

The non-linear fit was performed using GraphPad Prism version 4.0 for Windows (GraphPad Software San Diego, CA).

4.4.5 Luciferase Refolding

The luciferase refolding activity of DnaK WT and mutants were evaluated as described with minor changes [21]. Briefly, denatured firefly luciferase was prepared by beginning with a concentrated stock (8.2 µM) of luciferase with 6 M GuHCl in 25 mM HEPES buffer

(50 mM potassium acetate, 5 mM DTT, pH 7.2). This stock was incubated at room temperature for one hour and then diluted to 0.2 µM with the same HEPES buffer without GuHCl. This preparation was used as the stock solution for final sample preparation. Enzyme mix (10 µl) containing DnaK, DnaJ, GrpE, denatured firefly luciferase in 39 mM HEPES (170 mM potassium acetate, 1.7 mM magnesium acetate, 3 mM DTT, 12 mM creatine phosphate, 50 U/ml creatine kinase, pH 7.6) was first added into each well of 96-well white plate and then 4 µl of 3.5 mM ATP, dissolved in water, was added to start the reaction. The final concentration of DnaK was 1 µM, denatured luciferase was 8 nM, and ATP was 1 mM unless otherwise noted. The concentration of DnaJ and GrpE are reported for each experiment in the results section. After one hour of incubation at 37 °C, equilibrium was reached and 14 µl of 0.5% or 2% (v/v) SteadyGlo reagent in 50 mM glycine buffer (30 mM $MgSO_4$, 10 mM ATP and 4 mM DTT, pH 7.8) was added into each well, and the luminescence was measured. For each experiment, the signal from a negative control containing everything but DnaK was subtracted. The assay was also optimized for higher luciferase concentration (500 nM; **Appendix 4.5.11**), and the procedure was mostly the same with minor changes. Briefly, 61.3 µM luciferase denatured in 6 M GuHCl was first diluted into 12.5 µM by 100 mM Tris buffer (20 mM KCl, and 6 mM MgCl2, pH 7.4) before added into 22.9 mM HEPES buffer (200 mM potassium

acetate, 2 mM magnesium acetate, 3.6 mM DTT, 14.6 mM creatine phosphate, 63 units/ml creatine kinase, and 0.56 mg/mL BSA, pH 7.6) containing DnaK, DnaJ, and GrpE. Next, 15 µL of this enzyme-luciferase mix was added into each well of a 96-well plate and 10 µL of 2.5 mM ATP dissolved in ddH_2O was used to start the reaction. The reaction was quenched after 0, 10, 20, 30 minutes incubation at 37°C by adding 25 µL 4% (v/v) SteadyGlo reagent. The rate of refolding was obtained by converting the luminescence unit into luciferase concentration using standard curve shown in **Appendix 4.5.11**, and analyzing by linear regression fit using GraphPad Prism 4.0 (for Windows).

4.4.6 Malate Dehydrogenase (MDH) Refolding

The MDH refolding assay was optimized from a previous protocol [76] (**Appendix 4.5.12**). Briefly, 0.84 µM MDH was denatured at 47 °C for 30 minutes on PCR machine in 60 µL 20 mM MOPS buffer (2 mM magnesium acetate, 200 mM KCl, pH = 7.4) at the presence of the DnaK mutants (1.67 µM), DnaJ (0.42 µM), GrpE (0.2 µM), and DTT (5 mM). Next, 15 µL of the MDH heat denaturation mix was transferred into each well of a transparent 96-well plate (triplicate) and the refolding reaction was started by adding 10 µL of 2.5 mM ATP dissolved in the same 20 mM MOPS buffer (with 25 mM creatine phosphate and 87.5 U/mL creatine kinase). After 1.5 hour incubation at 30°C, 75 µL of MOPS buffer

containing 0.28 mM NADH, 0.5 mM OAA, and 1 mg/mL BSA was added to each well, and the decline of OD_{340} over 5 minutes was recorded by SpectraMax M5 spectrometer using kinetic reading. The slope of the OD_{340} (represent of the amount of refolded MDH) decline was obtained by linear regression fit using GraphPad Prism 4.0 (for Windows).

4.4.7 ELISA-based DnaK Binding Assay

The ELISA-based binding assay was optimized from a previous protocol [77] (**Appendix 4.5.3**). The assays were carried out on transparent 96-well plates. Both luciferase (61.3 µM) and MDH (55.4 µM) were denatured in 6 M GuHCl at room temperature for one hour. Next, 50 µL of PBS containing 100 nM denatured luciferase or MDH was added to each well and incubated at 37 °C for 30 minutes for immobilization. The unbound protein was washed away by TBS-T (0.05% Tween 20). Between all the binding steps were washing steps. In all the washing steps, 150 µL TBS-T was added to each well, after 3 minutes incubation on rocker, the buffer was discarded (repeat three times). After washing, 50 µL of 25 mM HEPES buffer (40 mM KCl, 8 mM $MgCl_2$, 100 mM NaCl, and 0.01% Tween 20) containing DnaK and ATP (1 mM) was added to each well, and discarded after a 12-hour incubation at room temperature (RT) on rocker. The plate was blocked by 100 µL 5% milk in TBS-T for 5 minutes, and the DnaK binding was detected by

adding rabbit anti-DnaK antibody, followed by HRP conjugated goat anti-rabbit antibody (50 µL, 1:5000 for both antibodies, diluted in TBS-T, and incubate at RT for 1 hour). After washing, 50 µL of TMB substrate (Invitrogen) was added to each well, incubated for 5 minutes in dark, and then 50 µL of 1 M HCl was added to quench the color change. The resulted OD_{450} was read by SpectraMax M5 spectrometer.

4.4.8 Holdase Activity

Native luciferase was diluted to 0.032 µM in 50 mM HEPES (10 mM $MgSO_4$, 300 mM KCl, 20 mM DTT, pH 7.5) and loaded into a 96-well PCR plate (Thermofisher) (5 µl/well). Next, 5 µl of 2 µM DnaK was added in triplicate into the wells containing luciferase. The reaction mixtures were heated to 39.5 °C for 8 minutes and the samples were transferred into a 96-well, opaque, white microtiter plate (Thermofisher). Next, 10 µl of 0.5 % v/v SteadyGlo reagent, as described in the previous section, was added to each well and the luminescence was measured.

4.4.9 Partial Proteolysis

The partial proteolysis protocol was adapted from a previously described method [11]. Briefly, we prepared samples of 6 µM DnaK in 40 mM HEPES buffer (20 mM NaCl, 8 mM

$MgCl_2$, 20 mM KCl, 0.3 mM EDTA, pH 8.0) with 1 mM nucleotide (ADP or ATP). Additives such as J-domain (residues 2-108, 4-fold molar equivalents) are noted when included. Samples were incubated at room temperature for 30 minutes. Trypsin (SIGMA Ec 3.4.2.1.4) was added at a 1:4 (trypsin:DnaK) molar ratio to bring the final volume to 50 µl. Proteolysis was carried out at room temperature for 20 minutes, unless otherwise noted. The reaction was quenched with the addition of 25 µl of SDS loading buffer (240 mM Tris, 6% (w/v) SDS, 30% (v/v) glycerol, and 16% (v/v) β-mercaptoethanol, 0.6 mg/ml bromophenol blue, pH 6.8) and heated to 95 °C for 3 minutes. Samples were analyzed using a 12% SDS-PAGE electrophoresis gel and stained with Coomassie blue.

4.4.10 Complementation of the Heat Shock Phenotype in a ΔdnaK Strain

Thermosensitive *E. coli ΔdnaK* (DE3) cells that expressed target genes under the T7 promoter were generated using λDE3 Lysogenization Kit (Novagen) based on the reported method of Sugimoto *et al.* [78]. pMCSG7 plasmids containing *dnaK* WT and mutant genes were transformed into *ΔdnaK* (DE3) *E. coli* cells, while transformation with an empty pMCSG7 vector served as a negative control. For the complementation assay, a single colony of each *dnaK* mutant was inoculated into 5 ml LB with 50 µg/ml ampicillin, and grown with shaking overnight at 30 °C. The next day, all the overnight cultures were

diluted to OD_{600} = ~0.055 by LB containing 50 µg/ml ampicillin and 4 µM IPTG. From the diluted culture, a 100 µl aliquot was loaded onto a transparent 96-well flat bottom plate (Corning) in triplicate. These samples were incubated at 43 °C with shaking for 6 hours and the OD_{600} value for each well was measured. The expression of DnaK protein in each clone was verified by adding 4 µM IPTG to the undiluted overnight culture, incubating at 37 °C for 5 hours, lysing the cultures, normalizing the protein content and then separating proteins by SDS-PAGE (**Appendix 4.5.22B**).

Notes

This work was partially published as "Mutagenesis reveals the complex relationships between ATPase rate and the chaperone activities of Escherichia coli heat shock protein 70 (Hsp70/DnaK)" **2010** J Biol Chem. 285: 21282-91.

Lyra Chang, Andrea Thompson, and Jason E. Gestwicki designed the experiments. Lyra Chang and Andrea Thompson conducted the experiments. In this study, Peter Ung helped design and purify ten DnaK mutants. The pMCSG7 vector was a gift from Clay Brown in Center for Structural Biology in University of Michigan. The original vectors containing J domain, DnaJ, DnaK, and GrpE were gifts from Prof. Erik R.P. Zuiderweg.

4.5 Appendix

4.5.1 Circular dichroism spectra of WT and mutant DnaK

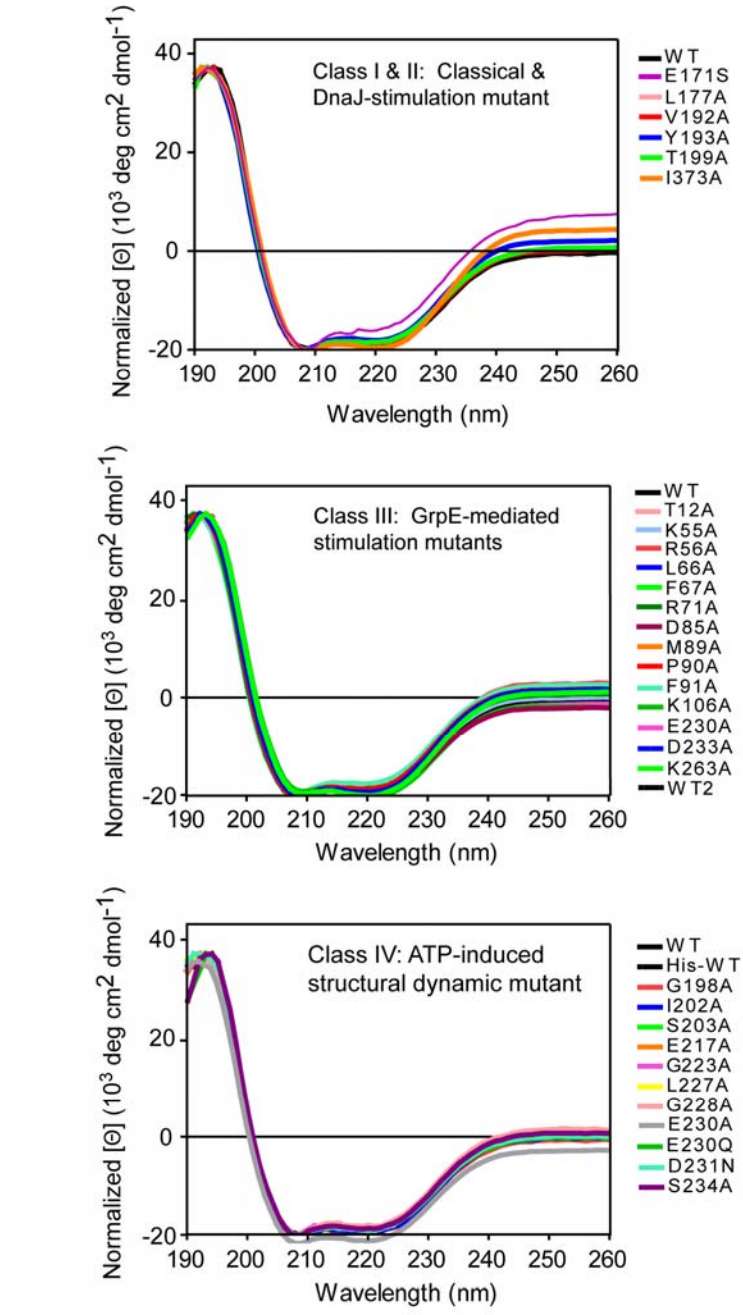

Appendix 4.5.1 Circular dichroism (CD) spectra of WT DnaK and mutants. CD spectra are normalized (deg cm^2 $dmol^{-1}$) for comparison. The mutant proteins show a similar spectra to WT DnaK, suggesting similar secondary structures in the folded proteins.

4.5.2 The holdase activities of DnaK mutants

	Holdase activity lum. x10^3	error stdev
no DnaK	**2.8**	**0.8**
WT	12.9	0.1
E171S	11.3	1.0
V192A	15.0	0.4
Y193A	13.3	0.8
T199A	14.8	0.7
L177A	21.4	0.8
I373A	17.5	0.8
T12A	29.3	0.7
K55A	21.0	1.1
R56A	25.1	1.3
F67L	22.1	1.4
R71A	20.4	2.2
D85A	17.5	1.4
M89A	25.4	0.7
P90A	20.6	1.6
F91A	21.8	1.5
K106A	26.1	1.6
D233A	22.5	1.0
K263A	18.8	1.1
G198A	16.2	1.0
I202A	15.5	1.0
S203A	16.7	1.1
E217A	15.8	1.3
G223A	15.9	0.5
L227A	17.7	0.4
G228A	17.4	0.4
E230Q	13.2	0.8
E230A	26.3	1.5
D231N	8.4	0.6
S234A	7.7	0.8

All mutants were tested at 1 µM.
Abbreviations are as follows;
luminescence (lum.), wildtype (WT),
standard deviation (stdev)

4.5.3 Optimization of the ELISA-based DnaK binding assay

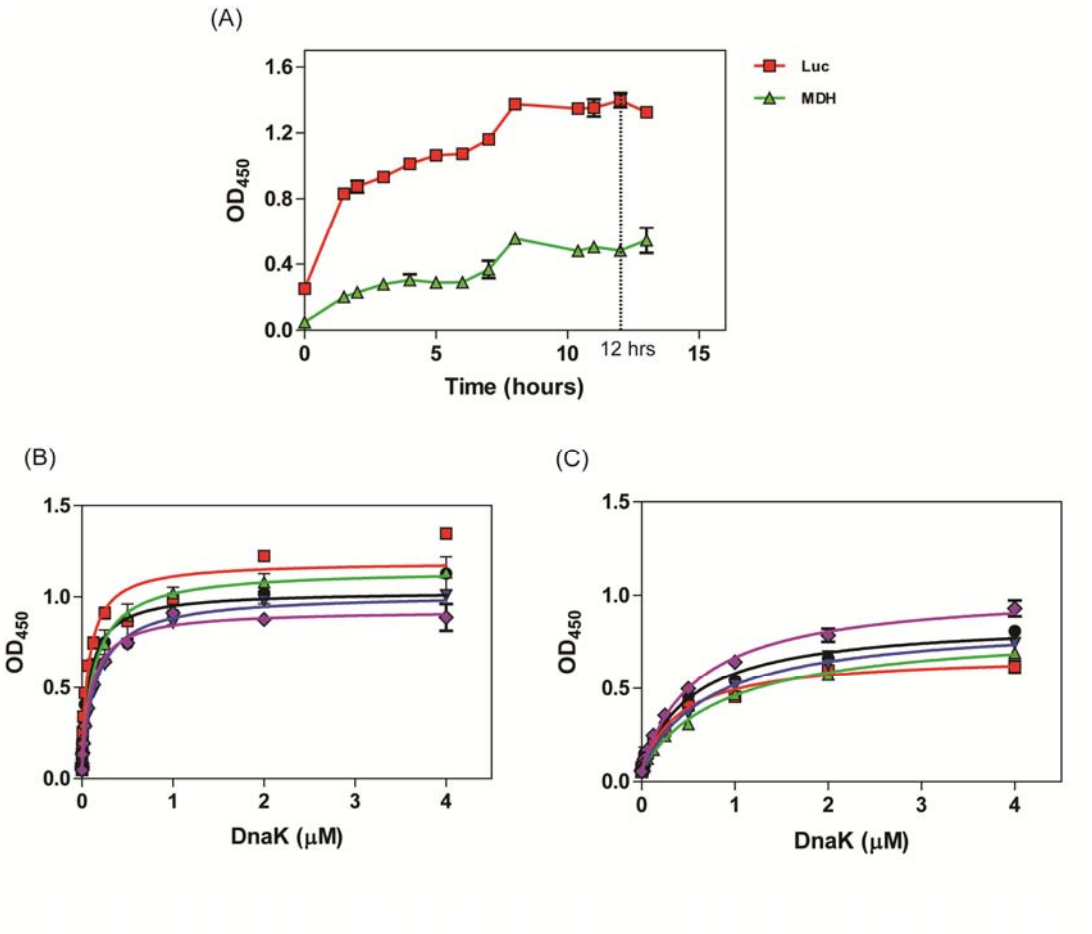

Appendix 4.5.3 Optimization of ELISA-based DnaK binding assays. (A) Time course of DnaK (1 μM) binding to immobilized 6 M GuHCl denatured luciferase (Luc) and MDH. In order to measure DnaK binding at equilibrium state, 12 hours incubation of DnaK with immobilized substrates was used in all ELISA-based binding experiments in this chapter. (B) and (C) After optimization of the ELISA-based binding assay, the binding assays became highly repeatable for both 6 M GuHCl denatured luciferase (B) and MDH (C). Each curve shown in (B) or (C) represents a seperate set of experiment. Wild type DnaK is used in all experiments at the presence of 1 mM ATP. Each data point is the average of triplicates and the error bars represent the standard error of the mean.

4.5.4 Dose-dependent binding curves of DnaK to denatured luciferase

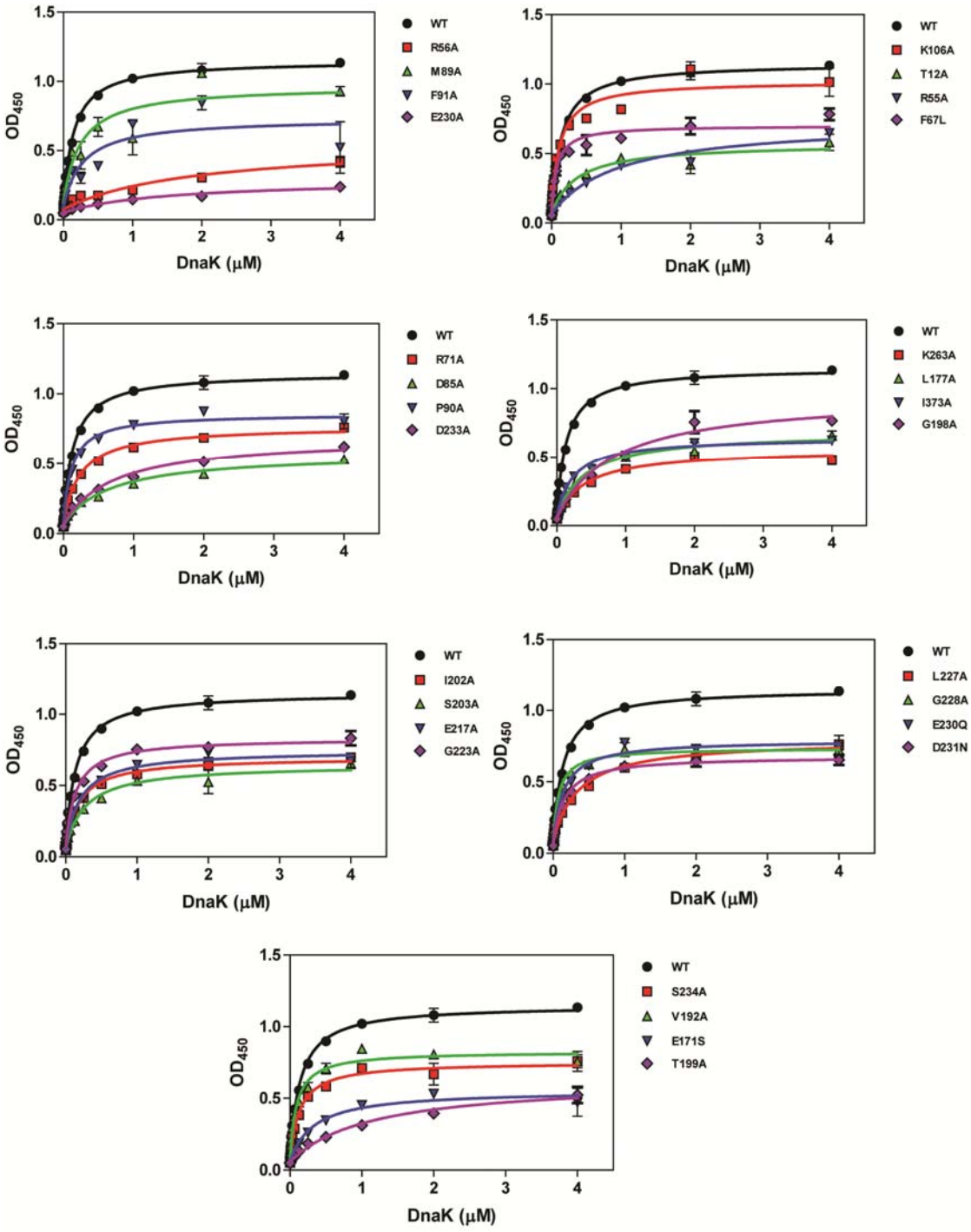

Appendix 4.5.4 Dose dependent binding curve of DnaK mutants to 6 M GuHCl denatured luciferase.The binding is measured by an ELISA-based assay (see material and method). Each data point is the average of triplicate and the error bar represents standard error of the mean.

4.5.5 Dose-dependent binding curves of DnaK to denatured malate dehydrogenase

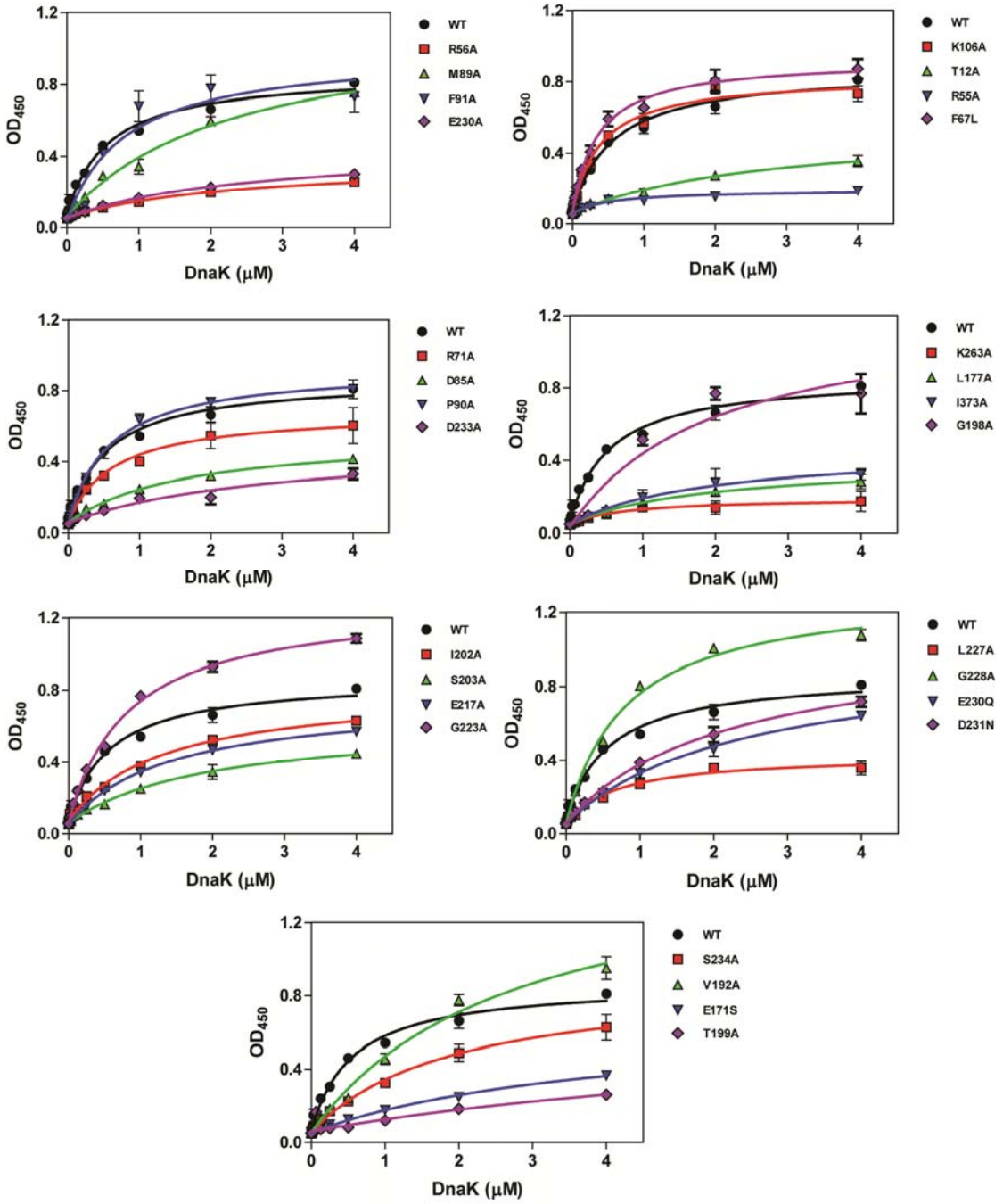

Appendix 4.5.5 Dose dependent binding curve of DnaK to 6M GuHCl denatured malate dehydrogenase. The binding is measured by an ELISA-based assay (see material and method). Each data point is the average of triplicate and the error bar represents standard error of the mean.

4.5.6 Summary table of the substrate binding activities of DnaK mutants

Appendix 4.5.6 The binding affinity and the maximal binding signal of each DnaK mutant against 6 M GuHCl denatured luciferase and MDH. The binding curves shown in appendix 4.5.4 and 4.5.5 were evaluated by fitting the data using a hyperbolic fit with a non-zero intercept; $y = B_{max}*x/(K_d+x)+b$ using GraphPad 4.0. B_{max} is the maximal binding signal shown in this table.

Mutant ID	DnaK binding to 6 M GuHCl denatured Luciferase		DnaK binding to 6 M GuHCl denatured MDH	
	K_d	Maximal Signal (OD_{450})	K_d	Maximal Signal (OD_{450})
R56A	1.91 ± 0.48	0.48 ± 0.05	2.43 ± 0.35	0.32 ± 0.02
M89A	0.25 ± 0.06	0.85 ± 0.05	2.30 ± 0.27	1.10 ± 0.06
F91A	0.28 ± 0.10	0.64 ± 0.06	0.80 ± 0.19	0.95 ± 0.07
E230A	1.51 ± 0.21	0.24 ± 0.01	2.62 ± 0.23	0.41 ± 0.02
K106A	0.12 ± 0.02	0.92 ± 0.03	0.39 ± 0.05	0.77 ± 0.03
T12A	0.35 ± 0.05	0.51 ± 0.02	2.71 ± 0.54	0.50 ± 0.05
R55A	0.98 ± 0.17	0.67 ± 0.04	0.52 ± 0.11	0.13 ± 0.01
F67L	0.07 ± 0.01	0.63 ± 0.02	0.35 ± 0.04	0.86 ± 0.03
R71A	0.24 ± 0.01	0.70 ± 0.01	0.65 ± 0.13	0.62 ± 0.04
D85A	0.66 ± 0.06	0.52 ± 0.01	1.63 ± 0.15	0.50 ± 0.02
P90A	0.12 ± 0.01	0.79 ± 0.01	0.59 ± 0.05	0.88 ± 0.02
D233A	0.71 ± 0.05	0.63 ± 0.02	2.89 ± 0.86	0.45 ± 0.07
K263A	0.41 ± 0.04	0.50 ± 0.01	0.76 ± 0.35	0.14 ± 0.02
L177A	0.41 ± 0.05	0.62 ± 0.02	2.00 ± 0.40	0.35 ± 0.03
I373A	0.24 ± 0.02	0.58 ± 0.01	1.95 ± 0.69	0.42 ± 0.07
G198A	0.84 ± 0.10	0.89 ± 0.04	2.02 ± 0.56	1.22 ± 0.15
I202A	0.19 ± 0.01	0.63 ± 0.01	1.32 ± 0.15	0.74 ± 0.03
S203A	0.28 ± 0.04	0.59 ± 0.02	1.99 ± 0.31	0.57 ± 0.04
E217A	0.20 ± 0.02	0.68 ± 0.02	1.43 ± 0.07	0.71 ± 0.01
G223A	0.14 ± 0.01	0.76 ± 0.01	0.82 ± 0.04	1.23 ± 0.02
L227A	0.34 ± 0.03	0.72 ± 0.02	0.71 ± 0.11	0.37 ± 0.02
G228A	0.08 ± 0.01	0.66 ± 0.01	0.80 ± 0.05	1.27 ± 0.02
E230Q	0.14 ± 0.02	0.72 ± 0.02	2.45 ± 0.28	0.93 ± 0.05
D231N	0.15 ± 0.01	0.61 ± 0.01	2.22 ± 0.23	1.02 ± 0.05
S234A	0.13 ± 0.01	0.68 ± 0.02	1.93 ± 0.33	0.84 ± 0.07
V192A	0.10 ± 0.01	0.74 ± 0.02	2.74 ± 0.37	1.55 ± 0.10
E171S	0.33 ± 0.06	0.50 ± 0.02	4.11 ± 0.48	0.63 ± 0.04
T199A	1.15 ± 0.17	0.57 ± 0.03	9.06 ± 8.73	0.65 ± 0.46
WT	0.14 ± 0.01	1.07 ± 0.01	0.56 ± 0.06	0.97 ± 0.02

4.5.7 Unstable DnaK mutants, L66A and F67A

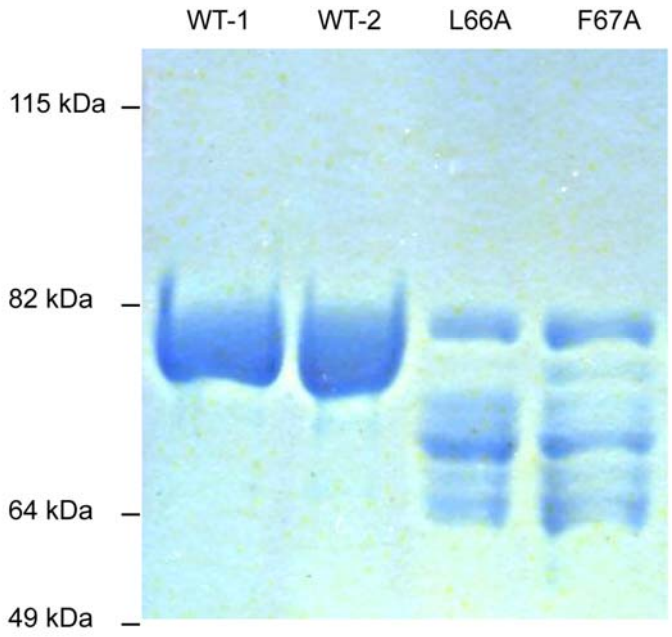

Appendix 4.5.7 Some mutations of DnaK create unstable proteins, which were removed from the study. During purification of the DnaK mutants, L66A and F67A were found to have poor stability durign storage. We were not able to express L227P. The gel shown is an 8% SDS PAGE gel with 4 mM protein loaded into each lane.

4.5.8 Co-chaperone ATPase stimulation curves

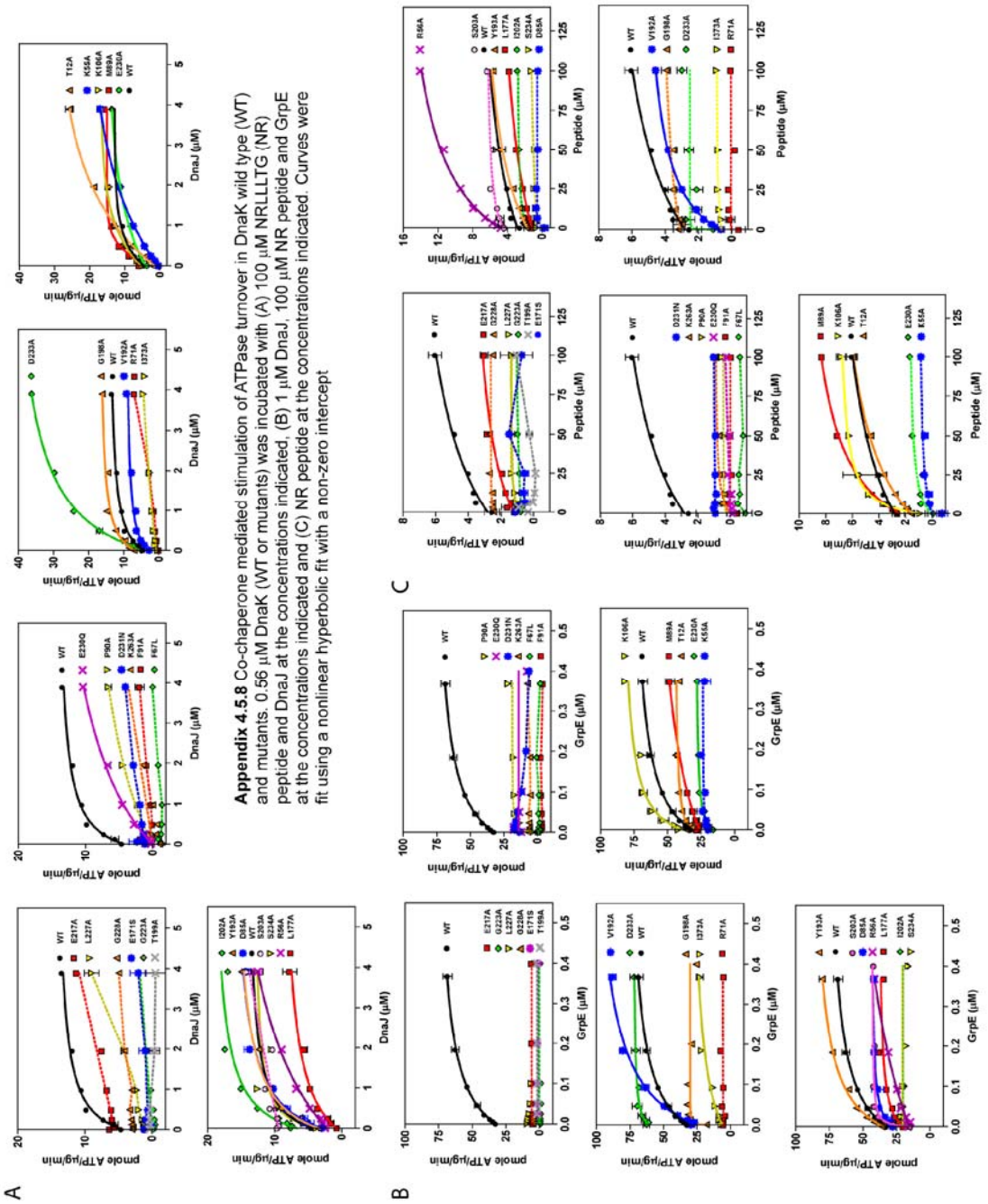

Appendix 4.5.8 Co-chaperone mediated stimulation of ATPase turnover in DnaK wild type (WT) and mutants. 0.56 μM DnaK (WT or mutants) was incubated with (A) 100 μM NRLLLTG (NR) peptide and DnaJ at the concentrations indicated, (B) 1 μM DnaJ, 100 μM NR peptide and GrpE at the concentrations indicated and (C) NR peptide at the concentrations indicated. Curves were fit using a nonlinear hyperbolic fit with a non-zero intercept

4.5.9 Surface topology plots of the co-chaperone dependency of DnaK's refolding and ATPase activities

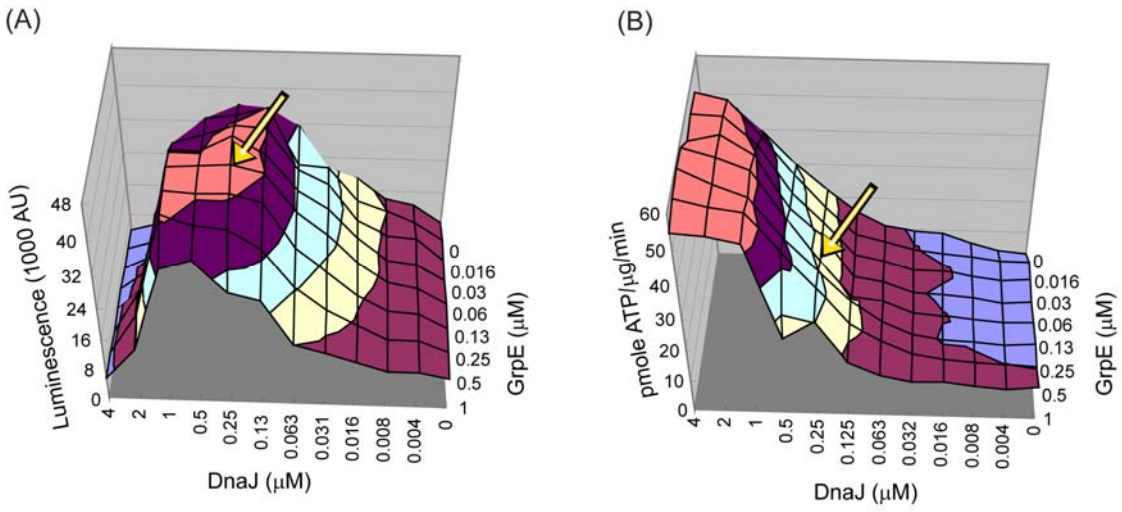

Appendix 4.5.9 Surface topology plots for the dependence of WT DnaK's ATPase and refolding activity on co-chaperones. WT DnaK demonstrated a different dose response to DnaJ and GrpE in luciferase refolding (A) and ATPase activity (B). In both (A) and (B), the final concentrations were: DnaK (1 μM), denatured luciferase (8 nM) and ATP (1 mM). The reaction temperature was 37°C for both. The optimal DnaJ and GrpE concentration (0.25 μM and 0.125 μM, respectively) for luciferase refolding (indicated by the arrow) were used in future experiments, including those shown in figures 2 and 5. The color code in (A) is as follows; blue 0-8, magenta 8-16, yellow 16-24, green 24-32, purple 32-40, orange 40-48. The color code in (B) is as follows; blue 0-10, magenta 10-20, yellow 20-30, green 30-40, purple 40-50, orange 50-60.

4.5.10 The correlations between the intrinsic/DnaJ-stimulated ATPase and luciferase refolding activities

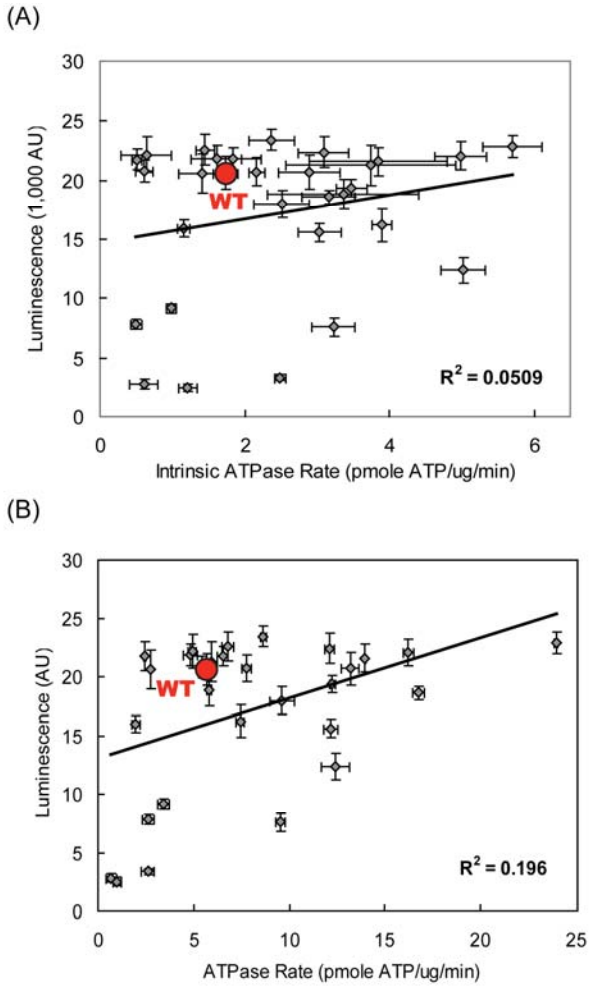

Appendix 4.5.10 The intrinsic and DnaJ-stimulated ATPase rates of DnaK mutants were not correlated with their luciferase refolding activities. (A) The luciferase refolding activity (in luminescence) is plotted against the intrinsic ATPase rate of each DnaK mutant. (B) The luciferase refolding activity (in luminescence) are plotted against the DnaJ-stimulated ATPase rate of each DnaK mutant. The luciferase refolding activities were measured using 1 μM DnaK, 0.25 μM DnaJ, 0.125 μM GrpE and 8 nM luciferase. The intrinsic ATPase rates were measured using 0.6 μM DnaK. The DnaJ-stimulated ATPase rate was measured using 0.6 μM DnaK and 0.5 μM DnaJ. 1 mM ATP was used in all experiments. Each data point is the average of triplicate and the error bars represent the standard error.

4.5.11 Optimizing the luciferase refolding assay for higher substrate concentration

(A)

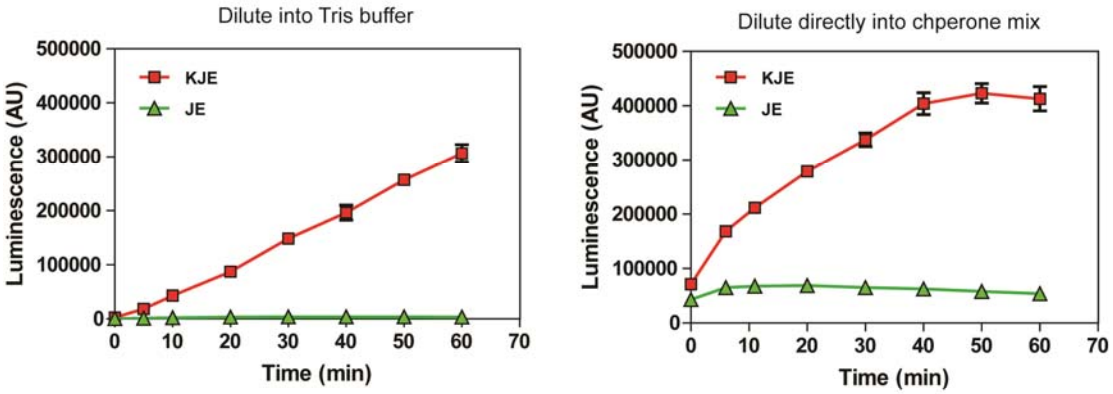

(B)

Luciferase (nM)	Luminescence (AU)
1000	8E+06 ± 443573
500	4E+06 ± 180772
250	2E+06 ± 93393
125	977035 ± 43091
62.5	473273 ± 26645
31.25	235560 ± 16414
15.625	117939 ± 6466
7.8125	58744 ± 3324
3.90625	30386 ± 1905
1.953125	15701 ± 1506
0.9765625	8255 ± 1109
0.48828125	4798 ± 623
0.244140625	2722 ± 342
0.122070313	1473 ± 233
0.061035156	951 ± 154
0	276 ± 100

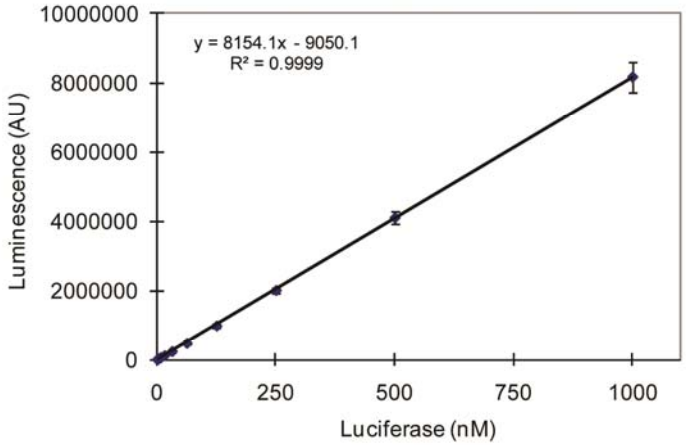

Appendix 4.5.11 Optimization of luciferase refolding assay. (A) Time courses of luciferase refolding by DnaK chaperone system at higher (500 nM) denatured luciferase concentration. Interestingly, constant refolding rate over 1 hour requires first dilute the 6 M GuHCl denatured luciferse into 100 mM Tris buffer (20 mM KCl, and 6 mM $MgCl_2$, pH 7.4) then to the refolding reaction mix containing DnaK chaperone system (shown in left panel). If dilute directly into DnaK-DnaJ-GrpE mix, the initial refolding rate will be higher, but reaches a plateau after 40 minutes (shown in right panel) while only ~ 50 nM of total (500 nM) denatured luciferase was refolded. The refolding activity was measured at 37°C in the presence of DnaK (1 μM), DnaJ (0.25 μM), GrpE (0.125 μM), and ATP (1 mM). In both panels, refolding mixes containing only DnaJ-GrpE (JE, shown in green) are used as control. (B) The standard curve of luciferase concentration versus luminescence after adding SteadyGlo reagent (1/25 original concentration). Each data point is the average of triplicates and the error bars represent the standard error of the mean in (A) while represent standard deviation in (B)

4.5.12 Optimizing the MDH refolding assay for high substrate concentration

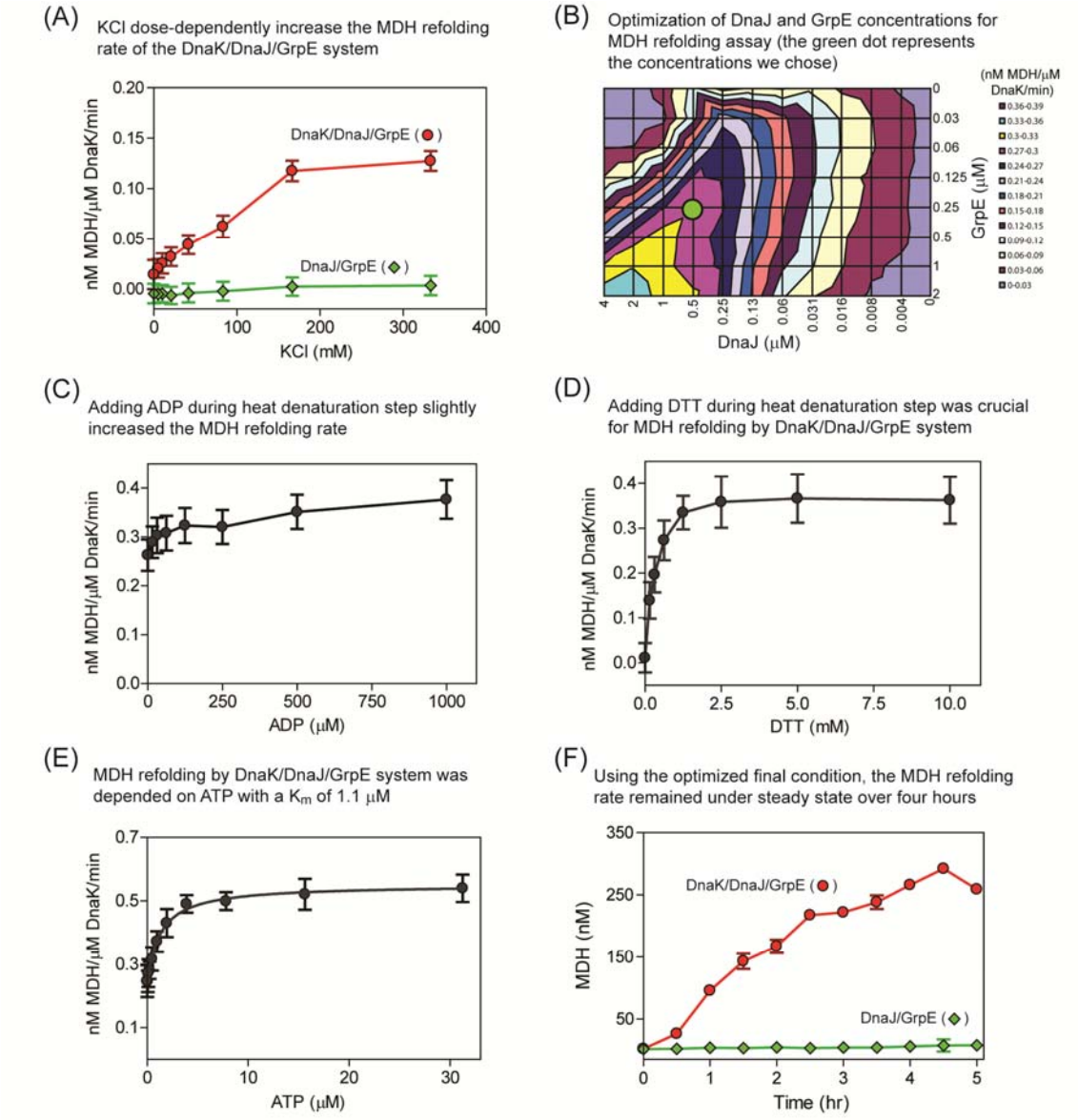

Appendix 4.5.12 Optimization of MDH refolding assay for characterizing the chaperone activity of DnaK/ DnaJ/GrpE system. (A) Potassium chloride significantly increased the MDH refolding rate (DnaK:DnaJ:GrpE = 3.5:0.7:0.35 μM).(B) Optimizing the DnaJ and GrpE concentration for MDH refolding assay (DnaK = 2 μM). (C) Adding ADP during the heat denaturation step only slightly increased the MDH refolding rate. (D) Adding DTT during heat denaturation dose-dependently increased the refolding rate. (E) The MDH refolding rate was dependent on ATP (K_m = 1.1 μM). (F) Using final optimized condition (indicated in material and method), the MDH refolding rate remained under steady state over four hours. For (D), (E) and (F), the DnaK:DnaJ:GrpE concentration was 2 μM:0.5 μM:0.25 μM. Each data point is the average of triplicates and the error bars represent standard error of the mean.

4.5.13 Correlations between ATPase and refolding activities (500 nM Luciferase)

(A)

Mutant ID	Luc Refolding Rate (pM Luc/µg DnaK/min)	ATPase Rate (pmole ATP/µg DnaK/min)
R56A	10.0 ± 1.7	20.3 ± 1.8
M89A	208.2 ± 5.4	87.1 ± 3.6
F91A	9.9 ± 0.9	47.4 ± 2.7
E230A	253.7 ± 14.4	99.3 ± 4.9
K106A	46.8 ± 1.7	56.8 ± 2.1
T12A	6.0 ± 1.4	113.8 ± 6.6
R55A	30.8 ± 2.0	89.2 ± 4.1
F67L	47.8 ± 2.8	52.7 ± 1.8
R71A	44.9 ± 3.0	116.1 ± 4.6
D85A	544.4 ± 20.4	56.5 ± 1.7
P90A	12.1 ± 1.8	47.5 ± 1.6
D233A	79.3 ± 4.2	124.9 ± 5.4
K263A	84.9 ± 5.2	51.9 ± 1.8
L177A	114.0 ± 6.0	44.3 ± 1.6
I373A	10.6 ± 1.9	63.4 ± 1.9
G198A	229.8 ± 6.7	76.0 ± 3.2
I202A	40.5 ± 2.0	88.8 ± 2.9
S203A	25.2 ± 1.0	75.1 ± 1.9
E217A	24.4 ± 1.5	42.1 ± 3.4
G223A	8.1 ± 0.8	66.8 ± 2.8
L227A	18.9 ± 1.3	87.5 ± 2.2
G228A	3.1 ± 1.2	56.0 ± 2.1
E230Q	134.2 ± 4.6	70.8 ± 1.9
D231N	77.0 ± 4.5	55.6 ± 1.9
S234A	136.0 ± 3.6	68.4 ± 3.4
V192A	79.5 ± 3.6	59.5 ± 2.7
Y193A	5.2 ± 0.6	109.5 ± 5.4
E171S	1.2 ± 0.7	ND
T199A	0.8 ± 0.4	-1.8 ± 1.0
WT	148.0 ± 2.8	61.2 ± 2.8

(B)

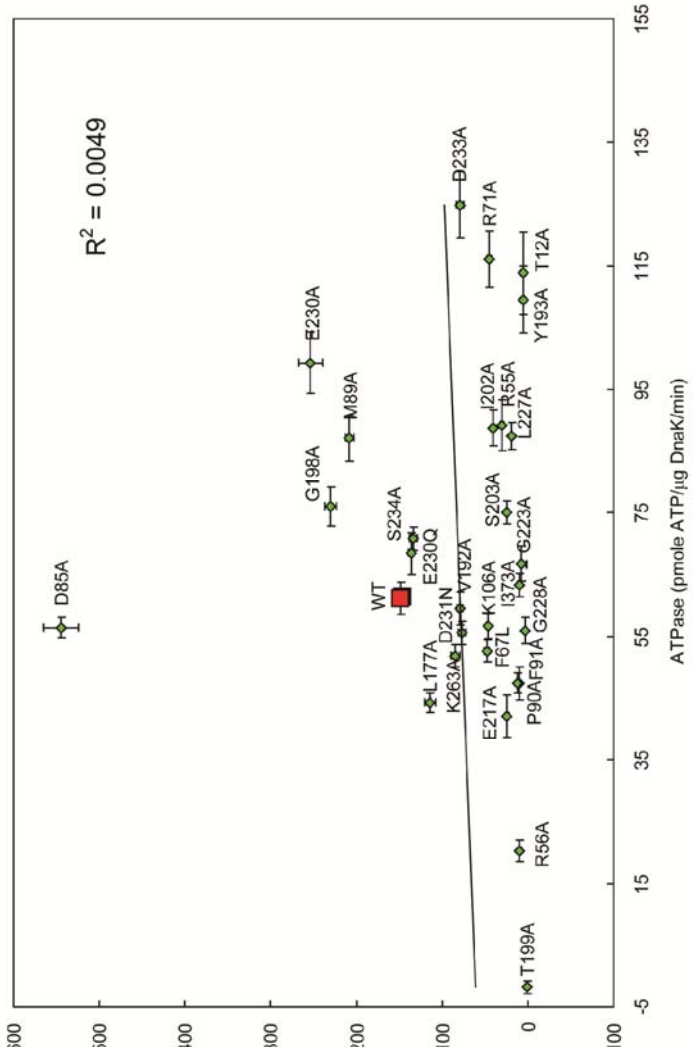

Appendix 4.5.13 At higher denatured luciferae concentration (500 nM), the ATPase rates of DnaK mutants are not correlated with their refolding rates. (A) The luciferase refolding and ATPase rates of DnaK mutants. (B) No correlation can be observed between the ATPase and luciferase refolding activities of DnaK mutants. In (A) and (B), the ATPase and luciferase refolding rates of DnaK mutants are measured in the presence of 500 nM 6M GuHCl denatured luciferase, 1 µM DnaK, 0.25 µM DnaJ, 0.125 µM GrpE, and 1 mM ATP at 37°C. The ATPase and refolding rates shown in both panels are the average of tripicates and the errors are standard error of the mean.

4.5.14 The correlations between the ATPase and MDH refolding activities (37°C)

(A)

Mutant ID	MDH Refolding Rate (pM MDH/μM DnaK/min)	ATPase Rate (pmole ATP/μg DnaK/min)
R56A	23.2 ± 2.3	6.2 ± 0.2
M89A	116.7 ± 6.9	19.9 ± 0.5
F91A	72.7 ± 6.3	17.1 ± 0.2
E230A	128.2 ± 7.3	23.7 ± 0.5
K106A	30.6 ± 2.7	13.6 ± 0.5
T12A	25.9 ± 2.1	40.6 ± 1.0
R55A	17.2 ± 5.7	18.4 ± 0.5
F67L	40.6 ± 8.8	10.9 ± 0.2
R71A	76.7 ± 4.4	35.4 ± 0.5
D85A	272.5 ± 14.4	14.3 ± 0.3
P90A	62.2 ± 2.5	17.7 ± 0.4
D233A	117.1 ± 3.3	42.2 ± 0.3
K263A	39.2 ± 5.8	11.5 ± 0.3
L177A	77.5 ± 3.6	11.0 ± 0.4
I373A	44.6 ± 4.0	19.6 ± 0.5
G198A	90.4 ± 26.3	17.0 ± 0.4
I202A	66.2 ± 7.8	19.2 ± 0.4
S203A	97.1 ± 7.1	31.3 ± 0.6
E217A	52.8 ± 2.6	11.9 ± 0.2
G223A	49.2 ± 2.7	26.9 ± 0.3
L227A	48.8 ± 2.3	32.1 ± 0.7
G228A	14.4 ± 4.4	33.5 ± 0.5
E230Q	103.7 ± 3.7	17.2 ± 0.3
D231N	94.8 ± 2.6	16.1 ± 0.4
S234A	92.1 ± 2.3	13.9 ± 0.4
V192A	105.2 ± 7.4	18.5 ± 0.5
Y193A	31.7 ± 3.4	34.2 ± 0.7
E171S	10.7 ± 3.8	ND
T199A	6.7 ± 4.9	0.1 ± 0.1
WT	69.8 ± 4.7	15.3 ± 0.5

(B)

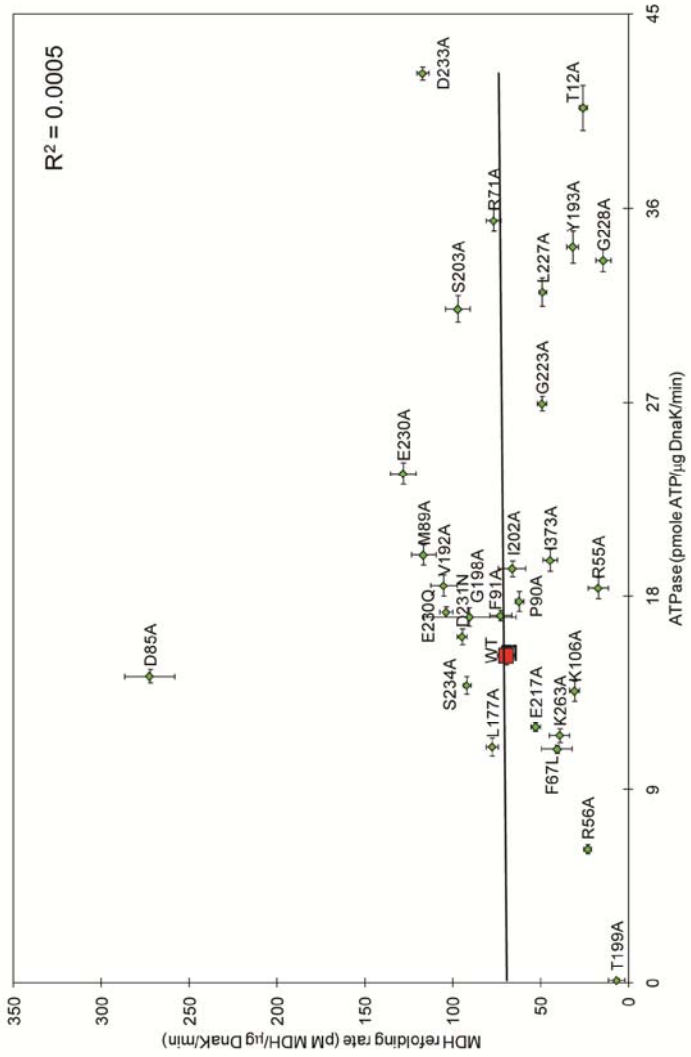

Appendix 4.5.14 The ATPase rates of DnaK mutants are not correlated with their MDH refolding rates at 37°C. (A) The MDH refolding and ATPase rates of DnaK mutants at 37°C. (B) No correlation can be observed between the ATPase and MDH refolding activities of DnaK mutants at 37°C. In (A) and (B), the ATPase and MDH refolding rates of DnaK mutants are measured in the presence of 500 nM MDH, 1 μM DnaK, 0.25 μM DnaJ, 0.125 μM GrpE, and 1 mM ATP. The ATPase and refolding rates shown in both panels are the average of tripicates and the errors are standard error of the mean.

4.5.15 The correlations between the ATPase and MDH refolding activities (30°C)

(A)

Mutant ID	MDH Refolding Rate (pM MDH/μM DnaK/min)	ATPase Rate (pmole ATP/μg DnaK/min)
R56A	10.2 ± 4.5	2.0 ± 0.1
M89A	243.7 ± 10.0	11.7 ± 0.4
F91A	150.5 ± 4.7	8.7 ± 0.5
E230A	234.7 ± 7.0	14.4 ± 0.4
K106A	41.7 ± 5.3	7.4 ± 0.3
T12A	25.1 ± 4.7	29.6 ± 0.7
R55A	10.1 ± 6.6	11.9 ± 0.3
F67L	67.5 ± 4.8	5.7 ± 0.2
R71A	156.4 ± 6.5	23.7 ± 0.1
D85A	545.0 ± 49.7	7.2 ± 0.2
P90A	63.2 ± 9.4	9.7 ± 0.2
D233A	211.3 ± 10.4	28.7 ± 0.3
K263A	14.6 ± 7.1	5.3 ± 0.2
L177A	111.2 ± 7.3	5.4 ± 0.1
I373A	69.3 ± 6.8	10.6 ± 0.2
G198A	181.9 ± 58.0	8.8 ± 0.2
I202A	94.5 ± 6.8	11.0 ± 0.3
S203A	189.8 ± 9.2	17.5 ± 0.4
E217A	91.1 ± 5.2	5.6 ± 0.1
G223A	73.1 ± 5.1	15.7 ± 0.3
L227A	95.1 ± 6.6	20.5 ± 0.4
G228A	-3.9 ± 5.4	20.6 ± 0.5
E230Q	193.6 ± 6.4	9.6 ± 0.3
D231N	143.1 ± 14.1	8.2 ± 0.2
S234A	207.0 ± 6.4	6.7 ± 0.1
V192A	152.6 ± 8.7	8.6 ± 0.3
Y193A	76.3 ± 5.5	21.8 ± 0.3
E171S	19.1 ± 5.7	ND
T199A	27.2 ± 5.9	-1.1 ± 0.1
WT	202.6 ± 10.9	7.5 ± 0.3

(B)

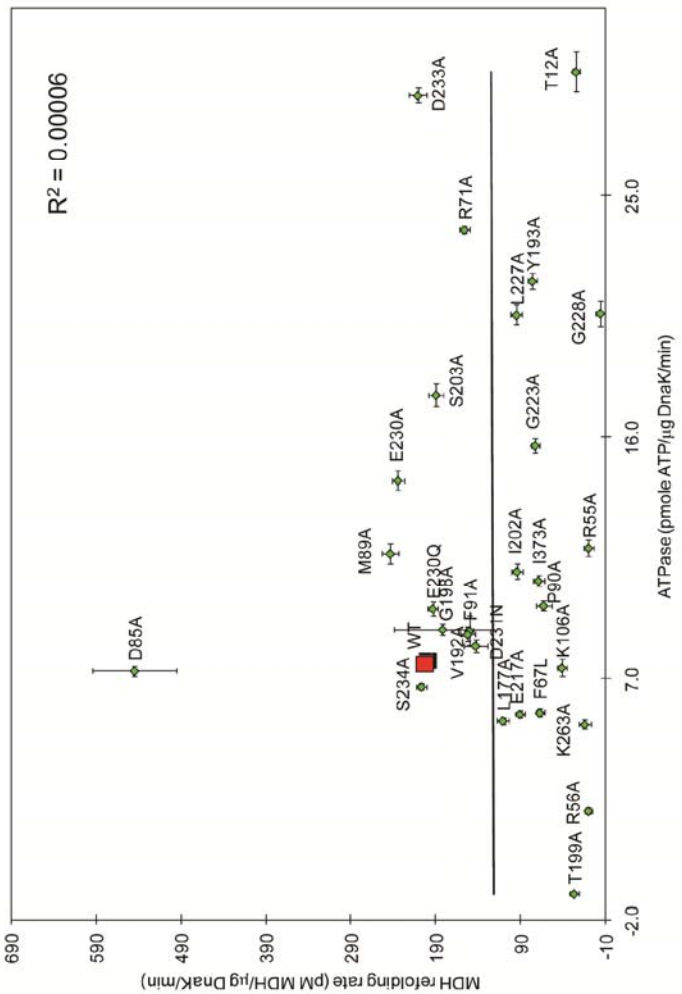

Appendix 4.5.15 The ATPase rates of DnaK mutants are not correlated with their MDH refolding rates at 30°C. (A) The MDH refolding and ATPase rates of DnaK mutants at 30°C. (B) No correlation can be observed between the ATPase and MDH refolding activities of DnaK mutants at 30°C. In (A) and (B), the ATPase and MDH refolding rates of DnaK mutants are measured in the presence of 500 nM MDH, 1 μM DnaK, 0.25 μM DnaJ, 0.125 μM GrpE, and 1 mM ATP. The ATPase and refolding rates shown in both panels are the average of tripicates and the errors are standard error of the mean.

4.5.16 ATPase activities of DnaK mutants are independent of the substrate identity

(A)

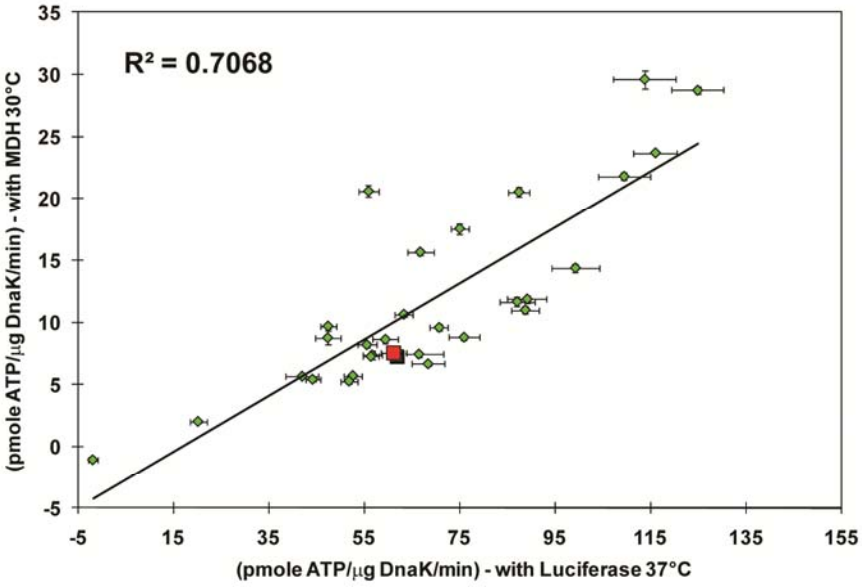

(B)

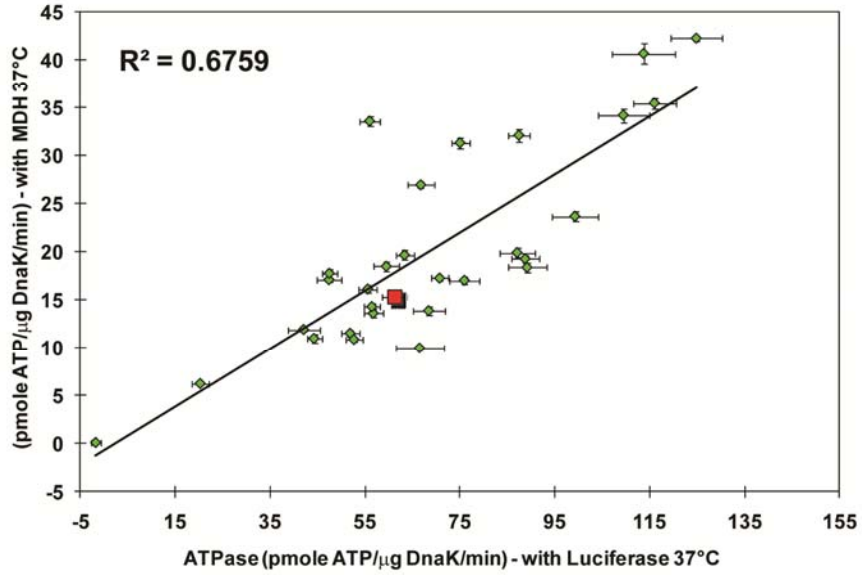

Appendix 4.5.16 The ATPase activities of DnaK mutants at the prescence of luciferase or MDH as protein substrates are moderately correlated. In both (A) and (B), the ATPase reaction mix contained 1 μM DnaK mutants, 0.25 μM DnaJ, 0.125 μM GrpE, 1 mM ATP, and 500 nM of either luciferase or MDH. The ATPase rate of DnaK mutants with malate dehydrogenase in (A) was measure at 30°C while the one in (B) was measured at 37°C. Each data point is the average of triplicates and the error bars represent the standard error of the mean.

4.5.17 Refolding activities of DnaK mutants are largely independent of substrate identity

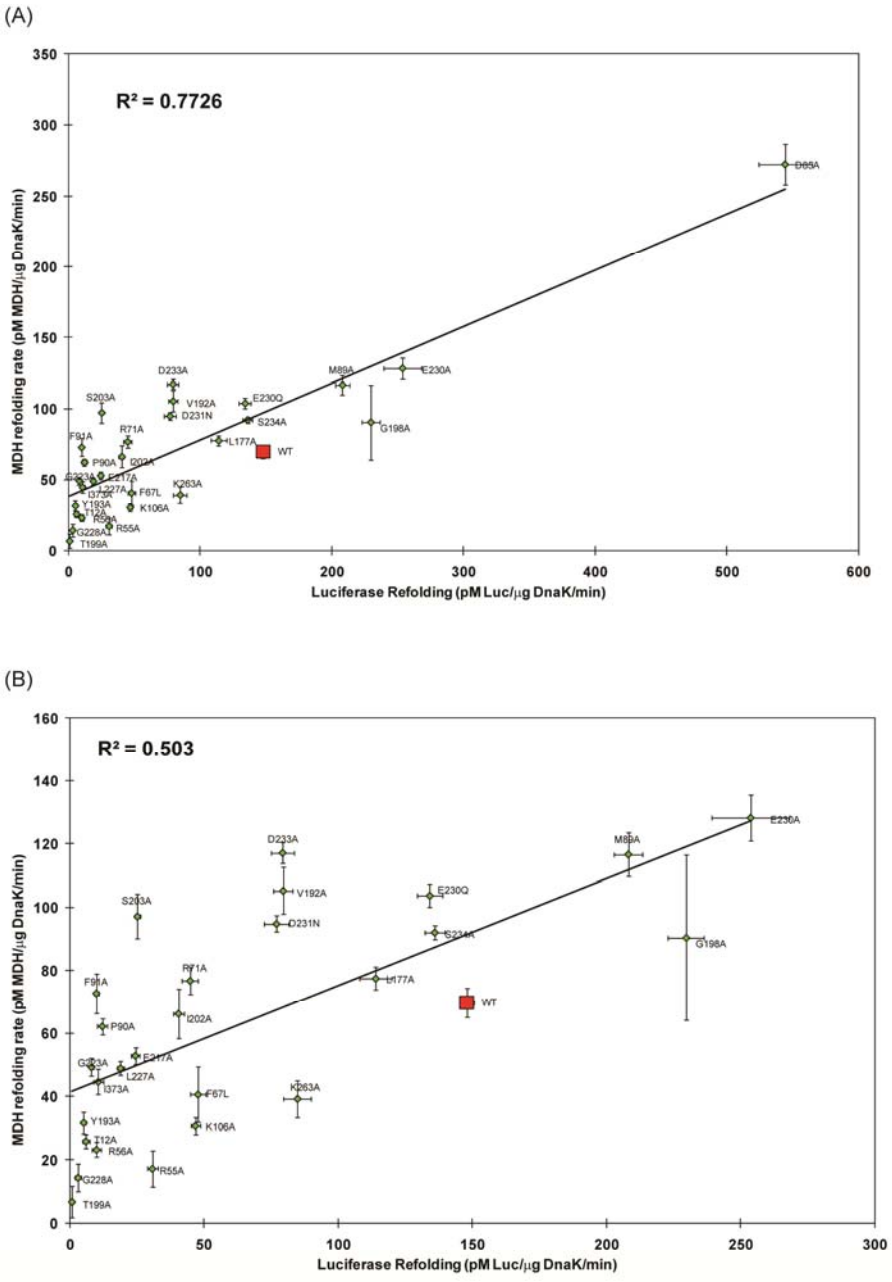

Appendix 4.5.17 The luciferase and MDH refolding rates of DnaK mutants are moderately correlated. In (A), all mutants are included, whereas in (B) the D85A mutant that has ~4-fold higher refolding activity than WT was omitted from the graph. In this graph, both luciferase and MDH refolding rates were measured at 37°C. In the refolding reaction mix, the concentration of both luciferase and MDH were 500 nM, DnaK was 1μM, DnaJ was 0.25 μM, GrpE was 0.125 μM, and ATP was 1mM. Each data point is the average of triplicates and the error bars represent the standard error of the mean.

4.5.18 The correlations between the luciferase (37°C) and MDH refolding (30°C) activities

(A)

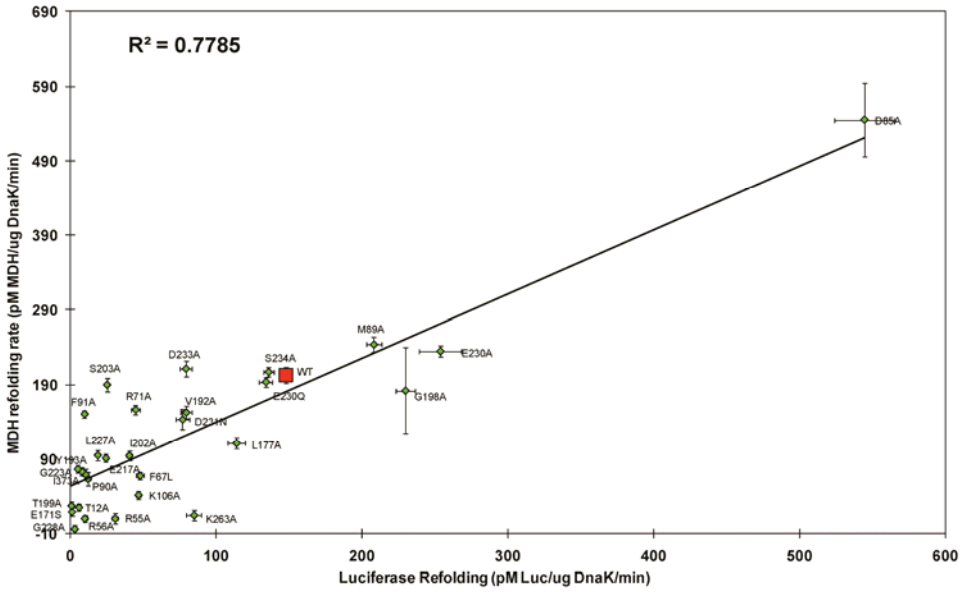

(B)

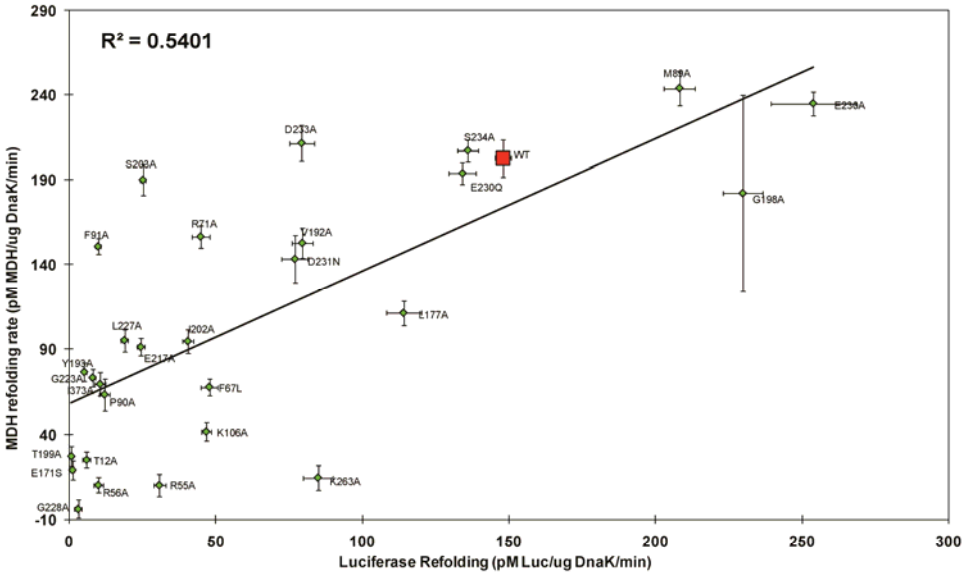

Appendix 4.5.18 The luciferase and MDH refolding rates of DnaK mutants are moderately correlated In (A), all mutants are included, whereas in (B) the D85A mutant that has ~4-fold higher refolding activity than WT was omitted from the graph. In this graph, the MDH refolding rate was measured at 30°C and luciferase refolding is measured at 37°C. In the refolding reaction mix, the concentration of both luciferase and MDH were 500 nM, DnaK was 1μM, DnaJ was 0.25 μM, GrpE was 0.125 μM, and ATP was 1 mM. Each data point is the average of triplicates and the error bars represent the standard error of the mean.

4.5.19 The Apparent K_d of substrate binding was not correlated with refolding activities (500 nM refolding substrate)

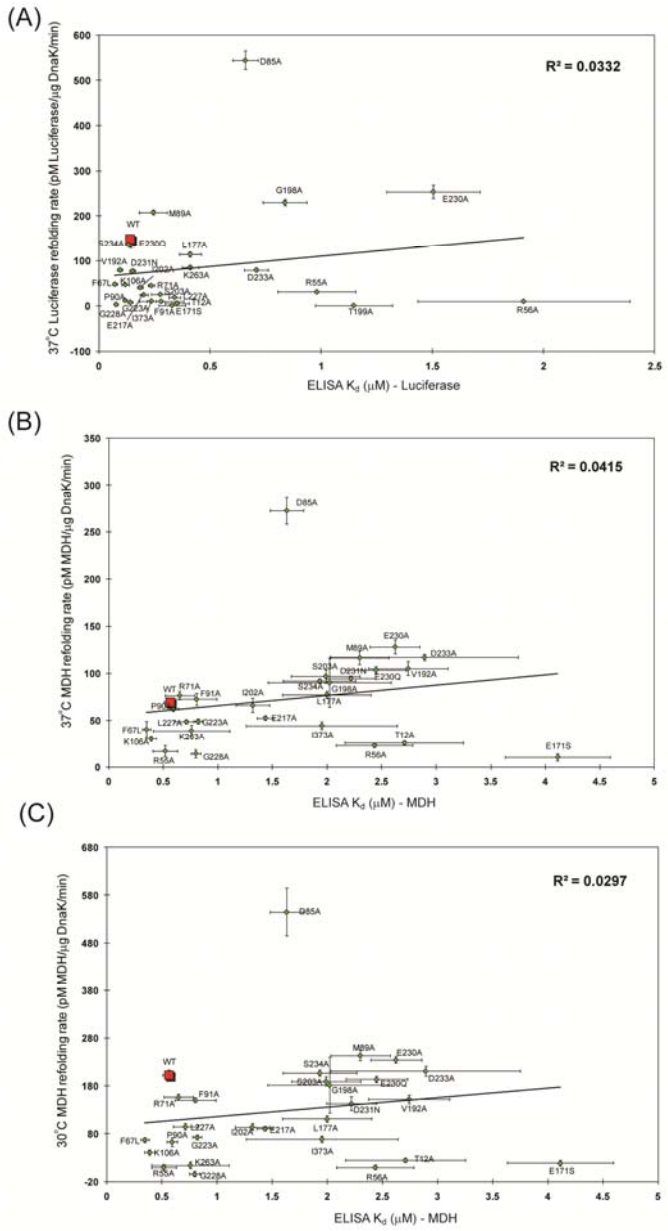

Appendix 4.5.19 The apparent K_d of DnaK mutants binding to immobilized 6 M GuHCl denatured luciferase or MDH in ELISA platform is not correlated with their refolding activity against the two protein substrates. (A) The correlations between apparent K_d of DnaK mutants to denatured luciferase and their luciferase refolding activities. (B) and (C) The correlations between K_d of DnaK mutants to denatured MDH and their MDH refolding activities at 37°C (B) and 30°C (C). All refolding activities are measured at the presence of 1 μM DnaK, 0.25 μM DnaJ, 0.125 μM GrpE, and 1 mM ATP. The binding affinity of DnaK to denatured luciferase and MDH is measured with 1 mM ATP added. Each data point is the average of triplicates and the error bars represent the standard error of the mean

4.5.20 Neither the apparent substrate-binding K_d nor the maximal binding signal were correlated with ATPase or refolding activities (500 nM refolding substrate)

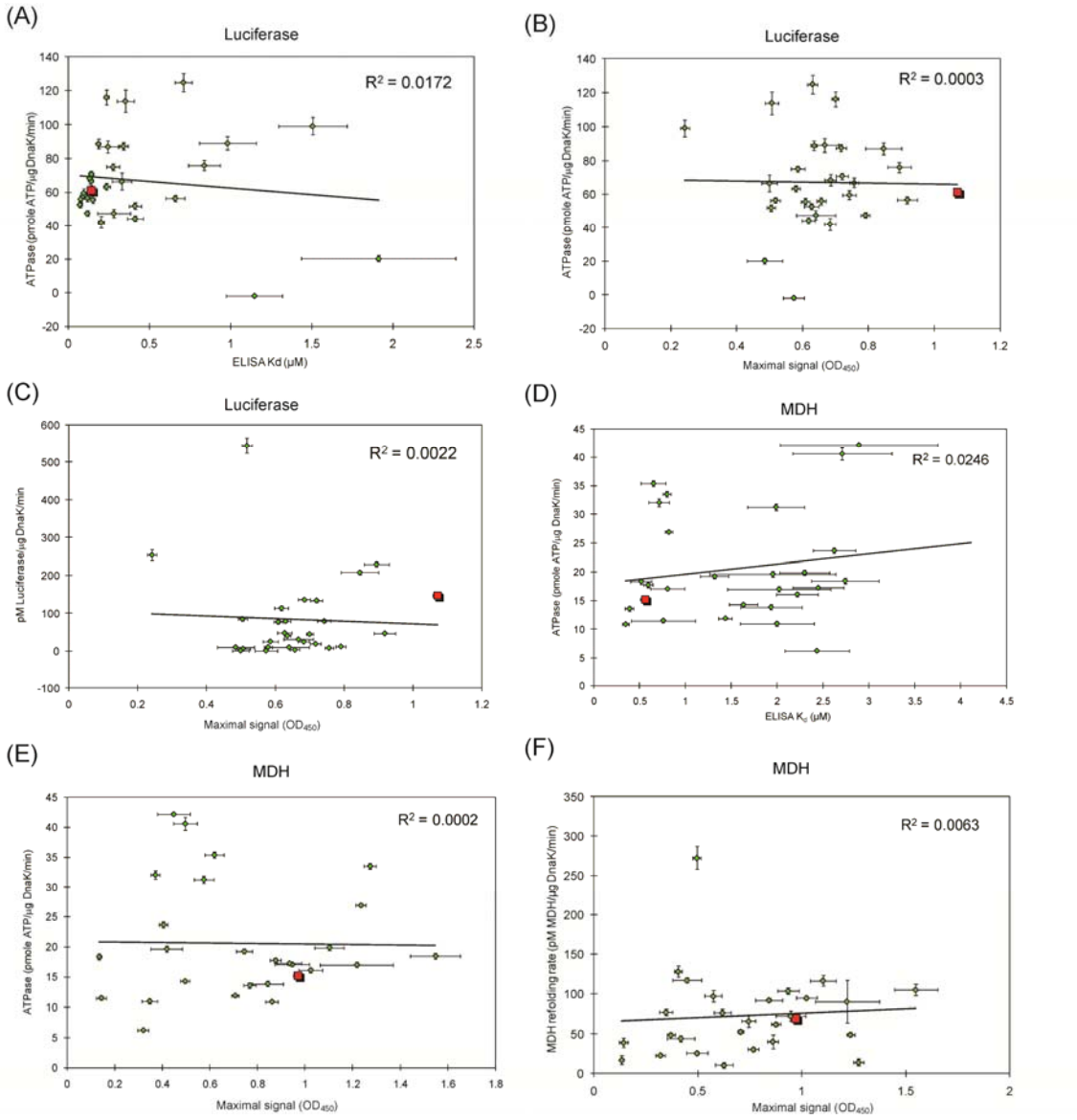

Appendix 4.5.20 The K_d or maximal signal of DnaK mutants binding to luciferase or MDH are not correlated with their ATPase or refolding activities. In (A), (B), and (C), denatured luciferase was used as substrate in all enzymatic assays while in (D), (E), and (F), denatured MDH was used. (A) and (D) show the correlations between apparent K_d and ATPase activity; (B)(E) and (C)(F) show the correlations between maximal binding siganl and ATPase or refolding activities, respectively. The ATPase and refolding activities were measured in the presence of 500 nM luciferase or MDH, 1 μM DnaK, 0.25 μM DnaJ, 0.125 μM GrpE, and 1 mM ATP at 37°C. Each data point is the average of triplicates and the error bars represent the standard error of the mean.

4.5.21 Partial proteolysis of IB subdomain mutants of DnaK

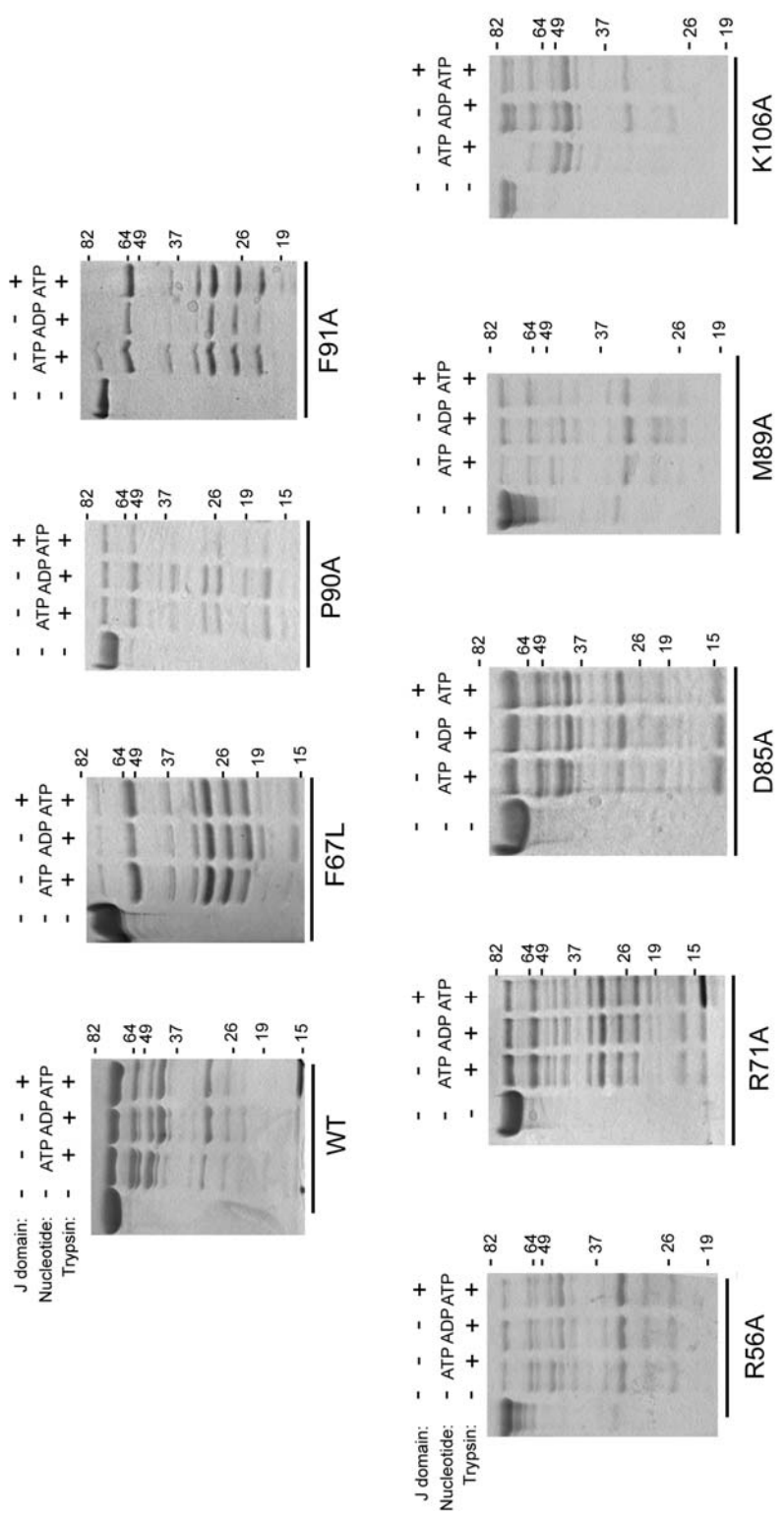

Appendix 4.5.21 Partial proteolysis of DnaK IB subdomain mutants. Trypsin digestion was carried out for 20 minutes using trypsin:DnaK (1:4) in the presence of a 4-fold excess of nucleotide or J-domain (2-108 of DnaJ). Note that the IB decoupling mutants, F67L, P90A, and F91A, had a distinct cleavage pattern and they did not undergo a nucleotide-dependent conformational change. Other IB subdomain mutants (such as R56A, R71A, D85A, M89A, and K106A) were more similar to WT DnaK

4.5.22 Control experiments for testing the *in vivo* heat shock rescue activities of DnaK mutants

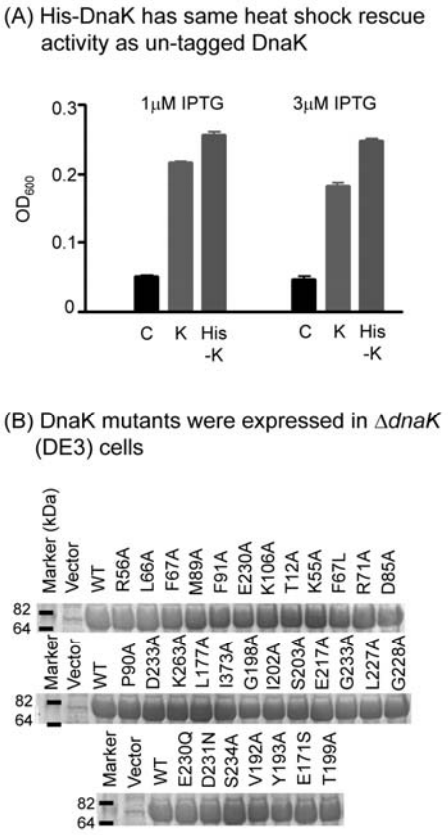

Appendix 4.5.22 Control experiments for testing the ability of DnaK mutants to complement the growth of Δ*dnaK* (DE3) *E. coli* cells under heat shock. (A) DnaK with uncleaved N-terminal His-tag (His-K) could rescue the growth of Δ*dnaK* (DE3) *E. coli* cells at 43°C as well as DnaK lacking the N-terminal His-tag (K). An empty vector was tested as a negative control (C). (B) Prior to testing the heat shock rescue activities of all 29 mutants (with N-terminal His-tags), we confirmed they all expressed in Δ*dnaK* (DE3) *E. coli* cells upon addition of 4 μM IPTG by SDS-PAGE electrophoresis.

4.6 References

1. Rensing, S.A. and U.G. Maier, *Phylogenetic analysis of the stress-70 protein family.* J Mol Evol, 1994. **39**(1): p. 80-6.
2. Parsell, D.A. and S. Lindquist, *The function of heat-shock proteins in stress tolerance: degradation and reactivation of damaged proteins.* Annu Rev Genet, 1993. **27**: p. 437-96.
3. Hesterkamp, T. and B. Bukau, *Role of the DnaK and HscA homologs of Hsp70 chaperones in protein folding in E.coli.* Embo J, 1998. **17**(16): p. 4818-28.
4. Patury, S., Y. Miyata, and J.E. Gestwicki, *Pharmacological targeting of the Hsp70 chaperone.* Curr Top Med Chem, 2009. **9**(15): p. 1337-51.
5. Paek, K.H. and G.C. Walker, *Escherichia coli dnaK null mutants are inviable at high temperature.* J Bacteriol, 1987. **169**(1): p. 283-90.
6. Szabo, A., et al., *The ATP hydrolysis-dependent reaction cycle of the Escherichia coli Hsp70 system DnaK, DnaJ, and GrpE.* Proc Natl Acad Sci U S A, 1994. **91**(22): p. 10345-9.
7. Liberek, K., et al., *The Escherichia coli DnaK chaperone, the 70-kDa heat shock protein eukaryotic equivalent, changes conformation upon ATP hydrolysis, thus triggering its dissociation from a bound target protein.* J Biol Chem, 1991. **266**(22): p. 14491-6.
8. Slepenkov, S.V. and S.N. Witt, *Detection of a concerted conformational change in the ATPase domain of DnaK triggered by peptide binding.* FEBS Lett, 2003. **539**(1-3): p. 100-4.
9. Schmid, D., et al., *Kinetics of molecular chaperone action.* Science, 1994. **263**(5149): p. 971-3.
10. Flynn, G.C., T.G. Chappell, and J.E. Rothman, *Peptide binding and release by proteins implicated as catalysts of protein assembly.* Science, 1989. **245**(4916): p. 385-90.
11. Buchberger, A., et al., *Nucleotide-induced conformational changes in the ATPase and substrate binding domains of the DnaK chaperone provide evidence for interdomain communication.* J Biol Chem, 1995. **270**(28): p. 16903-10.
12. Buczynski, G., et al., *Characterization of a lidless form of the molecular chaperone DnaK: deletion of the lid increases peptide on- and off-rate constants.* J Biol Chem, 2001. **276**(29): p. 27231-6.
13. Pierpaoli, E.V., et al., *The power stroke of the DnaK/DnaJ/GrpE molecular chaperone system.* J Mol Biol, 1997. **269**(5): p. 757-68.

14. Karzai, A.W. and R. McMacken, *A bipartite signaling mechanism involved in DnaJ-mediated activation of the Escherichia coli DnaK protein.* J Biol Chem, 1996. **271**(19): p. 11236-46.
15. Szabo, A., et al., *A zinc finger-like domain of the molecular chaperone DnaJ is involved in binding to denatured protein substrates.* Embo J, 1996. **15**(2): p. 408-17.
16. Goffin, L. and C. Georgopoulos, *Genetic and biochemical characterization of mutations affecting the carboxy-terminal domain of the Escherichia coli molecular chaperone DnaJ.* Mol Microbiol, 1998. **30**(2): p. 329-40.
17. Johnson, J.L. and E.A. Craig, *An essential role for the substrate-binding region of Hsp40s in Saccharomyces cerevisiae.* J Cell Biol, 2001. **152**(4): p. 851-6.
18. Liberek, K., et al., *Escherichia coli DnaJ and GrpE heat shock proteins jointly stimulate ATPase activity of DnaK.* Proc Natl Acad Sci U S A, 1991. **88**(7): p. 2874-8.
19. Ang, D. and C. Georgopoulos, *The heat-shock-regulated grpE gene of Escherichia coli is required for bacterial growth at all temperatures but is dispensable in certain mutant backgrounds.* J Bacteriol, 1989. **171**(5): p. 2748-55.
20. Sell, S.M., et al., *Isolation and characterization of dnaJ null mutants of Escherichia coli.* J Bacteriol, 1990. **172**(9): p. 4827-35.
21. Wisen, S. and J.E. Gestwicki, *Identification of small molecules that modify the protein folding activity of heat shock protein 70.* Anal Biochem, 2008. **374**(2): p. 371-7.
22. Barthel, T.K., J. Zhang, and G.C. Walker, *ATPase-defective derivatives of Escherichia coli DnaK that behave differently with respect to ATP-induced conformational change and peptide release.* J Bacteriol, 2001. **183**(19): p. 5482-90.
23. Klucken, J., et al., *A single amino acid substitution differentiates Hsp70-dependent effects on alpha-synuclein degradation and toxicity.* Biochem Biophys Res Commun, 2004. **325**(1): p. 367-73.
24. Bardwell, J.C. and E.A. Craig, *Major heat shock gene of Drosophila and the Escherichia coli heat-inducible dnaK gene are homologous.* Proc Natl Acad Sci U S A, 1984. **81**(3): p. 848-52.
25. Gragerov, A., et al., *Cooperation of GroEL/GroES and DnaK/DnaJ heat shock proteins in preventing protein misfolding in Escherichia coli.* Proc Natl Acad Sci U S A, 1992. **89**(21): p. 10341-4.
26. Mogk, A., et al., *Identification of thermolabile Escherichia coli proteins: prevention and reversion of aggregation by DnaK and ClpB.* Embo J, 1999. **18**(24): p. 6934-49.
27. Groemping, Y. and J. Reinstein, *Folding properties of the nucleotide exchange factor GrpE from Thermus thermophilus: GrpE is a thermosensor that mediates heat shock*

response. J Mol Biol, 2001. **314**(1): p. 167-78.
28. Grimshaw, J.P., et al., *Thermosensor action of GrpE. The DnaK chaperone system at heat shock temperatures.* J Biol Chem, 2003. **278**(21): p. 19048-53.
29. Kamath-Loeb, A.S., et al., *Analysis of three DnaK mutant proteins suggests that progression through the ATPase cycle requires conformational changes.* J Biol Chem, 1995. **270**(50): p. 30051-9.
30. McClellan, A.J. and J.L. Brodsky, *Mutation of the ATP-binding pocket of SSA1 indicates that a functional interaction between Ssa1p and Ydj1p is required for post-translational translocation into the yeast endoplasmic reticulum.* Genetics, 2000. **156**(2): p. 501-12.
31. Buchberger, A., et al., *The chaperone function of DnaK requires the coupling of ATPase activity with substrate binding through residue E171.* Embo J, 1994. **13**(7): p. 1687-95.
32. Grimshaw, J.P., et al., *The heat-sensitive Escherichia coli grpE280 phenotype: impaired interaction of GrpE(G122D) with DnaK.* J Mol Biol, 2005. **353**(4): p. 888-96.
33. Buchberger, A., et al., *Functional defects of the DnaK756 mutant chaperone of Escherichia coli indicate distinct roles for amino- and carboxyl-terminal residues in substrate and co-chaperone interaction and interdomain communication.* J Biol Chem, 1999. **274**(53): p. 38017-26.
34. Hu, S.M., et al., *Characterization of the L399P and R447G mutants of hsc70: the decrease in refolding activity is correlated with an increase in the rate of substrate dissociation.* Arch Biochem Biophys, 2002. **407**(1): p. 135-41.
35. Chang, T.C., et al., *The effect of mutating arginine-469 on the substrate binding and refolding activities of 70-kDa heat shock cognate protein.* Arch Biochem Biophys, 2001. **386**(1): p. 30-6.
36. Montgomery, D.L., R.I. Morimoto, and L.M. Gierasch, *Mutations in the substrate binding domain of the Escherichia coli 70 kDa molecular chaperone, DnaK, which alter substrate affinity or interdomain coupling.* J Mol Biol, 1999. **286**(3): p. 915-32.
37. Davis, J.E., C. Voisine, and E.A. Craig, *Intragenic suppressors of Hsp70 mutants: interplay between the ATPase- and peptide-binding domains.* Proc Natl Acad Sci U S A, 1999. **96**(16): p. 9269-76.
38. Jiang, J., et al., *Structural basis of J cochaperone binding and regulation of Hsp70.* Mol Cell, 2007. **28**(3): p. 422-33.
39. Jinwal, U.K., et al., *Chemical manipulation of hsp70 ATPase activity regulates tau stability.* J Neurosci, 2009. **29**(39): p. 12079-88.

40. Chang, L., et al., *High-throughput screen for small molecules that modulate the ATPase activity of the molecular chaperone DnaK.* Anal Biochem, 2008. **372**(2): p. 167-76.
41. Bhattacharya, A., et al., *Allostery in Hsp70 chaperones is transduced by subdomain rotations.* J Mol Biol, 2009. **388**(3): p. 475-90.
42. Harrison, C.J., et al., *Crystal structure of the nucleotide exchange factor GrpE bound to the ATPase domain of the molecular chaperone DnaK.* Science, 1997. **276**(5311): p. 431-5.
43. Woo, H.J., et al., *ATP-induced conformational changes in Hsp70: molecular dynamics and experimental validation of an in silico predicted conformation.* Biochemistry, 2009. **48**(48): p. 11470-7.
44. Sugimoto, S., et al., *A gram-negative characteristic segment in Escherichia coli DnaK is essential for the ATP-dependent cooperative function with the co-chaperones DnaJ and GrpE.* FEBS Lett, 2007. **581**(16): p. 2993-9.
45. Brehmer, D., et al., *Tuning of chaperone activity of Hsp70 proteins by modulation of nucleotide exchange.* Nat Struct Biol, 2001. **8**(5): p. 427-32.
46. O'Brien, M.C., K.M. Flaherty, and D.B. McKay, *Lysine 71 of the chaperone protein Hsc70 Is essential for ATP hydrolysis.* J Biol Chem, 1996. **271**(27): p. 15874-8.
47. Tanaka, N., et al., *The substrate binding domain of DnaK facilitates slow protein refolding.* Proc Natl Acad Sci U S A, 2002. **99**(24): p. 15398-403.
48. Theyssen, H., et al., *The second step of ATP binding to DnaK induces peptide release.* J Mol Biol, 1996. **263**(5): p. 657-70.
49. McCarty, J.S., et al., *The role of ATP in the functional cycle of the DnaK chaperone system.* J Mol Biol, 1995. **249**(1): p. 126-37.
50. Brehmer, D., et al., *Influence of GrpE on DnaK-substrate interactions.* J Biol Chem, 2004. **279**(27): p. 27957-64.
51. Laufen, T., et al., *Mechanism of regulation of hsp70 chaperones by DnaJ cochaperones.* Proc Natl Acad Sci U S A, 1999. **96**(10): p. 5452-7.
52. Wall, D., M. Zylicz, and C. Georgopoulos, *The conserved G/F motif of the DnaJ chaperone is necessary for the activation of the substrate binding properties of the DnaK chaperone.* J Biol Chem, 1995. **270**(5): p. 2139-44.
53. Cajo, G.C., et al., *The role of the DIF motif of the DnaJ (Hsp40) co-chaperone in the regulation of the DnaK (Hsp70) chaperone cycle.* J Biol Chem, 2006. **281**(18): p. 12436-44.
54. Linke, K., et al., *The roles of the two zinc binding sites in DnaJ.* J Biol Chem, 2003.

278(45): p. 44457-66.
55. Han, W. and P. Christen, *Mechanism of the targeting action of DnaJ in the DnaK molecular chaperone system.* J Biol Chem, 2003. **278**(21): p. 19038-43.
56. Mayer, M.P., et al., *Multistep mechanism of substrate binding determines chaperone activity of Hsp70.* Nat Struct Biol, 2000. **7**(7): p. 586-93.
57. Gamer, J., et al., *A cycle of binding and release of the DnaK, DnaJ and GrpE chaperones regulates activity of the Escherichia coli heat shock transcription factor sigma32.* Embo J, 1996. **15**(3): p. 607-17.
58. Liberek, K., D. Wall, and C. Georgopoulos, *The DnaJ chaperone catalytically activates the DnaK chaperone to preferentially bind the sigma 32 heat shock transcriptional regulator.* Proc Natl Acad Sci U S A, 1995. **92**(14): p. 6224-8.
59. Schuermann, J.P., et al., *Structure of the Hsp110:Hsc70 nucleotide exchange machine.* Mol Cell, 2008. **31**(2): p. 232-43.
60. Shaner, L., R. Sousa, and K.A. Morano, *Characterization of Hsp70 binding and nucleotide exchange by the yeast Hsp110 chaperone Sse1.* Biochemistry, 2006. **45**(50): p. 15075-84.
61. Sugimoto, S., et al., *In vivo and in vitro complementation study comparing the function of DnaK chaperone systems from halophilic lactic acid bacterium Tetragenococcus halophilus and Escherichia coli.* Biosci Biotechnol Biochem, 2008. **72**(3): p. 811-22.
62. De Los Rios, P., et al., *Hsp70 chaperones accelerate protein translocation and the unfolding of stable protein aggregates by entropic pulling.* Proc Natl Acad Sci U S A, 2006. **103**(16): p. 6166-71.
63. Barral, J.M., et al., *Roles of molecular chaperones in protein misfolding diseases.* Semin Cell Dev Biol, 2004. **15**(1): p. 17-29.
64. Brodsky, J.L. and G. Chiosis, *Hsp70 molecular chaperones: emerging roles in human disease and identification of small molecule modulators.* Curr Top Med Chem, 2006. **6**(11): p. 1215-25.
65. Fewell, S.W., et al., *Small molecule modulators of endogenous and co-chaperone-stimulated Hsp70 ATPase activity.* J Biol Chem, 2004. **279**(49): p. 51131-40.
66. Fewell, S.W., B.W. Day, and J.L. Brodsky, *Identification of an inhibitor of hsc70-mediated protein translocation and ATP hydrolysis.* J Biol Chem, 2001. **276**(2): p. 910-4.
67. Williamson, D.S., et al., *Novel adenosine-derived inhibitors of 70 kDa heat shock*

protein, discovered through structure-based design. J Med Chem, 2009. **52**(6): p. 1510-3.

68. Wadhwa, R., et al., *Selective toxicity of MKT-077 to cancer cells is mediated by its binding to the hsp70 family protein mot-2 and reactivation of p53 function.* Cancer Res, 2000. **60**(24): p. 6818-21.
69. Modica-Napolitano, J.S., et al., *Selective damage to carcinoma mitochondria by the rhodacyanine MKT-077.* Cancer Res, 1996. **56**(3): p. 544-50.
70. Britten, C.D., et al., *A phase I and pharmacokinetic study of the mitochondrial-specific rhodacyanine dye analog MKT 077.* Clin Cancer Res, 2000. **6**(1): p. 42-9.
71. Mamelak, D. and C. Lingwood, *The ATPase domain of hsp70 possesses a unique binding specificity for 3'-sulfogalactolipids.* J Biol Chem, 2001. **276**(1): p. 449-56.
72. Koren, J., 3rd, et al., *Facilitating Akt clearance via manipulation of Hsp70 activity and levels.* J Biol Chem. **285**(4): p. 2498-505.
73. Galam, L., et al., *High-throughput assay for the identification of Hsp90 inhibitors based on Hsp90-dependent refolding of firefly luciferase.* Bioorg Med Chem, 2007. **15**(5): p. 1939-46.
74. Stols, L., et al., *A new vector for high-throughput, ligation-independent cloning encoding a tobacco etch virus protease cleavage site.* Protein Expr Purif, 2002. **25**(1): p. 8-15.
75. Zheng, L., U. Baumann, and J.L. Reymond, *An efficient one-step site-directed and site-saturation mutagenesis protocol.* Nucleic Acids Res, 2004. **32**(14): p. e115.
76. Diamant, S. and P. Goloubinoff, *Temperature-controlled activity of DnaK-DnaJ-GrpE chaperones: protein-folding arrest and recovery during and after heat shock depends on the substrate protein and the GrpE concentration.* Biochemistry, 1998. **37**(27): p. 9688-94.
77. Wawrzynow, A. and M. Zylicz, *Divergent effects of ATP on the binding of the DnaK and DnaJ chaperones to each other, or to their various native and denatured protein substrates.* J Biol Chem, 1995. **270**(33): p. 19300-6.
78. Sugimoto, S., et al., *Construction of Escherichia coli dnaK-deletion mutant infected by lambdaDE3 for overexpression and purification of recombinant GrpE proteins.* Protein Expr Purif, 2008. **60**(1): p. 31-6.

Chapter 5

Understanding the Correlations between the Biochemical Activities of Human Hsc70 Mutants and their Abilities to Trigger Tau Degradation in Cultured Mammalian Cells

5.1 Abstract

The dysfunction and aggregation of tau protein is increasingly recognized as the main cause of tauopathies such as Alzheimer's disease. In collaboration with the Dickey laboratory (University of South Florida), our group discovered that tau is a substrate of Hsc70 and inhibiting the ATPase activity of Hsc70 by chemical modulators leads to tau degradation. Additionally, inhibitor-mediated removal of tau in the brain of transgenic mice was found to reverse cognitive defects even after the onset of dementia. Together, these results suggest the potential of alleviating tauopathies by chemically inducing tau degradation through Hsc70. However, the molecular mechanisms linking Hsc70 inhibitors to tau degradation are not clear. This lack of understanding makes it difficult to proceed with optimizing the compounds. In this study, we aimed to understand the

correlations between the *in vitro* biochemical activities of Hsc70 mutants and their abilities to trigger tau degradation. Specifically, we designed two Hsc70 mutants, D152K and E175S, based on the findings presented in Chapter 4. When over-expressed in cultured cells, two mutants (but not five distinct control mutants) triggered the degradation of tau protein. To understand this correlation, we performed biochemical characterization studies on the mutants and found that the tau-reducing mutants tended to have relatively poor luciferase refolding, activities. Using partial proteolysis, we also discovered that both E175S and D152K mutants assumed ADP-like conformations even in the presence of excess ATP. These results suggest that second-generation high throughput screening assays for refolding activity or the ability to induce the ADP-bound state of Hsc70 may facilitate discovery of compounds with the ability to trigger tau degradation. More generally, these findings provide an important link between the previously enigmatic biochemical properties of a highly allosteric molecular chaperone and one of its cellular activities.

5.1.1 Dysfunction of Tau Protein is correlated with Alzheimer's Disease

Alzheimer's disease (AD) is a currently incurable neurodegenerative disease and it is the fifth leading cause of death for adults aged 65 years or older in United States [1]. The

cause of AD is not fully understood. But evidences accumulated that the extracellular accumulation of amyloid plaques composed of Aβ peptide and the intracellular accumulation of insoluble neurofibillary tangles formed by tau protein are related to AD [2]. Recent reports suggested that, unlike Aβ amyloids, the level of neurofibillary tangles in brain is directly correlated with the progressing stages of AD [3-5]. Therefore, strategies that can modulate the protein level of tau in neuronal cell might be useful in combating AD.

5.1.2 The Normal Functions of Tau Proteins and Their Pathological Roles in AD

Tau is a group of intrinsically disordered proteins that interact with tubulin and stabilize the microtubules in neuron cells [6, 7]. There are six tau isoforms which are the differentially spliced product of one gene, the microtubule associated protein tau (MAPT) genes [8]. The tau isoforms bind to the negatively-charged microtubules via three or four repeats of the positive-charged C-terminal binding domain [6, 9, 10]. In the brain of AD patients, tau proteins dissociate from microtubules, become hyperphosphorylated, and forms neurofibrillary tangles [11, 12]. It is currently thought that tau contributes to AD by both gain-of-functions and lost-of-function mechanisms: the aggregated tau neurological tangles or oligomers are toxic to cells and the lost of stabilizing tau on

microtubules impairs the cargo transportation through microtubule in neuronal cells [2, 13].

5.1.3 Controlling Tau Protein Level through Chemical Modulating Hsp70s

As discussed in Chapter 1, Hsp70s have been linked to neurodegenerative disorders, including AD. One connection between this chaperone and AD arises from the fact that tau directly interacts with the Hsp70s' SBD by two motifs in its microtubule binding domain [14]. These motifs are also known to trigger tau aggregation [15]; thus, Hsp70s are thought to facilitate tau cycling on-and-off the microtubules, which is a normal process required for axonal transport in neurons [16, 17]. Moreover, Hsp70s also bind to free tau and preventing its aggregation when microtubules are disrupted [18]. Finally, Hsp70 has been implicated in tau turnover. Briefly, a complex between Hsc70-CHIP has been shown to be critical to ubiquitin-mediated degradation of tau and its hyperphosphorylated forms [16]. Thus, Hsp70s are important regulators of multiple aspects of tau biology and homeostasis.

Recently, the Dickey and Gestwicki groups found that inhibitors of Hsp70s' ATPase activity trigger tau degradation in HeLa and IMR32 cells, while activators increase tau

levels [19]. These cellular activities appear to be dependent on Hsp70s because overexpressing this chaperone potentiates the compound effects [18, 19]. These results suggest that there is a correlation between the ATPase activity of Hsp70s and their abilities to trigger tau degradation. However, as we discussed in Chapter 4, the ATPase activity of Hsp70s can readily be decoupled from refolding or *in vivo* heat shock rescue activities. Those studies clearly show that the relationship between ATP turnover and chaperone functions is complex.

Our chemical screening strategy (see Chapter 2), which yielded the compounds used in the tau degradation studies, involved identifying inhibitors of steady state ATPase activity. In theory, these active compounds could favor the ATP- or ADP-bound states and they could favor either tight or weak binding to substrates. Alternatively, as seen in Chapter 3, they might disrupt the interaction between Hsp70 and its cochaperones such as J proteins. Thus, the exact mechanism linking ATPase inhibitors to their outputs on Hsc70 activity in cells are not clear.

5.1.4 Our Strategies to Understand the Correlations between the Biochemical Activities of Hsc70 and Tau Protein Processing

To clarify these questions, we aimed to understand the correlations between different biochemical activities of the constantly expressed cytosolic Hsp70 homolog, Hsc70, and its ability to trigger tau degradation. Our strategy was to generate mutants of Hsc70 and test both their abilities to trigger tau degradation in mammalian cells and their *in vitro* biochemical activities (*e.g.* DJA2-stimulated ATPase activity, luciferase refolding activity, and tau protein binding affinity). From this study, we hoped to better understand which biochemical properties of Hsc70 are most directly correlated with its activities on tau in cells. From this understanding, we hoped to be better positioned to select *in vitro* screening assays that could be used to identify potent anti-tau compounds for AD.

5.2 Results

5.2.1 Selection of the Human Hsc70 Mutants

Seven human Hsc70 mutants were selected based on a series of criteria (**Figure 5.1**). Four mutants, F68L, E175S, S208A, and D234A, were selected based on the ATPase and refolding activities of their DnaK homologs (F67L, E171S, S203A, D233A) as indicated in Chapter 4. Briefly, compared to wild-type (WT), DnaK mutant F67L had lower ATPase but normal refolding activity, E171S had lower ATPase and refolding activities, S203A had higher ATPase activity but lower refolding activity, and D233A had both higher ATPase

and refolding activities (**Figure 4.2**). To supplement these mutants, we also selected the D152K mutant because it has been reported to have a high intrinsic ATPase rate but decreased clarthrin uncoating activity [20]. Finally, C17S, and C267S were selected because we found that methylene blue, an Hsp70 inhibitor with anti-tau activity,

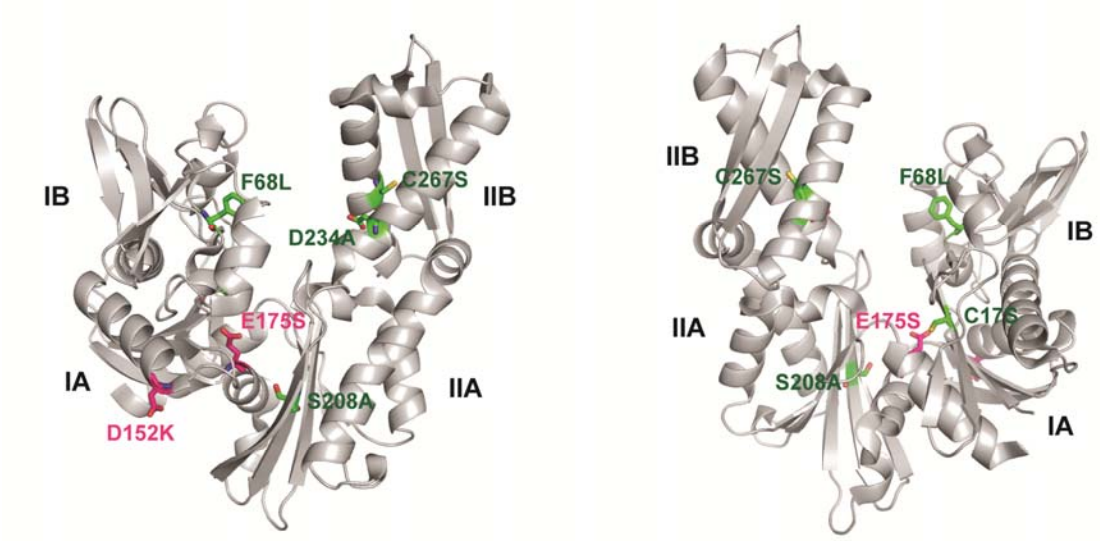

Figure 5.1 Locations of Hsc70 mutants. The structure of human Hsc70 NBD (PDB: 3FZF) is shown, with all subdomains labeled. The two mutants that induce tau degradation is shown in pink while the other five mutants are shown in green.

irreversible oxidizes these residues (Y. Miyata and J. E. Gestwicki, unpublished results). Together, this collection of mutants was intended to explore possible mechanisms of Hsc70-mediated degradation of tau.

5.2.2 Analyzing the Ability of Each Hsc70 Mutant to Trigger Tau Degradation

Wild-type (WT) Hsc70 and its seven mutants were cloned into pCMV6-XL6 vector and

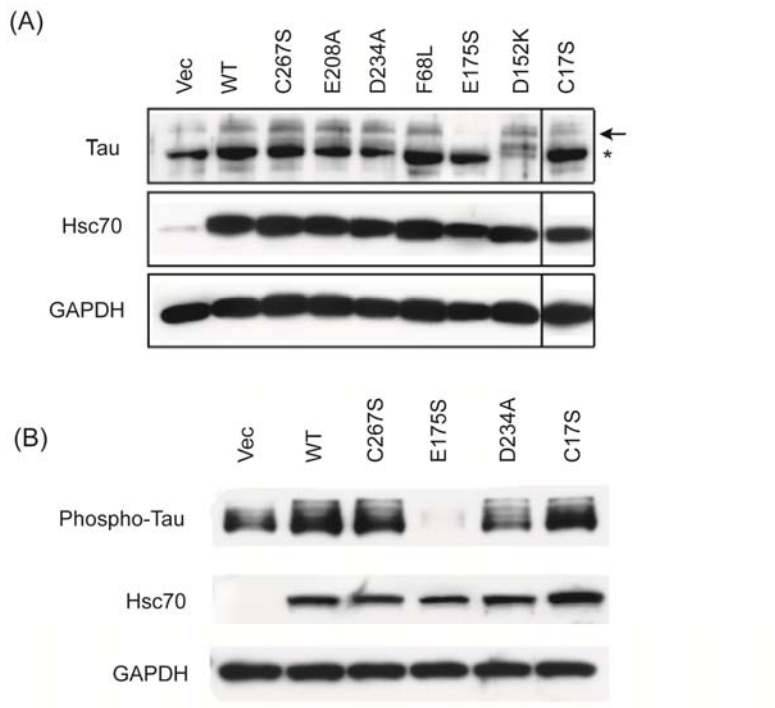

Figure 5.2 Two Hsc70 mutants (E175S and D152K) induced the degradation of tau protein in Hela cells. (A) Overexpressing of E175S induced the degradation of post-translational modified tau (pointed by arrow) while D152K induced the degradation of unmodified tau (*). (B) Overexpressing E175S specifically induced the degradation of phosphorylated tau. In both (A) and (B) the mutants were overexpressed in HeLa cell that constantly expressing tau protein. In (B), antibody that specifically recognized phosphorylated tau was used.

transformed into HeLa cells constitutively over-expressing human P301L tau protein. These studies revealed that over-expression of WT-Hsc70 slightly increased the level of both non-phosphorylated and phosphorylated tau when compared to vector control (**Figure 5.2**). Expression of Hsc70 mutants C17S, F68L, and C267S yielded similar effects as WT, whereas E208A and D234A did not increase tau level as much as WT. Interestingly, D152K induced the degradation of non-phosphorylated tau while E175S specifically triggered the degradation of phosphorylated tau (**Figure 5.2**).

5.2.3 Characterizing the ATPase Activities of the Hsc70 Mutants

Based on these findings, we were interested in understanding the biochemical differences between the tau-reducing mutants (E175S and D152K) and the WT and other mutants. Towards that goal, we purified recombinant Hsc70 and its mutants. The mutants were cloned into the pMCSG7 vector and the corresponding proteins expressed in Rosetta (DE3) cells. The Hsc70s were then purified by Ni-NTA resin, followed by an ATP column. All of the Hsc70s were stable and pure by SDS-PAGE (**Appendix 5.5.1**).

Table 5.1 Summary of the ATPase, refolding, and the substrate binding activities of Hsc70 mutants

Mutant ID	Intrinsic ATPase rate (pmole ATP/μg/min)	DJA2-Stimulated ATPase Activity		Refold Luciferase (Y/N)	Tau Binding (ELISA)		Tau Degradation (Y/N)
		K_m (μM)	V_{max} (pmole ATP/μg/min)		K_d (μM)	Maximal Signal (OD_{450})	
C17S	1.05 ± 0.23	1.08 ± 0.08	23.5 ± 0.5	Y	1.41 ± 0.27	0.67 ± 0.06	N
F68L	1.23 ± 0.24	1.15 ± 0.09	26.7 ± 0.6	Y	2.67 ± 1.26	0.92 ± 0.26	N
D152K	5.64 ± 0.30	0.16 ± 0.03	13.9 ± 0.8	N	0.78 ± 0.25	0.64 ± 0.07	Y
E175S	ND	NF	NF	N	1.86 ± 0.71	0.92 ± 0.18	Y
E208A	9.35 ± 0.29	0.25 ± 0.04	20.6 ± 0.9	Y	5.49 ± 5.48	1.38 ± 1.03	N
D234A	0.62 ± 0.17	0.32 ± 0.03	35.2 ± 0.9	Y	2.43 ± 0.78	0.85 ± 0.16	N
C267S	0.86 ± 0.31	0.23 ± 0.01	18.1 ± 0.3	Y	1.66 ± 0.46	0.77 ± 0.11	N
WT	4.03 ± 0.20	0.76 ± 0.16	6.0 ± 0.4	Y	1.11 ± 0.49	0.56 ± 0.10	N

Using these proteins, we measured their intrinsic ATPase activities. We found that the ATPase rates varied between 0 and ~9 (pmol ATP/μg enzyme/min) and that these values did not correlated with tau degradation (**Table 5.1**). For example, mutants F68L and

C267S had lower intrinsic ATPase activity (1.2 and 0.9 pmole ATP/µg/min, respectively) than WT (4 pmole ATP/µg/min), but their over-expression resulted in same tau level as WT (**Table 5.1**). Furthermore, E175S and D152K, the two mutants that triggered tau degradation had vastly different intrinsic ATPase rates: 0 and 5.6 pmole ATP/µg/min, respectively (**Table 5.1**).

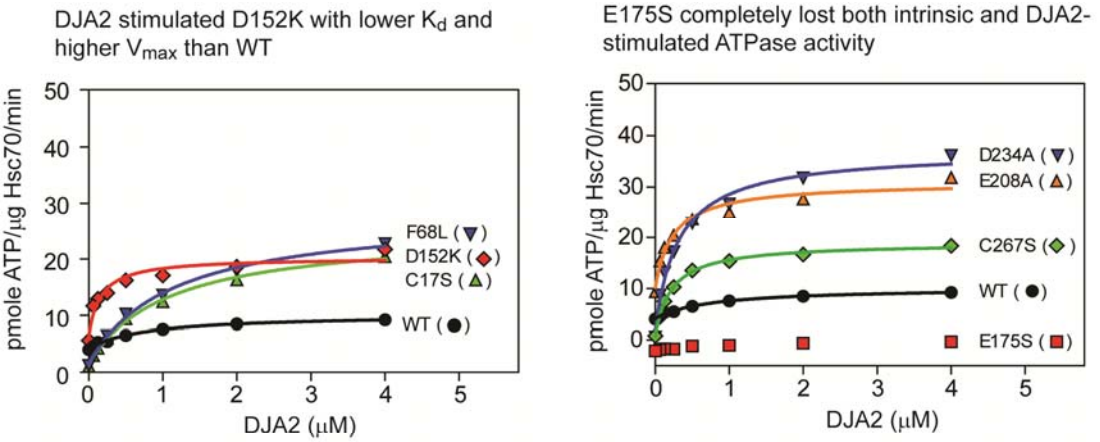

Figure 5.3 The ATPase activities of Hsc70 mutants were not completely predictive of their ability to trigger tau degradation. Two mutants that induced tau degradation behaved differently: DJA2 stimulated D152K with lower K_d and higher V_{max} than WT while E175S completely lost its intrinsic and DJA2-stimulated ATPase activities. In this experiment, 0.6 µM Hsc70 (mutant), 1 mM ATP, and 1 mM DTT was added to the reaction. Each data point is the average of triplicate and the error bar represents standard error of the mean.

Next, we measured the ability of the Hsc70 mutants to be stimulated by DJA2, a human J protein, using the ATPase assay. Interestingly, all of the mutants except E175S had higher V_{max} than WT whereas E175S could not be stimulated by DJA2 (**Table 5.1**, **Figure 5.3, and Appendix 5.5.2**). D152K was stimulated by DJA2 with lower K_d (0.2 µM) and higher V_{max}

than WT (14 and 6 pmole ATP/μg/min, respectively). The lower K_d value was not correlated with tau degradation, because three other mutants, E208A, D234A, and C267S, also had lower K_d (0.3, 0.3, and 0.2 μM, respectively), but had similar tau level as WT when overexpressed. In summary, we observed no obvious correlations between the relative ATPase activities of Hsc70 mutants and their abilities to induce tau degradation.

5.2.4 Characterizing the Luciferase Refolding Activities of the Hsc70 Mutants

In Chapter 4, we found that the luciferase refolding activities of DnaK mutants were more predictive of their *in vivo* heat shock rescue activity. Therefore, we hypothesized that the luciferase refolding activities of Hsc70 mutants might be more predictive of their abilities to trigger tau degradation. First, the refolding assay was optimized (**Appendix 5.5.3**) by measuring the time dependent refolding activity of WT-Hsc70 at the presence of DJA2 (1 μM Hsc70 and 0.25 μM DJA2) with different substrate concentrations. For all three luciferase concentrations we used, the refolding rate remained constant up to ~ 30 minutes, but the refolding yield reached a plateau after 40 minutes. Based on this result, we decided to use 100 nM denatured luciferase as substrate and measured the endpoint of refolding yield after 20 minutes incubation at 37 °C. Next, we measured the dose dependent stimulation effect of DJA2 against the

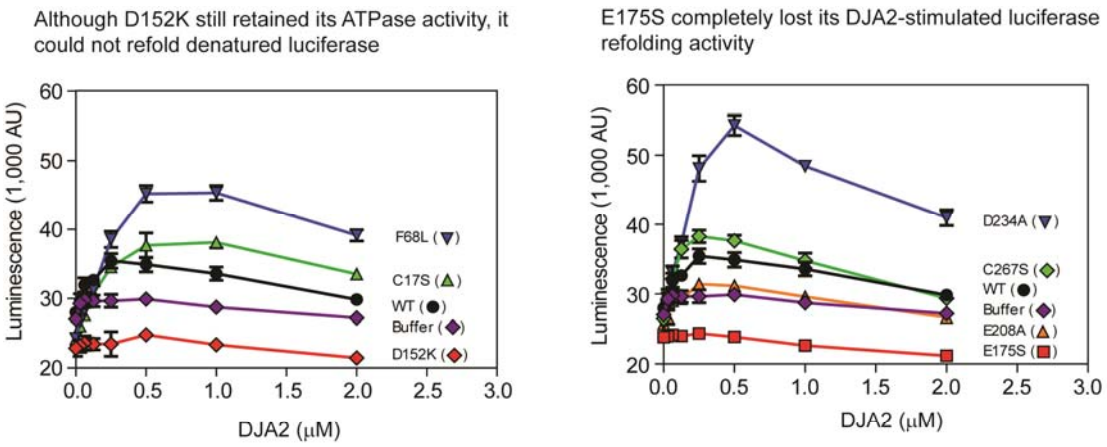

Figure 5.4 Both Hsc70 mutants that trigger tau degradation (D152K and E175S) lost their luciferase refolding activities. Although D152K has high intrinsic and DJA2-stimulated ATPase activity, it lost the ability to refold denatured luciferase. E175S mutant lost both its ATPase and refolding activities. The luciferase refolding assay appears to be more predictive of the tau degradation efficacy of Hsc70 mutants. In this experiment, 1 μM Hsc70, 1 mM ATP, and 100 nM of 6 M GuHCl denatured luciferase was added to the reaction mix. The incubation temperature was 37°C. Each data point is the average of triplicate and the error bar represents standard error of the mean.

luciferase refolding activities of Hsc70 mutants. The refolding activity of WT-Hsc70 was stimulated by DJA2 with patterns similar to prokaryotic DnaK-DnaJ system: DJA2 stimulated refolding at lower concentration, reached its optimal concentration at 1:4 (DJA2:Hsc70) ratio, and then started to inhibited refolding at higher concentration (**Figure 5.4**). Strikingly, we found that both of the mutants that triggered tau degradation, D152K and E175S, completely lost their luciferase refolding activity (**Figure 5.4**). On the other hand, F68L and D234A both had higher refolding activity than WT but no effect on tau levels (**Figure 5.2** and **Figure 5.4**). These results supported our hypothesis that the luciferase refolding activity of Hsc70 mutants is more predictive than ATPase activity for effects on tau degradation. However, higher luciferase refolding activities of mutants

were not correlated with any significant changes in tau level when overexpressed in cultured cells.

5.2.5 Characterize the Substrate Binding Activities of the Hsc70 Mutants

The current model of Hsc70-mediated tau degradation is that Hsc70 binds to tau and induces ubiquitination and degradation by recruiting the E3 ubiquitin ligase CHIP via its C-terminal EEVD domain [21, 22]. We expected this process to be influenced by the affinity of Hsc70 for its substrates and the "dwell time" of the substrate-Hsc70 complex. Thus, we hypothesized that the mutants that triggered tau degradation might have higher affinity to tau under equilibrium condition. To test this hypothesis, we immobilized Hsc70 mutants on a 96-well plate and measured their apparent K_d to tau by ELISA. Surprisingly, all mutants bound to tau with similar K_d and maximal signal to WT (Apparent K_d = 1.1 μM, $Signal_{max}$= 0.6) (**Table 5.1** and **Figure 5.5**). Although D152K had slightly lower K_d than WT (Apparent K_d = 0.8 μM), the difference was not significant (**Table 5.1** and **Figure 5.5**). This result suggests that there was no obvious correlation between the equilibrium tau binding affinities of Hsc70 mutants and their abilities to trigger tau degradation.

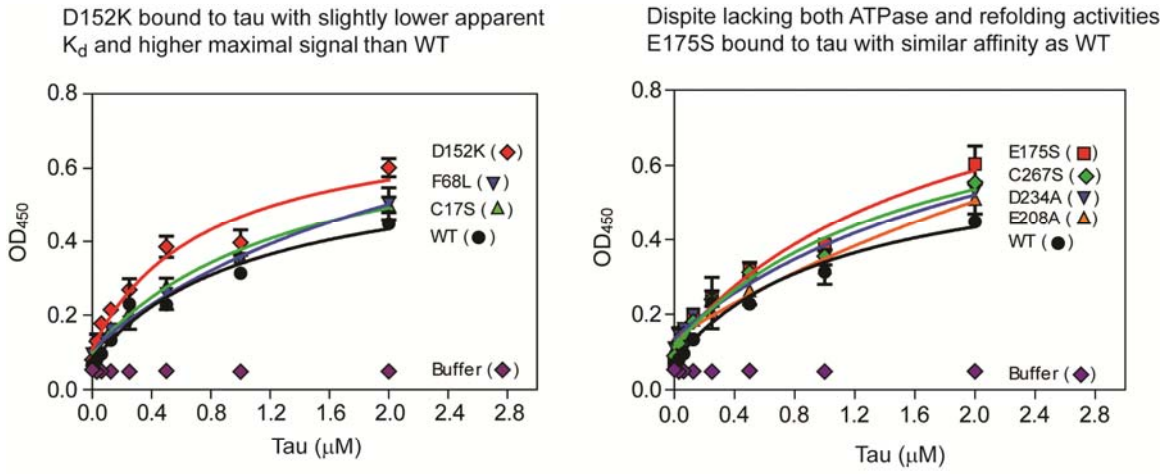

Figure 5.5 All Hsc70 mutants bound to tau protein with similar apparent K_d. The binding affinity of Hsc70 mutants to tau was measured by an ELISA-based assay. D152K bound to tau with slightly lower K_d while E175S binds to tau with similar affinity as WT. This result suggests that ELISA-based assay cannot be used to predict the tau degradation effects of Hsc70 mutants. Each data point is the average of triplicate and the error bar represents standard error of the mean.

5.2.6 Characterize the Partial Proteolysis Patterns of Hsc70 Mutants

Previously, we found that Hsc70s ATPase inhibitors such as methylene blue and myricetin induce the degradation of tau [19]. The inhibited ATPase activity suggests that the compound might “freeze” Hsc70 in certain conformation in the ATPase cycle that is important for tau degradation. Therefore, we hypothesized that the conformation of Hsc70 mutants under certain conditions might correlate with their abilities to trigger tau degradation. Although we did not have ready access to single molecule-based techniques to visualize the conformation of Hsc70 mutant, partial proteolysis provided a simple way to analyze their structure under equilibrium condition. First, we optimized the partial proteolysis assay for wild-type Hsc70 by pre-incubating the Hsc70 with ADP, ATP, ATP+NRLLLTG peptide ([23]; NR peptide), or ATP+J domain (DnaJ residue 2-108), and

then added trypsin and observed the time dependent changes in their partial proteolysis patterns (**Appendix 5.5.4**). We found that the most noticeable difference between different nucleotide states was the bands around 64 kDa: there were two bands at ADP-bound state and three bands at ATP-bound state. Interestingly, unlike its DnaK homolog, adding NR peptide and J domain to ATP-bound Hsc70 did not switched it from "ATP-bound" to "ADP-bound" form (**Appendix 5.5.4**). Next, we analyzed the partial proteolysis patterns of all Hsc70 mutants. Interestingly, D152A mutant constantly assumed ADP-bound conformation (two bands around 64 KDa) independent of all additives (**Figure 5.6**). On the other hand, the E175S mutant had normal ADP-like pattern when ADP was added; however, when ATP was added, it had two strong lower bands like ADP-bound form, but with very faint third upper band. Adding NR peptide or J domain to E175S-ATP did not change the pattern (**Figure 5.6**). The other five mutants (C17S, F68L, E208A, D234A, and C267S) had similar patterns as WT when ADP, ATP, or ATP+NR peptide was added (**Figure 5.6**). However, unlike WT, adding ATP and J domain to the five mutants switched them into ADP-bound form (**Figure 5.6**). In summary, both mutants that triggered tau degradation preferred to assume ADP-bound form even with excess ATP, and this result suggests a possible correlation between Hsc70 conformation and their ability to trigger tau degradation.

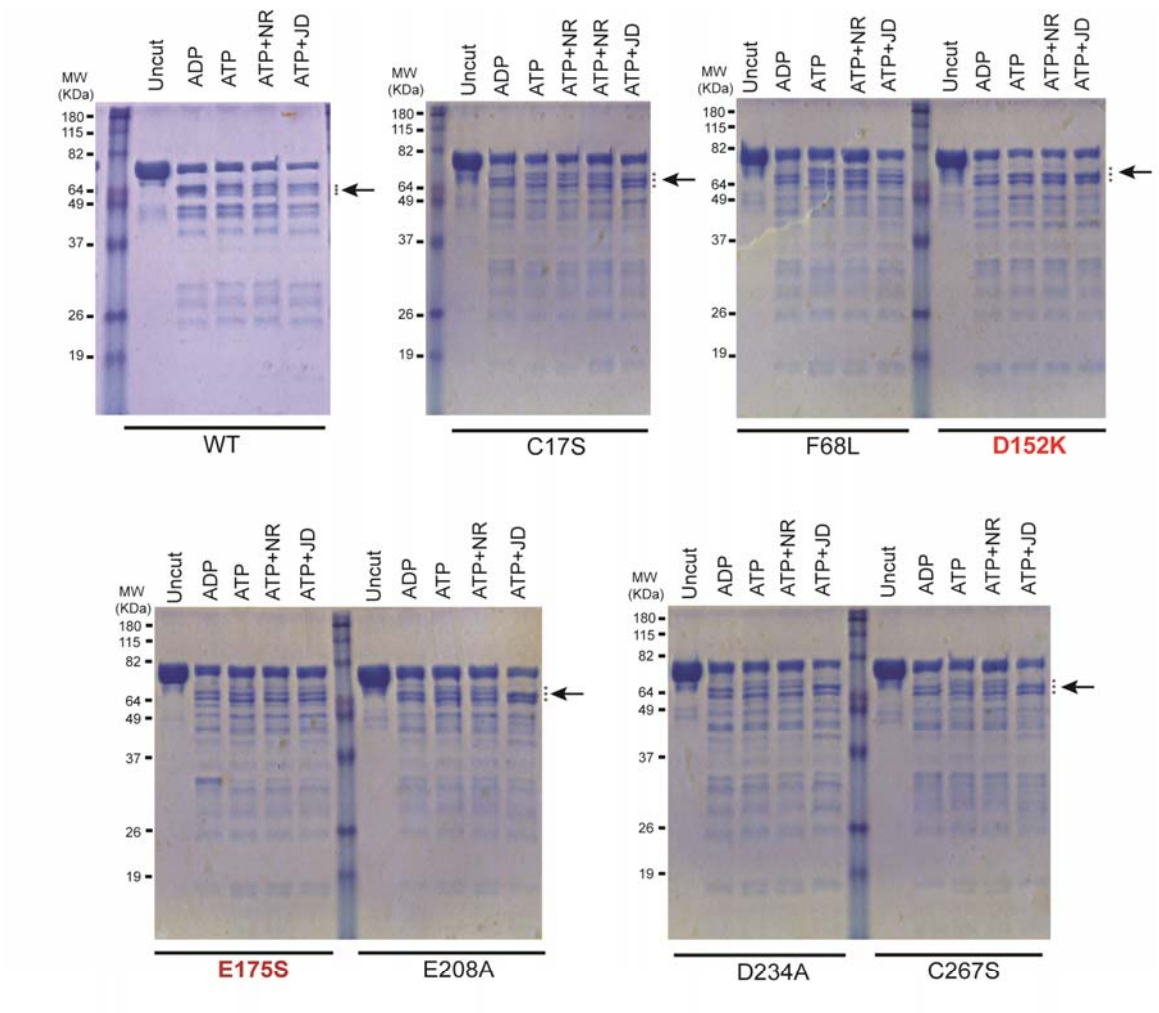

Figure 5.6 Partial proteolysis patterns of Hsc70 mutants. Similar to WT, most Hsc70 mutants also shown distinct parital digestion patterns between ADP and ATP-bound forms, especially for the bands around 64 kDa (marked by *). Interestingly, both mutants that triggered tau degradation, D152K and E175S, assumed ADP-like conformation even with excess ATP. Additionally, we found that except for D152K and E175S, adding J domain to other ATP-bound Hsc70 mutants switched them to ADP-bound (closed) state, which correlated well with their higher V_{max} for DJA2-stimulated ATPase activities

5.3 Discussion

In this study, we selected seven human Hsc70 mutants and analyzed the correlations between their effects on cellular tau level and their *in vitro* biochemical activities. We identified two mutants, D152K and E175S, that induced tau degradation. Through a

series of biochemical assays, we found that luciferase refolding activities and partial proteolysis patterns of Hsc70 mutants were more predictive of their abilities to cause tau degradation. Namely, among all mutants, only D152K and E175S lost their refolding activity and preferred to assume an ADP-bound structure even with excess ATP. Our results suggest that new primary or secondary screening assays for compounds that inhibit Hsc70 refolding activity or shift its structure to ADP-bound form would help us discover more compounds that trigger tau degradation through Hsp70.

5.3.1 Potential Mechanisms by Which Hsc70 Point Mutants Trigger Tau Degradation

When overexpressing WT-Hsc70 in cultured cells, it increased the level of both phosphorylated and non-phosphorylated tau. This effect is anticipated because Hsc70 is important for cycling tau on microtubules and protecting it from aggregation [14, 17, 18]. However, over-expressing D152K or E175S mutants of Hsc70 triggered the degradation of non-phosphorylated or phosphorylated tau, respectively. In addition to its roles in protecting tau from aggregation and degradation, Hsc70 has been shown to play a role in proteasomal degradation and turnover of tau [16, 18, 19]. Thus, it seems that the Hsc70 mutants shift the “retain” vs “degrade” signal towards degradation. Why might this occur? One potential insight comes from our observations that the tau-reducing

mutants, D152K and E175S, were in the ADP-bound, “lid-closed” form even with excess ATP. These results suggest that tight binding of Hsc70 to substrate in a “lid-closed”, ADP-bound conformation might be a trigger for degradation of tau.

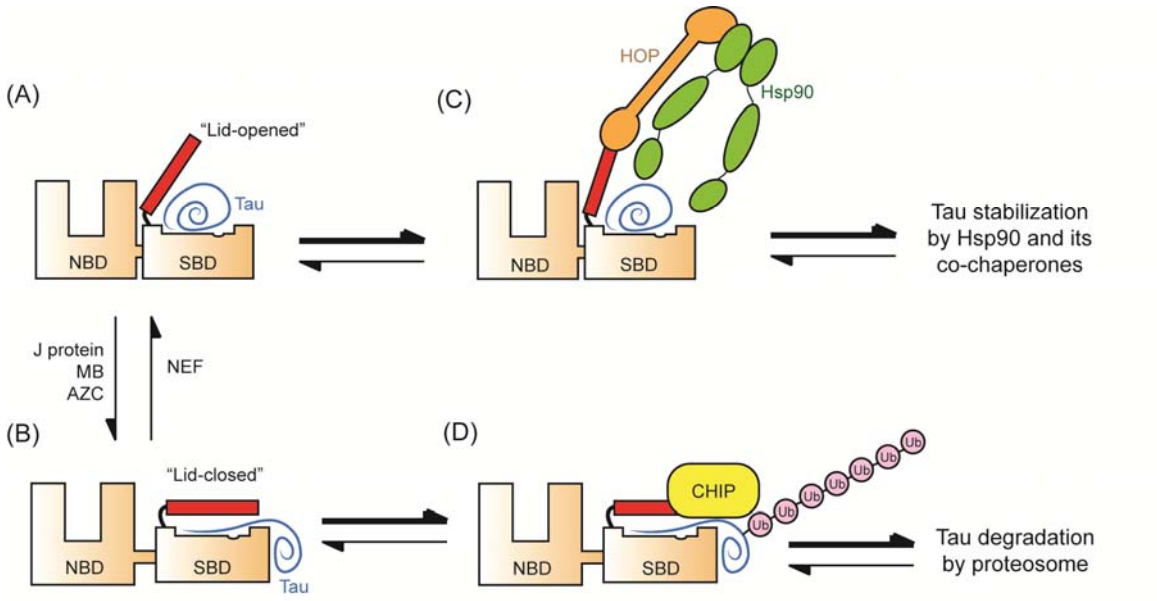

Figure 5.7 Model for tau processing by Hsc70 chaperone system. (A) and (B) In this proposed model, Hsc70 that binds to tau protein exists in an ensemble of “lid-opened” and “lid-closed” conformations. The addition of J protein or Hsc70 ATPase inhibitors such as methylene blue (MB) and Azure C (AZC) might shift the ensemble to the “closed” conformation while adding nucleotide exchange factor (NEF) might shift it to relative “opened” conformation. (C) The “lid-opened” conformation of Hsc70 might increase the affinity of Hsp70/Hsp90 organizing protein (HOP) to the EEVD tail of Hsc70, and thereby favor the transfering of tau protein to Hsp90. This route leads to the stabilization and accumulation of tau protein. (D) Alternatively, the “lid-closed” conformation might favor the binding of CHIP, an E3 ubiquitin ligase, to the C-terminal EEVD domain of Hsc70 and thereby leads to the ubiquitination and degradation of tau protein.

Based on this model, it is interesting to speculate about the molecular mechanisms linking the ADP-bound form to ubiquitination and degradation. The lid of the Hsc70 SBD contains the C-terminal EEVD motif that interacts with TPR-domain containing cochaperones, such as HOP and CHIP [21, 23, 24]. Thus, it is possible that, when the lid is open, it has higher affinity for the pro-folding co-chaperone HOP and thereby favors

transfer of substrates to Hsp90 for further folding [25] (**Figure 5.7**). Conversely, with the lid is closed, as would be expected in the ADP-bound state, Hsc70 might instead attract the binding of the E3 ubiquitin ligase CHIP and thereby induces the ubiquitination and degradation of the bound substrate [16] (**Figure 5.7**). However, this model is speculative and future work will be needed to clarify the mechanism. Regardless of the exact mechanism, this study provided useful insights into the triage of tau in the Hsc70 complex.

5.3.2 In Search of the Best Screening Assays for Compounds that Trigger the Degradation of Tau

As mentioned above and in Chapter 1, our previous reports suggested that reducing tau level in the brain using Hsp70s ATPase inhibitor rescues cognition defects in models of tauopathy [26]. We identified these compounds using the ATPase assays described in Chapters 2 and 3. Yet, in Chapter 4, we uncovered that the relationship between ATPase activity and downstream chaperone activities is complex. Therefore, if we depended entirely on ATPase activity for compound discovery, we might overlook molecules that modulate the chaperone activities of Hsp70s in other, important ways. Thus, in retrospect, we were fortunate to have identified compounds in the ATPases assays that

reduce tau levels in cells and animals [18, 19, 26]. A major goal of this Chapter was to formalize this process and, hopefully, reveal screening platforms that would more faithfully uncover compounds that work through Hsc70 to reduce tau levels.

In these studies, we found that the relative ability of each assay to predict mutants that triggered tau degradation was roughly as following: luciferase refolding (2/2 mutants) > ATPase (1/2 mutants) > tau-binding (0/2 mutants). Notably, only D152K and E175S lacked luciferase-refolding activity, suggesting that this assay is the most predictive of effects on tau. This result is somewhat reminiscent of the findings in Chapter 4 in which refolding activity was best correlated with recovery from heat shock. Why is this assay predictive of cellular chaperone functions? We suspect that the refolding assays allows measurement of multiple chaperone simultaneously because the refolding of a denatured substrate will likely require holdase and foldase activities, collaboration with cochaperones, and proper cycling between different conformations.

Together, the work in this thesis points to the potential of luciferase refolding assays. However, miniaturization and throughput of this platform has proven challenging in our group (S. Wisen, L. Chang and J. E. Gestwicki unpublished results). The technical reasons

for this are likely because most chemical compounds interfere with spontaneous refolding by interacting with exposed hydrophobic regions. Moreover, we have found that the enzymatic activity of luciferase is sensitive to inhibition by many compounds (L. Chang and J. E. Gestwicki unpublished results). Although these limitations currently render luciferase refolding assays unsuitable for HTS, we propose that other assays which measure global “chaperone activities”, such as substrate degradation assay (see chapter 6), might help identify compounds that trigger the degradation of tau.

5.4 Experimental Procedures

5.4.1 Plasmid and protein purification

WT-Hsc70, All Hsc70 mutants, and DJA2 were cloned into the pMCSG7 plasmid (Midwest Center for Structural Genomics, Bethesda, MD) by ligation independent cloning as previously described in Chapter 4 and the correct vector was transformed into Rosetta (DE3) cells for expression. To express Hsc70 mutant, 25 mL of overnight (37 °C) LB culture of Rosetta (DE3) culture was poured into 1 L of Terrific Broth. After 3 hours incubation at 37 °C, the culture was cooled down to 28 ^{o}C for 2 hours before overnigh induction of expression with 200 μM IPTG overnight, and the cell pellet was stored at -80 °C until use. The WT and Hsc70 mutants were purified using same procedures as

described except the addition of the EDTA-free protease inhibitor cocktail (Roche) (1/4 tablet for each sample) in the lysis buffer and the omitting of final Ni-NTA resin clean-up step for Hsc70 mutants. For large-scale expression of DJA2, a single colony of Rosetta (DE3) culture was inoculated into 5 mL LB. After 6 hours of incubation at 37 °C, the 5 mL starter culture was poured into 1 L Terrific Broth and the larger culture was incubated at 37 °C until OD_{600} reached 0.4 - 0.6. Next, DJA2 expression was induced by 500 μM IPTG under 18 °C for ~15 hours with shaking and the cell pellet was stored in -80 °C until use. DJA2 was purified by Ni-NTA His•Bind® Resin (Novagen, Darmstadt, Germany) as following. The DJA2 cell pellet was resuspended in His-binding buffer (25 mM Tris, 600 mM KCl, 5 mM imidazole, pH 8.5) supplement with protease inhibitor cocktail (1 tablet per liter of original culture) and the bacterial cells were lysed by sonication (3.5 minutes, 30 sec on/off cycle, 63%). The cell debris was removed by centrifugation at 20,000 rpm for 45 mins. The supernatant was incubated with Ni-NTA resin for 2 hours at 4 °C. To remove the contaminated ATPase activity in the DJA2 sample, the His-DJA2-bound Ni-NTA resin was washed extensively by 100 mL of His-binding buffer, 150 mL 25 mM Tris buffer (40 mM Imidazole, 300 mM KCl, 3% ethanol, pH 8.0), and finally with 500 mL 25 mM Tris buffer (30 mM imidazole, 100 mM KCl, 3% ethanol, pH 8.0). The DJA2 protein was eluted by His-elution buffer (50 mM Tris, 300 mM Imidazole, 150 mM KCl, pH = 8.0)

and the DJA2 protein was concentrated, exchanged into 25 mM HEPES buffer (150 mM KCl, 5 mM $MgCl_2$, pH 7.5) and stored at -80 °C until use.

5.4.2 ATPase Activity

The ATPase activity of Hsc70 (mutant) was measured as described in chapter 4 (see **4.4.4**).

5.4.3 Luciferase Refolding

The DJA2 stimulated refolding activity was characterized as following. Briefly, 54.4 µM luciferase denatured in 6 M GuHCl was first diluted into 5 µM by 100 mM Tris buffer (20 mM KCl, and 6 mM MgCl2, pH 7.4) before added into 34.3 mM HEPES buffer (300 mM potassium acetate, 3 mM magnesium acetate, 5.4 mM DTT, 21.9 mM creatine phosphate, 94.5 units/ml creatine kinase, and 0.84 mg/mL BSA, pH 7.6) containing Hsc70. Next, 10 µL of this enzyme-luciferase mix was added into each well of a 96-well plate, followed by the addition of 5 µL of 1:2 serial diluted DJA2 (in 100 mM Tris buffer, 20 mM KCl, and 6 mM MgCl2, pH 7.4). Finally, 10 µL of 2.5 mM ATP dissolved in ddH_2O was used to start the reaction. The reaction was quenched after 20 minutes incubation at 37 °C by adding 25 µL 4% (v/v) SteadyGlo reagent (as described in chapter 4). The

luminescence was measured immediately by SpectraMax M5 (Molecular Devices, Sunnyvale CA).

5.4.4 ELISA-based Tau Binding Assay

The ELISA-based binding assay was optimized from a previous protocol [27]. The assays were carried out on transparent 96-well plates. First, the Hsc70 (mutant) was immobilized onto the wells by adding 50 µL 0.1 mg/mL of Hsc70 (in 50 mM MES buffer, pH 5.2) to each well and incubate for ~ 14 hours at 37 °C. The unbound protein was washed away by TBS-T (0.05% Tween 20). Between all the binding steps were washing steps. In all the washing steps, 150 µL TBS-T was added to each well, after 3 minutes incubation on rocker, the buffer was discarded (repeat three times). After washing, 50 µL of 25 mM HEPES buffer (40 mM KCl, 8 mM MgCl2, 100 mM NaCl, and 0.01% Tween 20) containing Tau and ATP (1 mM) was added to each well, and discarded after a ~14-hour incubation at room temperature (RT) on rocker. The plate was blocked by 100 µL 5% milk in TBS-T for 5 minutes, and the bound tau protein was detected by adding rabbit anti-tau antibody (Tau H-150, Santa Cruz), followed by HRP conjugated goat anti-rabbit Ab antibody (50 µL, 1:5000 for both antibodies, diluted in TBS-T, and incubate at RT for 1 hour). After washing, 50 µL of TMB substrate (Invitrogen) was added to each well,

incubated for 6.5 minutes in dark, and then 50 µL of 1 M HCl was added to quench the color change. The resulted OD_{450} value was read by SpectraMax M5 spectrometer.

5.4.5 Partial Proteolysis

The partial proteolysis protocol was adapted from a previously described method . Briefly, we prepared 15 µL samples of 8 µM Hsc70 in 40 mM HEPES buffer (20 mM NaCl, 8 mM $MgCl_2$, 20 mM KCl, 0.3 mM EDTA, pH 8.0) with 1.33 mM nucleotide (ADP or ATP). Additives such as J-domain (residues 2-108, 5.3 µM) or NRLLLTG peptide (133 µM) are noted when included. Samples were pre-incubated at room temperature for 30 minutes. Next, 5 µL of 4 µM trypsin (SIGMA Ec 3.4.2.1.4) was added to bring the final volume to 20 µl. The final concentration of Hsc70 (mutant) was 6 µM, ADP/ATP was 1 mM, J domain was 4 µM, NRLLLTG peptide was 100 µM, and trypsin was 1 µM. Proteolysis was carried out at room temperature for 30 minutes, unless otherwise noted. The reaction was quenched with the addition of 10 µl of SDS loading buffer (240 mM Tris, 6% (w/v) SDS, 30% (v/v) glycerol, and 16% (v/v) β-mercaptoethanol, 0.6 mg/ml bromophenol blue, pH 6.8) and heated to 95 °C for 5 minutes. Samples were analyzed using a 12% SDS-PAGE electrophoresis gel and stained with Coomassie blue.

Notes

Lyra Chang and Jason E. Gestwicki designed the experiments. Lyra Chang conducted the experiments. Ying Jin in Chad Dickey's lab generated the Hsc70 mutant constructs in pCMV6-XL6 vector and Umesh K. Jinwal helped to test the effects of Hsc70 mutants had on tau degradation in cultured cells. Andrea Thompson and Anthony Emanuele optimized the ELISA-based tau binding assay against Hsc70.

5.5 Appendix

5.5.1 Analyzing Purified Hsc70 Mutants by SDS-PAGE and Native Gel

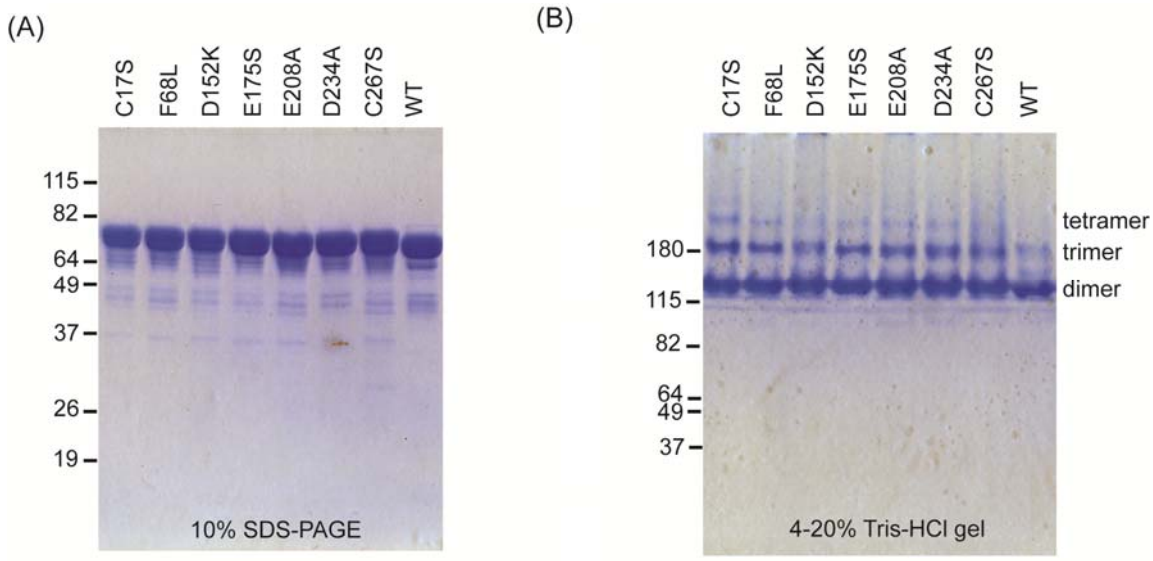

Appendix 5.5.1 Analyzing purified Hsc70 mutants by SDS-PAGE and native gel. In both (A) and (B), 10 μL sample was loaded into each well, and the final concentration of Hsc70 (mutant) was 4 μM after adding loading dye. 100 mM Tris buffer (20 mM KCl, and 6 mM $MgCl_2$, pH 7.4) was used to dilute sample in both (A) and (B). In (B), Hsc70 was pre-incubated with 1 mM DTT and 1 mM of ATP for 30 minutes before adding 1/2 volume of 3 x loading dye. The native gel was run in Tris-acetate buffer at 120 V for 6 hours (4°C). WT and Hsc70 mutants mainly formed dimer under the running condition while trimers and tetramers were also observed.

5.5.2 The Stimulation Effect of DJA2, Tau Peptide, and NR peptide against the ATPase Activity of Hsc70 Mutants in the absence of DTT

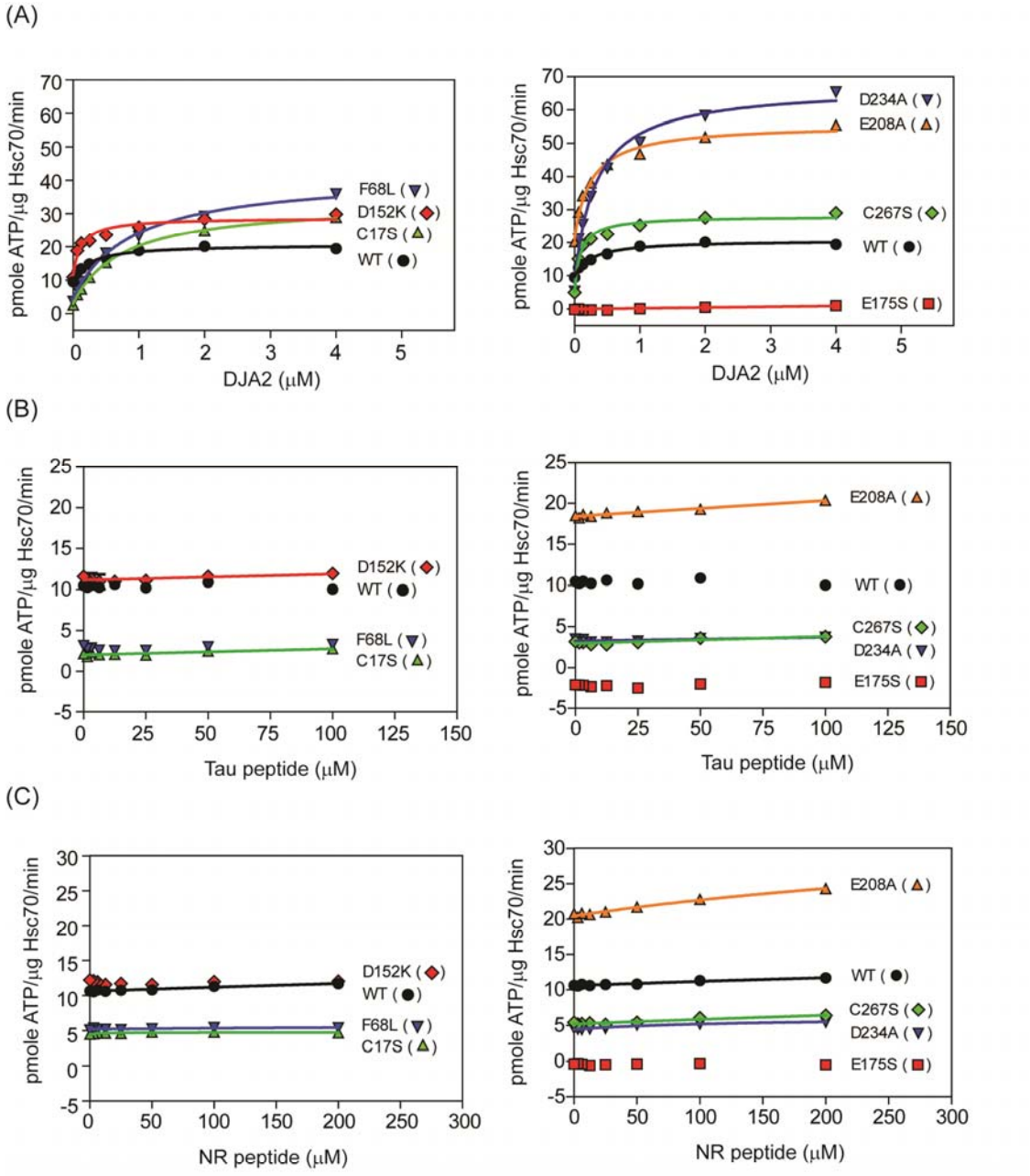

Appendix 5.5.2 The stimulation effect of DJA2, Tau peptide, and NR peptide against the ATPase activity of Hsc70 mutants in the absence of DTT. (A) DJA2 stimulated Hsc70 mutants with the same relative level as in the sample containing 1 mM DTT (see Figure 5.3). However, the overall ATPase rate is higher in the absence of 1 mM DTT. (B) and (C) Tau peptide and NR peptide did not stimulate the ATPase activities of Hsc70 mutants. In this experiment, 0.6 μM Hsc70 and 1 mM ATP was added to the reaction. Each data point is the average of triplicate and the error bar represents standard error of the mean.

5.5.3 The Time Courses of Hsc70-DJA2 Dependent Refolding of Denatured Luciferase

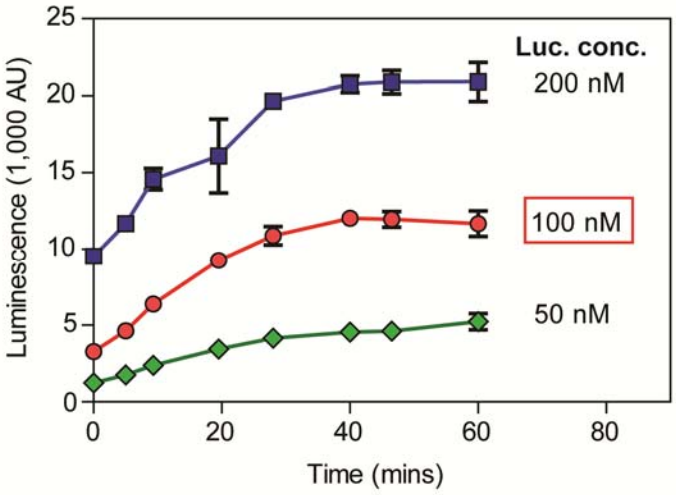

Appendix 5.5.3 The time course of Hsc70-DJA2 dependent refolding of denatured luciferase. In all three luciferase concentrations we tested, the refolding rate remain constant within ~30 mins but reach an abrupt stop after ~40 mins with no further increase in refolded luciferase observed. Based on this data, we decided to measure the refolding activity of Hsc70 mutants after 20 mins incubation at 37°C (endpoint measurement) and select 100 nM of denatured luciferase as substrate concentration for further study. In this experiment, 1 μM WT Hsc70, 0.25 μM DJA2, 1 mM ATP was added to the reaction mix. The incubation temperature was 37°C. Each data point is the average of triplicate and the error bar represents standard error of the mean.

5.5.4 Optimizing the Partial Proteolysis Conditions for WT-Hsc70

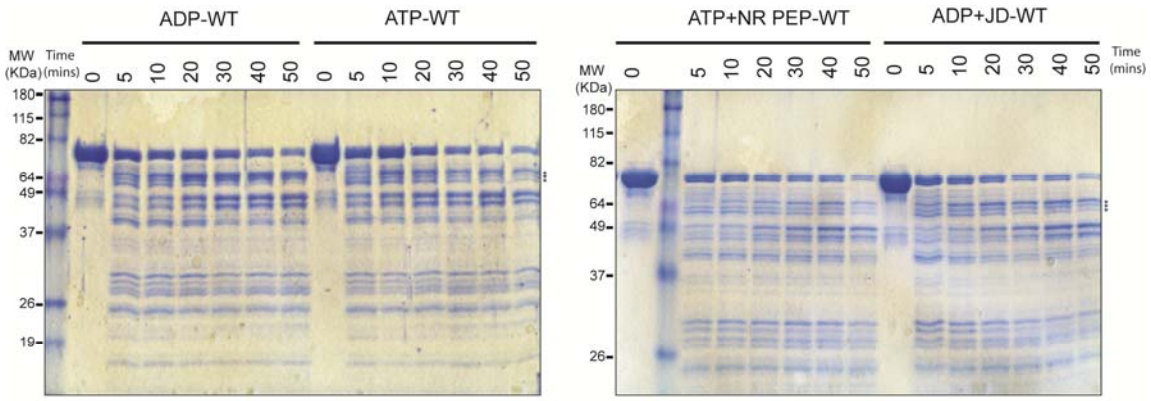

Figure 5.5.4 Optimizing the partial proteolysis condition for WT-Hsc70. In this experiment, ATP, ADP, model NR peptide substrate or J domain protein were added to purified Hsc70. After > 30 mins incubation, trypsin was added to start the partial digestion of Hsc70, and the reaction was quenched at time points indicated by adding SDS-PAGE loading dye followed by heat denaturation. We found that Hsc70 has distinct pattern of partial proteolysis at different nucleotide state, and the differences were most obvious around 64 KDa (marked by *). ADP-bound form had two bands (not seperated well on this gel) around 64 kDa while ATP-bound form has three bands. Interestingly, unlike the E. coli DnaK homolog, adding peptide susbstrate or J domain did not shilft the conformations of Hsc70 from ATP to ADP-bound form. This suggests that WT-Hsc70 favor "opened" conformation even at the presence of substrate and J domain. Based on this result, we decided to quench the partial digestion reactions in our future experiments after 30 mins incubation at room temperature.

5.6 References

1. *2011 Alzheimer's disease facts and figures.* Alzheimers Dement, 2011. **7**(2): p. 208-44.
2. Ittner, L.M. and J. Gotz, *Amyloid-beta and tau--a toxic pas de deux in Alzheimer's disease.* Nat Rev Neurosci, 2011. **12**(2): p. 65-72.
3. Braak, H. and E. Braak, *Neuropathological stageing of Alzheimer-related changes.* Acta Neuropathol, 1991. **82**(4): p. 239-59.
4. Mukaetova-Ladinska, E.B., et al., *Staging of cytoskeletal and beta-amyloid changes in human isocortex reveals biphasic synaptic protein response during progression of Alzheimer's disease.* Am J Pathol, 2000. **157**(2): p. 623-36.
5. Roberson, E.D., et al., *Reducing endogenous tau ameliorates amyloid beta-induced deficits in an Alzheimer's disease mouse model.* Science, 2007. **316**(5825): p. 750-4.
6. Lee, G., R.L. Neve, and K.S. Kosik, *The microtubule binding domain of tau protein.* Neuron, 1989. **2**(6): p. 1615-24.
7. Drechsel, D.N., et al., *Modulation of the dynamic instability of tubulin assembly by the microtubule-associated protein tau.* Mol Biol Cell, 1992. **3**(10): p. 1141-54.
8. Goedert, M., et al., *Tau proteins of Alzheimer paired helical filaments: abnormal phosphorylation of all six brain isoforms.* Neuron, 1992. **8**(1): p. 159-68.
9. Lee, G., N. Cowan, and M. Kirschner, *The primary structure and heterogeneity of tau protein from mouse brain.* Science, 1988. **239**(4837): p. 285-8.
10. Himmler, A., et al., *Tau consists of a set of proteins with repeated C-terminal microtubule-binding domains and variable N-terminal domains.* Mol Cell Biol, 1989. **9**(4): p. 1381-8.
11. Stoothoff, W.H. and G.V. Johnson, *Tau phosphorylation: physiological and pathological consequences.* Biochim Biophys Acta, 2005. **1739**(2-3): p. 280-97.
12. Bramblett, G.T., et al., *Abnormal tau phosphorylation at Ser396 in Alzheimer's disease recapitulates development and contributes to reduced microtubule binding.* Neuron, 1993. **10**(6): p. 1089-99.
13. Ballatore, C., V.M. Lee, and J.Q. Trojanowski, *Tau-mediated neurodegeneration in Alzheimer's disease and related disorders.* Nat Rev Neurosci, 2007. **8**(9): p. 663-72.
14. Sarkar, M., J. Kuret, and G. Lee, *Two motifs within the tau microtubule-binding domain mediate its association with the hsc70 molecular chaperone.* J Neurosci Res, 2008. **86**(12): p. 2763-73.
15. Giannetti, A.M., et al., *Fibers of tau fragments, but not full length tau, exhibit a cross*

beta-structure: implications for the formation of paired helical filaments. Protein Sci, 2000. **9**(12): p. 2427-35.

16. Petrucelli, L., et al., *CHIP and Hsp70 regulate tau ubiquitination, degradation and aggregation.* Hum Mol Genet, 2004. **13**(7): p. 703-14.
17. Dou, F., et al., *Chaperones increase association of tau protein with microtubules.* Proc Natl Acad Sci U S A, 2003. **100**(2): p. 721-6.
18. Jinwal, U.K., et al., *Hsc70 rapidly engages tau after microtubule destabilization.* J Biol Chem, 2010. **285**(22): p. 16798-805.
19. Jinwal, U.K., et al., *Chemical manipulation of hsp70 ATPase activity regulates tau stability.* J Neurosci, 2009. **29**(39): p. 12079-88.
20. Jiang, J., et al., *Structural basis of interdomain communication in the Hsc70 chaperone.* Mol Cell, 2005. **20**(4): p. 513-24.
21. Zhang, M., et al., *Chaperoned ubiquitylation--crystal structures of the CHIP U box E3 ubiquitin ligase and a CHIP-Ubc13-Uev1a complex.* Mol Cell, 2005. **20**(4): p. 525-38.
22. Graf, C., et al., *Insights into the conformational dynamics of the E3 ubiquitin ligase CHIP in complex with chaperones and E2 enzymes.* Biochemistry, 2010. **49**(10): p. 2121-9.
23. Stevens, S.Y., et al., *The solution structure of the bacterial HSP70 chaperone protein domain DnaK(393-507) in complex with the peptide NRLLLTG.* Protein Sci, 2003. **12**(11): p. 2588-96.
24. Scheufler, C., et al., *Structure of TPR domain-peptide complexes: critical elements in the assembly of the Hsp70-Hsp90 multichaperone machine.* Cell, 2000. **101**(2): p. 199-210.
25. Chen, S. and D.F. Smith, *Hop as an adaptor in the heat shock protein 70 (Hsp70) and hsp90 chaperone machinery.* J Biol Chem, 1998. **273**(52): p. 35194-200.
26. O'Leary, J.C., 3rd, et al., *Phenothiazine-mediated rescue of cognition in tau transgenic mice requires neuroprotection and reduced soluble tau burden.* Mol Neurodegener, 2010. **5**: p. 45.
27. Wawrzynow, A. and M. Zylicz, *Divergent effects of ATP on the binding of the DnaK and DnaJ chaperones to each other, or to their various native and denatured protein substrates.* J Biol Chem, 1995. **270**(33): p. 19300-6.

Chapter 6

Applying the 96-well Based Malachite Green Assay to Screen Compounds against GroEL and GroES Chaperone System

6.1 Abstract

In Chapter 2, we developed a 96-well based high throughput screening (HTS) assay against the Hsp70 ATPase activity. In this Chapter, we explored the generality of this method and found that it could be easily adapted to screen against GroEL-GroES (GroEL/ES), another ATP-powered chaperone system. We found that screening against GroEL/ES complex or GroEL alone yielded different “hits”, as our “gray box” screening strategy predicted (see Chapter 3). Thus, both the HTS assay we developed and the “gray box” strategy we proposed can be useful ways to identify chemical modulators of other ATPase systems.

6.1.1 Application of Our ATPase-based HTS Assay in Other ATPase Systems

In this thesis, we have developed both 96-well and 384-well based HTP assays against

the ATPase activity of Hsp70. Using this method, we identified both inhibitor and activators of Hsp70 ATPase, with some shown promising cellular activities such as inducing the degradation of tau and Akt [1-3]. Because many chaperones and important enzymes in cells, such as GroEL/GroES (GroEL/ES), chaperonin, Hsp90, Hsp104, and Vps4 are also ATPases [4-6], the HTS assay we developed might be easily adopted to screen against those medically important targets. In fact, we have used the 96-well based HTS strategies described in Chapter 1 to screen compound libraries against E. coli GroEL/ES and human Vps4 (**Figure 6.3** and **Appendix 6.4.1**). In this chapter, we will discuss the screen against GroEL/ES in further detail.

6.1.2 The Enzymatic Activity of GroEL/ES Chaperone System

Similar to the DnaK-DnaJ-GrpE system we described in this thesis, GroEL/ES is another chaperone complex in *E. coli* cells. GroEL is a 57 kDa protein that forms a large oligomer consisting of two cylinders each formed by seven GroEL monomers [7]. Each cylinder of the GroEL oligomer has an empty central cavity, which accommodates protein up to 60 kDa in size [8]. GroES is a 10 kDa protein that forms a heptamer that acts as a lid for the cavities of the GroEL oligomer [9]. Despite extensive studies, there is still debate on the refolding mechanism of the GroEL/ES complex (for a more thorough review of the

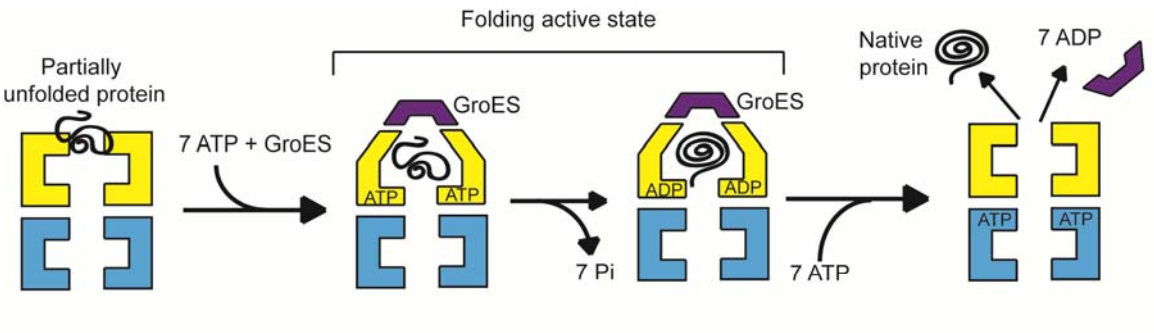

Figure 6.1 The schematic depiction of the tradiational model of GroEL/ES refolding cycle. The cycle starts with the binding of a partially unfolded protein to the hydrophobic regions of one cylinder of GroEL oligomer. Next, the binding of ATP and GroES heptamer encapsulates the protein substrate and allows it to fold in a protected condition while the ATP hydrolysis occurs. Finally, the binding of ATP to the other cylinder of GroEL oligomer releases GroES, ADP and the protein substrate. If folded, the native protein is released into cytosol while the incompletely folded protein will undergo another run of refolding with GroEL/ES or other chaperone system. (This model is redrawn based on the figure on http://www.biochem.mpg.de/hayer-hartl/).

GroEL/ES literature, see [10]). Briefly, the traditional model of GroEL/ES-mediated refolding is that the partially unfolded protein interacts in the cavity via exposed hydrophobic regions [11, 12]; which is followed by the binding of a GroES heptamer and seven ATP molecules (**Figure 6.1**). The binding of GroES seals the cylinder and releases the substrate in the central cavity of GroEL. By temporary encapsulating the partially unfolded protein, GroEL/ES allows it to fold, while also preventing non-specific interactions [10] (**Figure 6.1**). After a short time period (3 ~ 25 minutes), ATP is hydrolyzed, the GroES lid is dissociated, and the substrate is either released as a folded product or it undergoes another cycle of refolding [10] (**Figure 6.1**). Thus, GroEL is an ATPase and ATP hydrolysis powers the conformational changes required for the refolding reaction.

6.2 Results and Discussions

6.2.1 Establishing the Optimal Conditions for Screening against GroEL and GroEL/ES Complexes

In this preliminary study, we aimed to screen against either GroEL alone or the GroEL/ES complex. These studies were conducted in collaboration with Prof. Zhaohui Xu. To develop a HTS method, we first optimized the concentration of GroEL. In that process, we found that after three hours of incubation, the standard curve of GroEL

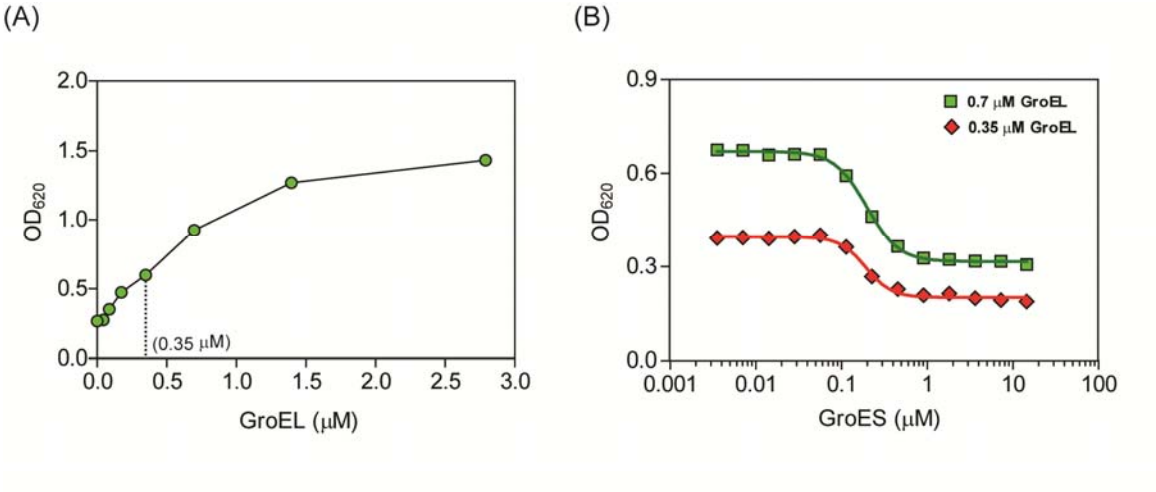

Figure 6.2 Optimization of the screen against the ATPase activities of GroEL and GroEL/ES complexes. (A) After three hours of incubation at 37°C, the standard curve of GroEL concentration versus OD_{620} (reflected the concentration of released phosphate) remained linear up to 1.4 μM. (B) GroES dose-dependently inhibited the ATPase activity of GroEL with K_d around 0.18 μM and 2-fold maximal inhibition. Based on the result, we decided to screen compounds against 0.35 μM GroEL at the presence or absence of 0.18 μM GroES. Each data point is the average of triplicates and the error bars represent the standard error of the mean. Note that the error bars are usually too small to be seen.

concentration versus OD_{620} values (representing released phosphate) remained linear up to 1.4 μM (**Figure 6.2A**). Next, we picked two concentrations of GroEL, 0.7 and 0.35 μM, and analyzed how increasing concentrations of GroES might affect its ATPase activity. In

that process, we found that GroES inhibited the ATPase activities of GroEL with an IC_{50} of ~0.18 μM and caused 2-fold inhibition at saturation (**Figure 6.2B**). Based on these studies, we decided to perform our screen using 0.35 μM GroEL with or without 0.18 μM GroES. We chose to screen with GroES concentration closed to its IC_{50} because compounds that affected GroEL/ES interaction would be more likely to be discovered.

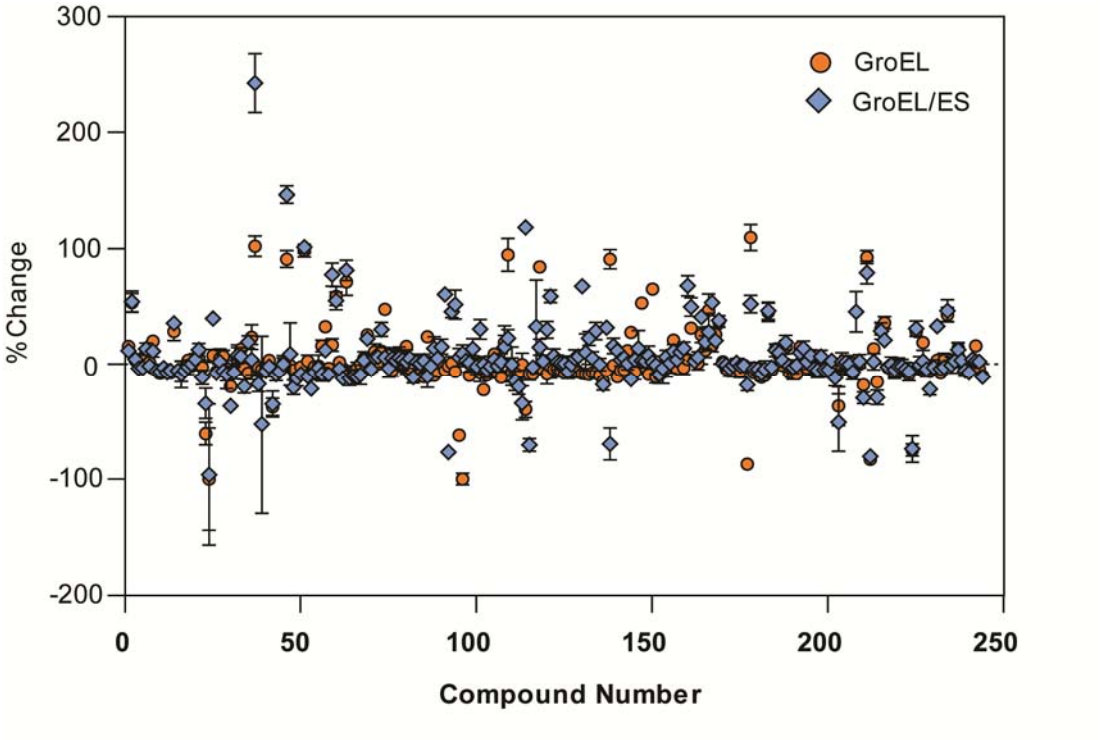

Figure 6.3 Consistent with our proposed "gray-box screening" strategy, screening against GroEL or GroEL/ES identified different hits. The screening concentration of compounds was 200 μM, GroEL was 0.35 μM, GroES was 0.18 μM, and ATP was 1 mM. The reactions were incubated at 37°C for 3 hours before quenched by the addition of malachite green (MG) reagent (as in Chapter 2). Since many compounds in this library had colors, the OD_{620} signals of controls that contained compound and ATP but not enzymes (also incubate for 3 hours at 37°C and developed by adding MG reagent) were subtracted from the signal of enzyme containing sample for each compound. The Z-factors of the screen against GroEL and GroEL/ES were 0.75 and 0.63, respectively. The percent signal change compared to the DMSO control is shown. Each data point is the average of triplicates and the error bars represent the standard deviations.

6.2.2 Screening a 246 compound library against GroEL and GroEL/ES Complexes

Next, we assembled a 246 compound library from our chemical inventory and screened it against the ATPase activities of GroEL or GroEL/ES complexes at 200 µM compound concentration. These compounds included many polyphenols and related bioactive compounds. Interestingly, as we predicted in Chapter 3, screening against different protein complexes of GroEL ("gray box" screening with or without GroES) generated different hits (**Figure 6.3** and **Appendix 6.5.2**). Samples that contained GroEL or

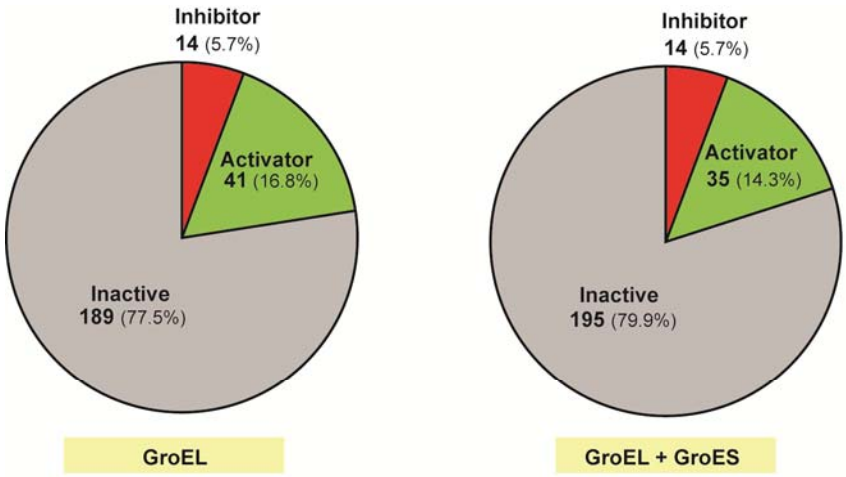

Figure 6.4 The "hit-rate" of the screen against GroEL or GroEL/ES complex. Compounds that decreased or increased the percent ATPase activity more than 3-fold standard deviation of the DMSO control were defined as inhibitors or activators. The relatively high "hit rate" was due to the enrichment of polyphenols that are known to interact with many protein targets in the compound library.

GroEL/ES, ATP, and DMSO were used as negative controls (no inhibition) whereas those with ATP and DMSO were used as positive controls (mimic 100% inhibition). The screen

against GroEL and GroEL/ES had Z factor of 0.75 and 0.63 and the hit rate was 22.5% and 20% when the “hits” were defined as compounds that inhibited or activated the percent ATPase activity more than 3 standard deviations of the negative controls. We identified 14 inhibitors and 41 stimulators in GroEL screen and 14 inhibitors and 35 stimulators in GroEL/ES screen (**Figure 6.4**). We expect that the “hit rates” were relatively high, because the library was enriched for promiscuous polyphenols.

6.2.3 Determine the Dose-dependent Effects of the “Hits” Found in the Screen

Based on these results, we selected 106 compounds to test their dose-dependence (**Appendix 6.4.3**). Interestingly, we observed two major types of dose-dependent effects: one type of compound stimulated the ATPase activities of both GroEL and GroEL/ES with high K_d values; the other type of compounds stimulated ATPase activity at lower concentration but inhibited it at higher concentration (**Figure 6.5**). Further follow-up studies are required to understand the stimulation or inhibition mechanisms of those compounds. But the preliminary data suggested that the HTS assays we developed can be easily adapt to screen for chemical modulators against other ATP-fueled enzymes.

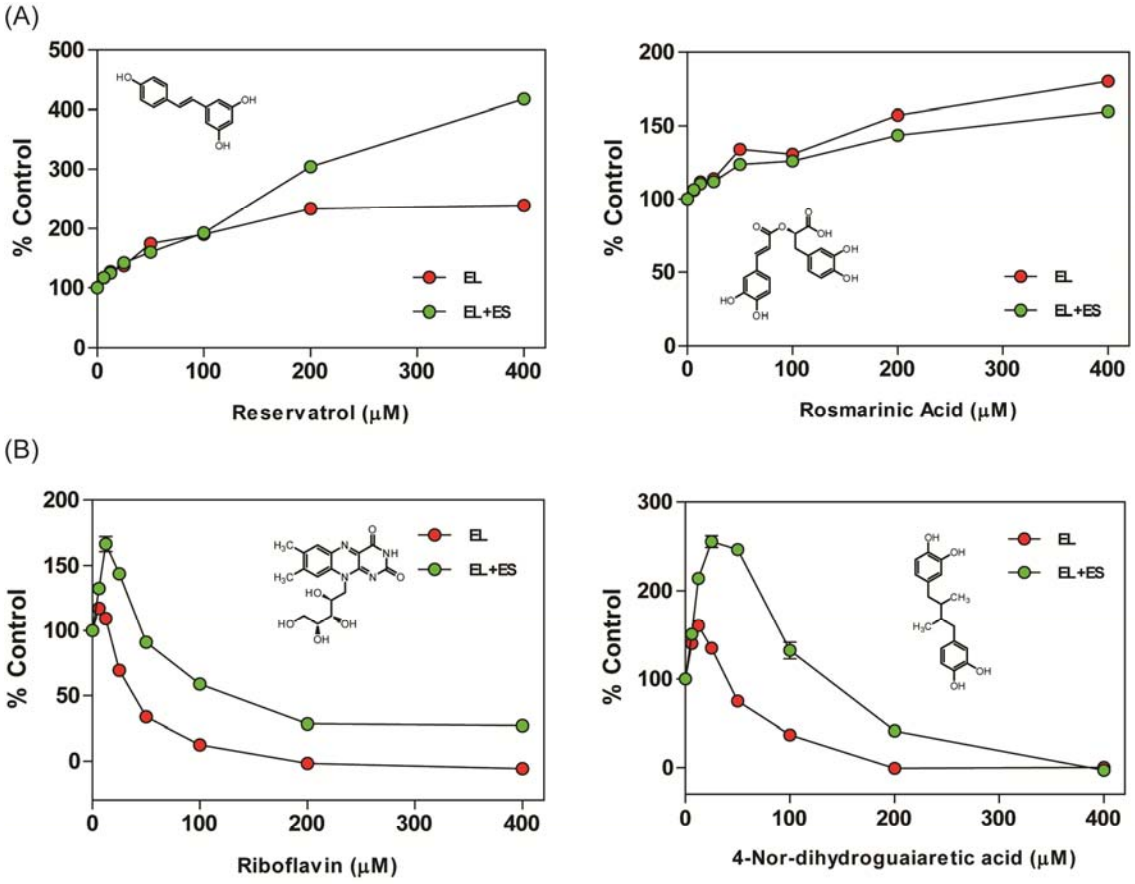

Figure 6.5 Examples of the two types of compound dose-dependent curves against GroEL and GroEL/ES. (A) One type of compounds stimulated the ATPase activty of both GroEL and GroEL/ES with a high EC_{50}, and (B) the other type of compounds stimulated ATPase activity of GroEL or GroEL/ES at low concentration but inhibited at higher concentration. The addition of GroES shift the dose-dependent curve of compounds, but did not affect the general trend. The concentration of GroEL was 0.35 μM, GroES was 0.18 μM, and ATP was 1 mM. For each data point, the signal of controls containing only serial diluted compounds and ATP was subtracted (as discribed in Figure 6.3). The percent ATPase signal compare to DMSO control (100%) is shown. Each data point is the average of triplicates and the error bars represent the standard error of the means.

6.3 Experimental Procedures

6.3.1 ATPase Assay

The ATPase activities of GroEL and GroEL/ES complexes were measured by same 96-well based method as described in Chapter 2.

Notes

Lyra Chang and Jason E. Gestwicki designed the experiments. Lyra Chang conducted the experiments. The purified GroEL, GroES, and Vps4 proteins were generous gifts from Prof. Zhaohui Xu.

6.4 Appendix

6.4.1 The Screening Result against the ATPase Activity of Vps4

(A)

Compound ID	% Change	Compound ID	% Change
1,3-diphenyl-2-propenone	-19.4	ellagic acid	22.9
3-(3-hydroxyphenyl)-1-(phenyl)-2-propen-1-one	-26.4	Eosin Y	-91.2
4-Methoxychalcone	13.5	epigallocatechin gallate	310.3
(2E)-3-(3,4-methoxyphenyl)-1-phenyl-2-propen-1-one	-28.5	fenofibrate	-14.1
Nordihydroguaiaretic acid	512.2	hematin	220.9
Benzophenone	-32.7	hemin	487.4
Resveratrol	-28.6	indomethacin	-18.3
Curcumin	288.6	juglone	535.5
4,4'-Methylenediphenol	-48.8	kaempferol	427.0
lacmoid	-83.6	melatonin	-17.6
3,5-bis(3-methoxy-4-hydroxybenzylidene)4-piperidinone	465.0	methyl orange	-25.3
BSB-p*	520.1	methyl red	12.6
ED*	-27.6	methyl yellow	128.3
DAB-FA dimer*	-0.1	methylene blue	-4.2
DAO-FA dimer*	95.8	minocycline	-77.7
m-xd-FA dimer*	321.1	myricetin	410.9
congo red	-13.9	naringenin	-8.7
crysamine G	-67.8	neocuproine	-22.8
1,3 (ver)2*	343.3	octadecysulfate	-48.8
1,2-Naphthoquinone	516.8	Orange G	-18.1
2,2'-dihydroxybenzophenone	56.2	o-vanillin	33.9
2,3,4-trihydroxybenzophenone	99.8	phenol red	-10.2
4,4'-dihydroxybenzophenone	262.1	pherphenazine	-54.5
apigenin	468.8	quercetin	564.3
Azure A	46.3	Rhodamine B	504.5
Azure C	64.3	Rifamycin	12.6
baicalein	428.7	Rolitetracycline	-0.6
catechin	-11.4	taxifolin	497.9
Chicago Sky Blue 6B	-3.8	tetracycline	-19.2
Chlorazol Black	-81.4	thionin	141.9
dopamine	-51.0	TMTDAB	-137.8

(B)

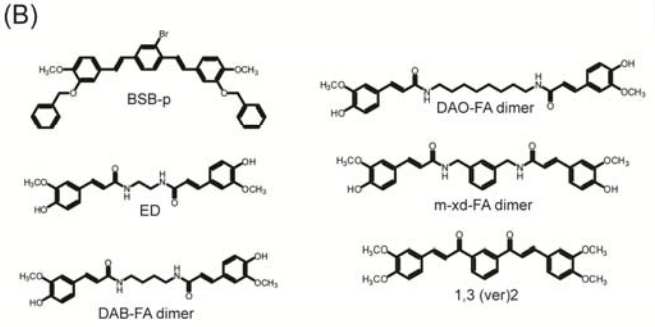

(C)

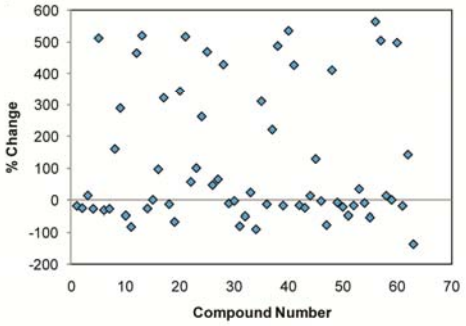

Appendix 6.4.1 The screening result against Vps4. (A) Compound effects on the percent ATPase activity of Vps4. The structure of the compounds marked by ⋆ are shown in (B). (C) The dot plot representation of the screening result. The compounds were screened at 200 μM and the concentration of Vps4 was 1 μg/well, ATP was 1 mM. The total volume of each well was 25 μL, and the reaction was incubated at 37°C for 3 hours before quenched by adding malachite green reagent (same as in Chapter 2). Each data point represents the result of one reaction (no replicate) with control signal (ATP + 200 μM compound) subtracted as discribed in Figure 6.3. The compound induced percent changes of Vps4 ATPase activities compared to its DMSO control (DMSO+Vps4+ATP) were shown.

6.4.2 The Screening Result against the ATPase Activities of GroEL and GroEL/ES Complexes

Appendix 6.4.2 The screening results against GroEL and GroEL/ES complexes

Compound Name	GroEL Screen (% Change)	GroEL/GroES Screen (% Change)
(+/-) Catechin Hydrate	15.6 ± 2.7	11.7 ± 1.7
5- ((((2-iodoacetyl)amino)ethyl)amino) (IAEDANS)	53.5 ± 7.8	54.5 ± 9.2
4- (1-Piperimidyl)-benzaldehyde	3.5 ± 3.3	4.4 ± 3.0
4- (2-Pyridyl)-benzaldehyde	-1.5 ± 2.4	-3.4 ± 2.8
1- (4-Amino-Phenyl)-3-phenyl-propenone	5.6 ± 2.9	-3.1 ± 3.7
N- (4-Bromobutyl)-phthalimide	12.7 ± 4.2	13.4 ± 5.3
3'- Amino acetophenone	1.9 ± 2.3	-1.3 ± 4.1
9- Aminoacridine Hydrochloride	20.2 ± 3.9	11.3 ± 4.7
4- Aminobenzylamine	-4.6 ± 1.9	-6.1 ± 3.1
4- Aminomethyl piperidine	-8.2 ± 2.2	-6.4 ± 2.6
3- Aminophenol	-7.5 ± 1.2	-3.1 ± 4.3
Amoxicillin trihydrate	-5.3 ± 3.0	-7.3 ± 2.7
Ampicillin Sodium Salt	-7.6 ± 3.1	-5.6 ± 2.9
1- anilinonapthalene-8-sulfonic acid (1,8-ANS)	28.7 ± 7.9	35.8 ± 2.7
p- Anisaldehyde	-6.5 ± 4.5	-5.7 ± 3.3
p- Anisidine	-6.2 ± 8.9	-8.8 ± 12.0
Anisole	-2.8 ± 2.6	-5.7 ± 4.2
9- Anthraldehyde	3.7 ± 3.6	-2.5 ± 6.3
Anthraquinone-1,5-disulfonic acid	-1.4 ± 3.7	0.2 ± 4.2
Anthraquinone-2,6-disulfonic acid	2.2 ± 6.4	4.4 ± 4.8
Apigenin	5.0 ± 5.2	12.7 ± 5.3
L- Ascorbic acid	-2.8 ± 6.4	-11.5 ± 6.1
Azure A	-60.5 ± 9.9	-34.2 ± 13.2
Azure C	-99.8 ± 44.3	-96.0 ± 61.0
Baicalein	7.5 ± 5.8	39.7 ± 3.1
Benzaldehyde	-6.5 ± 3.4	-7.8 ± 4.4
Benzidine dihydrochloride	5.3 ± 8.1	2.2 ± 3.7
Benzil	6.7 ± 5.6	-5.9 ± 3.8
Benzophenone	-4.1 ± 10.1	-8.9 ± 12.6
Benzyl Viologen dichloride	-19.2 ± 3.8	-36.3 ± 3.5
Benzylacetoacetate	-5.7 ± 4.4	-7.5 ± 5.8
3- Benzyloxy-4-methoxybenzaldehyde	3.9 ± 12.8	7.7 ± 7.2
4- Benzyloxy-benzaldehyde	13.1 ± 2.0	6.7 ± 5.2
1,1' Binaphthyl-2,2'-diamine	-3.6 ± 1.7	-19.4 ± 5.7
Chrysamine G	-7.9 ± 5.7	19.5 ± 5.1
bis-ANS	23.7 ± 10.7	3.8 ± 13.3
Bithionol	102.3 ± 8.8	242.7 ± 25.6
2- bromo-1,4-dimethyl benzene	-2.9 ± 5.2	-17.4 ± 6.7
4- Bromoaniline	-4.2 ± 3.7	-52.4 ± 76.8
4- Bromo-benzaldehyde	-4.5 ± 5.3	-6.1 ± 5.1
2- Bromobenzyl alcohol	3.7 ± 2.1	-1.7 ± 2.5
Bromocresol green	-37.2 ± 7.4	-34.8 ± 11.1
2- Bromo-p-xylol	-5.3 ± 4.6	-9.1 ± 5.4
5- Bromovanillin	-5.0 ± 3.9	-6.6 ± 2.9
4- Butylaniline	0.9 ± 6.7	0.2 ± 5.6
calcofluor white stain	91.2 ± 7.2	146.5 ± 7.3
d- Camphoric Acid	-1.0 ± 4.1	8.8 ± 27.2
Camptothecin	-5.2 ± 4.4	-20.1 ± 6.3
Chlorobenzene	-11.5 ± 7.3	-12.1 ± 3.8
2- chlorophenol	-2.1 ± 3.4	-8.6 ± 3.3
Chlorophenol Red	98.4 ± 5.4	101.3 ± 4.7
2- chlorophenothiazine	2.8 ± 5.2	-10.7 ± 2.4
Chrysin	-7.6 ± 5.5	-21.3 ± 3.2
trans- Cinnamaldehyde	-1.8 ± 3.8	-6.9 ± 3.6
Cinnamyl acetate	-1.3 ± 3.2	-3.0 ± 11.0
Congo red	16.1 ± 4.9	-8.7 ± 6.1
Coralyne Chloride Hydrate	32.5 ± 3.4	12.4 ± 4.3
Coumarin	-3.4 ± 4.0	-8.8 ± 4.4
Cresyl violet	16.8 ± 5.5	77.7 ± 9.9
Curcumin	59.1 ± 8.1	55.1 ± 7.7

Appendix 6.4.2 The screening result against GroEL and GroEL/ES complexes

Compound Name	GroEL Screen (% Change)	GroEL/GroES Screen (% Change)
Danslyamide	1.7 ± 4.0	-4.1 ± 3.1
1,3- Diacetylbenzene	-5.5 ± 4.3	-12.3 ± 3.4
5,7- Dibromo-8-hydroxy-quinoline	71.5 ± 11.7	81.4 ± 8.9
2,4- Dichlorobenzaldehyde	-7.8 ± 4.4	-12.1 ± 6.5
2,4- Dichlorophnenthylamine	-6.0 ± 5.1	-10.5 ± 5.5
2,5- Difluorobenzaldehyde	-3.5 ± 5.5	-10.9 ± 2.5
3,4, dihydro-2H-1,4-benzothiazine 1,1-dioxide	0.4 ± 4.5	-9.3 ± 8.5
2,3 dihydro-3-oxo-4H-1,4-benzothiazine-2-acetic acid	5.3 ± 5.6	3.4 ± 3.3
1,4- Dihydroxy-2-naphthoic acid	25.8 ± 4.1	22.2 ± 2.9
3,4- Dihydroxybenzaldehyde	-0.3 ± 6.4	-4.3 ± 3.0
4,4'- dihydroxybenzophenone	11.2 ± 6.5	5.9 ± 2.7
2,2'- Dihydroxybenzophenone	0.4 ± 3.0	6.4 ± 3.5
2,6- Dihydroxynaphthalene	11.3 ± 3.7	30.4 ± 6.1
L-3,4 dihydroxyphenylalanine	47.8 ± 3.6	6.2 ± 8.7
(S)-(-)-2,2'- Dimethoxy-1,1'-binaphthyl	-0.3 ± 4.1	-3.7 ± 7.9
4,5- Dimethoxy-2-nitrocinnamic acid	-5.1 ± 5.6	5.4 ± 8.2
2,3- Dimethoxybenzaldehyde	1.7 ± 2.2	3.6 ± 8.6
2,4- Dimethoxybenzaldehyde	8.6 ± 3.0	5.5 ± 9.6
3,5- Dimethoxybenzaldehyde	-1.9 ± 4.5	3.8 ± 8.9
2,6- Dimethoxybenzoic acid	15.8 ± 3.3	2.1 ± 10.8
5,5 dimethyl -1,3 cyclohexandione	-8.1 ± 2.6	5.2 ± 3.6
dimethyl yellow	-11.6 ± 3.1	-11.6 ± 4.8
4- Dimethylamino benzaldehyde	-10.9 ± 3.2	1.9 ± 4.7
4- dimethylamino pyridine	-8.8 ± 4.9	0.5 ± 8.4
3,5- dimethylphenylboric acid	-11.0 ± 2.9	3.0 ± 6.1
4,4- Dinitro-2-biphenylamine	23.9 ± 3.1	-10.8 ± 9.6
Diphenic acid	-10.0 ± 2.8	-1.8 ± 8.5
5,5- Diphenylhydantoin	-9.7 ± 2.8	14.0 ± 10.1
2,2'- Dipyridyl	-6.4 ± 4.7	5.2 ± 4.2
Dopamine hydrochloride	-0.1 ± 4.2	15.3 ± 6.4
ellagic acid	-5.1 ± 2.8	60.8 ± 4.3
Eosine y	-1.6 ± 1.8	-76.4 ± 3.1
Epicatechin monogallate	1.1 ± 5.7	45.5 ± 4.7
Epigallocatechin gallate from green tea	-6.4 ± 4.1	51.9 ± 12.5
Erythromycin	-61.9 ± 4.0	6.0 ± 7.8
N- Ethoxycarbonylphthalimide	-99.8 ± 5.2	9.3 ± 7.4
Ethyl 2-pyridylacetate	3.6 ± 3.1	3.2 ± 3.5
4- Ethynyl-N,N-dimethylaniline	-10.0 ± 3.7	1.3 ± 8.1
Eugenol	1.4 ± 4.2	13.4 ± 8.8
fenofibrate	2.7 ± 3.7	-1.7 ± 7.4
Flavone	-7.7 ± 7.5	30.5 ± 8.5
4- Fluoro-3-nitrobenzotrifluoride	-22.2 ± 4.3	-0.3 ± 7.3
4- Fluorobenzaldehyde	-9.2 ± 3.7	-4.6 ± 7.2
3- Fluorobenzaldehyde	0.1 ± 3.7	-1.8 ± 9.2
2- Fluorobenzaldehyde	8.9 ± 2.8	4.3 ± 4.1
Folic acid	-7.1 ± 5.3	-1.5 ± 5.3
G418 Sulfate	-11.3 ± 3.2	1.9 ± 7.6
galangin	19.1 ± 14.3	15.3 ± 9.8
Gallocyanine	94.8 ± 14.2	22.7 ± 7.5
Geldanamycin	-6.5 ± 12.1	-0.2 ± 15.3
18alpha glycyrrhetinic acid	-7.8 ± 4.6	-14.6 ± 8.7
hematin	-8.0 ± 3.6	-19.2 ± 7.4
Hemin	-0.2 ± 10.1	-33.8 ± 14.9
Hexachlorophene	-39.5 ± 6.8	118.5 ± 4.2
Hexadecyltrimethylammonium bromide	-8.8 ± 5.2	-70.1 ± 5.5
Hydrocinnamaldehyde	-8.5 ± 1.5	-2.8 ± 2.9
Hydrocortisone	-2.8 ± 2.1	32.6 ± 40.7
Hydroxocobalamin hydrochloride	84.2 ± 4.1	15.0 ± 6.8
2- Hydroxy-1,4-naphthoquinone	-4.7 ± 3.5	2.9 ± 4.9
5- hydroxy-1,4-napthoquinone	-8.7 ± 8.8	30.1 ± 7.3

Appendix 6.4.2 The screening results against GroEL and GroEL/ES complexes

Compound Name	GroEL Screen (% Change)	GroEL/GroES Screen (% Change)
2- Hydroxy-1-naphthaldehyde	-2.0 ± 10.1	59.0 ± 5.4
trans-4- Hydroxy-3-methoxycinnamic acid	-4.4 ± 6.7	7.4 ± 6.0
3- Hydroxybenzaldehyde	-4.1 ± 2.3	1.7 ± 6.6
2- Hydroxybenzyl alcohol	-5.4 ± 5.1	1.1 ± 5.5
m- Hydroxycinnamic acid	-7.7 ± 3.3	0.7 ± 6.7
3- Hydroxyflavone	-6.7 ± 4.1	-6.4 ± 6.3
5- hydroxymethyl fufural	-7.0 ± 3.1	-0.3 ± 4.6
Indole	-6.7 ± 5.2	5.4 ± 7.4
Indole-3-Carboxaldehyde	-6.9 ± 4.8	7.0 ± 3.8
Indomethacin	-8.1 ± 3.4	67.8 ± 4.3
4- Iodobenzoic acid	-8.4 ± 3.8	10.4 ± 15.9
4- Iodophenol	-9.0 ± 4.5	22.6 ± 6.1
5- Iodovanillin	-7.1 ± 3.5	5.3 ± 5.6
Kaempferol	-7.6 ± 3.9	29.1 ± 7.5
Kanamycin monosulfate	-9.9 ± 2.9	-0.2 ± 5.3
6- Ketocholestanol	-14.8 ± 2.3	-17.9 ± 4.8
Koparin	-5.7 ± 1.6	32.0 ± 4.6
Lacmoid	91.1 ± 8.3	-69.4 ± 13.9
luteolin	-1.0 ± 4.6	16.1 ± 6.7
Meclocycline sulfosalicylate	-11.0 ± 4.4	11.9 ± 4.4
Melatonin	-5.5 ± 3.0	3.9 ± 5.5
7 methoxy-1,4,benzothiazin-3(4H)one	-5.0 ± 4.0	5.5 ± 4.2
4- Methyl imidazole	11.9 ± 3.4	0.7 ± 5.3
Methyl red	27.6 ± 2.6	-13.3 ± 3.7
Methyl viologen dichloridehydrate	-7.0 ± 6.5	4.0 ± 2.8
1- Methyl-1-cyclohexane carboxylate	12.5 ± 4.5	14.0 ± 15.4
Methyl-3-formylbenzoate	53.3 ± 4.4	3.3 ± 4.9
Methyl-4-amino-benzoate	-2.1 ± 5.7	2.8 ± 5.9
DL-6- methyl-5,6,7,8-tetrahydropterine	-9.0 ± 4.2	7.7 ± 8.4
5- Methyl-5-phenylhydantoin	65.2 ± 4.4	1.8 ± 5.6
N- Methylaniline	-11.2 ± 5.2	-0.5 ± 7.8
Methylene blue	-9.5 ± 2.6	-8.9 ± 8.0
N- Methylisatoic anhydride	-7.1 ± 9.8	-3.5 ± 4.5
4- Methylmorpholine	-3.3 ± 7.8	6.3 ± 5.8
N- Methylpyrrole-2-carboxaldehyde	1.4 ± 5.5	1.1 ± 9.0
2- Methylthiobenzothiazole	21.2 ± 3.4	11.4 ± 5.9
4- Methylumbelliferyl-B-D-galactoside	-4.0 ± 3.4	3.9 ± 3.8
7- Methyl-1,4-benzothiazin-3(4H)one	7.1 ± 3.9	10.7 ± 4.8
minocycline hydrochloride	-3.3 ± 5.6	14.0 ± 5.4
morin hydrate	4.4 ± 2.1	68.1 ± 8.7
myricetin	31.4 ± 4.1	49.8 ± 7.8
2- Naphthaldehyde	3.7 ± 3.2	2.9 ± 4.2
1- Naphthaldehyde	1.2 ± 5.8	6.2 ± 4.7
1,2- Naphthoquinone	25.5 ± 6.6	41.2 ± 4.4
2- Naphthylacetic acid	12.2 ± 6.3	19.3 ± 5.6
Naphtol blue black	47.0 ± 14.1	28.1 ± 16.3
1,4- napthoquinone-2-sulfonic acid potassium salt	16.6 ± 5.6	53.6 ± 3.0
1,2- napthoquinone-4-sulfonic acid potassium salt	26.1 ± 5.1	20.7 ± 3.6
Naringenin	37.2 ± 5.1	38.2 ± 3.7
Neocuproine	2.3 ± 4.4	0.6 ± 4.1
Neomycin sulfate	-3.9 ± 4.5	-0.6 ± 4.4
Neopentyl glycol	-2.2 ± 5.8	-3.4 ± 7.1
Nicotinic acid	-5.8 ± 5.2	-1.0 ± 3.8
4- Nitrobenzene sulfonyl chloride	-1.2 ± 6.2	1.3 ± 4.5
4- Nitrobenzoic acid	-6.3 ± 5.4	-1.4 ± 3.9
5- Norbornene-2-Carboxamide	-0.8 ± 2.9	-1.0 ± 3.7
4- Nor-dihydroguaiaretic acid	-86.9 ± 2.7	-18.3 ± 4.7
octadecysulfate	109.8 ± 11.2	52.3 ± 7.5
Orange G	-7.6 ± 4.4	-4.1 ± 6.1
2- Oxazolidone	-7.2 ± 3.5	-4.5 ± 5.4

Appendix 6.4.2 The screening results against GroEL and GroEL/ES complexes

Compound Name	GroEL Screen (% Change)	GroEL/GroES Screen (% Change)
Paclitaxel	-11.4 ± 3.4	-8.2 ± 6.2
Penicillin-G Potassium	-9.6 ± 4.4	-4.4 ± 7.5
perphenazine	45.1 ± 7.9	46.4 ± 7.4
Phenetyl alcohol	-5.4 ± 2.6	-2.9 ± 3.4
Phenol Red	13.1 ± 3.7	12.3 ± 5.3
Phenothiazine	8.3 ± 3.2	10.1 ± 8.1
phenoxathiin	-1.2 ± 3.9	3.4 ± 5.6
Phenoxazine	15.1 ± 5.6	19.0 ± 6.1
Phenyl boronic acid	-7.4 ± 3.8	-1.4 ± 5.4
Phenyl trimethyl ammonium chloride	-8.3 ± 5.2	-2.9 ± 5.4
3- Phenyl-1-propanol	-8.5 ± 4.7	-0.9 ± 4.8
1,2- Phenylene diamine	14.8 ± 4.5	10.2 ± 4.0
1,3- Phenylene diamine	4.1 ± 8.0	13.8 ± 6.6
P- Phenylene diamine dihydrochloride	-3.0 ± 6.9	2.3 ± 6.7
o- phenylenediamine	7.2 ± 5.5	7.9 ± 4.9
N- Phenylglycine	-3.3 ± 4.7	-3.8 ± 6.4
Phenylmethanesulfonylfluoride	-6.1 ± 5.7	-5.3 ± 6.5
Phtalic anhydride	0.9 ± 4.9	7.0 ± 5.3
N- Phtaloylglycin	-6.4 ± 5.1	-4.6 ± 4.3
4- Picoline	-5.7 ± 4.3	-4.6 ± 4.9
2- Picoline	-1.7 ± 3.2	3.3 ± 4.6
Ponceau S	-10.2 ± 3.8	-11.7 ± 7.3
Procion red	-36.6 ± 17.0	-50.8 ± 24.9
Protocatechnic acid (3,4-dihydroxybenzoic acid)	-3.7 ± 3.5	2.2 ± 8.2
3,5- Pyridine carboxylic acid	-4.6 ± 4.4	1.7 ± 6.2
Pyridoxin HCl	-5.1 ± 1.8	-0.1 ± 6.1
L-2- Pyrrolidone-S-carboxylic acid	-8.1 ± 1.9	-6.7 ± 6.7
quercetin hydrate	3.4 ± 4.4	45.7 ± 17.6
Quinoline	0.3 ± 2.5	2.7 ± 5.8
Rapamycin	-18.1 ± 2.1	-29.5 ± 5.0
D(+)- Reservatrol	92.9 ± 5.8	79.4 ± 9.8
Riboflavin	-82.8 ± 2.5	-80.3 ± 4.3
Rifamycin SV, sodium salt	13.4 ± 3.6	2.2 ± 7.0
Ritanserin	-15.5 ± 3.1	-29.1 ± 6.2
Rolitetracycline	31.2 ± 5.4	29.0 ± 7.2
Rosmarinic Acid	36.2 ± 5.2	21.0 ± 4.4
Salicylic acid	-2.6 ± 3.3	-2.4 ± 4.2
Sodium L-ascorbate	-2.7 ± 2.3	-0.1 ± 6.7
Spectinomycin	-7.5 ± 5.2	-4.6 ± 6.8
Spermidine	-1.5 ± 7.0	-2.0 ± 6.3
Spermine	-4.9 ± 6.0	-2.0 ± 6.4
Spermine dihydrate	-5.9 ± 4.5	-4.4 ± 6.3
Streptomycin Sulfate	-8.9 ± 2.4	-6.4 ± 8.0
Tannic acid	-74.6 ± 5.4	-73.7 ± 11.6
taxifolin	28.5 ± 3.4	31.0 ± 6.6
terbutaline hemisulfate salt	-4.3 ± 2.1	-0.5 ± 7.2
Tetracycline-HCl	18.8 ± 4.1	2.8 ± 9.4
Thiamine HCl	-5.7 ± 3.7	-4.3 ± 6.6
Thiazolyl Blue Tetrazolium Bromide	-6.6 ± 2.9	-22.0 ± 4.8
Thioflavin T	-3.1 ± 3.6	-2.6 ± 6.4
thionin acetate	3.6 ± 3.9	33.3 ± 3.6
Thymine	-7.9 ± 3.3	-4.0 ± 4.8
Tiron	3.6 ± 6.0	-2.6 ± 3.7
2,3,4- Trihydroxy benzophenone	43.1 ± 6.4	46.5 ± 9.4
Triketo hydrindene hydrate	1.0 ± 2.3	-0.6 ± 7.0
Transtrismethoxy resveratrol	3.1 ± 4.7	2.9 ± 5.5
3,4,5- Trismethoxybenzophenone	13.8 ± 5.0	12.7 ± 5.8
ursodeoxycholic acid	2.5 ± 3.9	3.4 ± 4.0
Vanillin	-3.6 ± 5.2	-5.8 ± 5.0
o- Vanillin	-2.9 ± 5.6	-7.1 ± 3.5
Veratraldehyde	-2.0 ± 1.7	4.3 ± 2.4
Vitamin B12	16.1 ± 2.5	2.7 ± 3.3
Wafarin	-3.9 ± 2.5	2.3 ± 4.4
m- xylylenediamine	-10.1 ± 1.9	-11.1 ± 2.5

6.4.3 Dose-dependent Effects of Selected Compounds against the ATPase Activities of GroEL and GroEL/ES Complexes

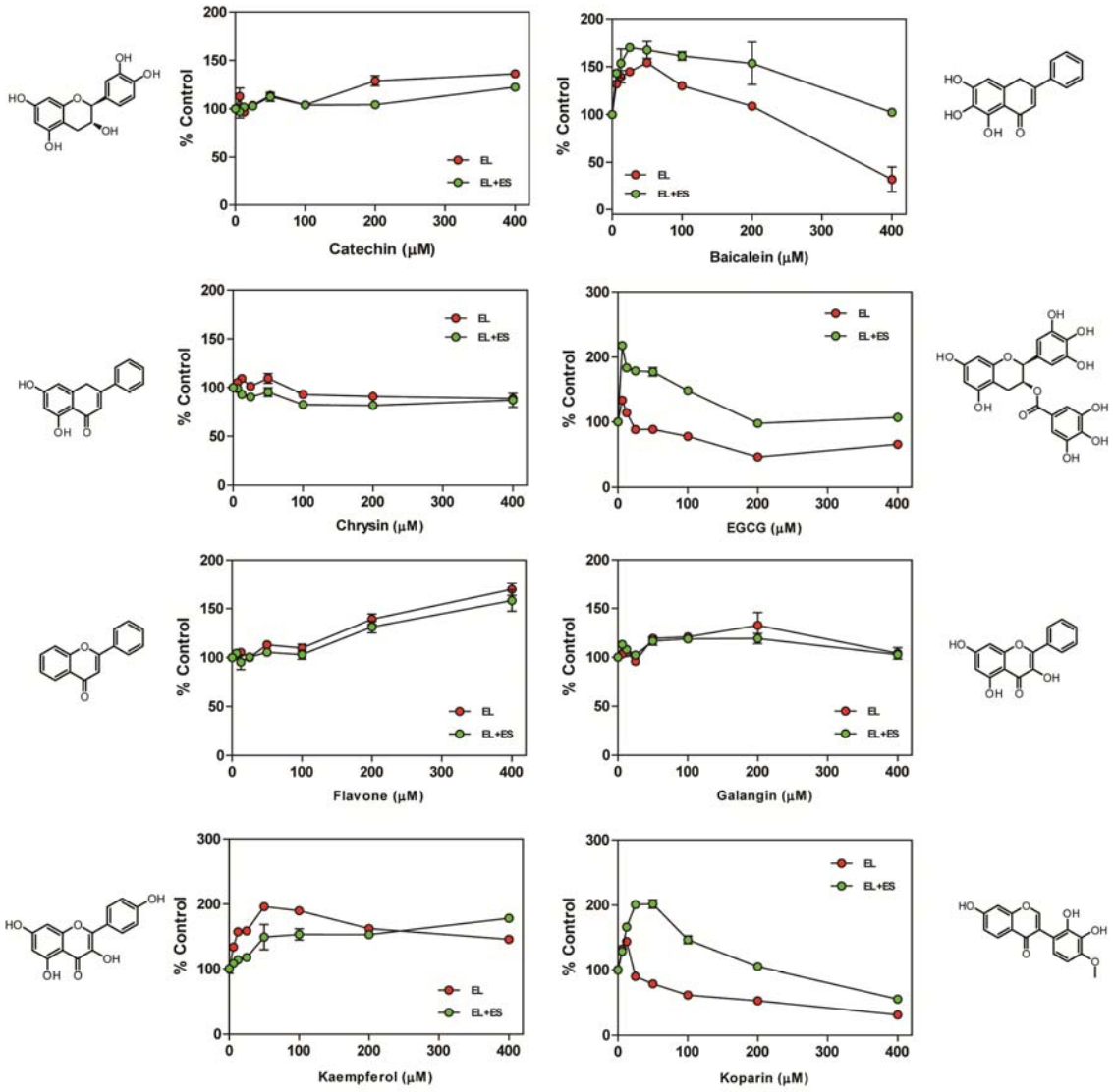

Appendix 6.4.3 The dose-dependent effect of selected "hits" from the GroEL and GroEL/ES high throughput screen. The concentration of GroEL was 0.35 μM, GroES was 0.18 μM, ATP was 1 mM, and the incubation condition was 37°C, 3 hours. The reaction volume was 25 μL and the phosphate released by ATP hydrolysis was detected by adding 80 μL malachite green reagent, followed by 10 μL 32% sodium citrate, and the OD_{620} value was measured after 15 mins incubation at 37°C similar to the protocols shown in chapter 1. The OD_{620} value of the control, buffer+specific compound at indicated concentration+ATP (with 3 hr 37°C incubation), was subtracted out from each data point. Each data point is the average of triplicates and the error bars represent the standard error of the mean.

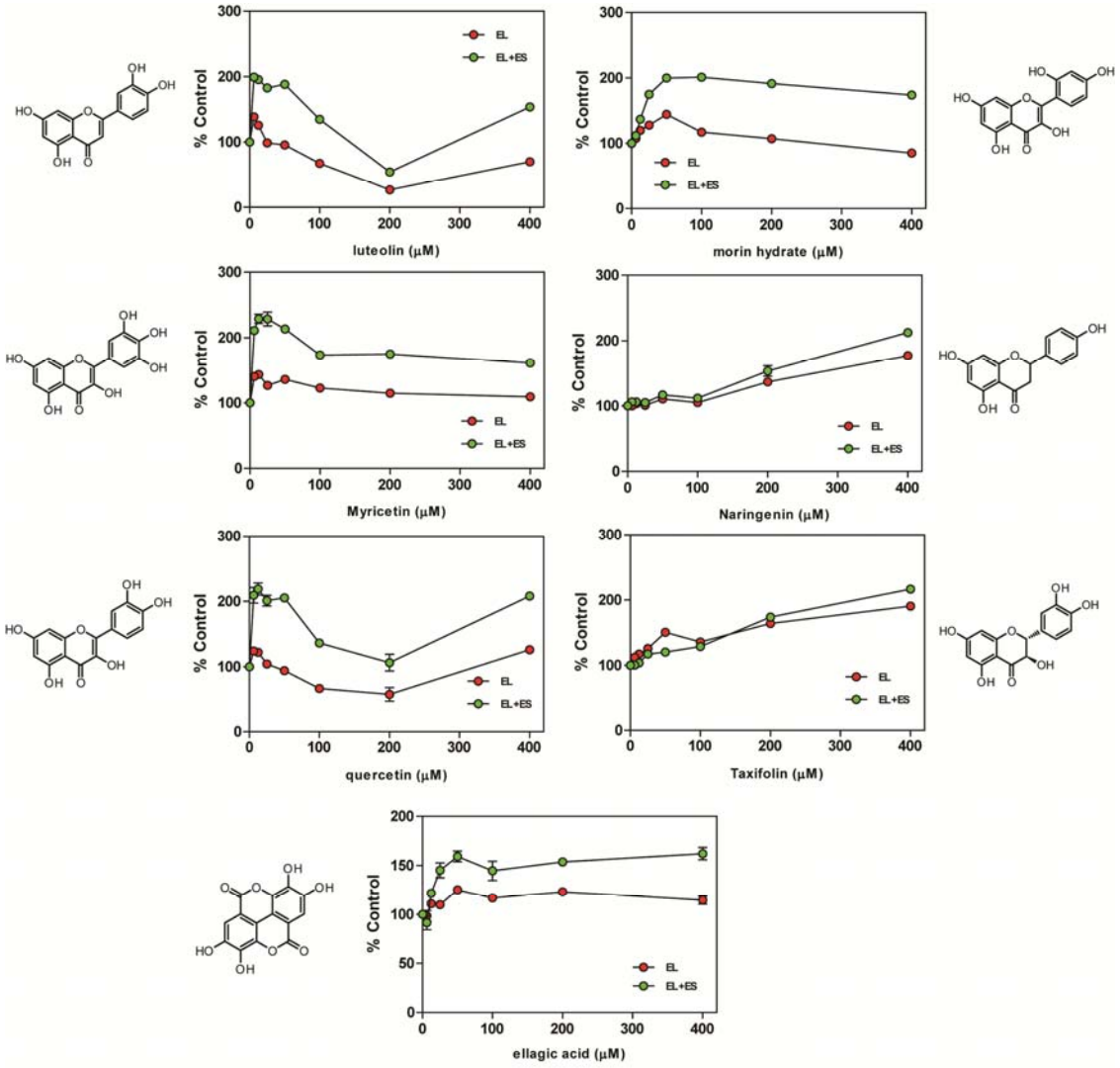

Appendix 6.4.3 The dose-dependent effect of selected "hits" from the GroEL and GroEL/ES high throughput screen. The concentration of GroEL was 0.35 μM, GroES was 0.18 μM, ATP was 1 mM, and the incubation condition was 37°C, 3 hours.The OD_{620} value of the control, buffer+specific compound at indicated concentration+ATP (with 3 hr 37°C incubation), was subtracted out from each data point. Each data point is the average of triplicates and the error bars represent the standard error of the mean.

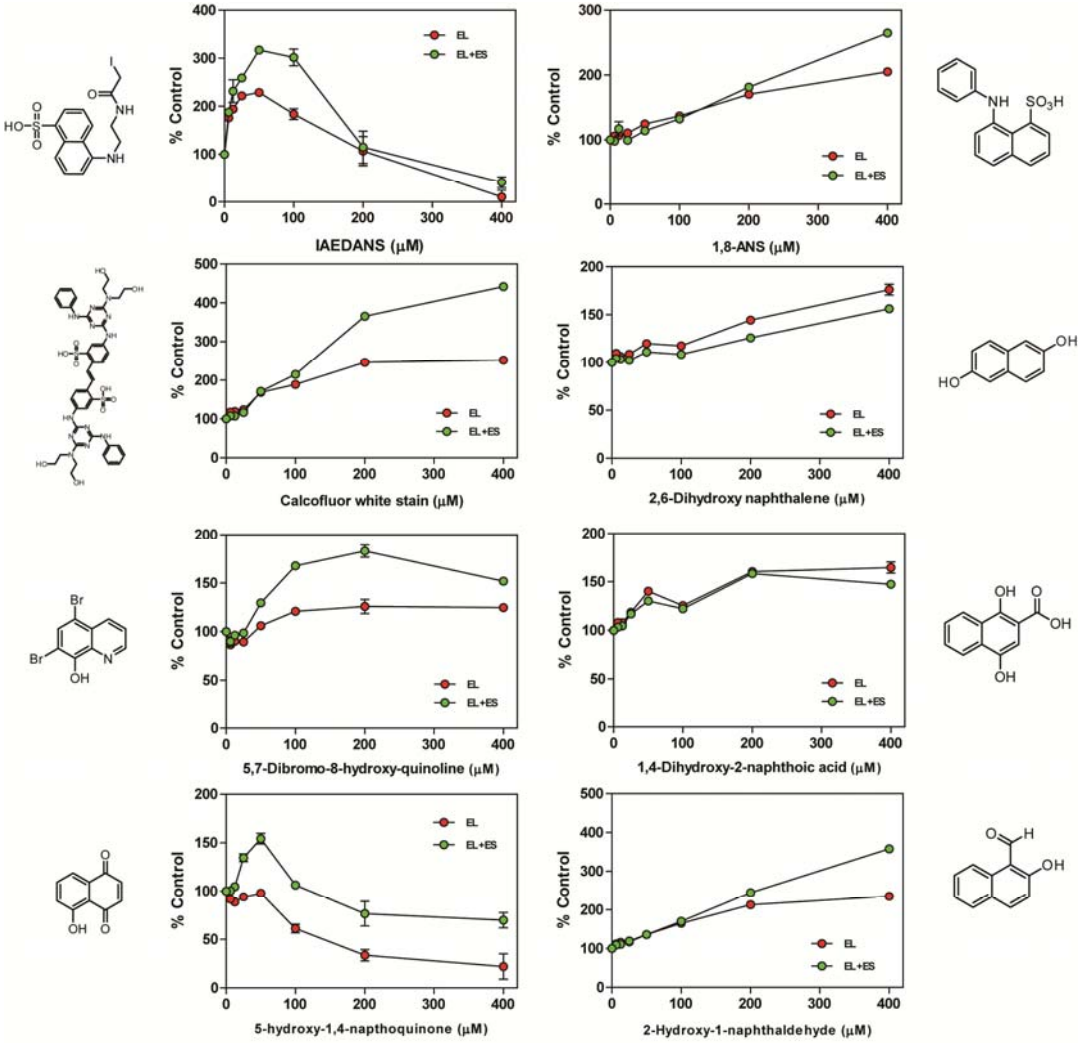

Appendix 6.4.3 The dose-dependent effect of selected "hits" from the GroEL and GroEL/ES high throughput screen. The concentration of GroEL was 0.35 μM, GroES was 0.18 μM, ATP was 1 mM, and the incubation condition was 37°C, 3 hours.The OD_{620} value of the control, buffer+specific compound at indicated concentration+ATP (with 3 hr 37°C incubation), was subtracted out from each data point. Each data point is the average of triplicates and the error bars represent the standard error of the mean.

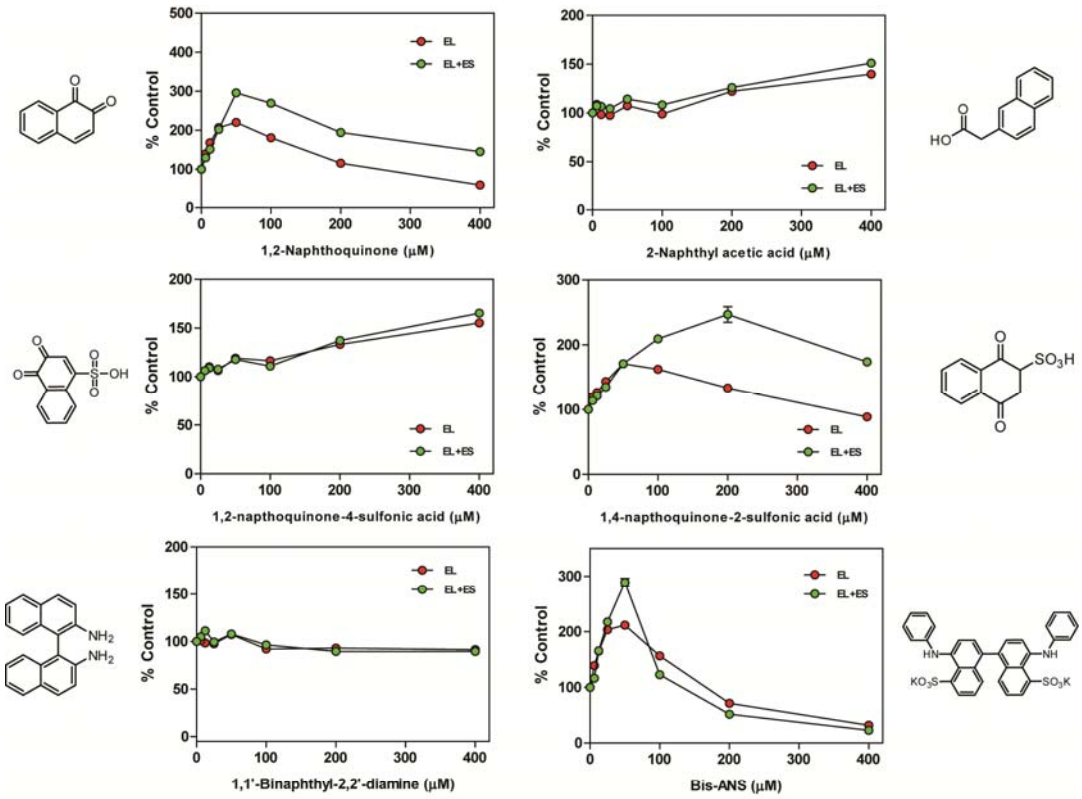

Appendix 6.4.3 The dose-dependent effect of selected "hits" from the GroEL and GroEL/ES high throughput screen. The concentration of GroEL was 0.35 μM, GroES was 0.18 μM, ATP was 1 mM, and the incubation condition was 37°C, 3 hours.The OD_{620} value of the control, buffer+specific compound at indicated concentration+ATP (with 3 hr 37°C incubation), was subtracted out from each data point. Each data point is the average of triplicates and the error bars represent the standard error of the mean.

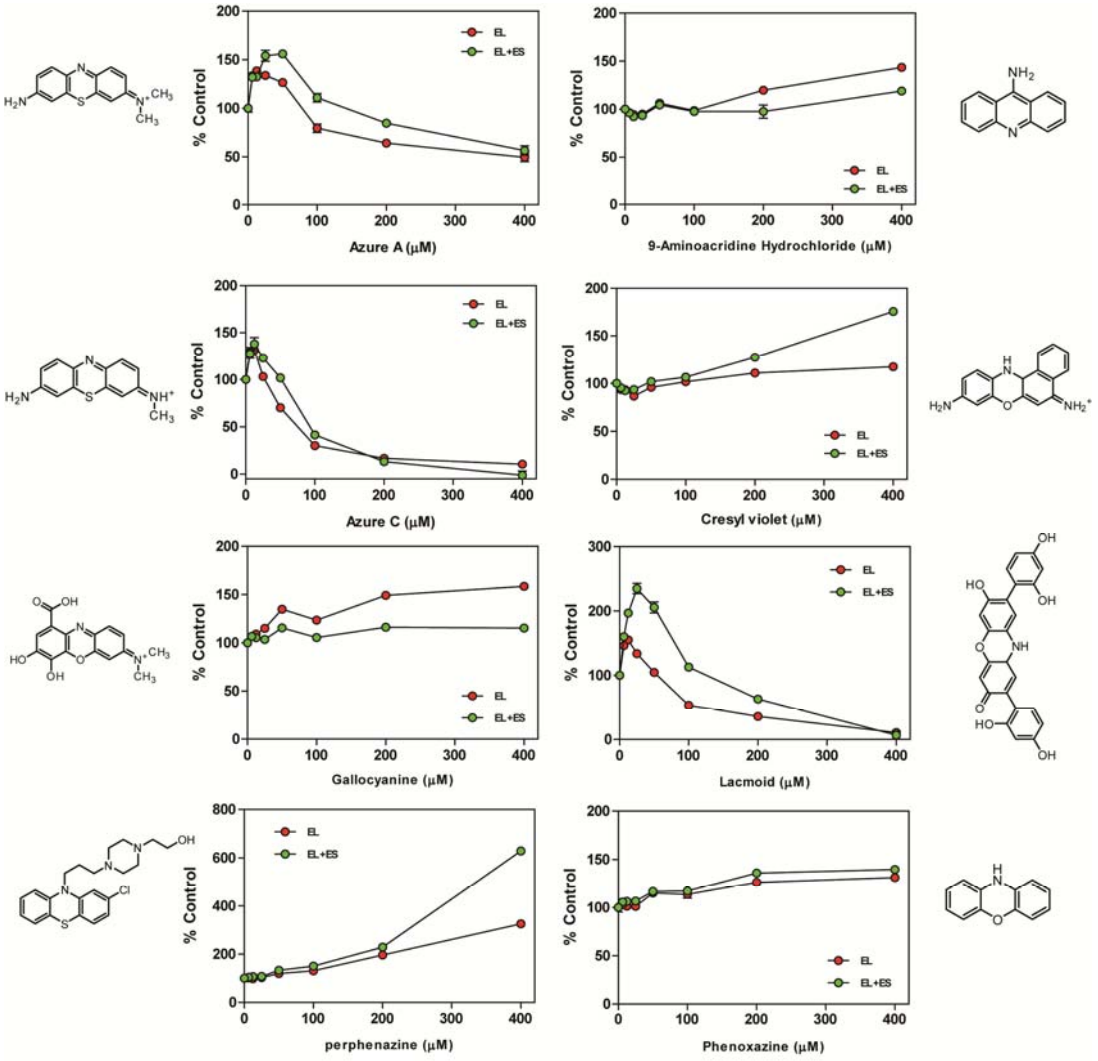

Appendix 6.4.3 The dose-dependent effect of selected "hits" from the GroEL and GroEL/ES high throughput screen. The concentration of GroEL was 0.35 μM, GroES was 0.18 μM, ATP was 1 mM, and the incubation condition was 37°C, 3 hours.The OD_{620} value of the control, buffer+specific compound at indicated concentration+ATP (with 3 hr 37°C incubation), was subtracted out from each data point. Each data point is the average of triplicates and the error bars represent the standard error of the mean.

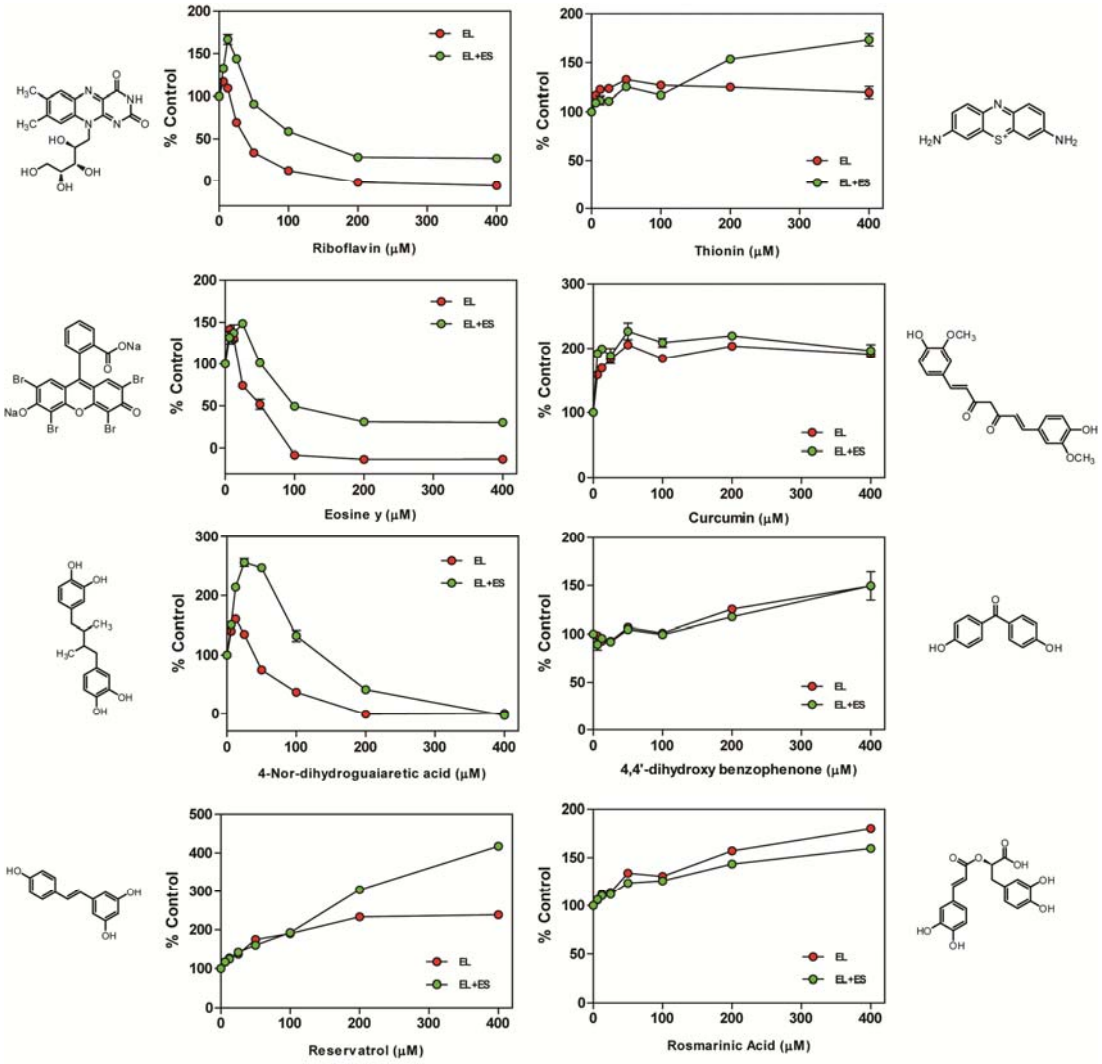

Appendix 6.4.3 The dose-dependent effect of selected "hits" from the GroEL and GroEL/ES high throughput screen. The concentration of GroEL was 0.35 μM, GroES was 0.18 μM, ATP was 1 mM, and the incubation condition was 37°C, 3 hours.The OD_{620} value of the control, buffer+specific compound at indicated concentration+ATP (with 3 hr 37°C incubation), was subtracted out from each data point. Each data point is the average of triplicates and the error bars represent the standard error of the mean.

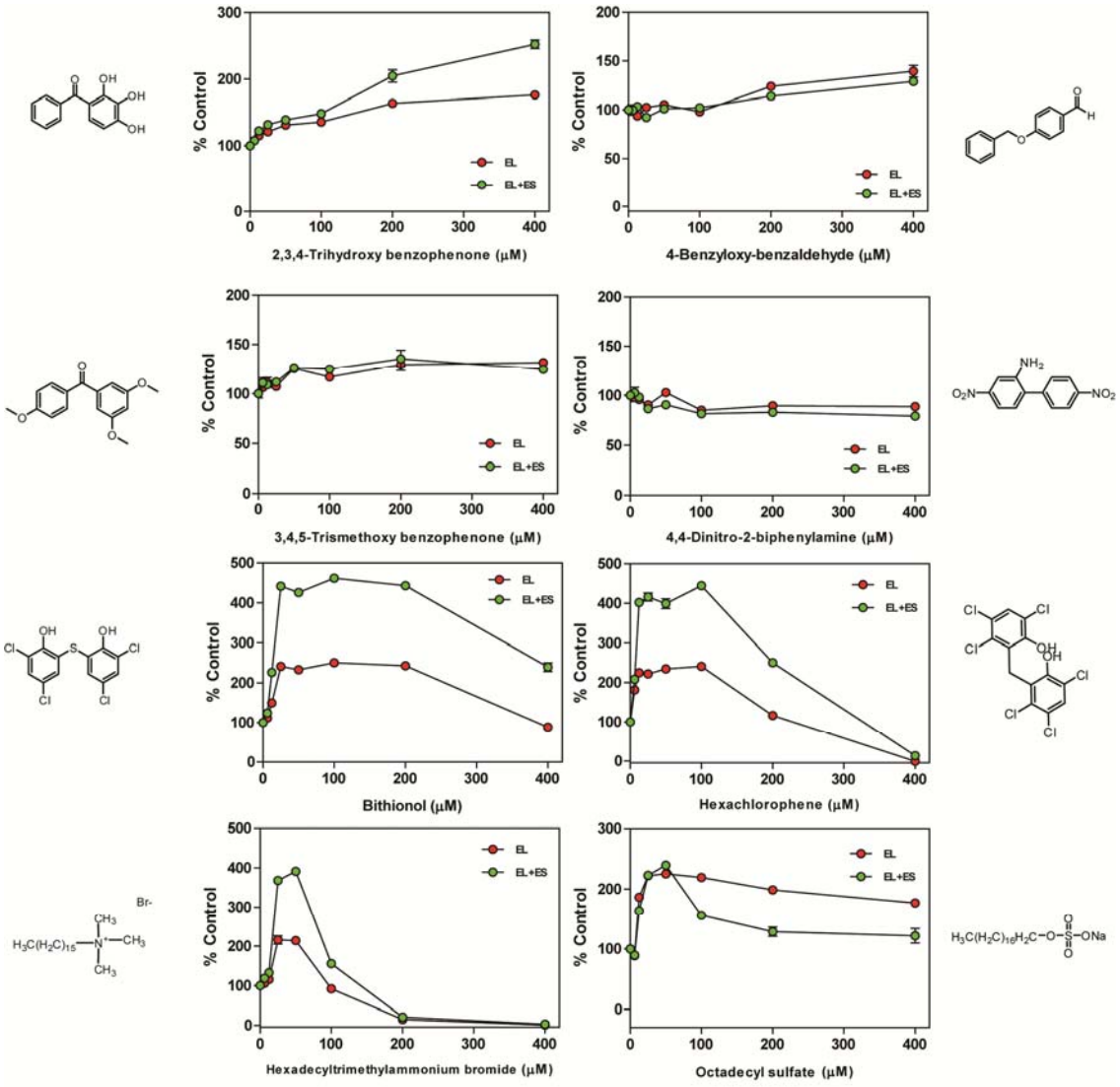

Appendix 6.4.3 The dose-dependent effect of selected "hits" from the GroEL and GroEL/ES high throughput screen. The concentration of GroEL was 0.35 μM, GroES was 0.18 μM, ATP was 1 mM, and the incubation condition was 37°C, 3 hours.The OD_{620} value of the control, buffer+specific compound at indicated concentration+ATP (with 3 hr 37°C incubation), was subtracted out from each data point. Each data point is the average of triplicates and the error bars represent the standard error of the mean.

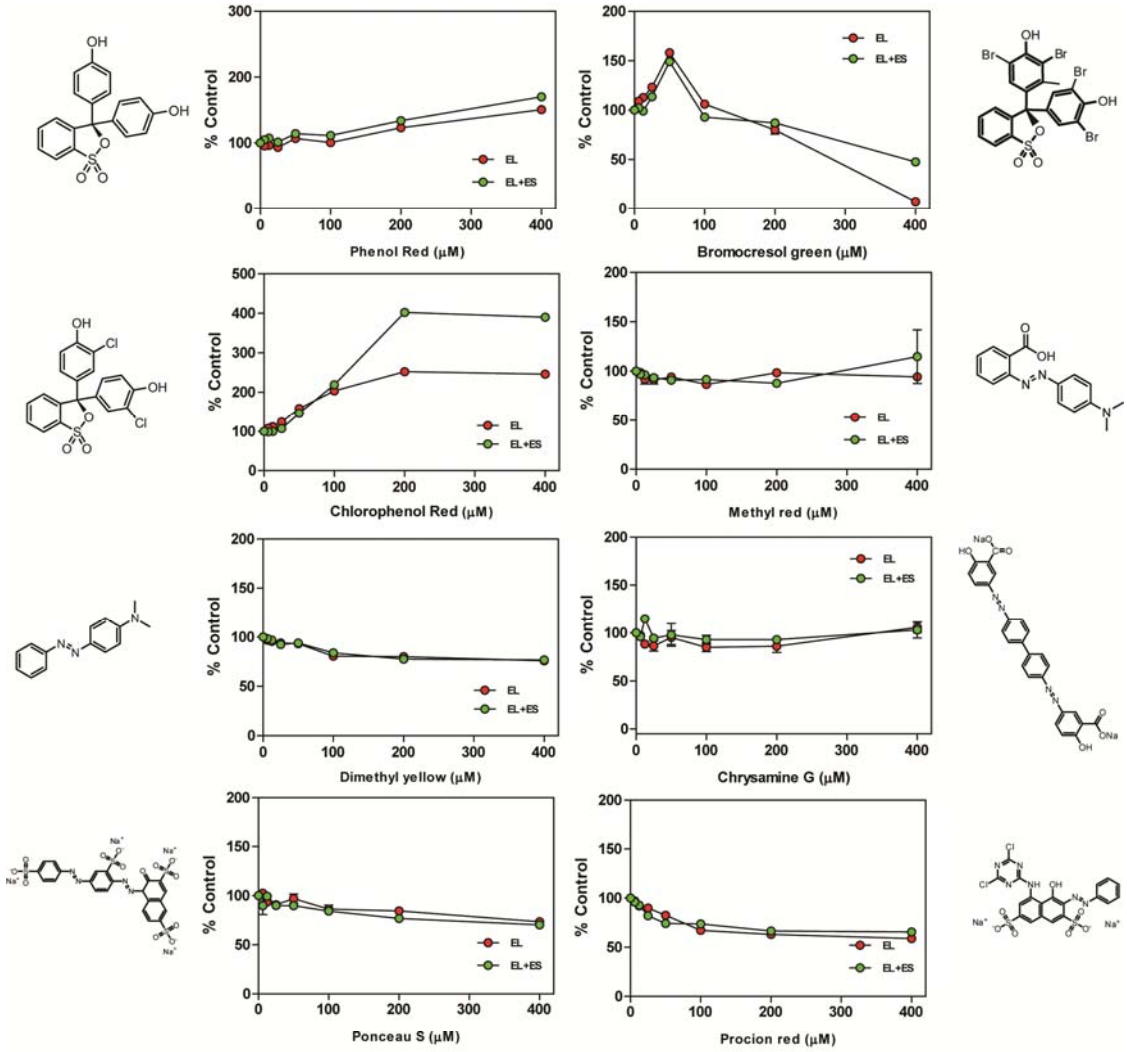

Appendix 6.4.3 The dose-dependent effect of selected "hits" from the GroEL and GroEL/ES high throughput screen. The concentration of GroEL was 0.35 μM, GroES was 0.18 μM, ATP was 1 mM, and the incubation condition was 37°C, 3 hours.The OD_{620} value of the control, buffer+specific compound at indicated concentration+ATP (with 3 hr 37°C incubation), was subtracted out from each data point. Each data point is the average of triplicates and the error bars represent the standard error of the mean.

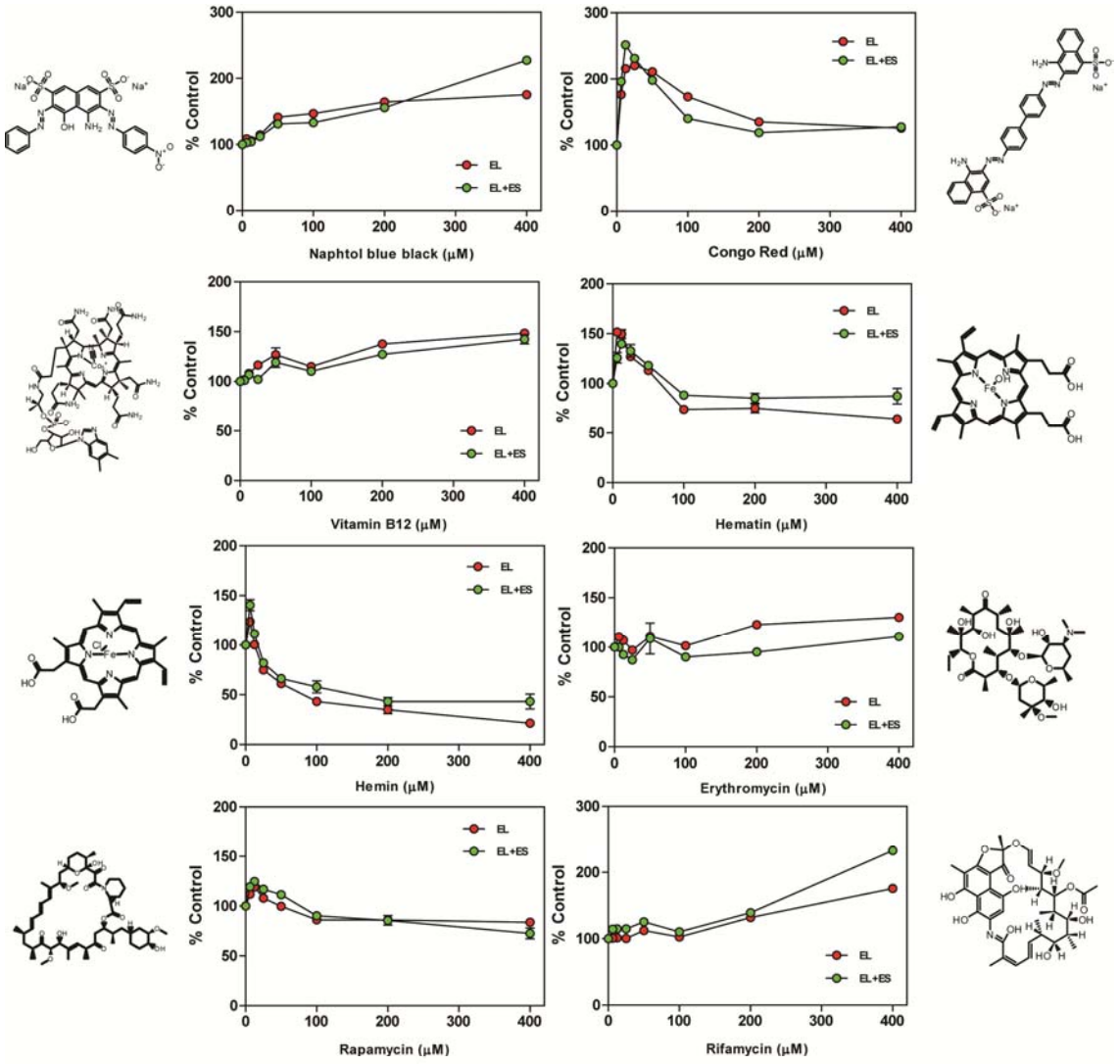

Appendix 6.4.3 The dose-dependent effect of selected "hits" from the GroEL and GroEL/ES high throughput screen. The concentration of GroEL was 0.35 μM, GroES was 0.18 μM, ATP was 1 mM, and the incubation condition was 37°C, 3 hours.The OD_{620} value of the control, buffer+specific compound at indicated concentration+ATP (with 3 hr 37°C incubation), was subtracted out from each data point. Each data point is the average of triplicates and the error bars represent the standard error of the mean.

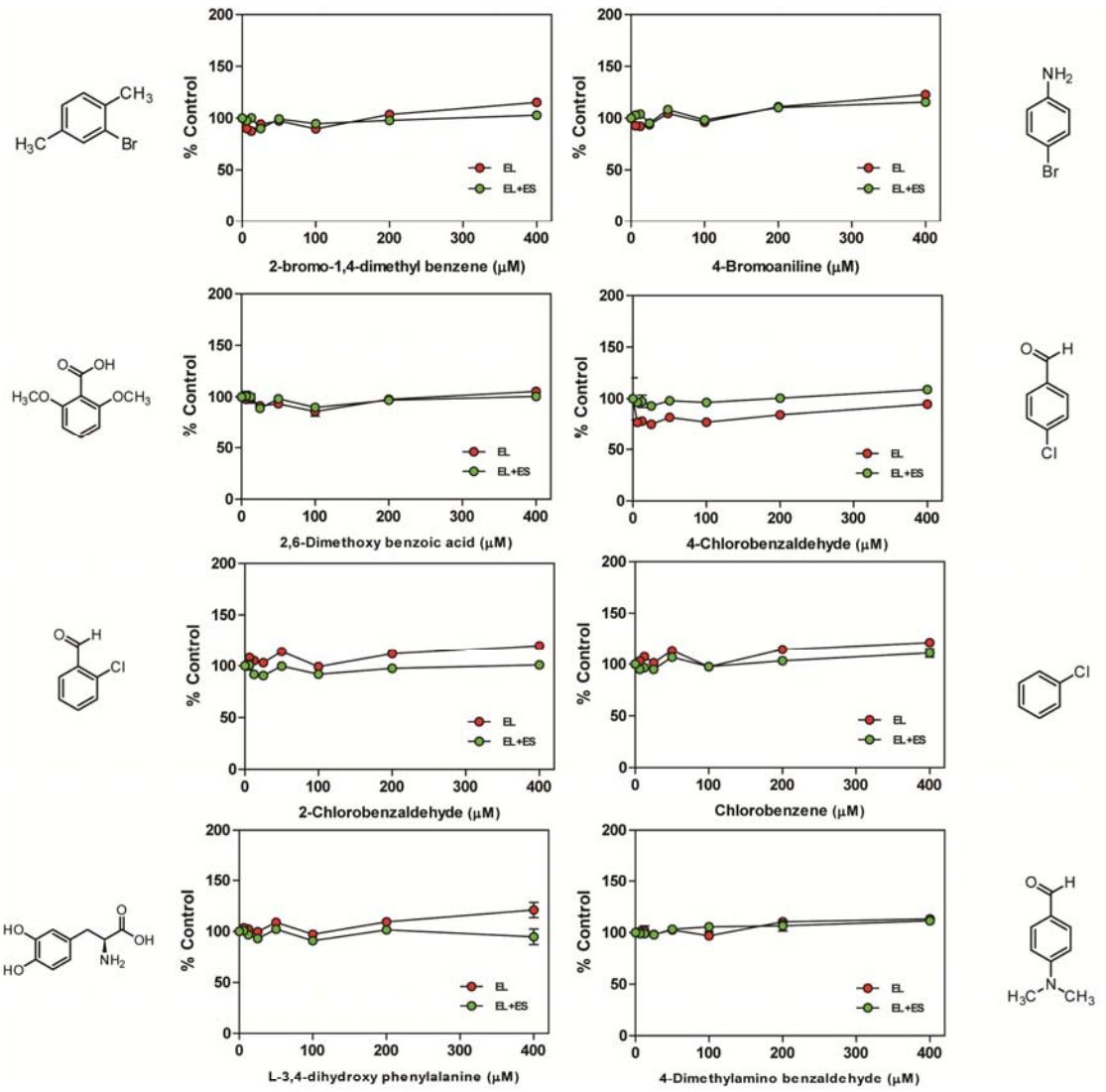

Appendix 6.4.3 The dose-dependent effect of selected "hits" from the GroEL and GroEL/ES high throughput screen. The concentration of GroEL was 0.35 μM, GroES was 0.18 μM, ATP was 1 mM, and the incubation condition was 37°C, 3 hours.The OD_{620} value of the control, buffer+specific compound at indicated concentration+ATP (with 3 hr 37°C incubation), was subtracted out from each data point. Each data point is the average of triplicates and the error bars represent the standard error of the mean.

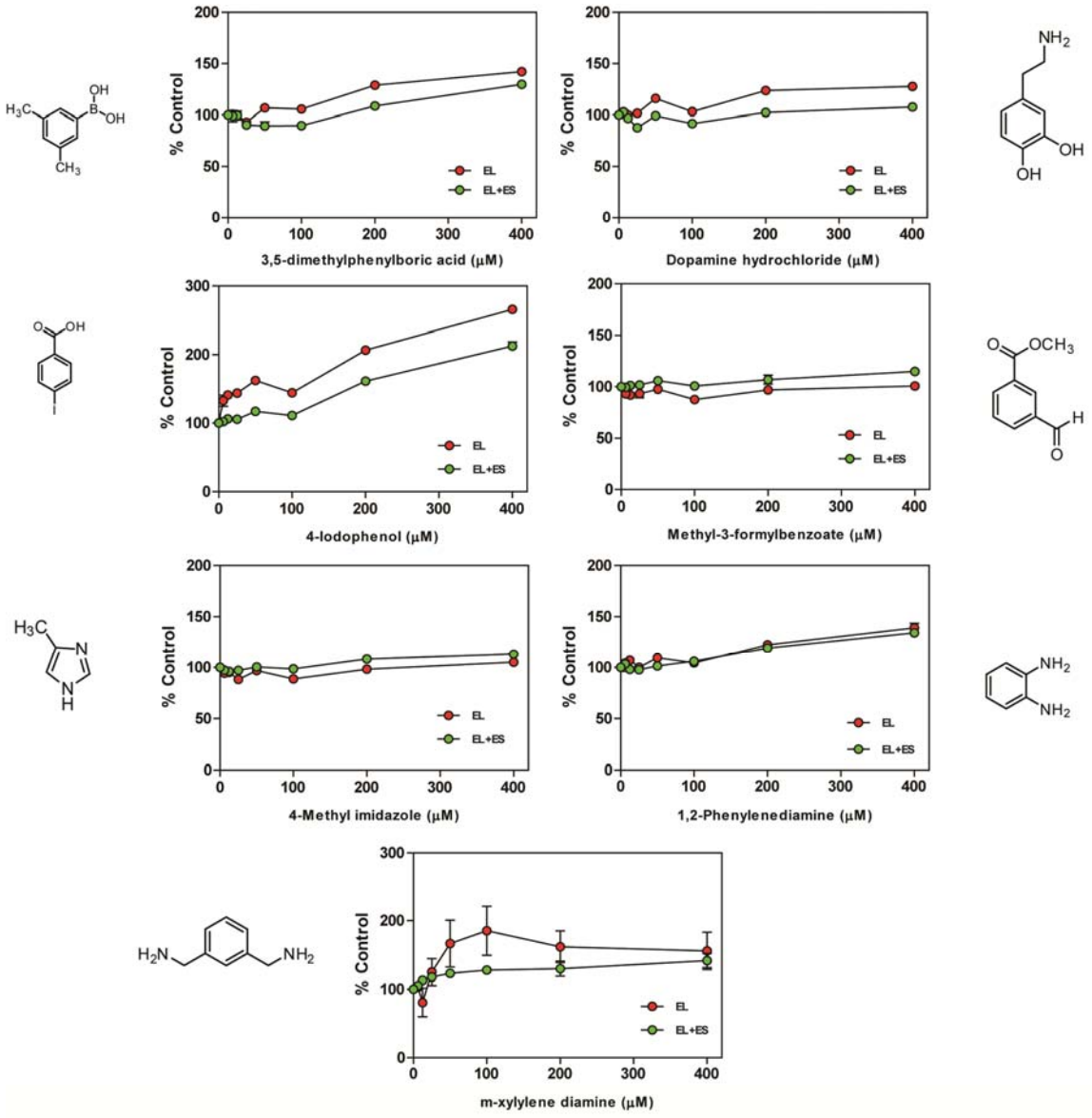

Appendix 6.4.3 The dose-dependent effect of selected "hits" from the GroEL and GroEL/ES high throughput screen. The concentration of GroEL was 0.35 μM, GroES was 0.18 μM, ATP was 1 mM, and the incubation condition was 37°C, 3 hours.The OD_{620} value of the control, buffer+specific compound at indicated concentration+ATP (with 3 hr 37°C incubation), was subtracted out from each data point. Each data point is the average of triplicates and the error bars represent the standard error of the mean.

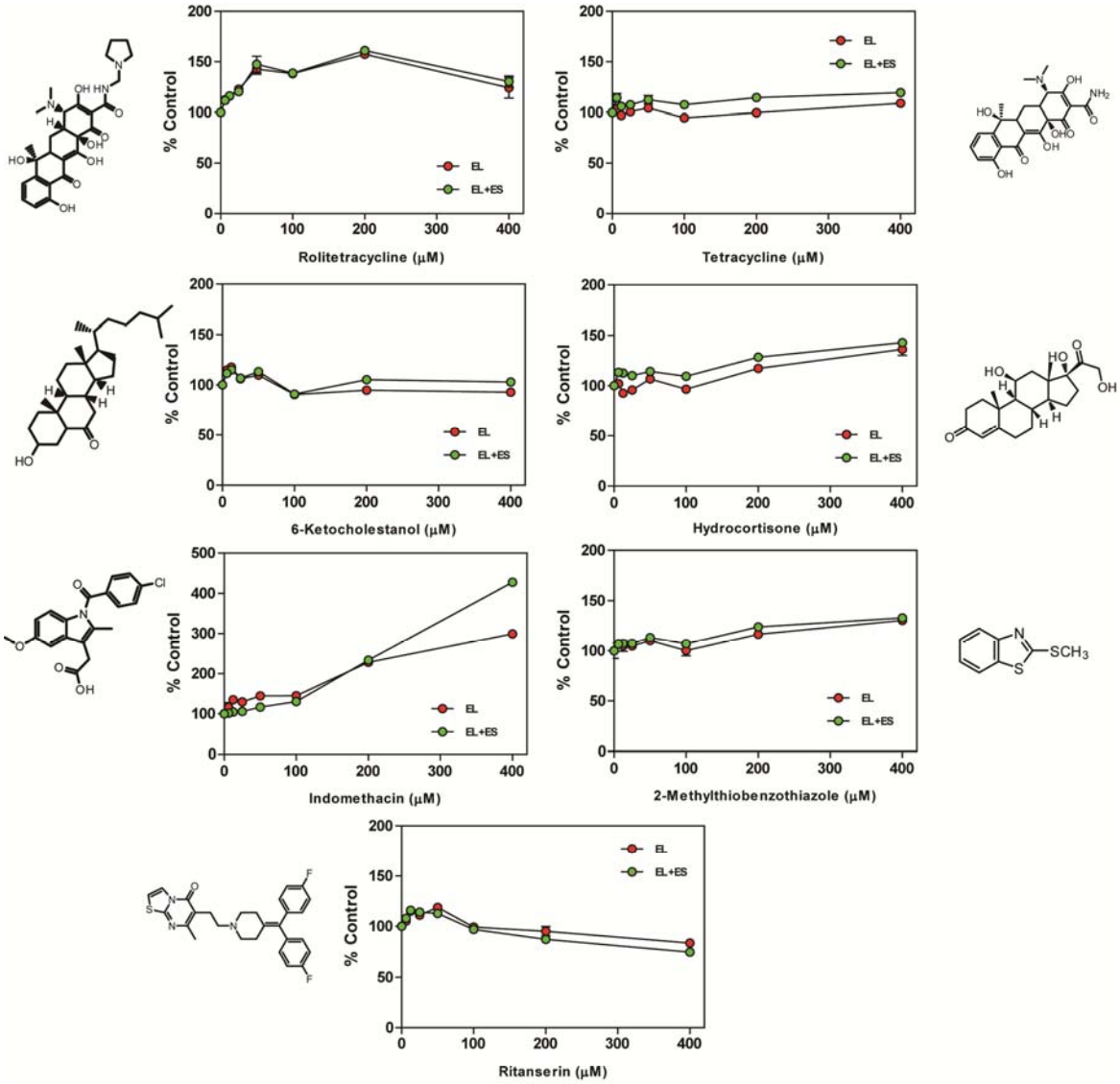

Appendix 6.4.3 The dose-dependent effect of selected "hits" from the GroEL and GroEL/ES high throughput screen. The concentration of GroEL was 0.35 μM, GroES was 0.18 μM, ATP was 1 mM, and the incubation condition was 37°C, 3 hours.The OD_{620} value of the control, buffer+specific compound at indicated concentration+ATP (with 3 hr 37°C incubation), was subtracted out from each data point. Each data point is the average of triplicates and the error bars represent the standard error of the mean.

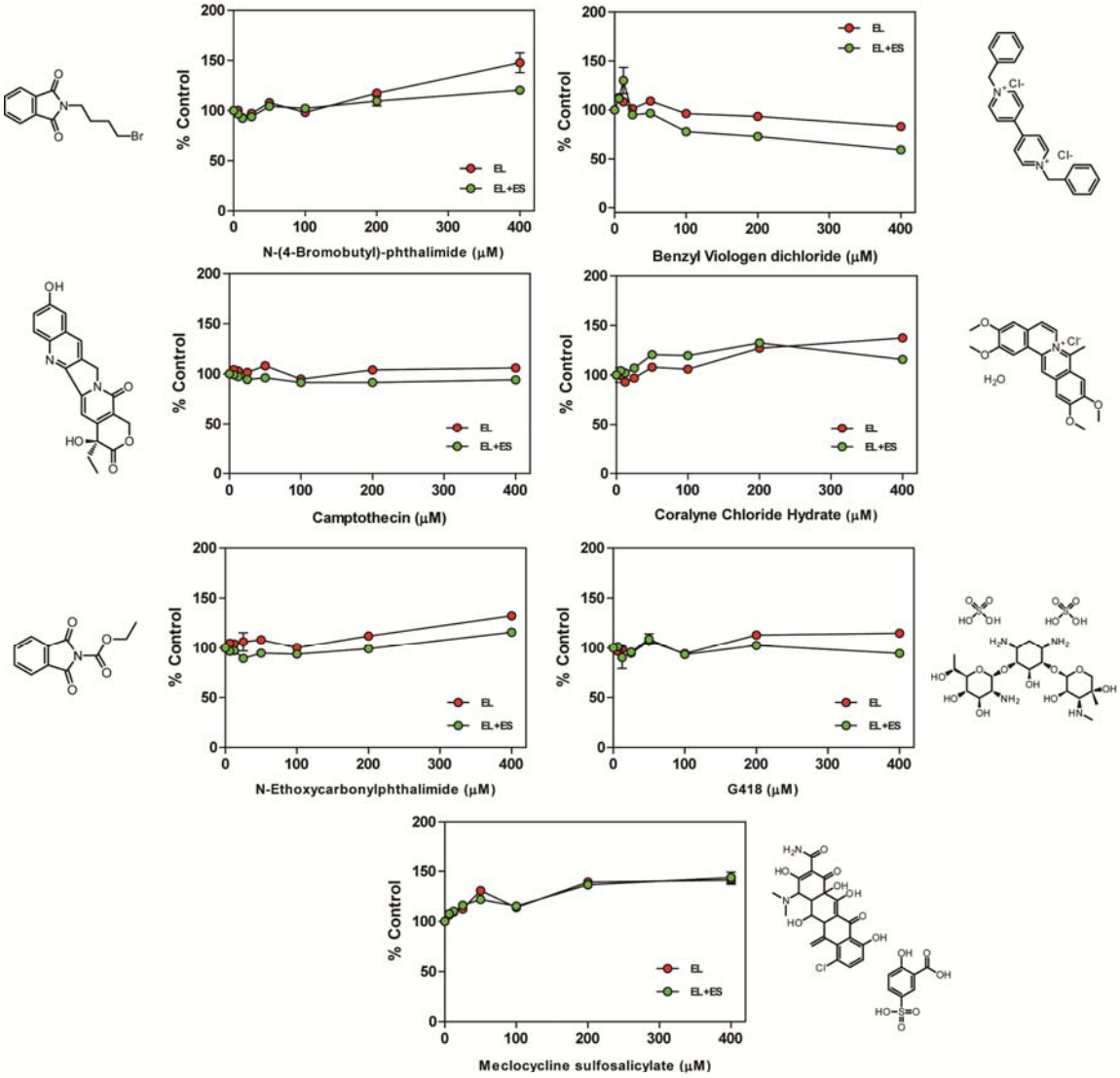

Appendix 6.4.3 The dose-dependent effect of selected "hits" from the GroEL and GroEL/ES high throughput screen. The concentration of GroEL was 0.35 μM, GroES was 0.18 μM, ATP was 1 mM, and the incubation condition was 37°C, 3 hours.The OD_{620} value of the control, buffer+specific compound at indicated concentration+ATP (with 3 hr 37°C incubation), was subtracted out from each data point. Each data point is the average of triplicates and the error bars represent the standard error of the mean.

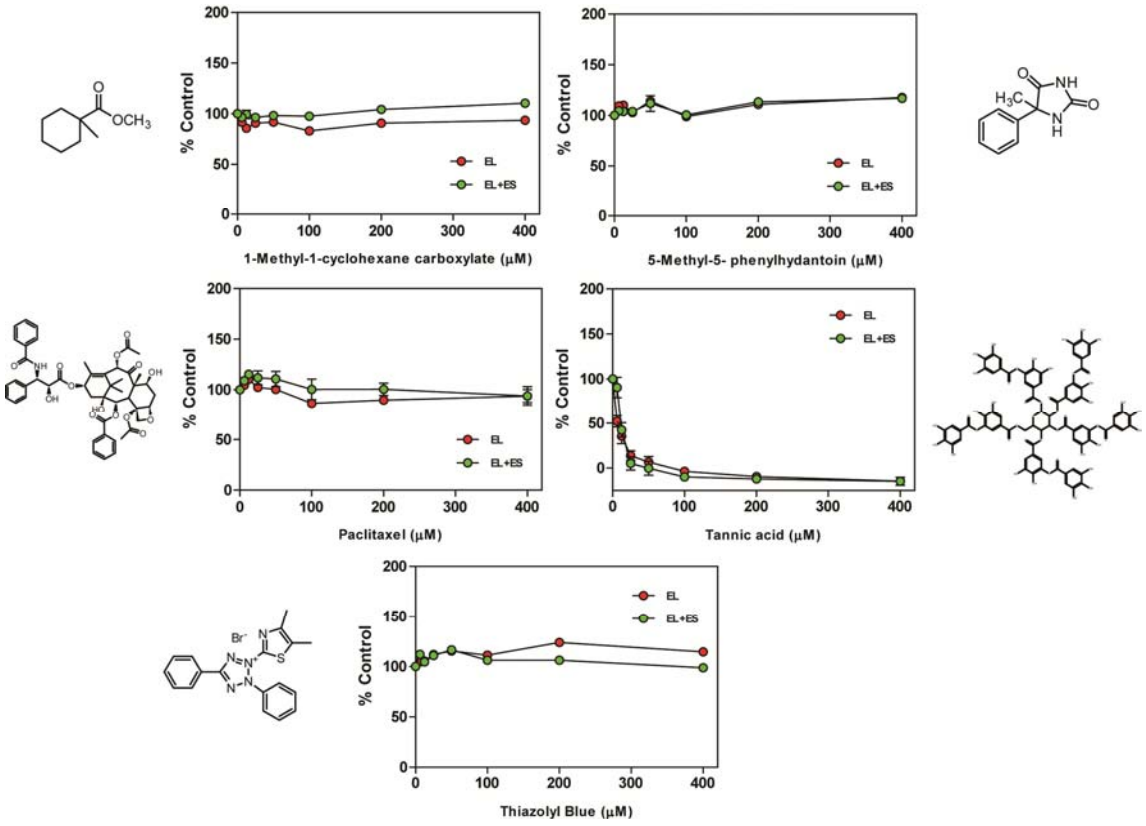

Appendix 6.4.3 The dose-dependent effect of selected "hits" from the GroEL and GroEL/ES high throughput screen. The concentration of GroEL was 0.35 μM, GroES was 0.18 μM, ATP was 1 mM, and the incubation condition was 37°C, 3 hours.The OD_{620} value of the control, buffer+specific compound at indicated concentration+ATP (with 3 hr 37°C incubation), was subtracted out from each data point. Each data point is the average of triplicates and the error bars represent the standard error of the mean.

6.5 References

1. Koren, J., 3rd, et al., *Facilitating Akt clearance via manipulation of Hsp70 activity and levels.* J Biol Chem, 2010. **285**(4): p. 2498-505.
2. Jinwal, U.K., et al., *Hsc70 rapidly engages tau after microtubule destabilization.* J Biol Chem, 2010. **285**(22): p. 16798-805.
3. Jinwal, U.K., et al., *Chemical manipulation of hsp70 ATPase activity regulates tau stability.* J Neurosci, 2009. **29**(39): p. 12079-88.
4. Horwich, A.L., et al., *Two families of chaperonin: physiology and mechanism.* Annu Rev Cell Dev Biol, 2007. **23**: p. 115-45.
5. Mayer, M.P., *Gymnastics of molecular chaperones.* Mol Cell, 2010. **39**(3): p. 321-31.
6. Xiao, J., et al., *Structural characterization of the ATPase reaction cycle of endosomal AAA protein Vps4.* J Mol Biol, 2007. **374**(3): p. 655-70.
7. Xu, Z., A.L. Horwich, and P.B. Sigler, *The crystal structure of the asymmetric GroEL-GroES-(ADP)7 chaperonin complex.* Nature, 1997. **388**(6644): p. 741-50.
8. Houry, W.A., et al., *Identification of in vivo substrates of the chaperonin GroEL.* Nature, 1999. **402**(6758): p. 147-54.
9. Hunt, J.F., et al., *The crystal structure of the GroES co-chaperonin at 2.8 A resolution.* Nature, 1996. **379**(6560): p. 37-45.
10. Jewett, A.I. and J.E. Shea, *Reconciling theories of chaperonin accelerated folding with experimental evidence.* Cell Mol Life Sci, 2010. **67**(2): p. 255-76.
11. Kerner, M.J., et al., *Proteome-wide analysis of chaperonin-dependent protein folding in Escherichia coli.* Cell, 2005. **122**(2): p. 209-20.
12. Hartl, F.U. and M. Hayer-Hartl, *Converging concepts of protein folding in vitro and in vivo.* Nat Struct Mol Biol, 2009. **16**(6): p. 574-81.

Chapter 7

Future Directions and Conclusions

7.1 Abstract

In Chapter 4 and 5, we concluded that all aspects of Hsp70 chaperone activities are not represented by ATP turnover. Thus, we anticipate the need to develop new screening assays against the Hsp70 chaperone system. In this Chapter, we discuss potential avenues towards that goal. Specifically, we explore the potential benefits of studying disease-related Hsp70-co-chaperone complexes using genetic and proteomic-based methods. Next, we discuss ways to develop Förster resonance energy transfer (FRET)-based assays that allow us to find compounds that affect the interactions between Hsp70 and its various co-chaperones or compounds that "freeze" Hsp70s in certain disease-related conformations. We also discuss how protein microarrays might be used to identify the specific peptide substrates of each Hsp70 or J protein homolog to enable screens for compounds that block the binding of the specific peptide ligand to target protein using fluorescent polarization-based assays. Finally, we describe the

possible use of substrate degradation assay to discover compounds that modulate Hsp70 chaperone activities. In summary, my thesis projects are our first step in targeting human disease through chemical manipulation of Hsp70 chaperone systems, and further studies toward this direction might leads to the discovery of new drugs that alleviate cancers or neurodegenerative diseases.

7.2 Future Directions – Developing New Screening Methods against Hsp70 Chaperone Complexes

7.2.1 Identifying the Target Human Hsp70 Complexes against Different Diseases

As we mentioned in Chapter 1, human Hsp70 chaperone system is a target for cancer and neurodegenerative diseases; however, its functional complexity poses a challenge for drug discovery. Specifically, Hsp70s performs multiple, different cellular activities and interacts with different sets of co-chaperones, including ~40 J proteins, nucleotide exchange factors, and TPR-domain containing proteins [1-4]. Therefore, the first step in targeting human Hsp70 system is likely to identify the specific Hsp70-co-chaperone complexes that are best linked to diseases. Towards that goal, expressing Hsp70 co-chaperones in cultured cells and identifying the ones that block degradation of Hsp70 substrates, such as Akt and tau proteins [5, 6], or trigger the aggregation of

polyglutamine-containing proteins might be used to focus attention on specific co-chaperone partners. Alternatively, we might be able to use an unbiased proteomics strategy to compare the different Hsp70 complexes formed in normal and diseased cells. For example, in chapter 5, we identified two Hsc70 mutants that trigger tau degradation when overexpressed; possibly, by comparing their "interactome" with those of wild-type Hsc70, we can identify Hsp70 complexes that are important for tau degradation. By combining both genetic and proteomic strategies, we might identify the drug target complexes of Hsp70 for each specific disease. In turn, these complexes would be good candidates for future chemical screening efforts, using the assays discussed in this thesis. Implicit in this argument is that different complexes can be selectively targeted. This hypothesis remains to be tested.

7.2.2 Förster Resonance Energy Transfer-based Screening Assays

One way to find compounds that target specific co-chaperone / chaperone complexes might be through the "gray-box" screening strategy we proposed in Chapter 3; namely, compounds that modulate the ATPase activity of the disease-related Hsp70 chaperone complexes, but not the "normal" complexes might be found. This strategy worked well for ATPase stimulators like J proteins, because any compounds that block the Hsp70-J

interaction will significantly inhibit ATP turnover and produce a measurable signal. Unfortunately, many potentially important co-chaperones, such as CHIP and BAGs only mildly affect Hsp70's ATPase activity (S. Patury and J. E. Gestwicki unpublished results).

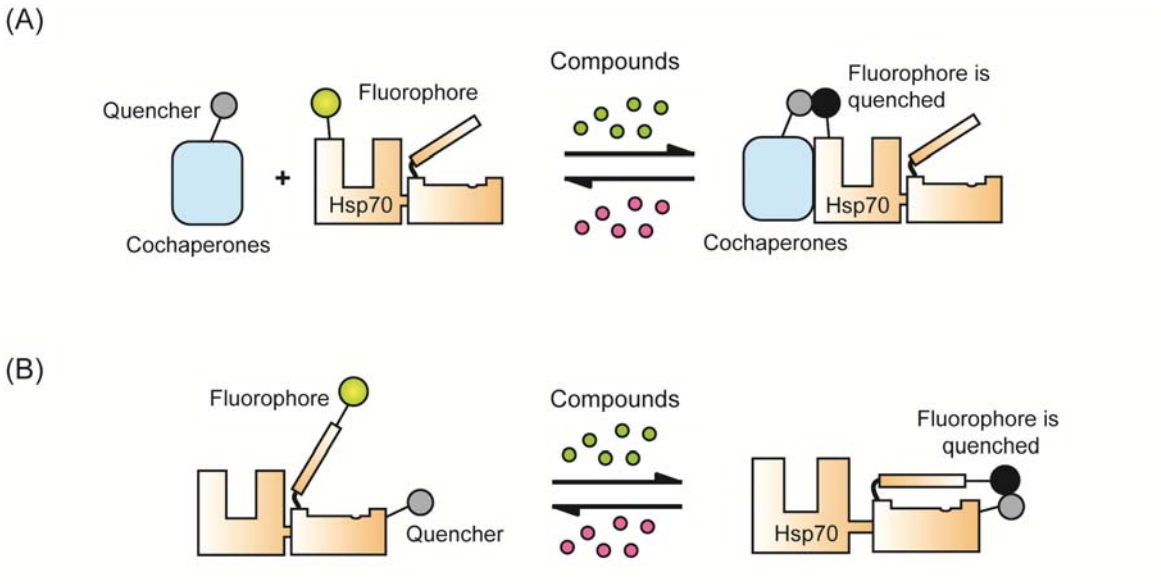

Figure 7.1 Designing new FRET-based assays. (A) We can attach a fluorophore donor on Hsp70 and an acceptor chromophore (quencher) on selected cochaperones and screen for compounds that affect the fluorescence quenching effects caused by protein-protein interactions. (B) We can also attach FRET pairs between different locations of Hsp70s, in this case between the lid and SBD, and screen for compounds that "freeze" Hsp70 in disease-related conformations.

Moreover, some co-chaperones have their own ATPase activity, such as the large T antigen of SV40 (a J protein) [7]. Therefore, we anticipate the need to develop new assays that permit discovery of compounds that modulate the physical interactions with cochaperones to supplement the ATPase approach.

Förster resonance energy transfer (FRET) refers to the transfer of energy from the donor chromophore to the acceptor chromophore through nonradiative dipole-dipole coupling. For FRET to occur, the emission spectra of the donor must overlap with the absorbance spectra of acceptor [8]. FRET pairs are useful for detecting protein-protein interactions, because they are sensitive to the distance between donor and acceptor chromophore and, thus, can be used as "molecular rulers" for two protein molecules [8]. We propose that labeling Hsp70 and its co-chaperones with FRET pairs will enable screening for compounds that inhibit or enhance their interactions (**Figure 7.1A**). In fact, in Chapter 3 we successfully applied the FRET-based method to prove that myricetin dose-dependently reduced the affinity between DnaK and DnaJ. Alternatively, FRET can be used to detect intra-molecular conformational changes for flexible proteins like Hsp70s. A recent report by Mapa et al. used FRET pairs on NBD/SBD and Lid/SBD to characterize the domain movements of yeast mitochondria Hsp70, Ssc1, and *E. coli* DnaK under different nucleotide states [9]. In Chapter 5, we found that the two Hsc70 mutants that triggered tau degradation, unlike negative controls, preferred to assume ADP-bound or "lid-closed" state even with excess ATP. Based on this result, we might discover compounds that trigger tau degradation by designing a FRET pair between the lid and SBD of Hsc70 and screen for compounds that stabilize its "lid-closed" conformation

under high ATP concentration (**Figure 7.1B**). Based on my past few years of studying the Hsp70 system, I think that FRET-based methods might be particularly powerful ways of investigating regulation in these proteins and screening for inhibitors.

7.2.3 Fluorescence Polarization-based Assay

The human genome contains more than 40 J proteins, and it is believed that each J protein binds and presents a different subset of substrates and thereby "specializes" the function of Hsp70s [1]. Although J proteins are suitable for the "gray-box screening" strategies we proposed, compounds discovered through this method might non-specifically interfere with all Hsp70-J protein interaction, because they all interact via a highly conserved J domain [1]. Thus, to specifically target J proteins, we might need to find compounds that target other, more specific functions; among them, the substrate-binding activities are likely the most "screenable". Prior to those studies; however, we will need to better understand the substrate-J interaction. In the literature, peptide microarrays have been used to scan for consensus J protein-binding peptide sequences [10, 11] (**Figure 7.2A**). We propose that these tight-binding peptides can be labeled and used as fluorescence polarization (FP) probes against the selected J protein, facilitating identification of compounds that block the specific binding between the

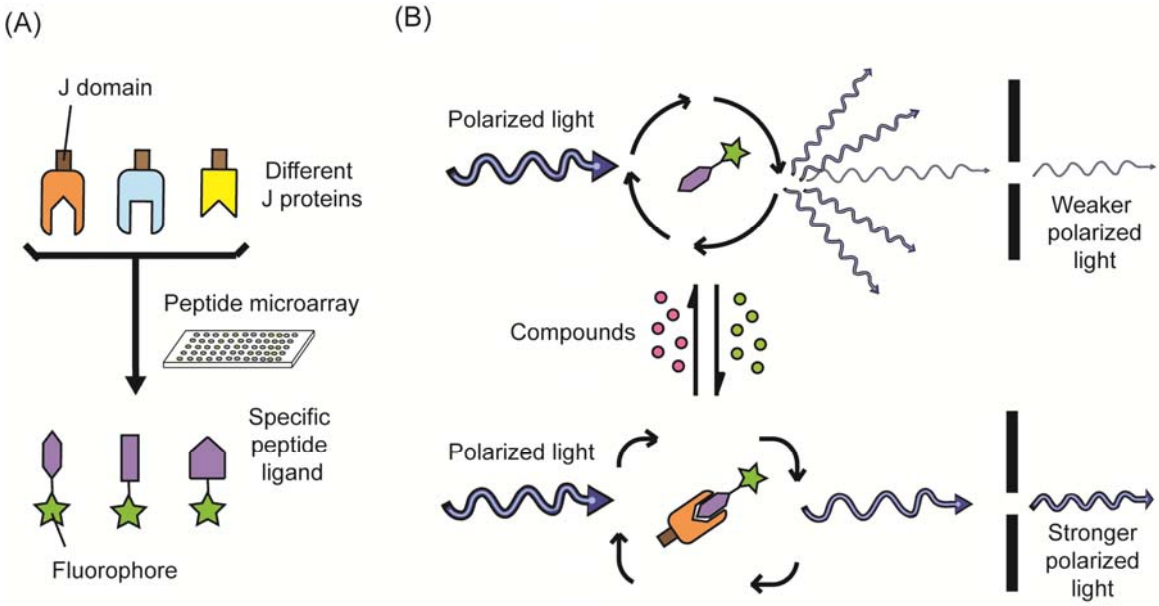

Figure 7.2 Fluorescent Polarization (FP)-based screening assays. (A) We can identify the specific peptide substrates of each J protein by peptide microarray, and labeled the selected peptides by fluorophore to use as probes against the target J proteins. (B) We can screen for compounds that block the interactions between the labeled peptide substrates and the target J proteins by fluorescent polarization assay. When compounds inhibit the peptide-J protein interaction, it will reduce the level of emitted polarized light, and vise versa.

peptide and J protein (**Figure 7.2B**). Briefly, FP assays detect the binding of small fluorophore-labeled ligands to their protein targets using plane-polarized light [12]. When a fluorophore is excited, the relative orientation of its emitted light will depend on whether it is bound or free in solution. FP-based assays are frequently used for HTS because of its high sensitivity [12]. Therefore, new FP-based HTS assays against J proteins might allow us to efficiently discover compounds that specifically inhibit the substrate-binding activities of disease-related J proteins.

7.2.4 Substrate Degradation Assay

In Chapter 5, we discovered that luciferase-refolding assays were the most predictive of tau degradation. The ability of this assay to predict chaperone biology is probably due to its ability to simultaneously measure multiple activities, including holdase, foldase

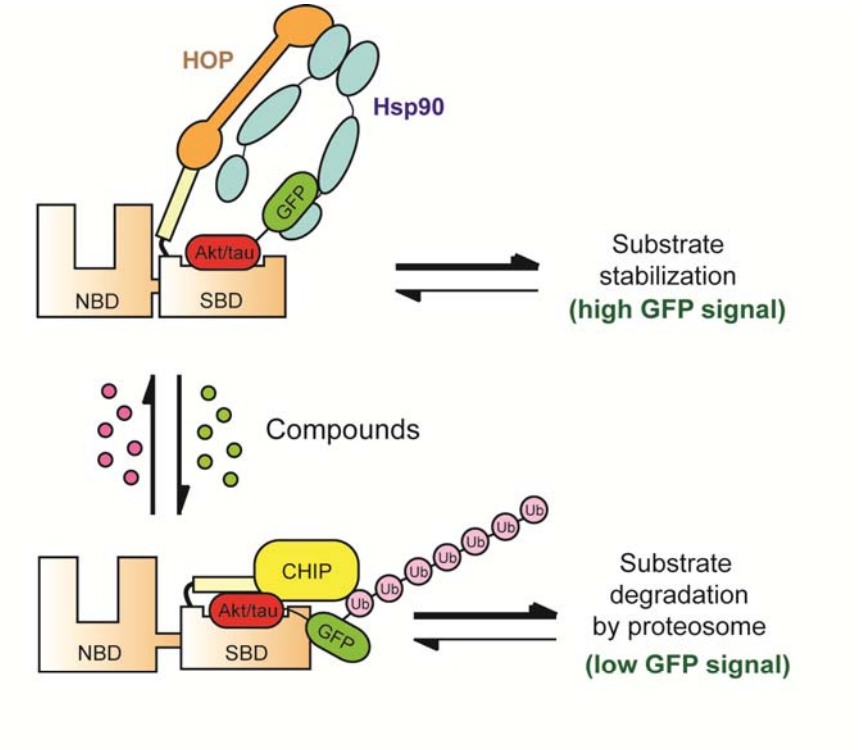

Figure 7.3 Substrate-degradation assay. We can label the Hsp70 substrate, such as Akt or tau, with GFP-tag and screen for compounds that trigger or inhibit their degradation by the changes in GFP fluorescence signal. This assay can be performed both in cultured cells that overexpress Hsp70 or by *in vitro* reconstituted systems using rabbit reticular lysate. We can also randomly label substrates with fluorophore and detect the proteolysis by fluorescent polarization assay, in which the un-digested labeled substrates will emit more polarized light than the free fluorophores.

activities and proper cooperation with co-chaperones. However, most refolding assays are vulnerable to artifacts, because typical small molecules are likely to nonspecifically bind to the exposed hydrophobic regions of the denatured protein. Additionally, the

enzymatic activity of the most commonly used refolding substrate, luciferase, is inhibited by many compounds. In fact, most Hsp70 ATPase inhibitors we identified were also luciferase inhibitors (L. Chang unpublished observations). This finding suggests that we need new assays that measure global chaperone activities that are more robust for chemical screening. One possible method is to screen for compounds that stimulate or inhibit the degradation of the known protein substrates of Hsp70 in cells (**Figure 7.3**). For example, we found that our Hsp70 inhibitors trigger the degradation of tau and Akt in an Hsp70-dependent process [5, 6, 13]. Thus, we might be able to label tau or Akt with a green fluorescent protein (GFP) tag to allow screening for compounds that induce its degradation or accumulation in human cell lines (**Figure 7.3**). Alternatively, we can do this experiment in a reconstitute *in vitro* system by adding purified Hsp70 and GFP-labeled tau or Akt to reticular cell lysate and screen for compounds that affect substrate degradation. We might also be able to detect substrate degradation using FP as described in 7.2.3 if we used measured release of fluorescence probes during substrate proteolysis. We expect that these more complex assays may have the advantages in measuring multiple chaperone activities.

7.3 Conclusions

When I first started as a graduate student, there were no HTS methods available for studying Hsp70 activity. This was a major technical hurdle in developing Hsp70 inhibitors. In this thesis, we developed the first economic and straightforward ATPase-based HTS assay against the Hsp70 system. In this Chapter, we showed that it is easily adapted to screen against other ATPases. We also proposed and validated the idea of “gray-box screening” strategy which allows us to find compounds that target specific Hsp70-chaperone complexes. Using myricetin as a model compound, we established a series of secondary assays that allows us to streamline the future hit characterization processes. Finally, using point mutants of DnaK and Hsc70, we discovered that the ATP-based screen, although has its merit, might overlook compounds that modulate other functional aspects of Hsp70s. Better understanding of the complicate Hsp70 chaperone system and further development of new screening strategies may allow us to cure neurodegenerative diseases, cancers, and many other Hsp70-related diseases through chemically manipulating the Hsp70 chaperone system.

7.4 References

1. Kampinga, H.H. and E.A. Craig, *The HSP70 chaperone machinery: J proteins as drivers of functional specificity.* Nat Rev Mol Cell Biol, 2010. **11**(8): p. 579-92.
2. Kabbage, M. and M.B. Dickman, *The BAG proteins: a ubiquitous family of chaperone regulators.* Cell Mol Life Sci, 2008. **65**(9): p. 1390-402.
3. Tzankov, S., et al., *Functional divergence between co-chaperones of Hsc70.* J Biol Chem, 2008. **283**(40): p. 27100-9.
4. Smith, D.F., *Tetratricopeptide repeat cochaperones in steroid receptor complexes.* Cell Stress Chaperones, 2004. **9**(2): p. 109-21.
5. Koren, J., 3rd, et al., *Facilitating Akt clearance via manipulation of Hsp70 activity and levels.* J Biol Chem, 2010. **285**(4): p. 2498-505.
6. Jinwal, U.K., et al., *Chemical manipulation of hsp70 ATPase activity regulates tau stability.* J Neurosci, 2009. **29**(39): p. 12079-88.
7. Giacherio, D. and L.P. Hager, *A poly(dT)-stimulated ATPase activity associated with simian virus 40 large T antigen.* J Biol Chem, 1979. **254**(17): p. 8113-6.
8. Roda, A., et al., *Nanobioanalytical luminescence: Forster-type energy transfer methods.* Anal Bioanal Chem, 2009. **393**(1): p. 109-23.
9. Mapa, K., et al., *The conformational dynamics of the mitochondrial Hsp70 chaperone.* Mol Cell, 2010. **38**(1): p. 89-100.
10. Kota, P., et al., *Identification of a consensus motif in substrates bound by a Type I Hsp40.* Proc Natl Acad Sci U S A, 2009. **106**(27): p. 11073-8.
11. Fan, C.Y., et al., *Exchangeable chaperone modules contribute to specification of type I and type II Hsp40 cellular function.* Mol Biol Cell, 2004. **15**(2): p. 761-73.
12. Smith, D.S. and S.A. Eremin, *Fluorescence polarization immunoassays and related methods for simple, high-throughput screening of small molecules.* Anal Bioanal Chem, 2008. **391**(5): p. 1499-507.
13. Jinwal, U.K., et al., *Hsc70 rapidly engages tau after microtubule destabilization.* J Biol Chem, 2010. **285**(22): p. 16798-805.